An integrated three-dimensional sound-intensity probe

Doekle Yntema

The research described in this thesis was carried out at the Transducers Science and Technology Group of the MESA+ Research Institute at the University of Twente, Enschede, The Netherlands. The project was financially supported by the Dutch Technology Foundation (STW).

Promotiecommissie:

Voorzitter

prof. dr. ir. P.J. Gellings	Universiteit Twente

Secretaris

prof. dr. ir. A.J. Mouthaan	Universiteit Twente

Promotoren

prof. dr. M.C. Elwenspoek	Universiteit Twente
prof. dr. ir. W.F. Druyvesteyn	Universiteit Twente

Assistent Promotor

dr. ir. R.J. Wiegerink	Universiteit Twente

Referent

dr. ir. H-E. de Bree	Microflown Technologies

Leden

prof. dr. ir. A. de Boer	Universiteit Twente
prof. dr. P.P.L. Regtien	Universiteit Twente
prof. dr. S. Weyna	Szczecin University of Technology
prof. dr. ir. G.J.M. Krijnen	Universiteit Twente

Yntema, Doekle
An integrated three-dimensional sound-intensity probe
Ph.D. Thesis, University of Twente, Enschede, The Netherlands
ISBN: 978-90-365-2733-0
Copyright © 2008 by D.R.Yntema, Enschede, The Netherlands

An integrated three-dimensional sound-intensity probe

PROEFSCHRIFT

ter verkrijging van
de graad van doctor aan de Universiteit Twente
op gezag van de rector magnificus
prof. dr. W.H.M. Zijm,
volgens besluit van het College voor Promoties
in het openbaar te verdedigen
op vrijdag 3 oktober 2008 om 15:00 uur

door

Doekle Reinder Yntema
geboren op 16 maart 1976
te Leeuwarden

Dit proefschrift is goedgekeurd door de promotoren:

prof. dr. M.C. Elwenspoek
prof. dr. W.F. Druyvesteyn

Contents

1 Introduction **3**
1.1 Introduction to sound . . . 3
1.1.1 Sound pressure and particle velocity . . . 4
1.1.2 The Microflown sensor . . . 5
1.2 Sound intensity . . . 7
1.2.1 Sound intensity measurement probes . . . 9
1.3 Some applications . . . 12
1.3.1 Acoustic impedance measurement . . . 13
1.3.2 Sound visualization . . . 13
1.4 Aim of this thesis . . . 15

2 Performance issues of particle velocity sensors **17**
2.1 Introduction . . . 17
2.2 Sensor performance issues . . . 17
2.2.1 Self noise level . . . 18
2.2.2 Self noise versus power consumption . . . 18
2.2.3 Self noise and sensor wire length . . . 19
2.2.4 Package gain . . . 19
2.2.5 Measurement of sensitivity and noise level . . . 20
2.3 Design considerations . . . 21
2.3.1 Sensor failure . . . 21
2.3.2 Decrease of performance due to wrong cutting of chips . . . 22
2.3.3 Mechanical resonances . . . 22
2.3.4 Maximum permissible operating temperature . . . 24
2.4 Self noise of two and three wire sensors . . . 26
2.4.1 Introduction . . . 26
2.4.2 Measurement setup . . . 27
2.4.3 Two wire sensor self noise . . . 28
2.4.4 Three wire sensor self noise . . . 32
2.5 Conclusions . . . 36

3 Three dimensional particle velocity sensor development **39**
3.1 Introduction to 3D sensors . . . 39
3.2 3D design on one chip . . . 40
3.3 Sound source localization with a four particle velocity sensor device . . . 43

3.3.1 One v-sensor . . . 43
3.3.2 Two sensors . . . 44
3.3.3 More v- sensors . . . 46
3.3.4 The four sensor device . . . 48
3.3.5 Experiments in a reverberant room . . . 49
3.3.6 Results . . . 49
3.3.7 Conclusions and future plans . . . 53
3.4 A first design of an integrated 3D particle velocity sensor . . . 54
3.4.1 Design choices . . . 54
3.4.2 Fabrication and packaging . . . 55
3.4.3 Simulation and measurement results . . . 56
3.5 An investigation of the deviation in sensitivity direction . . . 59
3.5.1 A four wire sensor measuring the directionality effect . . . 61
3.5.2 Difference between in-plane and out-of-plane sensitivity . . . 61
3.5.3 A rotational symmetrical sensor . . . 62
3.5.4 The shape of the polar pattern . . . 65
3.5.5 Influence of the element housing temperature . . . 66
3.5.6 Measurement on loose wires . . . 67
3.6 A second 3D integrated particle velocity sensor design . . . 67
3.6.1 Measurement results . . . 67
3.7 A particle velocity sensor with four wires . . . 69
3.7.1 Polar pattern and sensitivity . . . 70
3.7.2 Self noise difference between two and four wires . . . 70
3.8 An integrated four-wire 3D design . . . 71
3.8.1 Fabrication . . . 72
3.8.2 Measurement results . . . 72
3.9 Conclusions . . . 73

4 A silicon pressure sensor based on particle velocity sensing 75
4.1 Summary . . . 75
4.2 Introduction . . . 76
4.3 The Helmholtz realization . . . 77
4.3.1 Theory . . . 77
4.3.2 Measurements . . . 78
4.4 A standing wave tube . . . 79
4.4.1 Response of an undamped standing wave tube . . . 79
4.4.2 Damping effects . . . 83
4.5 Prototype construction . . . 87
4.5.1 Measurement results . . . 87
4.5.2 Sound pressure sensitivity measurement . . . 91
4.5.3 Temperature measurements . . . 91
4.6 Integration into a MEMS sensor . . . 92
4.6.1 Design . . . 92
4.6.2 Final discussion of the design . . . 93
4.6.3 Fabrication and assembly of the sensor . . . 94

4.6.4 Measurement results 95
4.7 A second implementation of a MEMS sound pressure device 98
4.7.1 Measurement results 100
4.7.2 Effect of ridges inside the sound pressure to particle velocity converter 101
4.8 Other designs 101
4.9 Fields of application 102
4.10 Conclusions 104

5 Fabrication and assembly 105
5.1 Introduction 105
5.2 Clean room fabrication 105
5.2.1 Fabrication of a single-sided particle velocity sensor 106
5.2.2 Fabrication of three-dimensional particle velocity sensors 111
5.2.3 Fabrication of pressure cavities 113
5.3 Assembly of sensors 114
5.3.1 Mounting in a Zero-Insertion-Force connector 115
5.3.2 Interfacing to MEMS devices by a soldered connection 116
5.3.3 Alignment by capillary force 118
5.4 Conclusions 119

6 Applications 121
6.1 Introduction 121
6.2 Acoustic Noise Source Finder application 122
6.2.1 Introduction 122
6.2.2 Description 122
6.2.3 Sound source localization 124
6.2.4 Implementation 125
6.2.5 Measurement results 125
6.2.6 Comparison between the sound pressure and particle velocity signal 127
6.2.7 Measurements with the ANSF and background noise 128
6.2.8 Conclusions 130
6.3 Very small sound source localization 130
6.3.1 Measurement setup 130
6.3.2 Measurement results 130
6.4 A portable sound intensity array system 135
6.4.1 The regular approach of an array system 135
6.4.2 A realization with a low data transfer rate 136
6.4.3 Measurements with the prototype 138
6.4.4 Design improvements 138
6.4.5 Applications with the SIMD 139
6.4.6 Conclusions 142

7 Conclusions and recommendations 143
7.1 Summary of conclusions 143
7.1.1 Recommendations and future research 146

A Appendix to section 3.3 **147**

B Propagation coefficient for a damped tube **151**

C Fabrication process sheet **153**

D Polar plot measurement **157**

References **163**

Summary **165**

Samenvatting **167**

Publications **169**

Dankwoord **171**

Chapter 1

Introduction

1.1 Introduction to sound

Sound is everywhere, it is used by many creatures to communicate, orientate, detect threats, locate prey, to deter enemies, for amorous reasons and so on. For humans it makes music and speech possible, but it can also be annoying. Although sound is a very common phenomenon, the understanding of sound is not trivial. Acoustic engineers try to understand sound by using measurement setups combined with theory to give explanations for acoustic situations, and in many cases with success.

Sound is measured for various reasons. Determining the sound level for regulatory purposes is a well known example. Another example is the qualification of a product in a factory by means of its generated sound. Exactly the opposite is also possible, the acoustic properties such as how sound does reflect on a certain product or how much it absorbs can be measured. Furthermore acoustic measurements can be used for the detection of events such as the passing of airplanes for regulatory or military purposes, thunder detection for meteorological purposes and gunshot detection in a military environment.

The best known method to measure sound is with a so called 'dB meter'. A dB meter measures the acoustic sound pressure and displays this in a logarithmic scale, so quantifying the amount of sound that we hear. Since sound pressure is a scalar value the direction of sound can not be measured when measuring with one sound pressure sensor. For some purposes, such as the determination of sound pressure in an indoor swimming pool for regulatory purposes, the measurement of sound pressure may suffice. For other measurement purposes such as determining the sound power emitted by a sound source or locating sound sources the measurement of sound pressure with a single sound pressure microphone is not sufficient.

Imagine a noisy engine. Measuring sound pressure with the dB meter near the engine results in a reading which is dependent on the measurement location, the influence of other sound sources and the influence of reflections. It can not even be discriminated whether the sound is generated by the engine or not. Determining the exact location of a sound source is useful though. The sound can be reduced by placing the engine in an

acoustically isolating box. But when the location where the sound is generated is precisely known the sound can be isolated more effectively, resulting in the same reduction with less insulation material or a better reduction. Determination of the location of this spot can also be used for finding defects in the engine. Furthermore it can be useful for optimization of the engine with respect to its emitted sound level, since the location where the sound is generated often coincides with the mechanical origin of the sound.

Although sound pressure does not have direction, sound does certainly propagate in a direction. When the direction of propagation is measured the location of the sound source can be found since the propagation starts there. The propagation of sound is three dimensional, requiring a three-dimensional sound probe to characterize the sound field completely. In the following sections the phenomenon 'sound' is explained further and a sensor able to determine the three-dimensional sound field is introduced.

1.1.1 Sound pressure and particle velocity

In everyday life sound is described as the sensation produced by oscillatory pressures acting on the ear. In the dictionary of acoustics [1] it is stated that sound is a disturbance in pressure that propagates through a compressible medium. More generally, sound can refer to any type of mechanical wave motion, in a solid or fluid medium, that propagates via the action of elastic stresses and that involves local compression and expansion of the medium.

When talking about sound the accent is mainly on pressure fluctuations, not least because the human ear is sensitive to the sound pressure signal, and indeed, sound fields are generally measured with microphones measuring sound pressure p. There is a difference between sound pressure and atmospheric pressure: sound pressure is a very small pressure fluctuation of the atmospheric pressure, in the order of micro Pascals to several Pascals, while the atmospheric pressure is around 10^5 Pascals. Sound pressure measurements show the sound pressure at the measurement location, but do not provide directional information since pressure is a scalar. Commonly sound pressure is given in Decibels, which is a logarithmic scale with as reference 20 μPa (or $SPL = 20 \cdot log_{10} \frac{Sound\ pressure\ [Pa]}{20 \cdot 10^{-6}\ [Pa]}$). The sensing of acoustic sound pressure is normally done with a sound pressure microphone. The most common variety of this type of sensor is a membrane covering an enclosed volume that moves through sound pressure fluctuations. These movements are detected and converted to an electrical signal. The movement of the membrane is detected electromagnetically, capacitively or even optically. The sound pressure microphone has been available for a long time and is a highly developed product.

Where the electrical domain is fully characterized by tension (defined in Voltage) and current (in Amperes) in the acoustical domain a similar configuration can be found. Sound pressure is analogous to tension in the electrical domain and electrical current is analogous to particle velocity in the acoustic domain. While sound pressure is a scalar and has only a magnitude, particle velocity is a three-dimensional vector value.

Particle velocity can be understood by imagining a number of imaginary particles

present in a certain volume where the number of particles per volume unit defines the pressure. A 'particle' can here be seen as a large number of neighboring air molecules. A flow of particles toward the volume will result in an increased pressure in this volume and vice versa. This (directional) movement of particles is equivalent to the 'particle velocity' or vector $\boldsymbol{u}$. In acoustics particle velocity is defined as the speed (in m/s) of an infinitely small volume of air due to an acoustic wave, not to be confused with the speed of sound c or the random thermal motion of molecules. Particle velocity has nothing to do with particles or dust. Similar to sound pressure measurement the particle velocity level or PVL is commonly represented in a logarithmic scale with as reference 50 nm/s as $PVL = 20 \cdot log_{10} \frac{Particle\ velocity\ [m/s]}{50 \cdot 10^{-9}\ [m/s]}$.

Sensors which are capable of measuring particle velocity are not as common as sound pressure microphones. A particle velocity sensor based on ultrasonic transduction has been proposed [2][3]. In this sensor two parallel ultrasonic beams are launched in opposite directions. The time difference in reception of the waves is proportional to the average particle velocity over the measurement distance. Another example of a particle velocity sensor is the ribbon microphone, which consist of a lightweight ribbon between two magnets moving with the air flow or particle velocity. This type of particle velocity sensor is relatively bulky mainly due to the large magnets used. Nowadays a sensor, the 'Microflown' [4], is available which is able to measure particle velocity in one particular direction and has a small size [5].

1.1.2 The Microflown sensor

In 1994 the 'Microflown' was invented, which is in fact a modified flow sensor [6]. The original inventor of the element used a mass flow sensor to measure on an engine air intake, and accidentally discovered that the sensor was capable of detecting sound. The sensor proved to be useful as a particle velocity microphone. In 1998 a company commercializing the sensor was started [7].

The actual particle velocity sensing element consist of two small wires with a length of 1.5 mm, thickness between 200 nm and 500 nm and width varying between 2 and 5 μm. A photograph of such a sensor is shown in Figure 1.1. The wires are made of a temperature dependent resistance material. When a voltage is applied across the wires they will heat up to some hundreds of degrees centigrade. A particle velocity signal in the direction perpendicular to, and in plane with the two wires will change the local temperature profile causing a temperature difference between the two wires. This temperature difference results in a change in resistance between the wires which is detected electrically. Particle velocity signals perpendicular to the sensitive direction result in an equal temperature change of both wires, which does not result in an output signal. Therefore, the particle velocity sensor is sensitive in one direction only.

Since the sensor wires are very small and dust particles can easily interfere with the fabrication, fabrication is done in a clean room environment. The sensor wires are made by lithographic processes combined with depositing and etching techniques. After fabri-

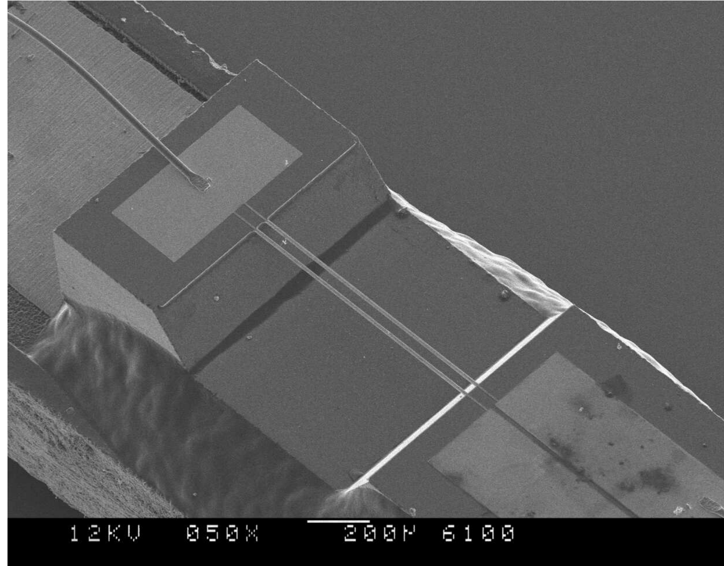

Figure 1.1: *Bridge type sensor.*

cation the sensors are placed on a carrier substrate and connected electrically. The carrier substrate can be partly seen in Figure 1.1. When using the sensor in a (commercial) measurement device it has to be packaged further, so that it is capable of operating outside the controlled laboratory environment.

The response of the sensor to particle velocity signals with a frequency between 100 Hz and 500 Hz is almost independent of frequency. Above 1 kHz the response starts to drop with 6 dB/ octave, due to the heat diffusion in air. At higher frequencies (around 10 kHz for commercially used sensor-heater-sensor configurations with 3 μm wire width), an additional low pass behavior results in a frequency response of -12 dB per octave. This is due to the heat capacity of the sensor wires [8] [9]. The amplitude and phase response of the element can be approximated successfully by a second order Resistor-Capacitor filter, an inverse Resistor-Capacitor filter is able to correct this response. At low frequencies (practically below 100 Hz) the sensitivity is also limited, this is very likely related to the thermal boundary layer of the sensor wires and the nearby packaging. In commercial products this is corrected either by software or electronically [10].

Compared with sound pressure microphones the equivalent acoustic noise of the Microflown element is higher than the equivalent acoustic noise of sound pressure microphones at frequencies above 1 kHz. A comparison in self noise between a 2-wire, a 3-wire, a small sound pressure microphone and a reference sound pressure microphone is given in Figure 2.1. In measurement setups the sound level is mostly high enough for good results [10]. Additional signal processing techniques can compensate for uncorrelated noise when using multiple sensors [11]. Measurements near (small) sound sources result in a comparatively high particle velocity signal due to the the near field effect [12][13]. In these situations measurement with a particle velocity sensor still results in a high signal to noise ratio compared with most sound pressure microphones.

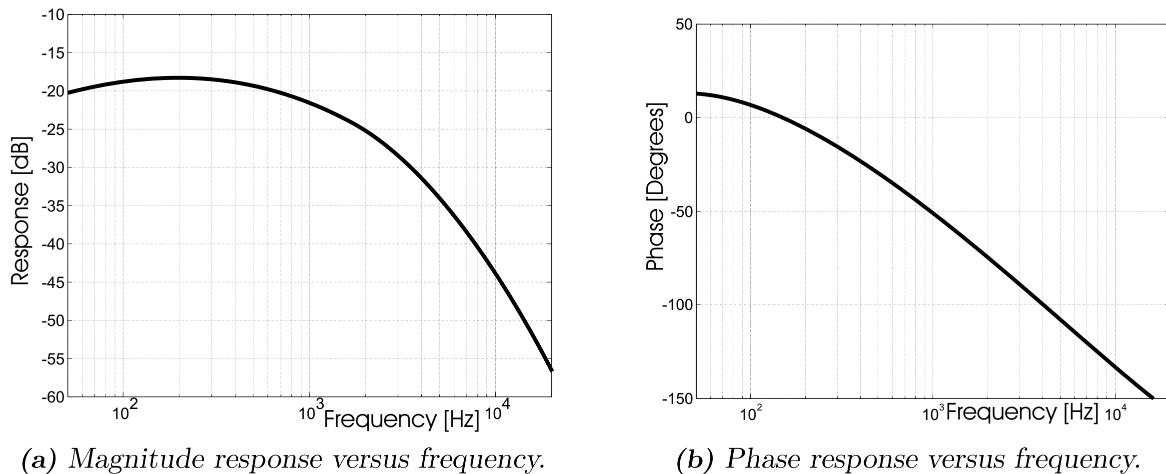

***(a)** Magnitude response versus frequency.* ***(b)** Phase response versus frequency.*

Figure 1.2: *Frequency response of a three wire sensor element, measured in a standing wave tube.*

Although the sensor can be used as a recording microphone for music its use is focused on acoustic measurement purposes. The high noise at frequencies above 1 kHz makes the sensor less suited for use in musical applications where sound levels are low. In some applications concerning the recording of music the sensors can still be of interest as shown in [14] and a prototype of a particle velocity based audio microphone suited for recording music is presented in [15].

A sensor capable of measuring particle velocity in a single direction was developed. Together with a sound pressure microphone the sound field can be characterized completely.

1.2 Sound intensity

Sound intensity is the product of sound pressure and particle velocity representing the amount of sound power moving through an area in W/m^2. Sound intensity is a vector quantity, describing both direction and magnitude. With sound intensity measurements the location of sound sources can be determined together with their acoustic strength.

Similar to the electrical domain where the measured voltage does not provide information on how much power is transferred in which direction the measurement of solely sound pressure cannot be used to measure sound intensity. Only in the rare case that the acoustic impedance at the measurement position is known sound pressure measurements can be sufficient. To be able to determine the three-dimensional sound intensity vector without knowing the acoustic impedance the three-dimensional particle velocity signal together with the sound pressure signal has to be measured.

While sound pressure is normally measured with a sound pressure microphone, the

particle velocity signal can be derived from differential sound pressure measurement. Since small particle velocity sensors (the Microflown sensor) are nowadays available it can also be measured by this particle velocity sensor. The method for measuring sound intensity where particle velocity is derived from the pressure gradient is called the P-P method, where the abbreviation P-P stands for Pressure-Pressure.) Using particle velocity sensors and a sound pressure sensor is called the P-U method, where U is a synonym for particle velocity.

For the determination of the instantaneous sound intensity the product of p and $\boldsymbol{u}$ is required:

$$\boldsymbol{I}(t) = p(t)\boldsymbol{u}^*(t) \tag{1.1}$$

where p is the pressure, expressed in a complex quantity thereby including phase information between the pressure and particle velocity signal, and $\boldsymbol{u}$ is the three dimensional complex valued particle velocity signal. The average intensity is obtained by averaging over time T:

$$\boldsymbol{I} = \frac{1}{T}\int_{-T/2}^{T/2} p(t)\boldsymbol{u}^*(t)dt \tag{1.2}$$

For a harmonic signal the value of T can be equal to the period of the signal, but in practical measurement situations the value of T is taken longer than the time needed for multiple periods of the lowest frequency that is measured.

An application where sound intensity measurement is of advantage is sound source localization. Locating sound with one stationary sound pressure sensor is an impossible task, since pressure is a scalar. When moving the sound pressure microphone amplitude variations are detected. In an environment with only few and soft reflections and a low amount of background noise this can eventually lead to finding the position of the noise source. Most measurement situations do not satisfy these conditions.

Measuring particle velocity with directional sensors has the advantage that information is obtained about where the sound field is directed to or where it comes from. Particle velocity moves both in the direction to and from a sound source in a symmetrical way. Measurement of the three dimensional particle velocity vector alone cannot tell whether the sound travels one or the other way in the direction of the particle velocity. Combining the measurement of particle velocity with sound pressure measurement can overcome this ambiguity in direction. In Figure 1.3 two sources are depicted, source A and source B. At the measurement point the particle velocity and sound pressure is measured. When sound source B is activated with a harmonic signal the particle velocity signal shown in Figure 1.4a is obtained. Activating sound source A with a harmonic signal results in the particle velocity signal shown in Figure 1.4b. A difference between both graphs is seen, in the first case the particle velocity signal has a 'positive' magnitude and in the second case a 'negative' one. In this example the time scales of the experiments are matched in time, but when only measuring the particle velocity signal it cannot be discriminated

whether the sign is positive or negative due to the symmetric signal. Sound pressure is not directional, thus the response to either sound source *A* or sound source *B* is similar. Combining the particle velocity signal with the pressure signal by multiplication results in the sound intensity signal, which has a uniquely defined direction.

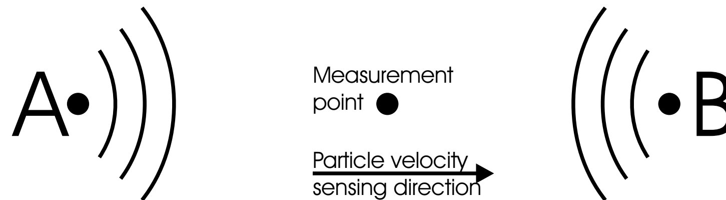

Figure 1.3: *Sound pressure multiplied with particle velocity results in a uniquely defined direction.*

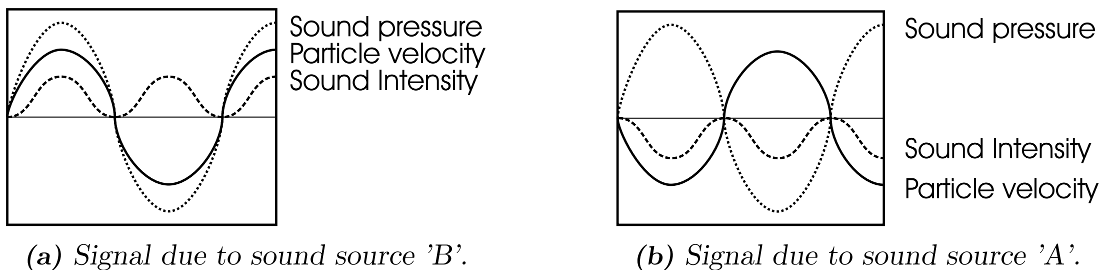

(a) Signal due to sound source 'B'. *(b) Signal due to sound source 'A'.*

Figure 1.4: *The relation between the time signals particle velocity, sound pressure and sound intensity are graphically represented. A sound intensity signal provides information whether the sound source is in front or behind the sensor.*

1.2.1 Sound intensity measurement probes

Sound intensity measurement systems have been available for some time, the best known method employs two sound pressure microphones spaced at a fixed distance. A distance of 12 mm is considered optimum for use between roughly 250 Hz to 10 kHz [16]. Indirectly the particle velocity signal is derived from a finite difference approximation of the pressure gradient. This conversion easily gives rise to errors because the conversion relies on precise phase matching of the sound pressure sensors and is affected by scattering and diffraction of the sound field. In [17] and [18] the principle is extensively explained. The sound pressure signal is evaluated as the average value of the two sound pressure signals.

The two sound pressure sensors are spaced at a certain distance from each other. This implies that the minimum size of a P-P measurement probe is equal to this separation distance plus the size of the sound pressure element. Since the sound intensity is evaluated between the sound pressure sensors the sound intensity cannot be measured closer than at least half the separation distance plus the size of a sound pressure sensor. Together with the measurement results a position where these results are obtained must be provided. This position must preferably be a well defined point in the measurement space. Using the

P-P method the sound intensity value is evaluated as the average value of sound intensity between the two sound pressure microphones, therefore the size of the measurement point is not infinitely small but actually a 12 mm long 'point'. Due to this the resolution in measurement position is about 12 mm.

Measuring particle velocity directly with a particle velocity sensor avoids the conversion step from pressure gradient to particle velocity and the problems encountered with the P-P method are avoided. The described Microflown sensor is sensitive for particle velocity in one direction, combining this sensor with a sound pressure sensor a one-dimensional sound intensity probe is made. A comparison between measuring with the P-P method and the P-U method is given in [16], [19] and [20]. Because the sensors can be placed closely together the size of the measurement point is smaller and therefore spatial resolution of the measurement point is higher.

3D-Sound Intensity sensors

A three-dimensional sound intensity probe can be made by combining three pairs of P-P probes, each pointed with its sensitivity axis in an orthogonal direction. A three dimensional sound intensity probe from G.R.A.S. is shown in Figure 1.5. The size of the probe is around 10 cm, which is physically limiting the minimum measurement distance from surrounding objects. Additionally the sound intensity is determined between the sound pressure sensors which are each 12 mm apart. For this probe the spatial resolution of the measurement point is roughly 12 mm.

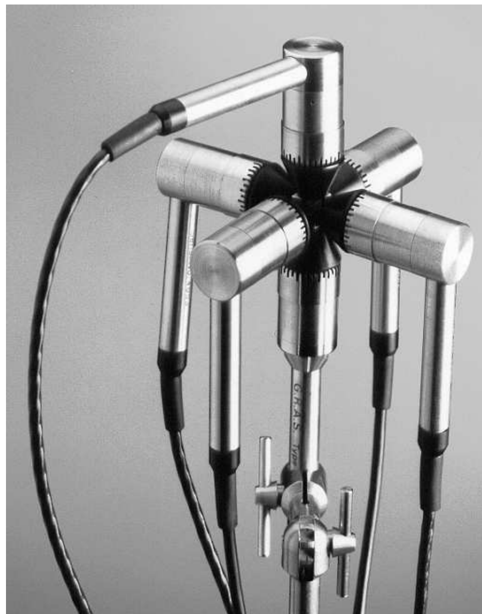

Figure 1.5: *A commercially available 3D sound intensity probe from G.R.A.S., six sound pressure sensors combined measure the three-dimensional sound intensity. The sound pressure element size is 1/2", the size of the complete probe is around 10 cm.*

The company 'Microflown Technologies' commercializes a 3D-sound intensity probe, based on a combination of manually assembled one-dimensional particle velocity sensors and a sound pressure sensor. See Figure 1.6 for a photo of such a probe. Small measurement distances are possible enabling measurement on small objects and in confined spaces. Due to its small size the probe has only little influence on the sound field which enables for reliable measurement results. Limitations for this probe do still exist. When measuring near to small sound sources the distance between the sensors is a limiting factor regarding measurement accuracy. For this probe the maximum sensor-to-sensor distance is around 6 mm, thus the size of the measurement point can be considered 6 mm. For a reliable point measurement a distance of at least two centimeters from the source is required. The frequency range in which sound intensity can be measured with this probe is from 10 Hz up to at least 10 kHz. For higher frequencies the distance between sensors is in the order of the wavelength, giving rise to errors.

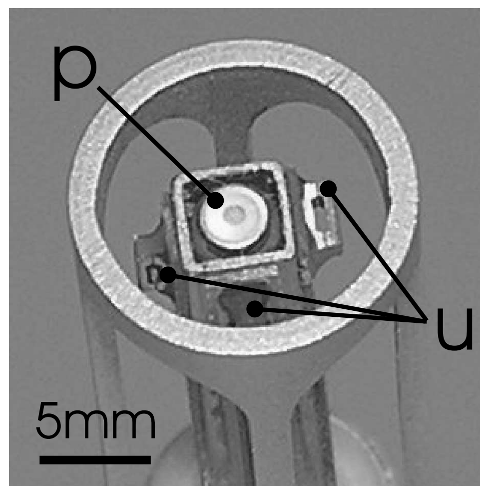

Figure 1.6: *A commercially available sensor from Microflown Technologies, three particle velocity sensors are combined with a sound pressure sensor to an 'USP', a three-dimensional sound intensity probe. Around the sensor a protective metal casing is placed.*

An integrated design

Although the existing sound intensity probe based on sound pressure and particle velocity measurement are already much smaller than systems based on the P-P measurement principle an even smaller sensor is desirable [21] . Both size and sensor separation determine the usefulness of the sensor. A smaller sensor has less influence on the sound field. Placing the sensors closer together results in a higher spatial resolution of the measurement point. High spatial resolution is required e.g. for measurement on small sound sources.

The orientation of the particle velocity sensors (and therefore the sensitivity directions) in an integrated particle velocity sensor chip is defined by lithography. Compared with the manual assembly of separate sensors of the probe shown in Figure 1.6 the precision in positioning the sensors is very high. Furthermore the sensors can be placed much closer to each other since there is no separate silicon carrier or electrical connection

necessary for every single sensor. In the designs as shown in the figure the size of the carrier and other mounting material determines by a large amount how close the sensors can be placed together. Several different realizations of an integrated 3D particle velocity sensor are described in chapter 3, of which each is an improved version of an earlier design.

The sound pressure sensor in the manual assembled three-dimensional probe (designated by the 'p' in Figure 1.6) still requires much space. Integrating a sound pressure sensor with the particle velocity the above described sensor chip can reduce the size further or the sound pressure sensor can be positioned more efficiently. Designs based on membrane deflection are not considered but instead a whole new type of sensor is developed and optimized for integration with particle velocity sensors. The fabrication of the sensor is compatible with the fabrication process of the particle velocity sensor designs. Integrating particle velocity sensors with a sound pressure sensor in a single chip results in a sensor capable of measuring the sound field with a smaller probe size than existing three-dimensional sound intensity probes. Together with decreasing size a higher spatial resolution of the measurement position is obtained. Additionally the precision in orientation of the sensors is higher than with a manually assembled probe.

1.3 Some applications

Many applications using the particle velocity sensor have been discovered since the invention of the Microflown sensor, and some of them are a commercial success [10] [22]. A small selection of existing applications is evaluated to gain insight in the possibilities of using particle velocity sensors, possibly combined with sound pressure microphones. In the described applications the probes that are already available are often well suited but a smaller sensor can be beneficial.

When scaling the size of the application, for example from measurements on a large diesel engine to measurements on a small dentist drill, the size of the measurement probe is of importance for a number of reasons. Obviously the probe must not physically interfere with the measurement setup, the probe must not have a large effect on the sound field and the measurement location must be known precisely. In these cases the application of a small integrated sound intensity probe is essential. Applications requiring a three-dimensional sound intensity probe can be scaled down when using a smaller sound intensity probe or the intrusiveness of the element in existing applications can be diminished.

Very near to a moving object the particle velocity is equal to the movement of the object, so by measuring the particle velocity very near to the object the movement of the object can be measured. As shown in chapter 3 the sensor chip can be made so small that measurement of particle velocity very close (practically down to 0.5 mm distance) to an object can be measured. With the presented four wire particle velocity sensor even the two-dimensional particle velocity can be measured at virtually the same measurement point at this small distance. Measuring the particle velocity very near to the measurement

object with a small sensor makes a high spatial resolution possible, enabling a detailed view of the vibration of the object.

In chapter 6 a number of applications are described in detail where the integrated sound intensity sensor chip is especially suitable. The focus is mainly on sound source localization and new applications involving a small integrated sensor.

1.3.1 Acoustic impedance measurement

Measurement of the acoustic impedance is important for many applications. For example wind instruments, horns, vocal tract and absorbing materials can be be characterized such [23]. In [24] the material is placed in a tube and with a sound source at one end and the signals from two sound pressure microphones the acoustic impedance is calculated. With the use of the particle velocity sensors the acoustic impedance can be measured in an easy way, enabling a hand held and non-destructive characterization of various types of materials. The method is named the 'in-situ surface impedance technique' and requires a one-dimensional sound intensity probe and a sound source. A sound probe with a one-dimensional particle velocity sensor and a sound pressure sensor is placed near the object to be characterized and the sound source is activated. From the measured particle velocity and sound pressure the acoustic impedance can be calculated. The in situ surface impedance technique has been proved valid in various papers [25] [26] [27] [28] [29].

Some applications require a very small sound probe to measure the acoustic impedance. An example of this is impedance measurement in the human ear canal. The functional operation of an ear can be characterized by measuring the acoustic impedance of the ear canal terminated with the eardrum. Since this requires a very small particle velocity sensor combined with a pressure sensor an integrated design can be a solution.

When measuring the acoustic impedance of small objects or when measurement is focused on a small surface the measurement probe must be placed very close to the object. Especially when measuring very near to an object it is of importance that the sound pressure and particle velocity sensor are at virtually the same place. Furthermore the probe must preferable not influence the measurement results. A small measurement probe is of advantage in this situation.

1.3.2 Sound visualization

Sound field visualization is the process of transforming a sound field into a visual image. In such an image sound pressure, particle velocity or sound intensity is visualized. By visualizing the sound field one can get an impression of the sound field over an area or volume in a simple way.

Acoustic holography and particle velocity

Acoustic sound field visualization is done with techniques such as Near-field Acoustic Holography (NAH), which is a famous example. This technique measures the sound pressure field at a certain distance from a sound source and calculates the particle velocity

and sound pressure as well as the sound intensity at the location of the sound sources [30]. A good summary of different methods capable of doing this is given in [31].

With the availability of particle velocity sensors it has become possible to measure the sound field near a sound source. Where the acoustical holography methods reconstructs the sound pressure and particle velocity from the sound pressure measurements at a larger distance the sound field can also be measured directly. The advantage of measuring the sound field directly is that the errors made in the propagation process are avoided resulting in a better description of the sound field. The method with particle velocity sensors is found to be superior, as published in [32] and [33]. A condition is that the measurement probes have to be placed close to the measurement object and that the probes must preferably not disturb the sound field.

An integrated three-dimensional sound probe is here of advantage, since the complete three-dimensional particle velocity signal is measured together with the sound pressure signal in a small size. The small size minimizes the disturbance of the sound field and the small sensor to sensor distance guarantees a good spatial resolution.

Sound field scanner

A straightforward but useful sound visualization technique is using the 'scan and listen' technique [34]. With this method a (sound emitting) surface is scanned by hand. Finding the shape of a vibration mode in a vibrating surface is done by locating the positions where sound pressure and particle velocity signals are zero or maximum.

Measuring the particle velocity near the surface in the direction perpendicular to the surface results in a first indication of the sound field. At places where the particle velocity signal in this direction is largest a maximum in excursion of the plate is found. At places where the signal is smallest a minimum is found. Furthermore the places with zero lateral velocity can be found when scanning the surface for minimum particle velocity in the lateral direction with the surface. For this the probe must be rotated since it is sensitive in a single direction only. A result of such a scan is shown in Figure 1.7 (figure taken from [34]). In the figure the lines are drawn by hand on the plate. The sound field of small devices such as a mechanical watch, cellphones and hard disks, but also the mode shapes of an acoustic instrument can be visualized quickly.

While this technique requires rotation of the probe head, a three-dimensional type of sensor would eliminate this need, enabling an even faster sound field mapping. For measurements on large objects a commercially available three-dimensional probe can be used. Also in this application small objects or measuring very close to the object requires a small probe.

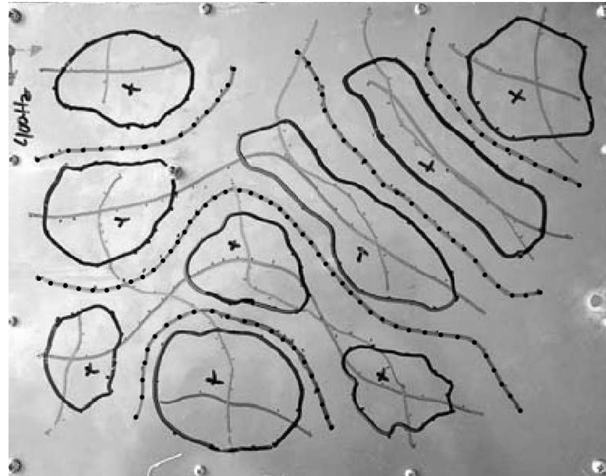

Figure 1.7: *A simple way to find a mode shape at 400 Hz. In gray, the lines with zero lateral velocity are shown. In black iso-velocity lines and in dotted lines the lines of zero normal velocity. The black crosses are the points of maximal normal velocity.*

1.4 Aim of this thesis

As shown in the previous sections the development of a particle velocity sensor opens up a new field of acoustic applications. Because particle velocity is a three-dimensional vector it requires a three-dimensional particle velocity sensor to measure it completely. A device capable of measuring the complete three-dimensional sound field is commercially available but significant improvements are possible. This research project has been initiated with the main goal to improve the design of the existing sensor by integrating all sensors in a single chip. By doing this a smaller sensor with a smaller sensor-to-sensor distance is obtained. This enables a very small measurement point with a minimum effect on the sound field.

To achieve these goals different sensors and their performance have been investigated. The results can be used for optimizing the final integrated sensor design. Furthermore some remarkable properties of the sensor are investigated and design rules to avoid problems are discussed. In chapter 2 the result of this research is shown. Positioning the sensors in a chip is a point of concern, together with the optimum orientation of the sensitivity directions. A discussion on various possibilities and research with a manually assembled four-particle-velocity sensor device results in a first design. The design evolves by the development and research on altered designs. Chapter 3 explains in detail how this is achieved.

A sound pressure microphone is developed based on a sound pressure to particle velocity transformer. Due to the similarity with the existing particle velocity sensor designs the fabrication of the sensor can be combined with the fabrication of the particle velocity sensors. This results in the integration of a sound pressure sensor with a three-dimensional particle velocity sensor on one chip.

The sensors have been fabricated in a clean room environment, using etching and

deposition of materials. Solutions for problems that are encountered in the fabrication process have been solved and design rules have been extracted. After fabrication the chip must be mounted and further prepared for use in a measurement setup. This requires a mechanical as well as an electrical connection. With the help of adapted mounting techniques for the made chip the assembly cost and the size of the assembly can be reduced further.

A large number of applications with particle velocity sensors has been discovered since the invention of the Microflown. Although the functionality of a three-dimensional sound intensity probe was already available in a manually assembled variety as used in [35] and [36], a much smaller sensor-chip has been developed here. This newly developed chip has a very small sensor-to-sensor distance, thus the sound field is measured at a small point in space. This small distance makes the chip especially suited for measurements on sound fields with a large gradient, such as the sound field near a small sound source. The sensor can be used for locating sound sources by measurement of sound intensity or particle velocity. Applications involving the use of the sensor are discussed in detail in chapter 6.

Chapter 2

Performance issues of particle velocity sensors

2.1 Introduction

In this chapter, the most important parameters that influence the performance of the basic particle velocity sensor structure are discussed. The results presented in this chapter were used to make better designs for a three-dimensional version of the sensor, which is presented in the next chapter.

First, in section 2.2 it is explained that the so-called *self noise* is an important measure for the quality of the sensor and a measurement setup for measuring the self noise is discussed. Next, in section 2.3 various other aspects needed for making a good sensor design are discussed, like robustness of the sensor, yield of the fabrication process and mechanical resonances.

In the last part of the chapter, systematic measurement results are presented for the self noise of two-wire (section 2.4.3) and three-wire (section 2.4.4) sensors as a function of wire spacing and power dissipation. These results are especially useful for design optimization.

2.2 Sensor performance issues

What is sensor performance? Sensor performance can be expressed in terms of temperature range, robustness, power consumption, size and so on. Quite often the sensitivity is used as a measure for the quality of a sensor, however only in combination with the noise level of the sensor this value is of any real importance. Sensitivity and sensor noise together define the lowest particle velocity level that can be detected. This minimum detectable level is called the *self noise* level.

For an integrated three dimensional sound intensity probe, which is the main goal of the research presented in this thesis, the performance must be good enough to compete with existing alternatives. That does not mean that every aspect of the sensors perfor-

mance has to be better, but there has to be a significant improvement in some aspects in order to make the sensor more suitable for certain measurements. As explained in chapter 1, obvious advantages of an integrated three-dimensional sensor include an almost perfect alignment and small overall sensor size. However, this may be at the expense of a degraded performance on other aspects. Most important will be to avoid an increase of the self noise level. Therefore, in this section we discuss the self noise level and the most important design parameters that influence the self noise. Other performance aspects are discussed in section 2.3.

2.2.1 Self noise level

From [37], it can be concluded that an optimum sensitivity can be attained with certain geometric properties of the sensor element. But when looking at sensor performance not only sensitivity but also noise level is of importance. Together with its sensitivity the noise of a sensor defines the lowest (sound) level that can be measured. When the generated noise level (in Volts) is divided by the sensitivity of the sensor (in Vs/m for a particle velocity sensor) this results in the apparent acoustic self noise. The apparent acoustic self noise is the amount of noise that is generated by the element, but treated as if the origin is acoustic. Self noise is therefore a key parameter when describing sensor quality.

Describing the acoustic self noise can be done conveniently with a logarithmic scale, with as reference the threshold of hearing at 1kHz. This threshold of hearing is defined as 20 μPa sound pressure level. Particle velocity and sound pressure are related by the acoustic impedance, which is in the free field equal to ρc (c=340 m/s and $\rho = 1.2$kg/m^3). Therefore the reference level for a 0 dB particle velocity level is taken as 50 nm/s, as found from dividing the reference sound pressure level by the acoustic impedance.

To illustrate the self noise level the self noise of two microphones and two particle velocity sensors is shown in Figure 2.1. The 'Titan' element is a three wire particle velocity sensor with packaging and the 'IO' sensor is an element with two wires. The signal gain due to packaging is estimated to be between 10 and 15 dB.

2.2.2 Self noise versus power consumption

It can be questioned what the most important quality comparison method is: a lower self noise level regardless of power consumption or self noise versus power consumption. When comparison of self noise versus power consumption is done the best sensor regarding power consumption can be found, but this noise level can still be higher than a less optimum sensor working at its optimum power level. Of course multiple sensors can be used in series or parallel thereby lowering the self noise, but then size is increasing.

Furthermore when power consumption is an important issue in the final application there is a strong reason to compare sensors using this method, otherwise, when simply an optimum sensor must be found the comparison method of self noise regardless of power consumption is more important. In the case of a measurement system the power consumption of at most 50 mW per sensor is not very large compared with the current consumption

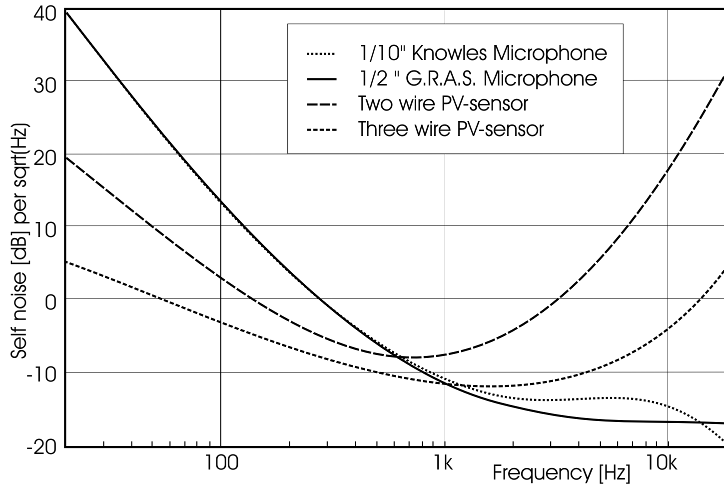

Figure 2.1: *Self noise in 1 Hz bands of a two wire and three wire particle velocity sensors packaged in a 1/2" housing. Together the self noise of a type 40-AC G.R.A.S. sound pressure microphone and a 1/10" FG-type Knowles microphone (Picture taken from [38]) are shown.*

of the other hardware normally used (such as analyzers and computer systems). Since the sensor is to be used mainly in such systems the focus is here on an optimum self noise level, regardless power consumption.

2.2.3 Self noise and sensor wire length

When two sensors are used instead of one and both signals are added, the signal level increases by a factor of two. The noise signal V_{ns} of two sensors is generally uncorrelated, and this can then be added as $\sqrt{V_{n1}^2 + V_{n2}^2}$, see for example [11]. Power consumption is doubled. So the signal level is doubled but the noise level is only increased by a factor $\sqrt{2}$, this gives a self noise 'gain' of $\sqrt{2}$. When using ten times as many sensors the self noise will be $\sqrt{10}$ times better, but the required power is ten times more. This demonstrates that the self noise using multiple sensors is directly proportional to the amount of sensors squared (or the amount of power squared). This is also valid when multiple sensors of the same type are formed to one single large sensor and all sensors are working under the same conditions, for example in an implementation in a design with elongation of the sensor wires. Total size does increase also.

Assuming that wire length is indeed equivalent to using multiple sensors (thereby disregarding wire support and other geometrical effects) the self noise divided by power requirement squared should give identical values. Therefore the parameter 'length of a sensor wire' is not varied in the experiments when comparing different sensor types.

2.2.4 Package gain

Through the effect of 'package gain', which is in short the effect of an object (housing of the sensor) in the vicinity of the particle velocity sensor on the output signal, the particle

velocity level at the place of the sensor is increased. This package gain has an effect on the particle velocity level as well as on the direction of the particle velocity [39]. Therefore the sensitivity of the total assembly increases. When the noise level stays the same the self noise level will decrease. Package gain for packages of size 15 * 15 mm can be up to 15 dB, thereby not increasing the noise level and thus lowering the self noise with 15 dB compared with an unpackaged sensor. When sensitivity increases, but the noise level increases with the same amount there will be no difference in sensor self noise level, apart from the fact that with increasing noise level lower demands are put on the pre-amplifier. Also whether an amplifier between the sensor and the analyzer is used does not have any influence on the self noise level, as long as the amplification for the sensitivity measurement and noise measurement is equal.

2.2.5 Measurement of sensitivity and noise level

Calibration of sensors is normally done by comparing a sensor with a reference sensor. For a particle velocity sensor there is no straightforward reference sensor available, so a workaround must be used. A method to calibrate the sensor with a reference particle velocity sensor is described in [40], but this requires expensive equipment and a delicate setup. In certain situations there is a well defined relation with sound pressure however, and reference sound pressure sensors are fully available.

When the acoustic impedance of a sound source is well known a sound pressure sensor can be used to calibrate the particle velocity sensor. This principle is used in the standing wave tube calibration [41]. The near field calibration and the piston in a sphere [42] [43] calibration setup relies on the known radiation impedance of the sources. For examining the sensitivity of the particle velocity sensors here the standing wave tube calibration technique is used. A short introduction is given below, a more detailed description can be found in [12] [44] or [45].

The standing wave tube calibration method

In a standing wave tube the sound field is well known. A sound source in the form of a loudspeaker is present on one side of the tube, generating particle velocity. On the surface of the loudspeaker the particle velocity is equal to the movement of the loudspeaker membrane. The other end of the tube is acoustically terminated, so sound reflects completely on this end. Furthermore at the closed end there is no particle velocity since the wall does not move and at the wall a sound pressure maximum exists. As a function of frequency and the input level the particle velocity level at a place x in the tube can be calculated.

Since there is a complete reflection on one end of the tube there is no energy transport in the tube; an amount of sound power is transferred to the closed end and an equal amount is reflected back to the end with the loudspeaker. Because the averaged intensity must be zero the phase shift between the sound pressure signal and the particle velocity signal must be 90 degrees. On the other hand the transfer function between the sound

pressure level at the closed end and the particle velocity is known, see [41] so when the response of the sound pressure sensor is known the response of the sensor is known. Without damping effects (which can be disregarded according to [12] and [44]) the relation between the particle velocity at a distance x from the closed end of the tube and the sound pressure signal at the end of a tube with length l:

$$\frac{u_{probe}}{p_{ref.}} = \frac{i}{\rho c} sin(kl) \tag{2.1}$$

Dividing the measured response of the particle velocity sensor by the response of the reference pressure microphone results in the response of the device in the standing wave tube. Dividing this result by the known response of the standing wave tube results in the response of the particle velocity sensor. An advantage of the standing wave tube calibration is that there is a clear distinction between the particle velocity signal and the pressure signal at place x, enabling investigating whether a device is sensitive to pressure or particle velocity or a combination of both. A disadvantage is the limited frequency range where the calibration tube works well, a fully closed tube allows measurement down to 10 Hz or even lower but above the 'cut off' frequency the equation (2.1) is not applicable anymore. This cutoff frequency is for a round tube $f_c = \frac{c}{1.71 \cdot d}$, with d the diameter of the tube. For the tube used the cutoff frequency is around 5 kHz.

Measurement of the noise level

The noise level of the sensor is measured with the same pre-amplification as used with the sensitivity measurement, but now in the absence of sound. This results in a signal that is generated by the element only and is the noise level. The signal is easily disturbed by electrical interference, noisy power supplies and acoustic disturbances resulting in an apparent higher noise level. Minimizing these disturbances is compulsory for a good measurement result.

2.3 Design considerations

In the process of designing a new type of sensor it is beneficial to investigate how existing elements operate, and how this operation can be improved. So from the results obtained through research on existing elements a better sensor can be designed. In the following part some problems are discussed and a solution is presented, together with an experiment revealing the maximum operating temperature of an element fabricated with the standard fabrication process.

2.3.1 Sensor failure

Sensor failure is mostly due to a mechanical origin, such as the touching of the sensor wires by (human) hairs or tools. Dropping the sensor or subjecting it to high gravitational forces generally does not result in damage (a sensor of size 5 * 7 mm can even be lifted by its own sensor wires). Pressurized air often used for cleaning devices is not recommended because it easily damages the wires. Submersion into a liquid such as water or ethanol does not result in damage when the sensor is not powered. The lifetime of a sensor at

normal use is only due to degradation of the sensing layer, but at the recommended power level this is in the order of years according to long term experiments [10].

Exceeding recommended power levels results in accelerated platinum degradation. The degradation of the wires is not due to atom migration caused by high electrical current, since the current needed for this transport phenomenon is orders of magnitude higher than needed for in-air operation of the sensor. Thermal degradation of the sensing layer is more plausible, at 600 degrees centigrade the platinum layer already begins to form island like structures [46]. At places where this has happened the electrical resistance does increase thereby increasing local power dissipation and therefore the local temperature will become even higher. This process continues until the so called 'hot spot' burns out and leaves an open circuit connection. When observed under a microscope there not always seem to be damage, because the silicon nitride support still remains in most cases. Closer observation reveals that halfway the length of the wire the structure of the platinum is dull and a small spot is visible at the place of the disconnection. Exceeding the maximum power level results in sensor damage. The maximum power level is here defined as the power level where the sensor continues operating for at least hours.

2.3.2 Decrease of performance due to wrong cutting of chips

With the testing of some elements a different type of noise is observed, resembling flicker noise. The noise exhibits itself as a 'rumbling, clicking and popping' type of noise. At higher applied voltages to the sensor element the noise level increases very fast. For some cases the noise level is so high that the element cannot be used anymore.

When sawing through the silicon and the metal connection pads the sensor often generates more noise than a well sawn sensor. This noise is of a 'rumbling and clicking' type. The only possible explanation for this effect is that the dicing process creates an electrical conducting path over the insulator material over short distances. Imagine a conducting piece of silicon with on top a layer of 200 nm silicon nitride. On top of that a metal layer of chromium and platinum is deposited. When sawing through these layers into the silicon a conducting path is created between the shattered and smeared out metal layer and the silicon substrate. When a current passes through this conducting path to the silicon bulk and again to an output connection this has an effect on the output voltage. When this current is not constant this manifests itself as an added signal in the form of noise. The connection between the silicon and metal layer is far from perfect resulting in a varying current.

A solution to the problem is to avoid sawing through the metal layer. When using break out structures etched in potassium hydroxide, as discussed in 5, the problem does not occur.

2.3.3 Mechanical resonances

Measurement of the frequency response of various sensor structures and at various operating powers has revealed that mechanical resonances can occur. In the frequency response

this becomes visible as a dip in the response at a certain frequency. At low heating powers up to about 10 mW this dip does not appear. That is, it is not visible in the measured frequency range from 0 to 20 kHz but it may of course be present at a higher frequency. At higher power levels the effect can be very noticeable. The frequency of resonance is not the same for every sensor and mounting the sensor also affects the resonance frequency.

The fact that the origin of the dip is a mechanical resonance was confirmed by changing the tension in the sensor wires while measuring the frequency response. As illustrated by Figure 2.2c the tension in the wires can be reduced by slightly bending the sensor chip. In that case, the dip moves to a lower frequency. Bending the other way, i.e. increasing the tension in the wires moves the dip to a higher frequency and out of the measurement range. Of course, the tension of the wires is also influenced by the heating power, which explains why the dip only appears at higher power levels. As a very rough approximation, one could say that the heated wire will expand and thus the tension will decrease with the heating power. As a result, the resonance frequency shifts to lower frequencies with higher applied power, which has been confirmed by measurements (see Figure 2.3). In practice, the wire not simply expands, but there are deformations due to temperature gradients and bi-morph effects as well. Observing the heated wire under a microscope confirms that the wire deforms due to the heating: the center of the wire moves downward by a couple of micrometers when the power is switched on (see Figure 2.2b).

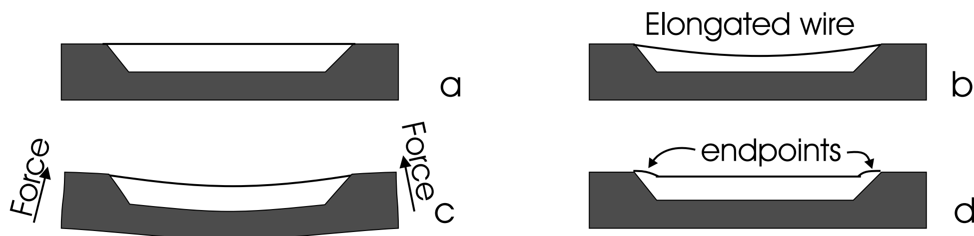

Figure 2.2: *The effect of high wire temperature and mechanical stress on the tension of the wires. The effects are depicted exaggerated.*

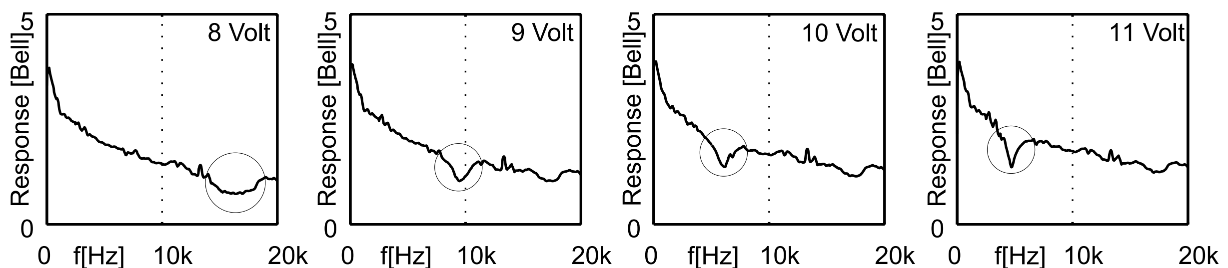

Figure 2.3: *Shift of the resonance frequency due to the increased power level. The dip is pointed out with a circle and observed in the graph as a dip in the frequency response, at high power level the frequency where this occurs is lower.*

Exact modeling of all effects is difficult and not very useful because of the many parameters that are involved. Some of these parameters are well understood and can be

controlled within certain limits like the stress in the silicon nitride and platinum layers. However, other parameters like the type of glue that is used for mounting the chip in a package and the exact mounting procedure have a large influence but are difficult to control. Therefore, a solution was sought that would eliminate the resonance by ensuring sufficient tensile strain in the wires under all circumstances. A practical solution was found by exploiting the difference in stress between the silicon nitride and platinum layers. Sensor wires have the tendency to curl downwards, which is easily seen when they break. The effect can also be seen in Figure 2.4: clearly the edges of the square piece are bent downwards. By broadening the ends of the wire we can use this effect: the broadened ends tend to deflect and in this way the wire is kept under tension, even when it elongates due to elevated temperatures or when the substrate is deformed slightly due to packaging.

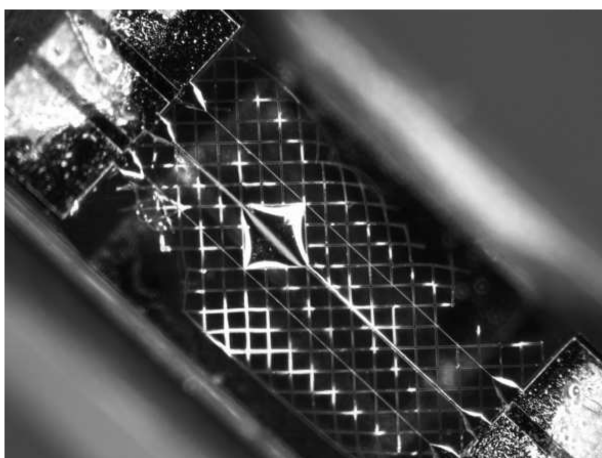

Figure 2.4: *A small square piece of siliconnitride and Cr/Pt on top tends to bend inwards. Broader wire endpoints act as springs to keep the sensor wires stretched.*

Figure 2.4 clearly shows the triangular-shaped broadened ends of the wires. In designs containing such wire ends the mechanical resonances have not been observed. Inspection under a microscope showed that the end points bend downward but the wire itself remains straight and under tension as indicated in Figure 2.2d. Measurement of the frequency response at high power levels and relatively large bending forces on the chip did not result in reappearance of the dip, so the solution seems to be very effective.

2.3.4 Maximum permissible operating temperature

An important class of applications such as measurement close to or inside combustion engines involves operation at several hundreds degrees centigrade. Therefore, some tests were performed to investigate the performance of a particle velocity sensor element at high temperatures.

The wires of an operating particle velocity sensor element can sustain temperatures well above 400 ^{o}C as tested in experiments and also in [45]. At these high temperatures degradation of the sensor wires occurs more quickly, reducing the lifetime of the sensor. When operating not only the sensor wires but the whole sensor in a high temperature environment places extra demands on the silicon bulk material and mounting of the element.

The electrical insulation of the silicon nitride layer decreases at higher temperatures.

Normally the sensor wires are insulated from the silicon bulk by a layer of 200 nm silicon nitride. At higher temperatures than 300 degrees centigrade the insulation diminishes and a current will flow [47], which fluctuates and results in an increased noise.

Test setup

A test setup was realized that allows measurement of the leakage current through the silicon nitride layer as a function of temperature. The sensor chips need to be mounted on a carrier which can withstand high temperatures. In this case a ceramic printed circuit board of aluminum-oxide with silver wiring was used. First the sensor is glued to the carrier board and wire bonded. When heated, the glue will evaporate and to assure that the sensor will remain in place additional ceramic glue is applied on the chip. Connections from the carrier substrate to the measurement unit outside the high temperature environment are made with tin plated copper wires. The wires are fixed to the board with ceramic glue and welded to the silver patterns. This welding is done by forcing a large current during a short time through the wire and pattern while keeping the wire fixed on the silver pattern. A good electrical but mechanically very weak contact is made, therefore additional high temperature resistant ceramic cement is used. Figure 2.5a shows a photograph of a sensor element mounted on the ceramic printed circuit board.

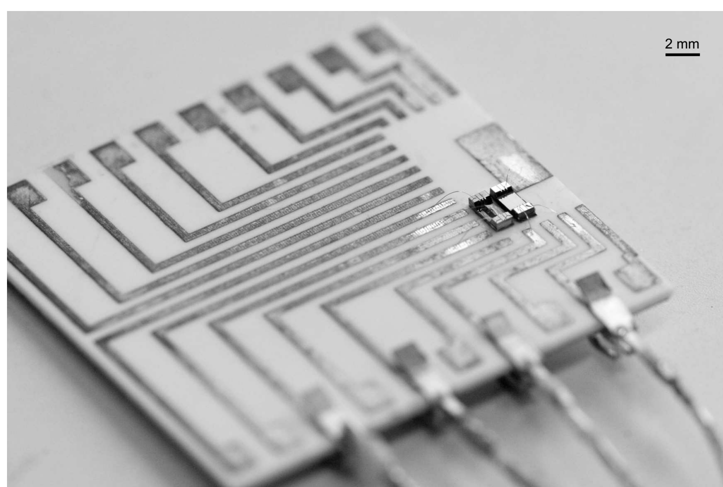

(a) Photograph of the mounted sensor.

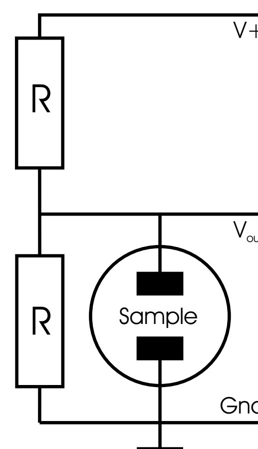

(b) Equivalent electrical circuit of the measurement setup.

Figure 2.5

Results

A measurement with a standard particle velocity element without sensor wires was performed so that only the effect of leakage through the silicon nitride layer was measured. The sensor wires are replaced by standard metal film resistors. The equivalent electrical

schematic is shown in Figure 2.5b. Without leakage, the output voltage is equal to half the supply voltage.

At room temperature the noise level was as expected equal to the output noise of the used amplifier and the noise of the resistors. Next, the printed circuit board was heated on a hotplate up to a maximum of 450 ^{o}C. Roughly beyond 300 ^{o}C the silicon nitride layer starts to conduct, which is in agreement with the experimental results presented in [47].

At even higher temperatures a fluctuating current with spurious peaks starts to flow through the silicon nitride, see Figure 2.6 for a detailed plot of the measured output voltage and leakage current. After lowering the temperature the leakage current disappears again. Contrary to the results shown in [47] there is no short circuit after cooling, probably because of the limited amount of current during break through.

Another chip was tested with between the silicon nitride and the silicon bulk an additional 900 nm thick layer of thermally grown wet silicon oxide. Wet silicon oxide is made by oxidizing silicon in an environment with water (in gas phase) present. No significant difference was found between both types of chips regarding breakthrough. Around 350 ^{o}C both types of sensors experience electrical breakdown. As observed in [47], wet oxide is not a good insulator material above 300 ^{o}C.

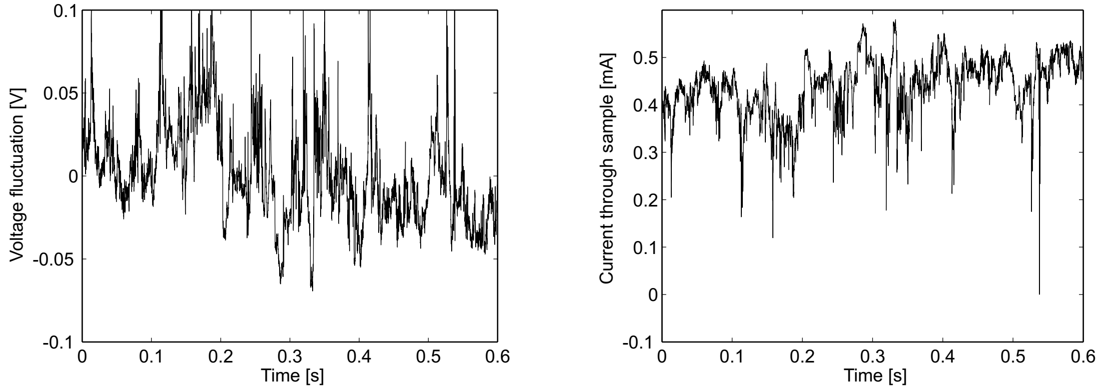

(a) Signal due to silicon nitride breakthrough at 450 degrees centigrade.

(b) Current through the silicon nitride layer at 450 degrees centigrade.

Figure 2.6: *Current and output voltage of the element subjected to a temperature of 450 degrees Centigrade.*

2.4 Self noise of two and three wire sensors

2.4.1 Introduction

As mentioned before the self noise of a sensor is an important property. In the following measurements of the self noise of two and three wire sensors with varying wire separation

distance are presented. The results are used for design optimization of the integrated three dimensional sound intensity probe.

For the sensor as used in the experiments a number of parameters are fixed. Sensor wire thickness is defined as the silicon nitride construction layer of 220 nm thickness and a platinum sensing layer of 150 nm. Sensor thickness contributes to the electrical resistance in a direct way: double platinum layer thickness results in an approximately twice as low wire resistance but also in an increased thermal mass. The thermal mass influences the high frequency response of the sensor, since this influences the speed of temperature change. Sensor wire width is for all sensors set to 2 μm. See also Figure 1.1 for a photograph of the sensor.

A more important limiting factor in terms of high frequency response is the heat diffusion in air, the response is largely influenced by the wire separation distance [37].

2.4.2 Measurement setup

The particle velocity sensor must operate with power applied, and the amount of power influences both sensitivity and the noise level. Resulting from these two quantities the self noise can be calculated and the self noise level at a certain power level is found. Two wire sensors as well as three wire sensors are discussed and the optimum power to the sensor and heater wires is measured. The experiment was performed for two and three wire sensors with several different wire distances. A standing wave tube was used as a calibration setup and calibration measurements at multiple power levels were performed.

The sensors were placed in a standing wave tube of 5 cm * 5 cm * 30 cm (w*h*l) at a distance of approximately 6 cm from the reference pressure microphone. On the other end a small loudspeaker generating white noise was placed. The transfer function between the particle velocity sensor and the pressure sensor is measured. At the point of the particle velocity sensor at a distance l from the pressure microphone the particle velocity signal at place l from the pressure sensitive device is equal to $p\frac{i}{\rho c} \cdot sin(kl)$ [41] with k the wavenumber, defined as $k = \omega/c$. From the imaginary unit number $i = \sqrt{-1}$ it is seen that the particle velocity signal has always 90 degrees phase difference compared with the reference sound pressure signal. Dividing the measurement result by the transfer function of the tube results in the sensitivity characteristic of the sensor. For increasing power levels the sensitivity was measured. Just after measuring the sensitivity, the noise level of the sensor was measured.

The use of a standing wave tube can deliver erratic results when used at frequencies above its cut off frequency. At these frequencies the standing waves do not travel solely in the length axis of the tube. This cut off frequency for a tube with rectangular cross section is equal to $c/2d$ with d the length of a side [48]. For this tube the cut off frequency is 4 kHz, nevertheless for frequencies up to 7 kHz the result measured matches well with other calibration techniques.

The noise level was measured in the same standing wave tube without loudspeaker excitation and in a quiet environment. The power spectral density of the sensor signal was measured. This is directly the (electrical) noise level generated by the sensor. This noise level has a very small amplitude, too small to be measured directly with an analyzer. A low noise amplifier is used to increase the signal level to a more convenient level for the analyzer system. The amplifier must add as little noise as possible to the signal not to affect the measurements. Without any power to the sensor wires (with a typical resistance of 1..2 kΩ) the thermal noise floor is still present. When the particle velocity element is powered this noise level is higher. For a 1 kΩ resistor this noise level is equal to 4 nV/$\sqrt{Hz}$ or -168 dBV. With the amplifier used for both the noise measurements and the sensitivity measurements (amplification 40 dB) the measured noise level was nearly -168 dBV. Therefore the amplifier was considered to have a low enough noise floor for the reliable noise measurement of the sensors.

From the obtained measurement results of the sensitivity and noise level the self noise is calculated for the given power levels. For a reliable result an automated measurement setup is used and the sensor voltages and heater voltages are controlled by the same computer that controls the signal analyzer.

The sensors to be measured were connected with glue to a small substrate and wire bonded. No glue was used to protect the wire bonds and no further packaging. From previous experimental results the maximum allowable power level for a number of sensors is determined. The power level in the experiments is kept just below that value. Before starting the measurement the sensors were operated at a moderate power level of approx 30 mW to 'burn in'. No sensors showed malfunction or noticeable degradation for measurement times at least up to 4 hours at the maximum power level.

2.4.3 Two wire sensor self noise

Sensitivity of the sensors

In Figure 2.7 the result of measurements of the sensitivity level of a two wire sensor with wire spacing of 300 μm is shown. Clearly the sensitivity increases with increased applied power and seems to reach to a maximum around 50 mW. This is due to the logarithmic scale of the graph, sensitivity increases here almost linearly with applied power. Still a logarithmic scale is preferred to be able to observe the frequency response more clearly. The response at 94 dB Particle Velocity Level (PVL), which is equal to 2.4 mm/s, is given in dBV.

For low power levels the response at higher frequencies cannot be measured well because the noise level of the sensor is too high compared to the signal level. Furthermore at 3.3 kHz the actual particle velocity level at the place of the sensor is very low due to the standing wave pattern in the tube; at this frequency $1/sin(kl)$ equals zero. The frequency characteristic may be interpolated with a straight line here.

A dip in the frequency response of the sensor at higher power levels and between 4

and 5.5 kHz is not an artifact of the standing wave tube but the so called 'resonance' effect. This effect is due to movement of sensor wires thereby lowering the sensitivity at that frequency, discussed in the section 2.3.3.

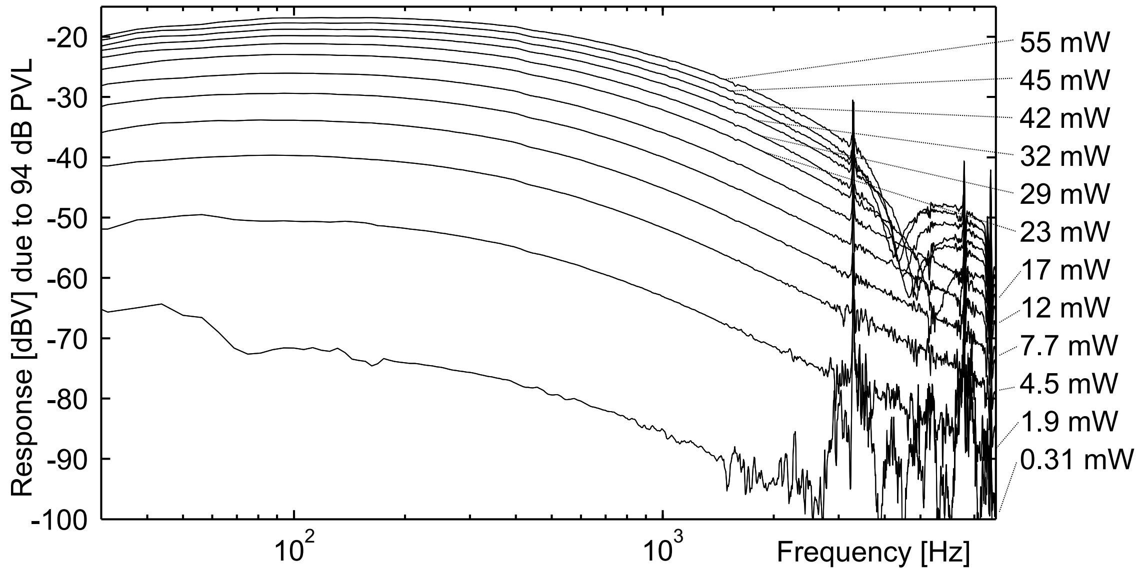

Figure 2.7: *Sensitivity for 2.4 mm/s at different power levels. The amplification is 40 dB.*

Noise level

The noise level of the sensor with 300 μm wire spacing has been measured. The results are shown in figure 2.8a. Without power applied there still is the thermal noise from the electrical resistance of the wires. This noise is measured and equals $\sqrt{4KTRB_w}$. The measured noise is almost independent of frequency. At higher power 1/f noise becomes dominant quickly. At low frequencies and low power peaks can be seen in the figure. These peaks are at multiples of 50 Hz and are due to the mains power grid which operates at 50 Hz.

When looking at the noise level at a number of fixed frequencies and plotting the noise level as a function of power to the sensor Figure 2.8b is obtained, which shows that the noise level increases almost linearly with the power squared. This is found to be valid over a broad frequency range.

Self noise levels

Dividing the noise level by the measured sensitivity for 94 dB PVL results in the self noise in dB with reference 2.4 mm/s (which is the particle velocity level at 94 dB). Preferably the threshold of hearing is used as reference, so 94 dB must be added to the result.

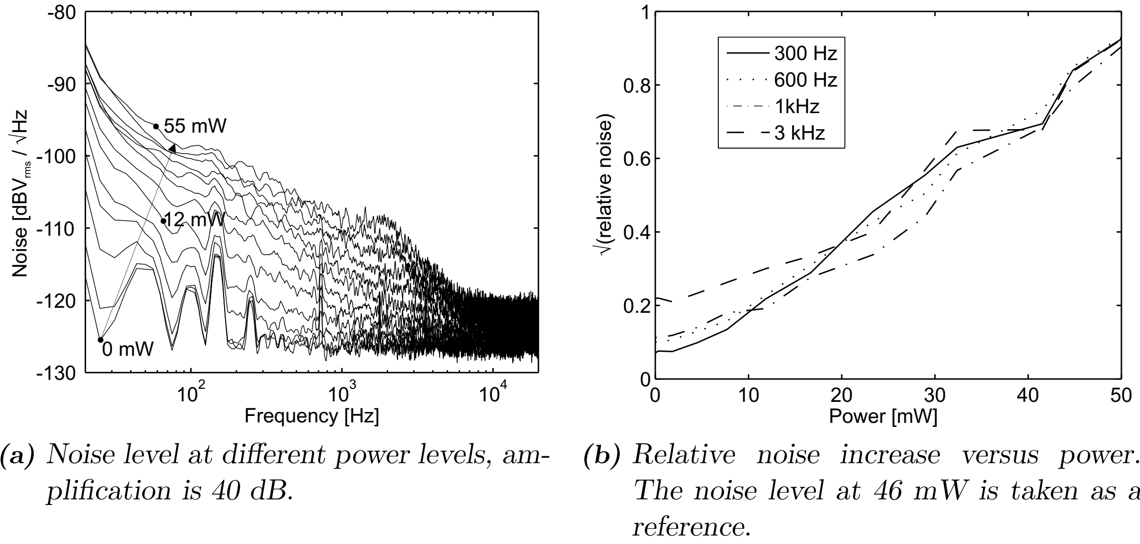

(a) Noise level at different power levels, amplification is 40 dB.

(b) Relative noise increase versus power. The noise level at 46 mW is taken as a reference.

Figure 2.8: *Noise level versus power dissipated in the wires.*

Since sensitivity is found to increase roughly linearly with dissipated power and noise increases with the power squared, there must be an optimum power at which the self noise is minimum. It is seen from figure 2.9 that the self noise decreases with increasing power but above 30 mW the self noise does not decrease any further. There is indeed an optimum power where the sensor works best.

Plotting the self noise versus power at a number of frequencies the results shown in figure 2.10 are obtained. At low power the self noise decreases fast with power increase but at higher power levels than 40 mW the self noise starts to increase again. An optimum power level is found at 30 to 40 mW. Power levels above 50 mW have a negative effect on the lifetime of the sensor, which is then decreasing rapidly to hours and shorter.

For two wire sensor elements with different sensor wire separation distances the measurements have been repeated. Wire distance was varied between 150 to 600 μm. The results from every sensor with the lowest self noise at a certain power are plotted in Figure 2.11. From this result it is clear that a wire separation distance of 150 μm exhibits the lowest self noise of the measured sensors, especially for frequencies above 1 kHz. From the graph a sort of 'corner frequency' can be observed, below this frequency the wire separation distance is less important for the optimum self noise. For a sensor with wire separation distance of 300 μm this 'corner frequency' is at 250 Hz. The closer the sensor wires the higher this corner frequency.

A short summary of the results on the optimum voltage and power of these sensors is given in table 2.1. Possibly a slightly lower self noise can be reached with an even smaller sensor wire separation.

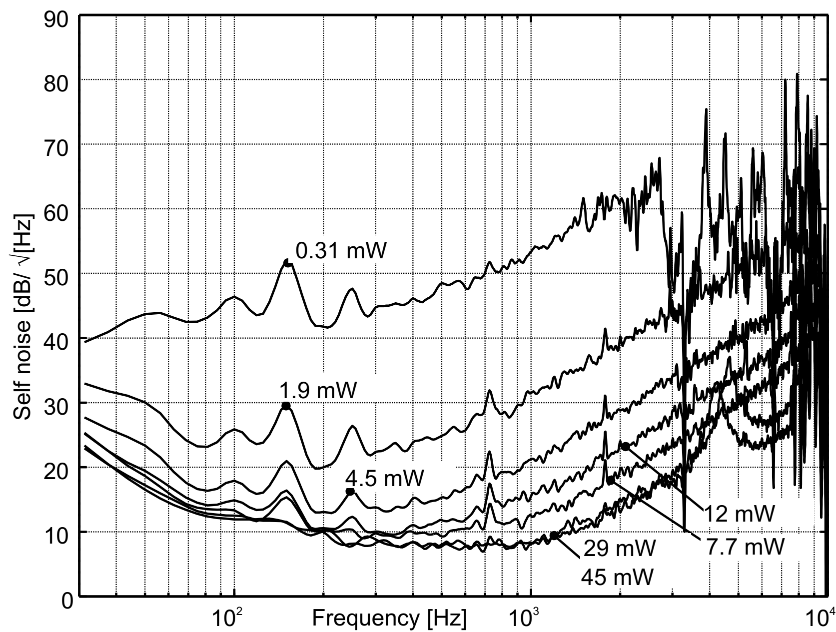

Figure 2.9: *Self noise at different power levels. Increasing the power above 30 mW does not decrease the self noise.*

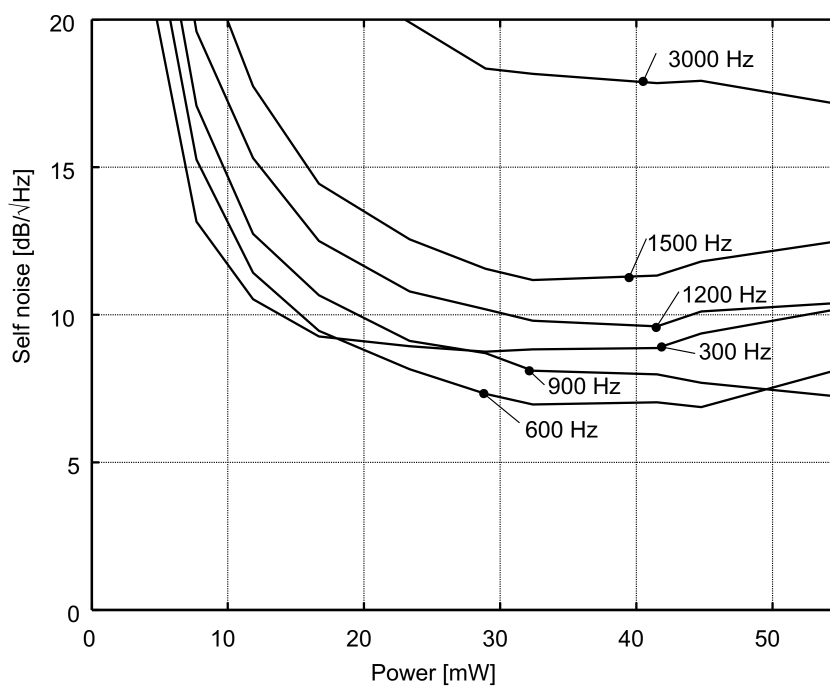

Figure 2.10: *Self noise as function of power dissipation in the sensor wires.*

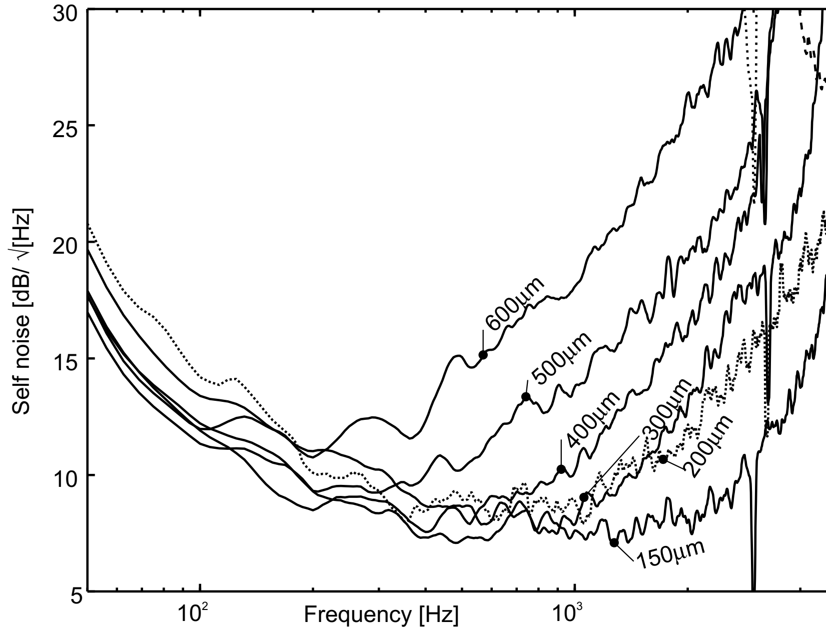

Figure 2.11: *Optimum self noise for two wire elements, with wire separation distance ranging from 150 μm to 600 μm.*

Table 2.1: *Optimum values for different two-wire sensor geometries*

Sensor wire spacing [m]	$\mathbf{V}_{sensor}$ **[V]**	$\mathbf{P}_{sensor}$ **[mW]**
150 μ	9	25
200 μ	7	15
300 μ	10	32
400 μ	11	36
500 μ	9	30
600 μ	9	30

2.4.4 Three wire sensor self noise

In the case of a three wire sensor a heater between the two sensor wires is incorporated. The heat generated by this wire results in a different shaped heat profile around the wires, due to this the sensitivity changes. For the three wire sensor types the heater is of the same length and thickness as the sensor wires, but the width is 10 μm. The three wire sensors seem to have a lower self noise than two wire sensors, especially at higher frequencies. This performance is dependent on parameters such as the wire distance and power to the wires [37].

Various sensors with sensor wire separation distances of 75, 100, 150, 250, and 300 μm are investigated, with a heater wire between the sensor wires. The design of the three wire sensor is similar to the two wire sensor designs, that is the sensor wires are placed on to a

silicon substrate which is etched away leaving the sensor wires free hanging. Wire length is 1.5 mm, the thickness of the wire is around 300 nm and sensor wire width is 2 μm. This results in a sensor wire resistance of about 1 to 2 kΩ per sensor wire. The heater wire is of the same length and thickness, but is 10 μm meter in width. The resistance of the heater wire is between 200 and 400 Ω. Experiments with a sensor wire width of 1 μm and sensor wire separation distance of 300 μm have been added to investigate whether a small wire has advantages over normal sensor width. The yield of working sensors is estimated to be 50% instead of the regular yield of about 95% (estimated before dicing chips from the wafer).

Measuring the sensitivity characteristic of the three wire sensor is done similar to the experiments with the two wire sensor, except for the fact that the three wire sensor has an additional connection, namely for the heater. This heater can have a different applied power than the sensor wire pair. Power to and temperature of the heater wire are linked and therefore of influence on the performance of the sensor.

Measurement results with a 250 μm sensor wire distance

Measurement results of the sensitivity and noise at different power levels are converted to self noise. For a sensor with 250 μm sensor wire separation distance and a heater the self noise as function of frequency at different power levels is plotted in Figure 2.12.

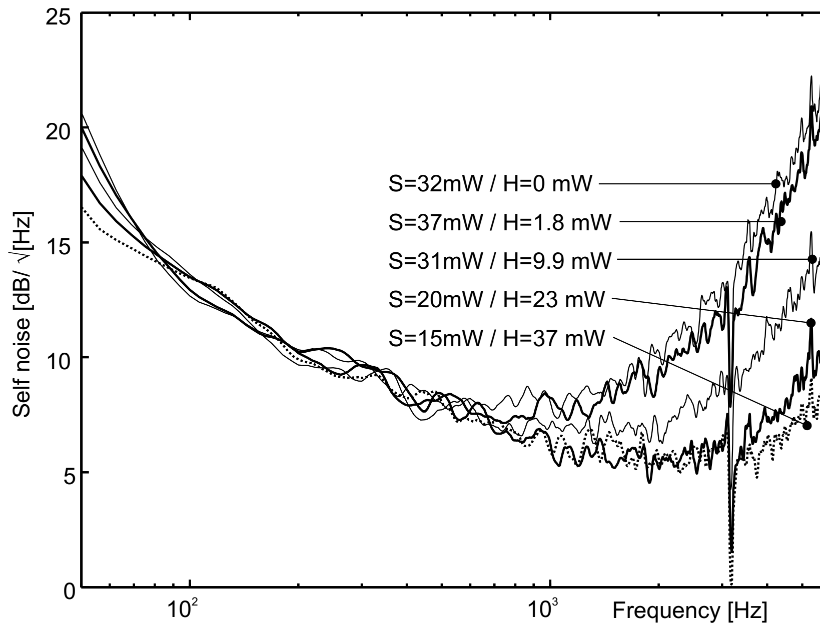

Figure 2.12: *Self noise as function of heater and sensor power for three wire sensors with spacing 250 μm.*

Similar to the two wire sensor experiment the optimum power dissipation in the sensor

wires is determined but now the power in the heater wire also affects the self noise. For five steps of different heater powers this optimum self noise of the sensor is determined. It is observed that especially at frequencies above 1 kHz the effect of the heater power is of importance on the self noise. Furthermore the optimum power to the sensor wires decreases with increasing heater power. Since the heater is thermally coupled with the sensor wires by the surrounding air the temperature of the sensor wires is affected by the heater power.

For high heater power (higher than displayed here) the heater malfunctions after a few hours. At the displayed power (that is below 40 mW) the sensor continues to operate without noticeable degradation for at least 2 hours.

Comparison between sensors with other wire distances

Repeating the experiment with other sensors having different sensor wire distances similar graphs are obtained. From these graphs a 'best value' can be found for every heater value. In figure 2.13 for every type of sensor the effect of the heater power on the optimum self noise can be seen.

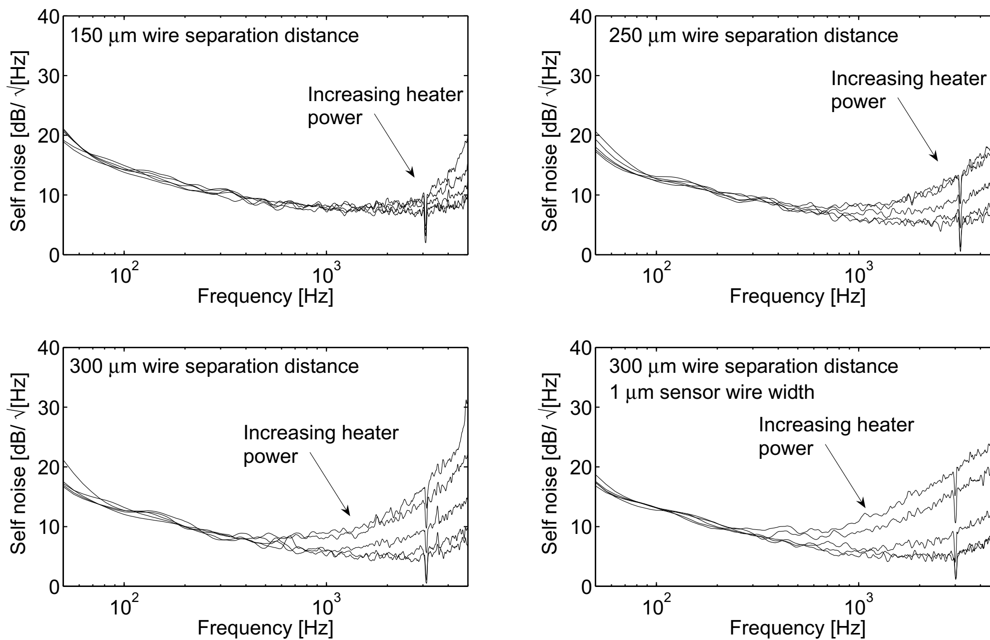

Figure 2.13: *Self noise for different 3-wire sensors as a function of heater power.*

With increasing distance between the wires the effect of the heater on the self noise becomes more pronounced, the self noise lowers rapidly with increased heater power, especially at frequencies above 1 kHz. Sensors with large wire separation distance perform less good at low heater powers compared with sensors with small wire separation distance at low heater powers. At high heater power this is reversed; the sensors with larger (up to

300 μm) wire separation distances perform much better than the ones with shorter wire separation distances. With increasing power dissipation to the heater wire the optimum power dissipation in the sensor wires is lower.

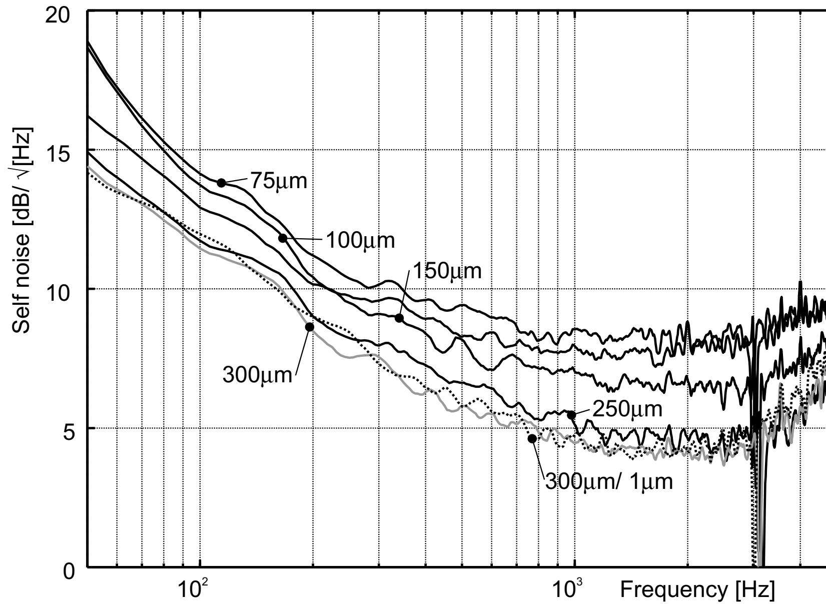

Figure 2.14: *Optimum self noise for different 3 wire sensors.*

Measurement results of a sensor with smaller sensor wires

In the graph shown in Figure 2.14 the measurement results of an another sensor with a 300 μm sensor wire separation distance is shown. This sensor has a sensor wire width of 1 μm instead of the regular 2 μm. At high heater power the performance is similar to the same sensor with 2 μm wires, at lower heater power levels the 1 μm sensor has a worse self noise. Regarding power consumption the sensor with 1 μm wire width seems to be a slightly better choice, but fabrication is more delicate and fabrication yield is much lower.

Due to the lower thermal mass of the sensor wires the low pass behavior due to the thermal mass must be shifted to higher frequencies. Since the effect of this behavior was already around 10 kHz for 2 μm wires, for this sensor this must be even higher. Due to the limited bandwidth of the measurement setup this is not observed. The power dissipation is lower however.

The optimum sensor operating at optimum power

In figure 2.14 a comparison between the optimum self noise of all sensors is given. From this it is observed that sensors with the sensor-heater-sensor configuration with sensor to

sensor distance of 300 um perform best. From the relative decrease in self noise between the smaller distances (75 to 250 μm) and the difference between 250 and 300 μm it is concluded that the optimum wire distance for the sensor-heater-sensor configuration is 300 μm but possibly slightly higher.

It is observed that the optimum value for the heater power is reached at the highest power levels, but with higher power levels the self noise does not decrease substantially anymore. Since at high power heater wire failure is common the power level just below the maximum measured here will still gives a satisfactory performance and a good lifetime.

A survey of the optimum sensor and heater power levels for the sensors which are investigated is given in Table 2.2.

Table 2.2: *Optimum levels for different three wire sensor geometries*

Sensor wire spacing [m]	$\mathbf{V}_{sensor}$ **[V]**	$\mathbf{P}_{sensor}$ **[mW]**	$\mathbf{P}_{heater}$ **[mW]**
75 μ	10	35	30
100 μ	7	25	30
150 μ	7	15	35
250 μ	8	15	35
300 μ	7	15	35
300 μ (1μ wide)	7	10	35

2.5 Conclusions

Sensor performance has been investigated and more insight in the particle velocity sensor gained. The required power is not a very important issue for the use of the sensor in a measurement setup. A solution to a wire resonance phenomenon is found and a design rule is derived. For temperatures below 300 ^{o}C the insulating properties of the silicon nitride insulation layer has been found to be good enough for operation of a particle velocity sensor. Dicing through a metal layer on silicon bulk material with silicon nitride in between can result in a conduction path between neighboring metal layers through the bulk material.

Altogether a power level of 30 to 40 mW is found to be a good choice for two wire particle velocity sensors, almost independent of sensor geometry, more power not necessarily contributes to more sensitivity but certainly to a shorter lifetime. Some sensors have a small decrease of self noise with increasing power level above 40 mW but this is not more than 1 dB and depends on the measured frequency. Two wire sensors with wire separation distance of 150 μm exhibit the lowest self noise regarding the high frequency response, for low frequency response the sensor with the larger separation distance of 500 μm is preferred. The elements survived at the highest measured powers for at least four hours. At the optimum power the sensor lifetime is expected to be much longer.

For three wire particle velocity sensors operating at their optimum heater and sensor power the sensor with a wire separation distance of 300 μm has the lowest self noise and is therefore the best configuration. Wire separation has the most pronounced effect at frequencies above 1 kHz, for lower frequencies the distance is of less effect on the self noise. The optimum heater power is around 30 mW, which is close to the maximum power this wire can sustain for a longer time without deteriorating. Furthermore the optimum self noise is reached at a sensor power between 15 and 35 mW.

For frequencies below 1 kHz both types of sensors show similar performance with respect to self noise but two wire sensors have a lower power consumption. For higher frequencies the three wire sensors have a lower self noise. A sensor with sensor wire distance of 150 μm exhibited the lowest self noise, with the possibility that a shorter distance can exhibit an even lower self noise.

Chapter 3

Three dimensional particle velocity sensor development

3.1 Introduction to 3D sensors

Sound fields consist of sound waves traveling in all directions, dependent on the shape and place of sound sources and reflections on other objects. Measurements with a one dimensional sound probe will suffice when the geometry of the sound field is known or when the sound field is fully stationary. In practical acoustical situations, this is often not the case. When the sound field is stationary and a one dimensional sound intensity probe is used the direction of the sound intensity can be found by rotating the probe until a maximum is detected, and the magnitude in this direction can be measured. Obviously, this is a time consuming task. For non-stationary sound fields this method is impossible and a three-dimensional sound probe must be used to measure the sound field.

A three-dimensional sound probe has been made with the P-P method and with particle velocity sensors combined with a sound pressure sensor. An early realization of such a probe is similar to the three-dimensional P-P probe described in chapter 1. In Figure 3.1a the mounting of three particle velocity probes and a sound pressure microphone fixed in a steel mounting frame is shown. The assembly proved to be successfully usable as shown in [49] and [50] and [51].

This sensor-assembly only differs from the 3D P-P probe because it measures particle velocity directly, the large size of approx 20 * 20 * 4 cm makes it look similar to a P-P probe. For measurements on small sound sources, in confined spaces or for non-intrusive measurements, size is of concern. Since the actual particle velocity sensor element is very small, a logical step in the development process of a new sound probe is to integrate the particle velocity sensors into a smaller housing. A design where this is done is shown in Figure 3.1b. Around a small sound pressure microphone inside a metal frame, three particle velocity sensors are placed. The particle velocity sensors are aimed at mutually perpendicular directions. A similar probe is used in [52]. With the small sizes of the elements combined with manual alignment, a misplacement of several degrees is easily possible. Furthermore every sensor is manually equipped with a small protection cap,

whose placement too is of influence on the response and size of the sensor.

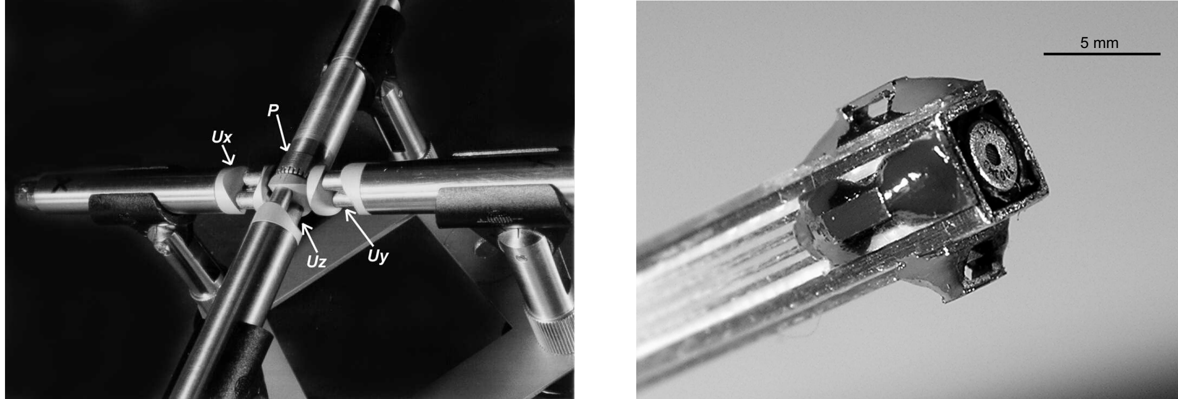

(a) A combined three-dimensional sound probe.(Photo taken from [49].) *(b) A small three-dimensional sound probe.*

Figure 3.1: *three-dimensional sound probes.*

The advantage of integrating a three-dimensional particle velocity probe in one piece of silicon is therefore obvious. The sensor placement can be very precisely controlled, since the sensor wires are positioned by photolithography. A misalignment is maximally in the order of some micrometers instead of tenths of millimeters when mounted by hand. In case an integrated element is used, the mounting on a carrier board must be done only once and there is only one board that has to be mounted in a probe (instead of three and a sound pressure microphone). A disadvantage of using a completely integrated sensor is that the yield of good sensors drops. When one sensor in the multiple-sensor-chip is defective, the whole chip is useless.

A three-dimensional particle velocity sensor integrated on one chip has been developed before, see [53]. The sensor was made using a double side polished silicon wafer with two particle velocity sensors in the silicon wafer plane with the directions of sensitivity orthogonal. Another sensor was aimed with its sensitivity direction 'through the wafer'. Here one sensor wire is on the top side of the wafer and one on the bottom, forming one sensor pair. For an impression of this sensor see figure 3.2, the photo is taken from [53]. The wafer used for this sensor had a thickness of 0.3 mm. The self noise of this sensor was not very good, but this could have been caused by the solder process used as described in section 5.3.2. Further research of this sensor was not carried out.

3.2 3D design on one chip

In chapter two, the differences between two- and three-wire sensors were investigated. From this, it became clear that the three-wire design is preferable when it comes to self noise at frequencies above 1 kHz. Apart from the self noise, the feasibility of the fabrication is certainly of importance for a good design.

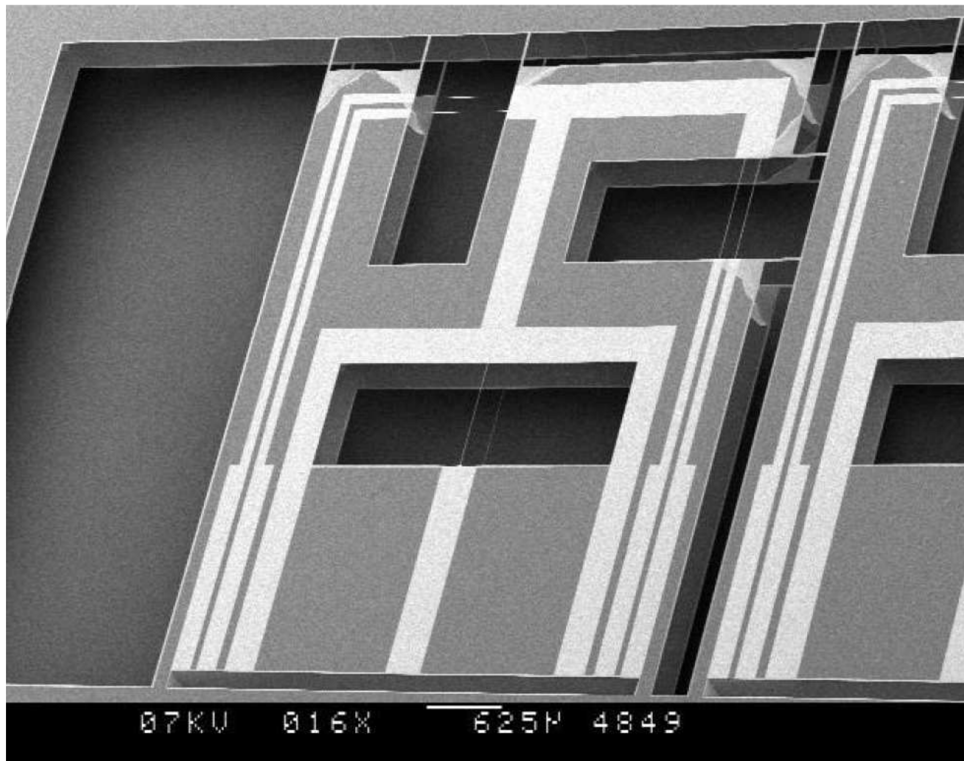

Figure 3.2: *A three-dimensional particle velocity sensor in one chip. (Photograph taken from [53]).*

For a two-wire design a double sided wafer process can be used. A way of fabricating a particle velocity sensor is to place sensor wires on both sides of a silicon wafer. When the silicon between the sensor wires is etched away, an out-of-plane sensor is obtained. This type of design is by far the most straightforward one and has a high possibility of succeeding. Some possibilities of combining two-wire sensors in one chip are listed below.

- Three sensors in one chip: one sensor with its two sensor wires in plane and one sensor with wires on both sides of the wafer. Trough the wafer sensors can have dissimilar wires compared with other sensors, since this wire is made separately from the other wires (at least not at the same time). This can lead to different sensor performance within the same chip. A design such as this is shown in Figure 3.2. Schematically the design comes down to a combination of the sensor orientation as shown in Figure 3.3a.

- Three sensors in one chip: sensors with a sensor wire on the upper side of the wafer and one on the bottom side as shown in Figure 3.3b.All sensors are identical, they only differ in rotation.

- Four sensors in one chip: two pairs of sensors with sensitivity perpendicular to each other and pointed 45 degrees out of plane, and another pair of sensors rotated 90 degrees in the plane. A schematic drawing of this orientation is given in Figure 3.3c. All four sensors are identical having only a difference in orientation. An

advantage of the four-sensor type is that for every direction of particle velocity there are at least two sensors picking up a signal, so cross correlating two sensor signals is possible for every direction of incidence. This is explained in more depth in section 3.3. When cross-correlating signals is not required simply one channel can be omitted or four channels can be (electronically) combined to three channels, saving one analyzer-input channel.

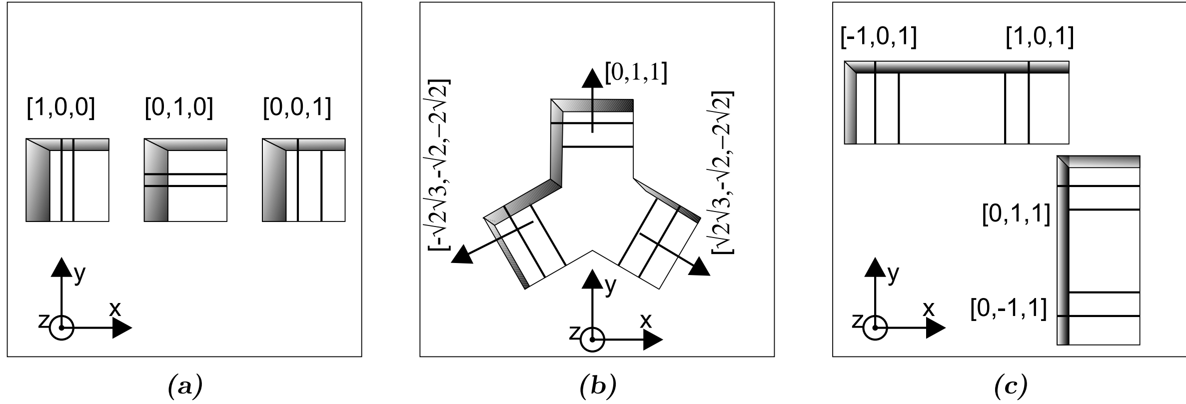

Figure 3.3: *Sensor orientation possibilities for a two-wire design. The sensor wires are the black lines in the figure.*

Three-wire sensors are favorite because of their good (high frequency) performance. Therefore a possible three-wire design is to be taken into account. The sensitivity directions of the sensors can be similar to the directions for the two-wire sensors. The fabrication of an out-of-plane three-wire design is not straightforward. Some options for fabricating a three-wire sensor are described hereafter.

- The first method is patterning a wafer such that halfway the wafer a heater wire is placed. While patterning a wire on both the top and bottom is relatively simple, placing a wire halfway in a wafer is not. An idea is to start with a double side polished wafer and depositing and patterning wires on both sides. After patterning the wafer is etched to half its thickness and a central wire is made. The process is complex since after etching the silicon at least one vulnerable sensor wire is exposed. This makes handling difficult and the number of available processes very limited.

- A second method is to use a two wafer structure. The design can consist of one chip with a sensor wire on the bottom side and a heater wire on the top layer. Between the two wires, the silicon is etched away, leaving a hole through the wafer. Another chip with one sensor wire and a through-the-wafer hole can be mounted on top of the first chip. Schematically this is shown in Figure 3.4. A disadvantage is that the mounting precision of both wafers is of direct influence on the directivity of the sensor. When using alignment slits this mounting precision can be improved. For an optimal wire distance, thin wires must be used, but this process is promising.

From this it is concluded that the two-wire design has a high chance of succeeding with reasonable sensor performance. Secondly, the three-wire design has a lower self noise

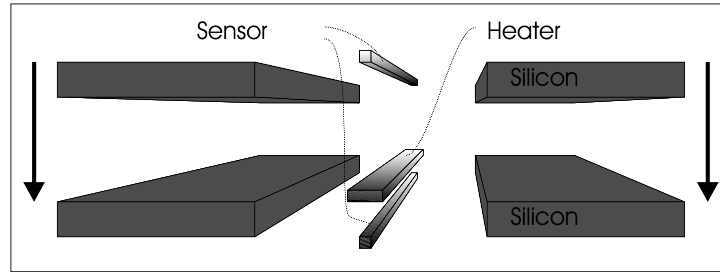

Figure 3.4: *A two wafer process for fabrication of a three-wire sensor.*

at higher frequencies but requires a fabrication process that is more complex than the two-wire design. A design based on the two-wire sensors can be adjusted to a three-wire design since the sensor orientation can be the same. A good choice seems to be to start with the development of a two-wire sensor. With the knowledge gained from this the design can be transferred to a three-wire design with better performance.

3.3 Sound source localization with a four particle velocity sensor device

In the next section experiments with four particle velocity sensors are presented. The three dimensional sound field is calculated from measurement data and the advantages of a cross correlation technique is demonstrated. The next section is a copy of a part of the article presented in the Journal of the Acoustic Society of America (JASA)[54], omitting some parts that are already discussed in this thesis separately. The part that is copied is designated with a line on the left side of the page.

Since particle velocity ($\boldsymbol{v}$) is a vector, while the sound pressure (p) is a scalar, more information about the sound field can be obtained when using a particle velocity sensor instead of a sound pressure sensor (microphone). Four particle velocity sensors are combined in to one (small) device. In a reverberant room the four auto-spectra and the six cross-spectra are determined. Interpretation of the measured results gives information of the free field (sound field without a contribution of reflections) as well as of the reverberant field.

3.3.1 One v-sensor

As a sensor for the particle velocity we used the "Microflown" [7]. This sensor consists basically of two thin wires, parallel to each other, which are heated up to about 200-300 ^oC by an electrical current. The temperature profile around the wires is influenced by the particle velocity of an acoustic disturbance, resulting in a small resistance change of the wires. In fact, the sensor detects the particle velocity component in a direction perpendicular to the length of the wires and in the plane of the wires. Define a unit vector $\boldsymbol{\mu}$, perpendicular to the length of the wires and in the plane of the wires, then the electrical signal of the sensor is proportional to the inner scalar product $\boldsymbol{\mu} \cdot \boldsymbol{v}$. In the

text throughout this paper we denote this unit vector as the sensitivity unit vector of the sensor. We often take the proportionality constant equal to one and write for the sensor signal s(t):$s(t) = \boldsymbol{\mu} \cdot \boldsymbol{v}(t)$. The directional characteristic of this v-sensor is independent of the frequency and follows from this relation as: $\boldsymbol{\mu} \cdot \boldsymbol{v} = |\boldsymbol{v}| \cdot cos(\alpha_{\boldsymbol{uv}})$, where $\alpha_{\boldsymbol{uv}}$ is the angle between $\boldsymbol{v}$ and $\boldsymbol{\mu}$. A detailed model is presented in [8].

Consider now the sensor signal. For stationary signals the rms value, or the auto spectrum, is measured, the latter being: $A = \frac{1}{T}\int_0^T s(t) \cdot s^*(t)dt$

Suppose a sound source is present at the origin of a Cartesian coordinate system emitting plane waves, propagating in the x-direction and a v-sensor is placed on the x-axis at a distance much larger than the wavelength and dimensions of the source (far field situation). When the sensitivity unit vector is along the x-axis, $\boldsymbol{\mu}$ =[1,0,0] the free field and a contribution of the reverberant field will be measured. If however, the sensor is rotated such that $\boldsymbol{\mu}$=[0,1,0] or $\boldsymbol{\mu}$=[0,0,1] no contribution of the free field will be measured and only (a part) of the reverberant field is detected. In a pure diffuse reverberant sound field, where the distances from the mirror sources to the sensor are much larger than the wavelength and much larger than the dimensions of the sources, the relation between the rms value of the sound pressure and particle velocity is given by: $v^2_{rev.} = p^2_{rev.}/(\rho c)^2$. In a purely diffuse reverberant sound field the three components v^2_x, v^2_y and v^2_z are equal thus $v^2_x = v^2_{rev}/3$ or $v^2_x = (1/3).p^2_{rev}/(\rho c)^2$; this relation will be discussed in more detail in section 3.3.2. When the v-sensor is used for direct recording experiments with a sound source at the x-axis it is interesting to listen to the cases where $\boldsymbol{\mu}$=[1,0,0] and $\boldsymbol{\mu}$=[0,1,0]. For the former case the direct- and reverberant field is heard, while for the latter case one listens to only the reverberant field. It is also interesting to listen to the reverberant field in the room at different positions.

3.3.2 Two sensors

In this section the response of two v-sensors for stationary signals is discussed; the orientation of the two v-sensors is given by $\boldsymbol{\mu_1}$ and $\boldsymbol{\mu_2}$. Three spectra can now be determined, two auto spectra and one cross-spectrum, the latter being:

$$C_{ij} = \frac{1}{T}\int_0^T s_i(t) \cdot s^*_j(t)dt \tag{3.1}$$

The two auto-spectra A_i and A_j are found from equation (3.1) by taking $j = i$. Consider first the noise level of these signals. In most cases the noise level in the cross spectrum is lower than in the separate auto spectra. The reason for this is that in the cross spectrum the product of the noise of sensor i and the noise of sensor j vanishes if the noise signals are uncorrelated and if the integration time T is taken long (the same holds for the product of the signal times the noise). Gordienko et al, [55] reported already in 1993 a reduction of the ocean noise field in the cross correlation of two sensors. Also Shchurov [56] reported an increase in the signal to noise ratio (SNR) when an intensity probe is used. For isotropic (diffusive) noise even an increase in the SNR of 20-30 dB was found. For the case of two microflowns a reduction of the noise, down to 30 dB for frequencies above 600 Hz, has been reported [11]. The reason for this enormous reduction is, that for frequencies above 600 Hz the dominant noise is the resistance noise (or Johnson noise).

One expects that the resistance noise from one wire (resistance) powered by one battery is uncorrelated with the noise from another wire (resistance) powered by another battery. For lower frequencies 1/f noise appears, resulting in a much smaller reduction of the noise in the cross correlation [11]. The reason for this is that the decrease in the noise of the cross correlation spectrum is most effective for flat, broadband, frequency spectra. If a 1/f shaped component is present, there is a correlation between subsequent sample points x_i and x_j, while in a flat spectrum there is no correlation between points x_i and x_j $(i \neq j)$ in the series of data points [11]. Secondly another remarkable quality of the signal is that the influence of the reverberant sound field on the cross spectrum on one hand and the auto spectra on the other hand is completely different. For the cross spectra the contribution of the reverberant field can even be zero, if $\boldsymbol{\mu_1} \cdot \boldsymbol{\mu_2} = 0$, as will be explained below.

A simple two-dimensional case is worked out first. Two v-sensors at the origin of the x-y plane are present, with $\boldsymbol{\mu_1} = [1, 0]$ and $\boldsymbol{\mu_2} = [0, 1]$. The two dimensional purely diffuse reverberant sound field is modeled as four mirror sources $M_1 \cdots {}_4$ on a circle making an angle β, $\pi - \beta$, $\pi + \beta$ and $2\pi - \beta$ with the x-axis. Consider the contribution to the product of $s_1(t)$ and $s_2(t)$ when for each mirror source the velocity is directed inwards or outwards. For source M_1 the product of $s_1(t) \cdot s_2(t)$ will be positive ($s_1(t)$ and $s_2(t)$ are both negative for an inward velocity , since $\boldsymbol{\mu_1} = [1, 0]$, $v_x < 0$ and $\boldsymbol{\mu_2} = [0, 1]$, $v_y < 0$; $s_1(t)$ and $s_2(t)$ are both positive for an outward velocity, since $\boldsymbol{\mu_1} = [1, 0]$, $v_x > 0$ and $\boldsymbol{\mu_2} = [0, 1]$, $v_y > 0$. So the product $s_1(t) \cdot s_2(t)$ is positive). For source M_2 the product $s_1(t) \cdot s_2(t)$ is negative ($s_1(t) > 0, s_2(t) < 0$ for an inward velocity and $s_1(t) < 0, s_2(t) > 0$ for an outward velocity, for M_3 the product is positive and for source M_4 again negative. So for all mirror sources, equally distributed over the circle and a long integration time, the total contribution will be zero.

Now consider the more general situation with a three dimensional pure diffuse reverberant sound field with two v-sensors in the origin with vectors $\boldsymbol{\mu_1} = [\mu_{1x}, \mu_{1y}, \mu_{1z}]$ and $\boldsymbol{\mu_2} = [\mu_{2x}, \mu_{2y}, \mu_{2z}]$. Define first $v^2_{rev.}$ Suppose a hypothetical omni-directional v-sensor is in the origin (this is certainly not a Microflown, which has a $cos(\alpha_{\boldsymbol{\mu v}})$ dependence, see section 3.3.1). The mirror sources are equally distributed over a sphere. An arbitrary mirror source makes makes an angle α with the z-axis and an angle β in the x-y plane, thus $v_x \propto sin(\alpha) \cdot cos(\beta)$, $v_y \propto sin(\alpha) \cdot sin(\beta)$ and $v_z \propto cos(\alpha)$. Take the v_{rms} value from the sources within a solid angle $d\Omega = sin(\alpha).d\alpha d\beta$, as v_m. The signal of the hypothetical omni-directional sensor is proportional to:

$$v^2_{rev} = \int v^2_m d\Omega = \int_0^\pi sin(\alpha) d\alpha \int_0^{2\pi} d\beta . v^2_m = 4\pi v^2_m \tag{3.2}$$

In the far field approximation $v^2_{rev.} = \frac{p^2_{rev.}}{(\rho c)^2}$. The signal of the v-sensor with $\boldsymbol{\mu_1}$ is: $s_1 = \boldsymbol{\mu_1} \cdot \boldsymbol{v_m} = v_m \cdot \mu_{1x} \cdot sin(\alpha) \cdot cos(\beta) + \mu_{1y}.sin(\alpha) \cdot sin(\beta) + \mu_{1z} \cdot cos(\alpha)$, thus the cross spectrum from the two v-sensors with $\boldsymbol{\mu_1}$ and $\boldsymbol{\mu_2}$ becomes:

$$C_{12} = \int_0^\pi sin(\alpha) d\alpha \int_0^{2\pi} d\beta . (\boldsymbol{\mu_1} \cdot \boldsymbol{v_m})(\boldsymbol{\mu_2} \cdot \boldsymbol{v_m}) = \frac{v^2_{rev.}}{3} (\mu_1 \cdot \mu_2) \tag{3.3}$$

Equation (3.3) follows from simple straightforward algebra and is written out in appendix A. Equation (3.3) shows that if $\boldsymbol{\mu_1}$ and $\boldsymbol{\mu_2}$ are orthogonal to each other, there is

no contribution of the reverberant sound field to the cross-spectrum, and only the direct sound field of the source is measured. This is similar to the measurement of the real part of the sound intensity, for which also the reverberant sound field vanishes [17]. If $\boldsymbol{\mu_1} = \boldsymbol{\mu_2}$ (two v-sensors in the same direction, in order to obtain a low noise level, as compared to the noise level in the auto-spectrum of one v-sensor) the contribution of the reverberant field is $v_{rev.}^2/3$. In section 3.3.3 the case of $\boldsymbol{\mu_1} = [1,1,0]/\sqrt{2}$ and $\boldsymbol{\mu_2} = [0,1,1]/\sqrt{2}$ is discussed; for this configuration the contribution of the reverberant field in the cross spectrum will be $v_{rev}^2/6$. Thus when using two orthogonal oriented v-sensors it is possible in a reverberant room to determine the direct sound field ("free field measurements") of a source, as well as the reverberant sound field in the room.

3.3.3 More v- sensors

When using two v-sensors it is possible that with a sound source in a room no direct sound is detected in A_1, A_2 and C_{12}. For example if the sound source is at $[0,0,0]$ and the sensors at $[1,1,0]$ with $\boldsymbol{\mu_1} = [-1,1,0]$ and $\boldsymbol{\mu_2} = [0,0,1]$ no direct sound is detected: $A_1 = A_2 = v_{rev.}^2/3$ and $C_{12} = 0$. It seems logical then to use three v-sensors with $\boldsymbol{\mu_1} = [1,0,0]$, $\boldsymbol{\mu_2} = [0,1,0]$ and $\boldsymbol{\mu_3} = [0,0,1]$ and to use the three low-noise cross-spectra for the source localization. However, for that case it may occur that all three cross-spectra are zero; e.g. source at $[0,0,0]$ and sensors at x-axis (or y-axis or z-axis).

In order to anticipate on this, four v-sensors should be used. In the device discussed below we used: $\boldsymbol{\mu_1} = [1,0,1]/\sqrt{2}$, $\boldsymbol{\mu_2} = [0,1,1]/\sqrt{2}$, $\boldsymbol{\mu_3} = [-1,0,1]/\sqrt{2}$ and $\boldsymbol{\mu_4} = [0,-1,1]/\sqrt{2}$. As measured spectra we now have four auto-spectra and six cross-spectra. The contribution of the free field to the time averaged auto- and cross-spectra can be found as follows. Write the free field particle velocity vector and its time dependence as $\boldsymbol{v}(v_x, v_y, v_z).a(t)$, where the vector $\boldsymbol{v}(v_x, v_y, v_z)$, with (the real) components v_x, v_y and v_z represents the directional-vector of the free field particle velocity and $a(t)$ the time dependence of the source signal. Write for the signal of sensor A, divided by the sensor sensitivity (in Volt/(m/sec)), the symbol $S_A(t)$, then

$S_A(t) = (\boldsymbol{\mu_A} \cdot \boldsymbol{v}).a(t) = (\mu_{xA} + \mu_{yA} + \mu_{zA}).a(t)$; $\boldsymbol{\mu}_a = [\mu_{xA}, \mu_{yA}, \mu_{zA}]$ is the sensitivity unit vector of sensor A. The time averaged auto-spectrum of sensor A is thus equal to $\overline{(\mu_{xA} \cdot v_x + \mu_{yA} \cdot v_y + \mu_{zA} \cdot v_z)^2.a(t).a^*(t)}$. Similarly the time averaged cross-spectrum of the signals of sensor A and sensor B, the latter with sensitivity unit vector $\boldsymbol{\mu}_B = [\mu_{xB}, \mu_{yB}, \mu_{zB}]$ is equal to: $\overline{(\boldsymbol{\mu_A} \cdot \boldsymbol{v})\ .(\boldsymbol{\mu_B} \cdot \boldsymbol{v}).a(t).a^*(t)}$ or $\overline{(\mu_{xA}.v_x + \mu_{yA}.v_y + \mu_{zA}.v_z).(\mu_{xB}.v_x + \mu_{yB}.v_y + \mu_{zB}.v_z).a(t).a^*(t)}$.

In the auto- and cross-spectrum the same term $a(t).a^*(t)$ appears, and in a comparison between these spectra this term can thus be omitted. For the four v-sensors, as defined above, the four auto-spectra and the six cross-spectra are:

$$A_1 = \frac{1}{2}v_x^2 + \frac{1}{2}v_z^2 + v_x v_z + \frac{1}{3}v_{rev.}^2 \tag{3.4}$$

$$A_2 = \frac{1}{2}v_y^2 + \frac{1}{2}v_z^2 + v_y v_z + \frac{1}{3}v_{rev.}^2 \tag{3.5}$$

$$A_3 = \frac{1}{2}v_x^2 + \frac{1}{2}v_z^2 - v_x v_z + \frac{1}{3}v_{rev.}^2 \tag{3.6}$$

$$A_4 = \frac{1}{2}v_y^2 + \frac{1}{2}v_z^2 - v_y v_z + \frac{1}{3}v_{rev.}^2 \tag{3.7}$$

$$C_{12} = \frac{1}{2}v_z^2 + \frac{1}{2}v_x v_y + \frac{1}{2}v_x v_z + \frac{1}{2}v_y v_z + \frac{1}{6}v_{rev.}^2 \tag{3.8}$$

$$C_{13} = -\frac{1}{2}v_x^2 + \frac{1}{2}v_z^2 \tag{3.9}$$

$$C_{14} = \frac{1}{2}v_z^2 - \frac{1}{2}v_x v_y + \frac{1}{2}v_x v_z - \frac{1}{2}v_y v_z + \frac{1}{6}v_{rev.}^2 \tag{3.10}$$

$$C_{23} = \frac{1}{2}v_z^2 - \frac{1}{2}v_x v_y - \frac{1}{2}v_x v_z + \frac{1}{2}v_y v_z + \frac{1}{6}v_{rev.}^2 \tag{3.11}$$

$$C_{24} = -\frac{1}{2}v_y^2 + \frac{1}{2}v_z^2 \tag{3.12}$$

$$C_{34} = \frac{1}{2}v_z^2 + \frac{1}{2}v_x v_y - \frac{1}{2}v_x v_z - \frac{1}{2}v_y v_z + \frac{1}{6}v_{rev.}^2 \tag{3.13}$$

In an experiment one thus determines ten spectra and there are four unknown quantities, v_x, v_y, v_z and $v_{rev.}$ As an approximation for the best solution of the ten equations (3.4)-(3.13) the following algebraic procedure was used. From the equations (3.4)-(3.13) the products of $v_i.v_j$ are estimated:

$$v_x.v_y = \frac{1}{2}\{C_{12} - C_{14} - C_{23} + C_{34}\} = C_{xy} \tag{3.14}$$

$$v_x.v_z = \frac{1}{4}\{A_1 - A_3 + C_{12} + C_{14} - C_{23} - C_{34}\} = C_{xz} \tag{3.15}$$

$$v_y.v_z = \frac{1}{4}\{A_2 - A_4 + C_{12} - C_{14} + C_{23} - C_{34}\} = C_{yz} \tag{3.16}$$

Use as variables $u = v_x^2$, $v = v_y^2$ and $w = v_z^2$, then one obtains the six following equations:

$$u - v = A_1 - A_2 + A_3 - A_4 = A_0 \tag{3.17}$$

$$-u + w = 2.C_{13} \tag{3.18}$$

$$-v + w = 2.C_{24} \tag{3.19}$$

$$u = \frac{(v_x.v_y).(v_x.v_z)}{(v_y.v_z)} = \frac{C_{xy}.C_{xz}}{C_{yz}} = C_u \tag{3.20}$$

$$v = \frac{(v_x.v_y).(v_y.v_z)}{(v_x.v_z)} = \frac{C_{xy}.C_{yz}}{C_{xz}} = C_v \tag{3.21}$$

$$w = \frac{(v_x.v_z).(v_y.v_z)}{(v_x.v_y)} = \frac{C_{yz}.C_{xz}}{C_{xy}} = C_w \tag{3.22}$$

These six equations with three unknown variables are solved using the least mean square method; the expression:

$$(u-v-A_0)^2+(-u+w-2C_{13})^2+(-v+w-2C_{24})^2+(u-C_u)^2+(v-C_v)^2+(w-C_w)^2 \tag{3.23}$$

should have a minimum value. Differentiating with respect to the three variables gives:

$$\partial/\partial u = 0: \qquad 3u - v - w - A_0 + 2C_{13} - C_u = 0 \tag{3.24}$$

$$\partial/\partial v = 0: \qquad -u + 3v - w + A_0 + 2C_{24} - C_v = 0 \tag{3.25}$$

$$\partial/\partial w = 0: \qquad -u - v + 3w - 2C_{13} - 2C_{24} - C_w = 0 \tag{3.26}$$

Solving these equations gives as the best solutions:

$$4u = 4v_x^2 = A_0 - 2C_{13} + 2C_u + C_v + C_w \tag{3.27}$$

$$4v = 4v_y^2 = -A_0 - 2C_{24} + C_u + 2C_v + C_w \tag{3.28}$$

$$4w = 4v_z^2 = 2C_{13} + 2C_{24} + C_u + C_v + 2C_w \tag{3.29}$$

from which the free field particle velocity vector and the reverberant field can be solved. If the S/N (signal to noise ratio) in $A_1 - A_4$ is low, but high in C_{ij} then the auto-spectra should not be used in equations [(3.15) and (3.16). An alternative and practical method to obtain the best solution of equations (3.4)-(3.13) is to use a simple straightforward numerical procedure (on a PC) to find the minimum value of the expression:

$(\frac{1}{2}v_x^2 + \frac{1}{2}v_z^2 + v_xv_z + \frac{1}{3}v_{rev.}^2 - A_1)^2 + (\frac{1}{2}v_y^2 + \frac{1}{2}v_z^2 + v_yv_z + \frac{1}{3}v_{rev.}^2 - A_2)^2 +$
$(\frac{1}{2}v_x^2 + \frac{1}{2}v_z^2 - v_xv_z + \frac{1}{3}v_{rev.}^2 - A_3)^2 + (\frac{1}{2}v_y^2 + \frac{1}{2}v_z^2 - v_yv_z + \frac{1}{3}v_{rev.}^2 - A_4)^2 +$
$(\frac{1}{2}v_z^2 + \frac{1}{2}v_xv_y + \frac{1}{2}v_xv_z + \frac{1}{2}v_yv_z + \frac{1}{6}v_{rev.}^2 - C_{12})^2 + (-\frac{1}{2}v_x^2 + \frac{1}{2}v_z^2 - C_{13})^2 +$
$(\frac{1}{2}v_z^2 - \frac{1}{2}v_xv_y + \frac{1}{2}v_xv_z - \frac{1}{2}v_yv_z + \frac{1}{6}v_{rev.}^2 - C_{14})^2 + (\frac{1}{2}v_z^2 - \frac{1}{2}v_xv_y - \frac{1}{2}v_xv_z + \frac{1}{2}v_yv_z + \frac{1}{6}v_{rev.}^2 - C_{23})^2 +$
$(-\frac{1}{2}v_y^2 + \frac{1}{2}v_z^2 - C_{24})^2 + (\frac{1}{2}v_z^2 + \frac{1}{2}v_xv_y - \frac{1}{2}v_xv_z - \frac{1}{2}v_yv_z + \frac{1}{6}v_{rev.}^2 - C_{34})^2$

The values of v_x, v_y and v_z, as found from equations (3.26)-(3.28) and $v_{rev.}^2 \geq 0$ can be used as starting values in this numerical procedure.

3.3.4 The four sensor device

A photo of the four v-sensor device is shown in figure 3.5. Four small printed circuit boards, each with one microflown on it are combined. The orientations of the four v-sensors are: $\boldsymbol{\mu_1} = [1, 0, 1]/\sqrt{2}$, $\boldsymbol{\mu_2} = [0, 1, 1]/\sqrt{2}$, $\boldsymbol{\mu_3} = [-1, 0, 1]/\sqrt{2}$ and $\boldsymbol{\mu_4} = [0, -1, 1]/\sqrt{2}$. For the configuration, as shown in figure 3.5 the directional characteristics

of each sensor corresponds to $cos(\alpha_{\mu v})$ see figure 3.6. It is necessary that the encapsulation is not done by combining the four printed circuit boards on a fixed bar, since this seams to lead more to (frequency dependent) deviations of the directional characteristics as given in section 3.3.1 as $cos(\alpha_{\mu v})$. The distance between the four sensors is only 5 mm. The main electronics are encapsulated in the holder and a 7-pins connector is used for the power supply and connection to a sound card or analyzer.

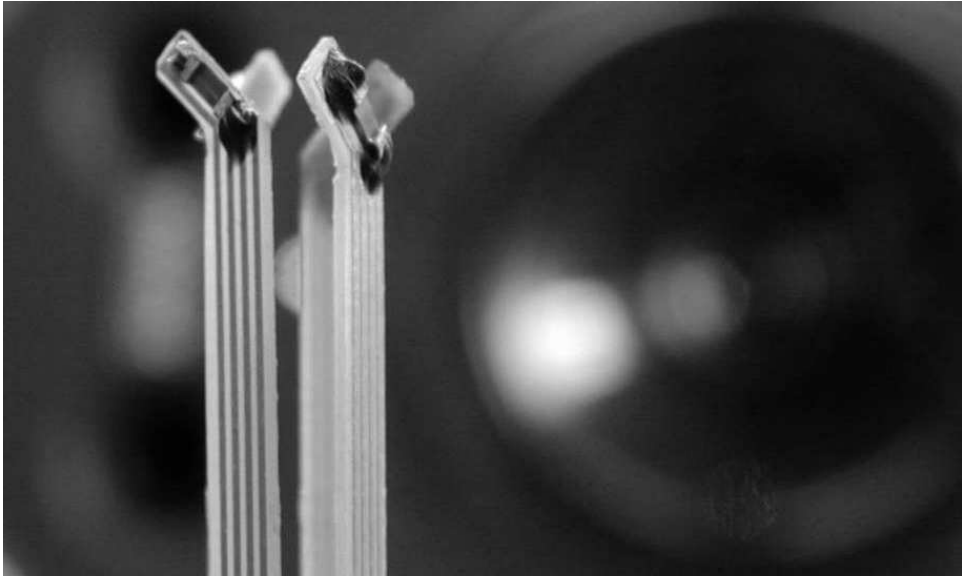

Figure 3.5: *The four sensor device, the elements are mounted on an epoxy carrier.*

3.3.5 Experiments in a reverberant room

In a reverberant room with dimensions of about 9 * 7 * 4 m a loudspeaker box with dimensions 0.4 * 0.2 * 0.2 m was used as a sound source. The four v-sensor device was placed at various locations in the room, in such a way that the inclination- (angle δ with the probe holder) and rotation angle (angle γ in a plane perpendicular to the probe holder) were varied. The source-sensor distance was also varied in order to create a situation where $v^2_{direct}/v^2_{reverberant} < 1$ and $v^2_{direct}/v^2_{reverberant} > 1$. When the inclination angle was taken as δ, the rotation angle as γ and the sound source- sensor distance as r, the response was measured for r= 0.5 m, 1 m and 2 m, δ as well as γ =0, 30, 60 and 90 degrees; so in total 48 responses. As signal to the loudspeaker white noise was used; the same (white noise) time signal was used in the 48 experiments. The auto- and cross-spectra were averaged over 4 seconds. A four input channel device, (product name Siglab) and a sound card in a PC were used as input for calculating the auto- and cross-spectra.

3.3.6 Results

In acoustic measurements it may well be that one is primarily interested in the free field properties of a sound source; on the other hand there are situations where one is primarily interested in the properties of the reverberant sound field. An example of the first case is

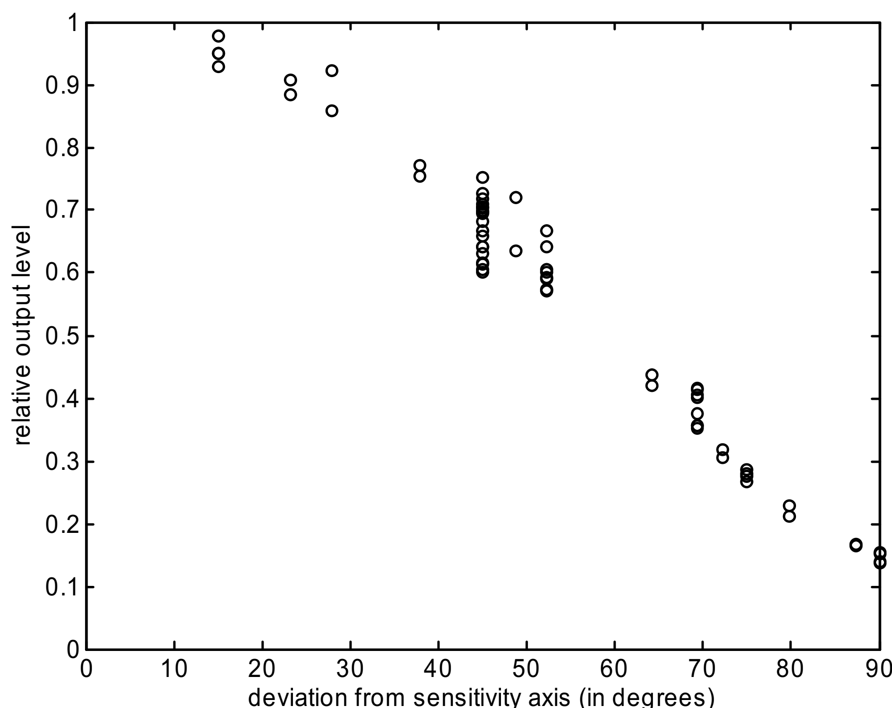

Figure 3.6: *Directionality of a sensor. A sound in the sensitivity direction of the sensor results in a relative output of 1. Sounds with a different results in less signal from the sensor, clearly the sensor is directional.*

that the one wants to know the radiated power (noise) of a machine while it is placed in a reverberant room. An example of the second case is that one is interested in the quality of a concert hall where the properties of the reverberant field are of interest. When using a p-sensor it is quite difficult or even impossible to measure the free- and the reverberant field separately. When the distance r, between sound source and sensor is larger than the reverberation distance r_r, of the room it is difficult to measure accurately the free field on the other hand, when the distance is small it is difficult to determine the properties of the reverberant field (the reverberation distance r_r is defined as the distance from the source where the rms value of the free field is equal to the rms value of the reverberant field). However with the 4-v-sensor device a number of possibilities appear. In the first subsection the emphasis is on the determination of the free field, in the following section the determination of the reverberant field is discussed. In the next two sections it will be shown that even in the case of $r > r_r$ it is possible to determine the free field, while for the case of $r < r_r$ the properties of the reverberant field can be determined.

Free field, localization of the sound source

The free or direct sound field is calculated from the measured 10 auto- and cross-spectra as was explained in section 3.3.2. From the ratios of v_x/v_y, v_x/v_z, and v_y/v_z, of the direct field the direction of the sound source seen from the sensor is calculated and compared with the theoretical value as deduced from the experimental set up. In table 3.1 results for the case r=1m are given; the bold numbers refer to the angles in degrees of the

experimental setup, the "theoretical angles". The other numbers for the angles in degrees are the results of the calculations from the experimental results. In e.g. 29.1 \ 1.1 the value of 29.1 refers to the value of δ, and 1.1. to the value of γ.

The (numerical) calculated values for v_x and v_y for the case $\delta = 90^o$ have no meaning and are placed between brackets. When $\delta = 90^o$, $v_x = v_y = 0$ and a value of $arctan\frac{v_x}{v_y}$ is undefined. In practice such a situation is recognized when the solutions for the components of the vector v are such that $v_x \ll v_z$ and $v_y \ll v_z$ while v_x and v_y are of the same order. Of course the numerical procedure gives values for v_x and v_y , but the ratio in has no meaning here.

Table 3.1: *Results for one meter distance to the source, the bold numbers are actual angles, the measured angles are given in the table*

Incl,$\delta \downarrow$ \ Rot,γ	**0**	**30**	**60**	**90**
0 μm	-0.79\1.2	1.47\31	0.93\61.1	0.74\89.6
30 μm	29.1\1.1	29.0\28.3	29.4\57.8	28.2\86.6
60 μm	57.4\ $-$ 1.9	57.0\29.8	57.0\59.5	56.1\91.1
90 μm	87.7\(17)	86.0\($-$7)	86.7\($-$9)	85.9\($-$30)

Table 3.2: *Measurement and errors, β is the deviation in degrees averaged over 16 measurements*

r(m)	$v^2_{dir.}/v^2_{rev.}$	$cos(\beta)$	$\beta(deg)$	$sin(\beta)$	σ	$\beta(deg)$
0.5	13.2	0.9984	3.3	0.0513	0.025	3
1	3.15	0.9989	2.7	0.0435	0.017	2.5
2	0.72	0.9900	8	0.1322	0.049	7.5

Table 3.3: *Reverberant field v^2_{rev}, calculated from two sensors at the time, values were normalized with respect to v^2_{dir} at $r = 1m$.*

$r\backslash\gamma\backslash\delta$	$v^2_{rev.}(1,2)$	$v^2_{rev.}(1,3)$	$v^2_{rev.}(1,4)$	$v^2_{rev.}(2,3)$	$v^2_{rev.}(2,4)$	$v^2_{rev.}(3,4)$
0.5\60\0	0.400	0.413	0.360	0.280	0.320	0.288
0.5\90\0	0.331	0.251	0.332	0.266	0.422	0.265
0.5\90\30	0.314	0.347	0.377	0.435	0.368	0.338
0.5\0\60	0.389	0.406	0.325	0.404	0.301	0.379
1\30\0	0.323	0.377	0.304	0.286	0.330	0.289
1\60\30	0.331	0.274	0.317	0.274	0.318	0.265

The average reverberant sound field $v^2_{rev.}$ is also calculated from these experimental values. In the second column of table 3.2 an averaged value of the ratio direct-/reverberant particle velocity, $v^2_{dir.}/v^2_{rev.}$ is given. For a more detailed comparison between experimental- and theoretical directions the inner, scalar, vector product of the theoretical particle velocity vector, taken as unit vector and denoted as $\boldsymbol{v}_{th}$,and the experimental particle

Table 3.4: *Reverberant field measured, normalized with respect to v^2_{dir} at r=1 m, and standard deviation.*

r(m)	$v^2_{rev.}$	σ
0.5	0.358	0.066
1	0.310	0.041
2	0.299	0.074

velocity vector, denoted as $\boldsymbol{v}_{exp.}$, is calculated. The deviation between the directions of $\boldsymbol{v}_{th}$ and $\boldsymbol{v}_{exp}$, denoted as β is then found from: $cos(\beta) = |\boldsymbol{v}_{th}.\boldsymbol{v}_{exp}|/|\boldsymbol{v}_{exp}|$. This deviation angle β can also be found from the inner vector product as: $sin(\beta) = |\boldsymbol{v}_{th} \times \boldsymbol{v_{exp}}|/|\boldsymbol{v}_{exp}|$, where the symbol $\times$ is used for the vector product. In terms of δ and γ the theoretical particle velocity vector is written as:

$\boldsymbol{v}_{th} = i[cos(\delta).cos(\gamma)] + j[cos(\delta).sin(\gamma)] + k[sin(\delta)]$

In the third and fifth column of table 3.2, the averaged values of $cos(\beta)$ and $sin(\beta)$ are given, the averaging is done over the 16 different directions given by δ and γ. For the deviation expressed by $sin(\beta)$ also a standard deviation s is given, calculated from: $\sigma = \sqrt{var} = \frac{1}{n}\sqrt{\sum(value - mean)^2}$, with n=16. The table shows a fairly good similarity between experimental found direction of the source and the real direction. So it is thus possible to measure the direct sound field in a reverberant environment using this 4-v-sensor device. Even for the case where the sound source - sensor distance is larger than the reverberation distance the results are within 8 degrees.

The reverberant field

The fact that in the auto-spectrum of a v-sensor only $\frac{1}{3}v^2_{rev}$ is measured means that only a part of the reverberant field contributes to it. Thus by measuring a number of auto-spectra (or cross-spectra) information about different parts of the reverberant field can be obtained. For example if there are three v-sensors, with $\boldsymbol{\mu_1} = [1, 0, 0]$, $\boldsymbol{\mu_2} = [0, 1, 0]$ and $\boldsymbol{\mu_3} = [0, 0, 1]$, then the signal of sensor one will contain the reverberant field around the x-axis, sensor two the field around the y-axis and sensor three the field around the z-axis.

When the free field is known, it is in principle possible to calculate the reverberant field from the difference of the auto-spectrum and the free field. However, this will not be a good method when $r < r_r$ since the reverberant field is smaller than the free field; consider e.g. the situation with r=0.5m in table 3.2, where $v^2_{dir}/v^2_{rev} = 13.2$. It seems better to calculate it from experimental values, which, in the case of no reflections, should be zero. An example is the expression $A_i.A_j - C^2_{ij}$. In the case of no reflections $A_i = (\boldsymbol{v}.\boldsymbol{\mu}_i)^2$, $A_j = (\boldsymbol{v}.\boldsymbol{\mu}_j)^2$ and $C_{ij} = (A_i.A_j) = (\boldsymbol{v}.\boldsymbol{\mu}_i).(\boldsymbol{v}.\boldsymbol{\mu}_j)$ thus $A_i.A_j - C^2_{ij}$ vanishes. In the case of reflections $A_i.A_j - C^2_{ij}$ can be written as a quadratic expression of v^2_{rev}, which then can be solved; the simple and straightforward algebra for the cases $i = 1$, $j = 2$ and $i = 1$ and $j = 3$ is given in appendix A. A reason for taking $A_i.A_j - C^2_{ij}$ is that this quantity is not sensitive to deviations in the sensitivity or orientation vector $\boldsymbol{\mu}$ of the separate sensors, or to a (small) deviation in the orientation of the 4-v-sensor with respect to the desired experimental set up. However, the noise and S/N ratio can be different for A_i and $_{ij}$. For

the 4-v-sensor device there are six independent values of $A_i.A_j - C_{ij}^2$, thus six different contributions of the reflections to the total reverberant field.

Some examples of results for v_{rev}^2 are given in table 3.3. In this table $r\backslash\gamma\backslash\delta = 0.5\backslash 60\backslash 0$ refers to the experimental set up where the distance is 0.5 m, the inclination $\delta = 0$ and the angle $\gamma = 60^o$; $v_{rev}^2(1,2)$ is the result using $A_1.A_2 - C_{12}^2$. The values of v_{rev}^2 in table 3.3 have been normalized with respect to the average value of v_{dir}^2 for $r = 1m$. This is done because a value of v_{rev}^2 in $(m/sec)^2$ does not give any information, unless the excitation used is known, together with the knowledge of a number quantities, as e.g. the loudspeaker efficiency, the radiation impedance etc. A direct measure for comparison is the direct (or free) sound field v_{dir}^2 (the choice of r=1 m is of course arbitrary).

So by measuring and calculating the parts of the reverberant field information can be obtained about the contributions from different directions to the total reverberant sound field, which in turn gives information about the acoustics of the room. In this paper, with emphasis on the 4-v-sensor device, we will not discuss these aspects. In general one is inclined to think that the average reverberant sound field is independent of the distance r. For the three distances r= 0.5,1 and 2 m the results are given in table 3.4; in the second column the average value of v_{rev}^2 , again normalized with respect to v_{dir}^2(r=1m), in the third column the standard deviation, σ. The values of v_{rev}^2 for the different distances are not exactly equal; however their differences are within the standard deviation.

3.3.7 Conclusions and future plans

A 4-particle velocity sensor has been described with which the free field and the reverberant sound field can be detected in a reverberant environment. The strength of these sound fields is not expressed in terms of the sound pressure but in terms of the particle velocity. Since the latter is a vector, while the sound pressure is a scalar, more information can be obtained when using a particle velocity sensor instead of a sound pressure sensor (microphone). Free field measurements are desired for determining the radiated noise of a source, when it is positioned in a reverberant environment. In (concert) hall acoustics a precise and detailed knowledge of the reflection pattern and reverberant sound field is desired. From measurements in a reverberant room the free field sound field, as well as the reverberant sound have been deduced. This has been done for a source- sensor distance as well as smaller as larger than the reverberation distance of the room. Also information about the directional characteristics of the reverberant field is obtained by comparing the various auto and cross correlations of the four sensors.

The separate four v-sensors are quite small (4 * 1.5 * 1.5 mm) and are encapsulated close to each other, so that the sensing volume (the volume in which the three vector components of the particle velocity are measured) is small as well; about 5 * 5 * 5 mm.

Many separate v-sensors were processed on a wafer in a thin film technology. They were cut, glued on a small printed circuit boards with electrical contact areas. The four printed circuit boards were encapsulated together to one device.

The next step in the integration process is to integrate all sensors on one die (a piece of silicon). The mounting of the sensor is much simpler (only one printed circuit board with electrical contacts is needed). More important the directions of the four unit vectors $\boldsymbol{\mu_i}$ are now precisely defined by a lithography process step and also the equality of the

four v-sensors in one device is expected to be better.

3.4 A first design of an integrated 3D particle velocity sensor

The research described in the previous section illustrates the extended possibilities when using a four sensor device. Fabrication of four sensors on one chip offers the possibility of a very symmetrical design, which has advantages regarding simulation and measurement results. Four input channels are normally required for this design, but this can be reduced to three when not using the cross correlation technique for every direction of particle velocity. Cross correlating signals results in a higher signal to noise level, but when signals are strong enough this is not necessary. Assume again four sensors with directivity $\mu_1 = [1,0,1]/\sqrt{2}$, $\boldsymbol{\mu_2} = [0,1,1]/\sqrt{2}$, $\boldsymbol{\mu_3} = [-1,0,1]/\sqrt{2}$ and $\boldsymbol{\mu_4} = [0,-1,1]/\sqrt{2}$. Then the value of v_x,v_y and v_z can be easily obtained by subtracting the signal of $\boldsymbol{\mu_3}$ from the signal of $\boldsymbol{\mu_1}$ to obtain v_x, and to subtract the signals of $\boldsymbol{\mu_4}$ from the signal of $\boldsymbol{\mu_2}$ to obtain v_y and adding the signals of all sensors to obtain v_z. This can be done electrically when all sensors are equal, or when they are electronically corrected such that they are equal. From four signals now three remain.

As discussed in section 3.2 the fabrication of an out-of-plane two wire sensor design has a high chance of succeeding and the design can eventually be up-scaled to a three wire design. The next step is to integrate four two-wire sensors with similar orientation as described in the previous section (3.3). The disadvantage that two wire type sensors have a lower self noise performance can be compensated by using cross correlation of sensor signals.

In the next part a monolithically integrated 3D sensor is presented consisting of four sensors integrated on one silicon die. This results in very good sensor reproducibility in terms of direction of sensitivity (since sensor location and direction of sensitivity is now determined by lithography instead of manual mounting sensors), easier mounting and a very small sensor-to-sensor distance. A small sensor-to-sensor distance allows for accurate single point measurements. Initial measurements performed show that three dimensional noise source finding is possible with this sensor, see also [57].

3.4.1 Design choices

Figure 3.7 shows a photograph of the realized sensor. Instead of integrating 3 sensors perpendicular to each other we chose to integrate 4 sensors at angles of 45 degrees with the chip surface. In Cartesian coordinates this corresponds to directions of maximum sensitivity of $\frac{1}{\sqrt{2}}(1,0,1)$, $\frac{1}{\sqrt{2}}(0,1,1)$, $\frac{1}{\sqrt{2}}(-1,0,1)$ and $\frac{1}{\sqrt{2}}(0,-1,1)$. This configuration has some interesting properties; firstly, modeling is more reliable due to the symmetry and secondly it provides the possibility of calculating cross spectra between two signals in any direction. Taking the averaged cross spectrum between two signals provides less (uncorrelated) sensor noise, [11] thus allowing to measure lower particle velocity. The four-sensor configuration provides at least two signals in any direction [54]. Due to the

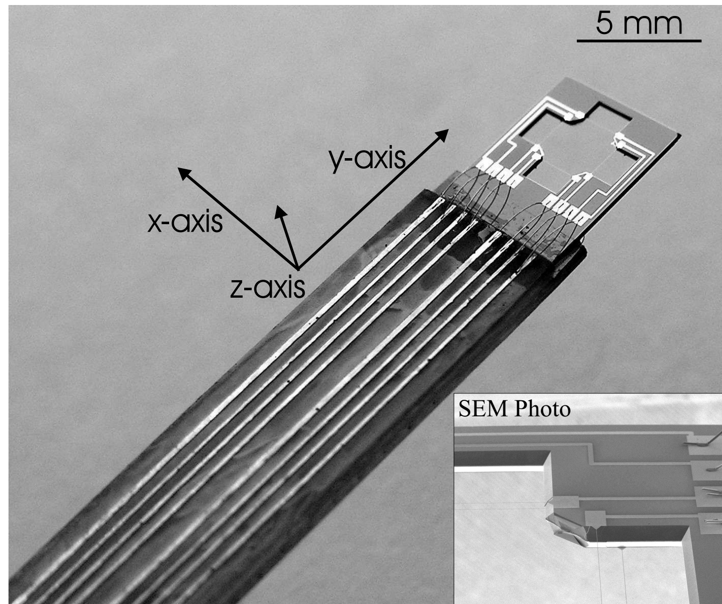

Figure 3.7: *A photograph of the integrated 3D particle velocity sensor.*

integration in one die the sensor can be extremely flat (250 μm thick), this can be of benefit when measuring close to surfaces. Seen in the y direction the sensor is of size 5 mm*5 mm*0.25 mm, which is not smaller in surface than existing 3D microflown sensors, but the sensors are more closely spaced (max. 2.5 mm). This allows almost single point particle velocity measurement, which can be useful when measuring close to very small sources or at high frequencies.

3.4.2 Fabrication and packaging

Special 250 μm thick double-side polished wafers are used because the wafer thickness defines the distance between the sensor wires in this design. To obtain a sensitivity direction of 45 degrees to the wafer surface the sensor wires are displaced by 250 μm with respect to each other. In this way the distance between the wires becomes 354 μm. This distance is not optimal in terms of self noise but smaller distances are much harder to accomplish due to the thin wafers required. When optimizing the design thinner wafers can be used. The wire thickness is 350 nm, due to the 200 nm silicon nitride and 150 nm chromium/platinum. The wire width is defined as approximately 2 μm (due to the used lift off technique and mask inaccuracies this is not precisely defined). Fabrication of the sensor is done by two sided processing of the wafer which is discussed more in depth in chapter 5.

The sensor yield is approximately 25%; on one standard 4 inch wafer approximately 20 working pieces can be made. By far most defects occur because of sensor wire breakage. With thicker sensor wires the yield can be increased significantly; however this decreases sensor performance at higher frequencies. When looking closely, the wires are not smooth at the edges and wire breakage occurs due to bad patterning of the platinum layer.

Furthermore in this design the inner, protruding edges of the etched silicon are etched significantly (see figure 3.7, SEM-photo), however not too much to destroy the wire supports. The amount of etching was controlled by using sacrificial structures at these edges. A too large sacrificial structure could result in sensor wire breakage due to remains of silicon nitride (the remaining KOH mask material) colliding with the wires.

To keep a slight tension on the wires to prevent phenomena like wire resonance effects and to provide a better support small triangular shaped ends are used. The triangular shapes tend to bend to the interior of the wafer. As shown in the same figure, SEM Photo, the wires are on both sides of the wafer and the triangular shapes are visible at each end of the sensor wires.

Before using the element in a measurement setup, it is mounted on a printed circuit board carrier. When the sensor will be used more frequently it must be packaged further since the constructed element is still very fragile. The sensor is operated by connecting every pair of sensor wires in series and powering them with a low noise voltage supply. Amplifying the series tap signal with a low noise amplifier results in a reasonable signal for further processing. All four channels have a separate output connection.

3.4.3 Simulation and measurement results

When plotting an absolute valued cosine function and letting the lower horizontal axis disappear in a single point and the upper horizontal axis to a circle a polar plot is made. Altogether when a vector (reflecting the direction of the sound) is multiplied with the sensitivity vector of the sensor the response of the sensor is equal to the magnitude of these vectors times the angle between them. Plotting the response of such a sensor versus the different directions of incoming sound waves results in a polar sensitivity plot.

As measurement setup, an acoustically damped box is used with a loudspeaker as sound source. The loudspeaker generates a white noise signal. In the center of the box, the device is placed together with a reference sound pressure microphone. The transfer function between the device and the reference sensor is measured. After every measurement the device is rotated around a small angle with a stepper motor and the measurement is repeated. Although this is not considered a good calibration technique, since the acoustic impedance of the setup is not known. Measuring the transfer function and only rotating the small sensor around its axis is still a good measurement for measuring the directivity of the element since the sound field does not change during rotation. A photo of the measurement setup is shown in Figure 3.8

Initial measurements were performed at a frequency of 600 Hz using a measurement setup that allowed rotation of the sensor along the two symmetry axes, namely the x-axis and z-axis (see figure 3.7 for orientation). The result of the measurement with rotation around the x axis is shown in Figure 3.9, rotation around the z-axis is shown in 3.10. The direction of sensitivity is dependent on the measurement frequency in this setup,

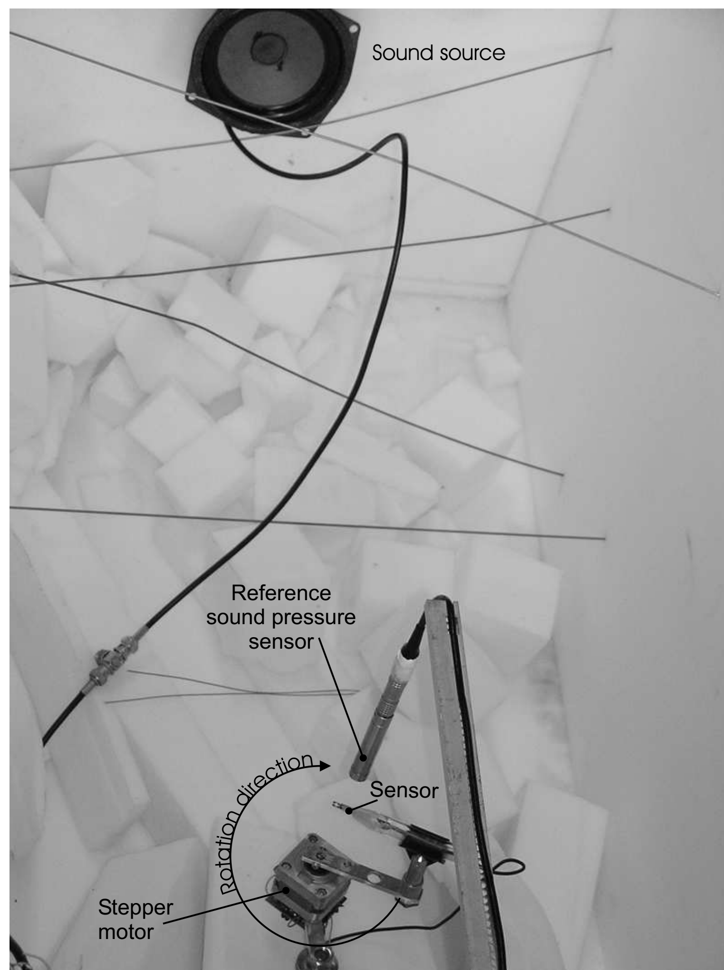

Figure 3.8: *Measurement setup. The sensor is rotated around its axis in an acoustically damped box with a sound source some distance away. The transfer between the sensor and a reference pressure sensor nearby is used for the polar pattern.*

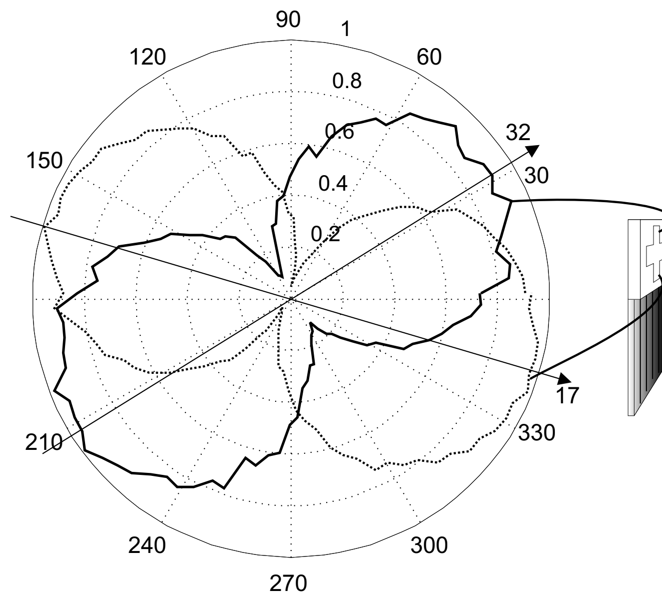

Figure 3.9: *Sensitivity pattern of the sensors at 600 Hz, rotated along the x-axis. The shown sensors should have a sensitivity direction at 45 degrees and -45 (315) degrees. Measurements are done in an acoustically damped box and results are linear scaled. The direction in the polar plot represents the direction of the incoming sound wave relative to the shown chip orientation.*

but the deviation is still within some degrees over a frequency range between 600 Hz and 3 kHz. A constant deviation (of at least ten degrees) of the sensitivity out of plane is found.

There is a clear figure-of-eight (or vector) response for each sensor, but the expected direction of sensitivity is not matching the measured direction perfectly. Channel 1, 2 and 4 are aligned 15 degrees off, but channel 3 is more than 20 degrees off. Since sensor 3 is the sensor nearest to the mounting carrier board, the deviation is probably the result of the package around the sensor. In the figure, an arrow represents the angle of sensitivity, found directly from another measurement in a standing wave tube. Further explanation of this setup is done in section 3.6. An analytical solution to this problem is not readily available, although the simulations predict this effect.

Measurements of the frequency response and sensitivity reveals that the sensors are nearly equal and have less than 6 dB difference in sensitivity. The sensitivity difference is partly due to the inequality of the sensor wire pairs; the resistance varies between 7 and 10 kΩ per sensor pair. Clearly, the sensor nearest to the mounting carrier board has by far the largest sensitivity, and this is most probably due to the particle velocity disturbance near the relatively large obstacle. Measurements were performed at a sensor voltage of 10 volts (5 Volts per sensor wire) and a current of approximately 1.3 mA (depending on the sensor). This gives a 'hot' resistance of 7.7 kΩ and a power consumption of 13 mW per sensor. This can be increased to approximately 60 mW before the sensor ceases working. When measuring the sensitivity and the electrical noise the equivalent acoustic noise can be found by dividing sensitivity by the electrical noise. In figure 3.11 the results on the

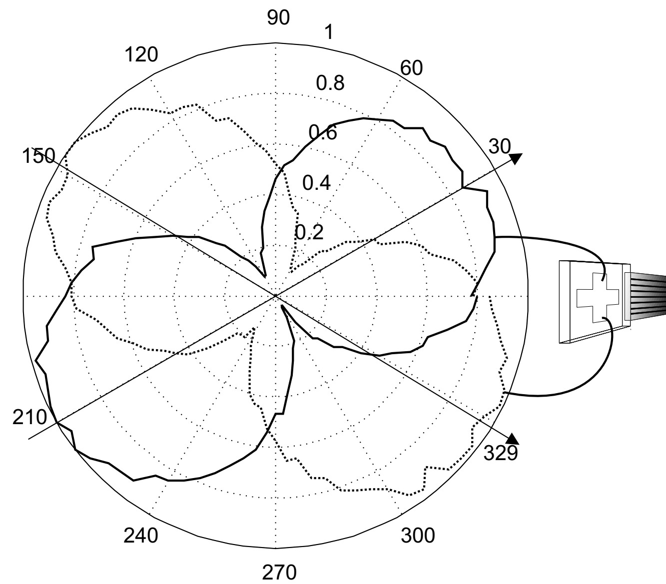

Figure 3.10: *Sensitivity pattern of the sensors at 600 Hz, rotated along the y-axis. All channels are expected to have a 45 degrees angle with the x- or y- axis. The data is plotted in linear scale.*

self noise of this sensor are shown. The sensitivity is divided by the electrical noise. Peaks are due to the calibration method used. The scaling is adjusted so that 0 dB is equivalent to 0 dB acoustic sound pressure in free field; 0 dB particle velocity is equivalent to 50 nm/sec. A fitted line shows the self noise for each power level. An optimal self noise is found at 40 mW (at 20 Volts and 2 mA). Since the sensor wires are smaller than the used sensors in chapter 2 where sensors are compared, a much higher voltage can be applied and the optimal power is therefore found at a higher voltage.

3.5 An investigation of the deviation in sensitivity direction

From the polar pattern in Figure 3.9 and 3.10 it is seen that the directivity of the sensor is not what it is expected to be. The direction of maximal sensitivity is rotated in the direction out of the chip plane. It is at this point not clear what the reason for this deviation is. There are several trivial things that could have been the cause of the deviation, the most obvious are explained briefly below.

- Physical misalignments are the most obvious explanation. Minute optical inspection reveals that there is not any physical misalignment that explains the difference in directivity.

- Crosstalk between signal lines. The 3D particle velocity sensor chip has multiple sensors whose electrical output signals are transmitted over a multiple conductor cable. Through capacitive coupling between the signal wires or the power supply wires the signal from one sensor could be coupled to other signal lines. By this

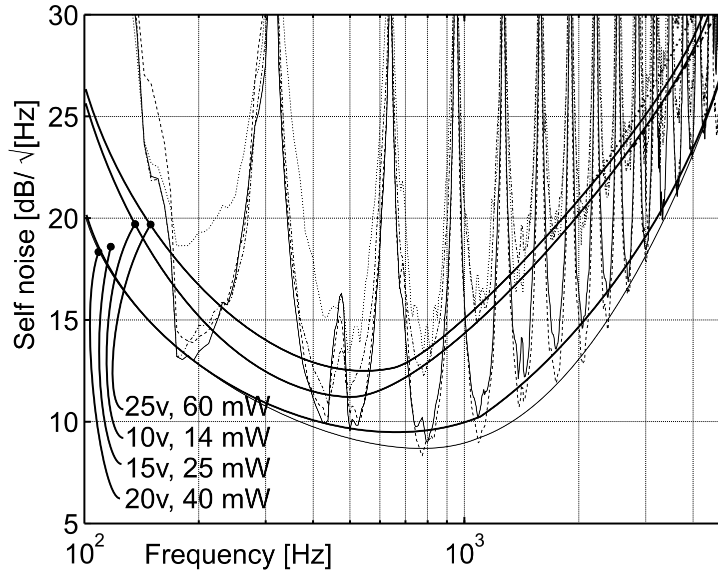

Figure 3.11: *self noise results for the sensors. A line is drawn through the measured minimum levels, this is the selfnoise level.*

effect the signal of the other sensor is influenced. In this way a certain amount of (correlated) signal is added to the electrical output of other sensors. Since the signal is correlated it is not easy to see whether there is crosstalk or not. With this effect it is possible that the apparent direction of sensitivity is changed.

A measurement with only one sensor connected and all other sensors disconnected showed the same deviation. This proves that the crosstalk is not the reason for the deviation, however it is an issue to keep in mind for future designs.

- Sound field effects. The sensor is tested in a standing wave tube, which has a well defined direction of particle velocity. In this setup the sensor is rotated until minimum and maximum values are measured. The measurement results were consistent with the polar plots measured earlier.

- When the thermal distribution near the sensor wires is changed due to heat sinks or sources this may lead to a different sensitivity (pattern). A nearby piece of silicon can act as a heat sink.

- Objects near the sensor may alter the local flow-profile near the sensor. Together with thermal effects this effect is named 'Package gain'.

After exclusion of the first three possibilities the remaining possibilities are an effect that disturbs the flow profile around the sensor wires, or a thermal effect. Further investigation to the directivity of the sensor is conducted with a symmetrical sensor with multiple wires. A more theoretical description of the observed effects is given in [58][39].

3.5.1 A four wire sensor measuring the directionality effect

For research purposes a sensor with four sensor wires is made. All sensor wires are designed equal, although small differences exist due to the fabrication process. The wire resistance is measured and is about equal. This four wire sensor can be connected in various ways, making it possible to investigate the deviation effect further. Two parallel wires at a distance of 250 μm are placed on one side of a silicon chip and two are placed on the other side of the chip. In Figure 3.12a a photograph of the sensor is shown. A cross sectional view of the sensor is given in Figure 3.12b, here the orientation of the wires becomes clear.

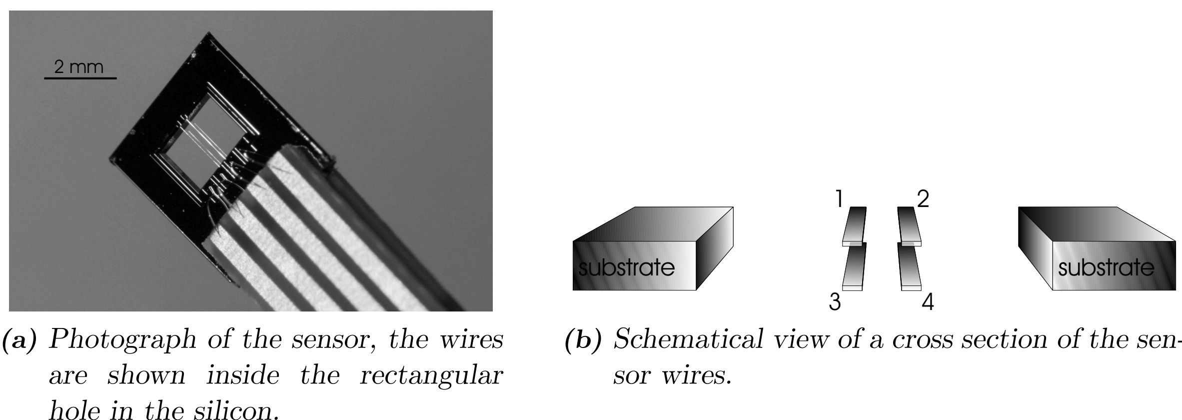

(a) Photograph of the sensor, the wires are shown inside the rectangular hole in the silicon.

(b) Schematical view of a cross section of the sensor wires.

Figure 3.12: *A Four wire sensor.*

When using wire pair 1 and 3 or pair 2 and 4 as sensor wires a sensor is made with its sensitivity direction perpendicular to the chip surface. Using wire pair 1 and 2 or 3 and 4 together a sensor is made with its sensitivity in the direction parallel with the surface of the chip. Since the sensor wires and their mutual distances are equal the effect of the surrounding silicon frame can be determined by this setup.

3.5.2 Difference between in-plane and out-of-plane sensitivity

Sensor wire pair 1 and 3 are connected such that they form a sensor. Following the sensitivity direction of the sensor is found by rotating the sensor in a standing wave tube until a maximum sensitivity is found. This is both done for a sensor with sensor wires 1 and 3 and sensor wire pair 2 and 4. For both sensors the maximum sensitivity is found when the direction of sound is perpendicular to the surface of the chip.

The same is done with the sensor wires pair 1 and 2. Now the direction of maximum sensitivity is found in plane with the surface of the sensor chip and perpendicular to the length-axis of the sensor wires. For these sensor configurations the measured direction of sensitivity is equal to the expected direction. The verification pair (the sensor with sensor wires 3 and 4) performed equally.

The sensitivity in the direction perpendicular to the plane (figure 3.13 'perpendicular') is about 6 dB (a factor two) higher than in the other direction (figure 3.13 'in plane').

A resemblance with the 'package gain' effect is observed, and the effect is dependent on the orientation of the package. Since the noise of the sensors is about equal for all configurations, so the self noise is lower when the sensor is used in the direction perpendicular to the sensor plane.

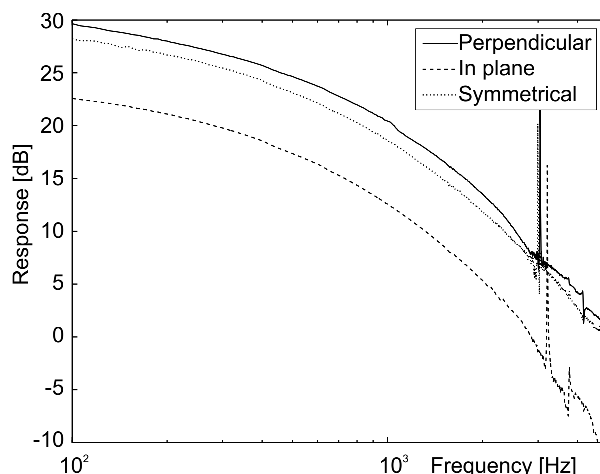

Figure 3.13: *On and off axis sensitivity measurement results, the effect of the surrounding package is observed.*

3.5.3 A rotational symmetrical sensor

An adjustment is made to the sensor. A second sensor without sensor wires is diced into two parts, and the parts are mounted on the existing 4-wire sensor. See figure 3.14. Furthermore the mounting carrier board is shaped into a more or less round shape with the application of clay.

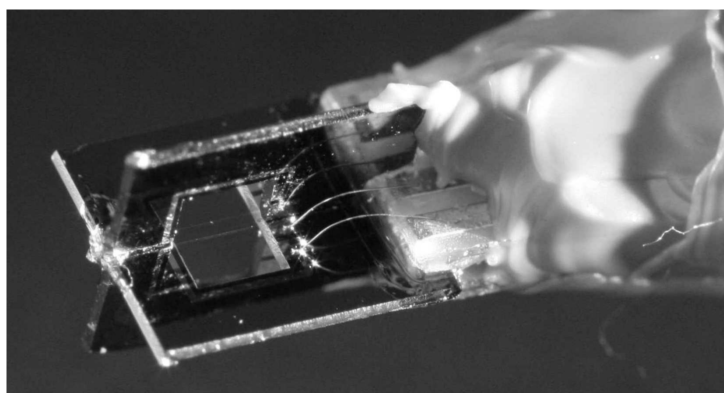

Figure 3.14: *A rotational symmetrical four wire sensor.*

The influence of the sensor wire orientation

The sensor wires are not round, but flat (2-3 μm width and approximately 300 nanometers thick) which could be of influence on the directivity or sensitivity of the sensor. Repeating

the experiment described in 3.5.2 can show whether the wire geometry has a detectable influence. Because the silicon frame is symmetrically oriented with the sensor wires the only difference between both measurement situations is the wire orientation. In Figure 3.15 this is shown.

The measurement principle is explained (see Figure 3.15) by comparing the sensitivity of sensor wires 1 and 3 to a vertical particle velocity with the sensitivity of sensor wires 1 and 2 to a horizontal particle velocity.

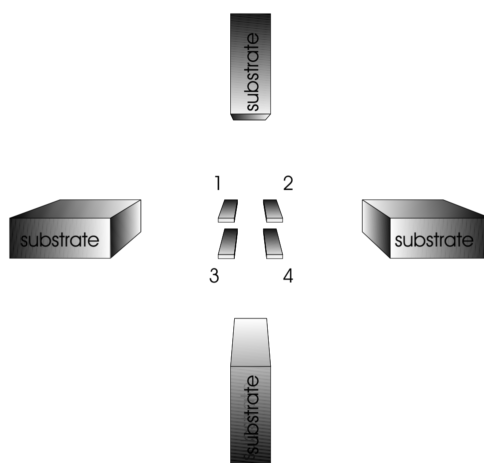

Figure 3.15: *A schematic representation of the symmetrical sensor.*

From measurements it is clear that both configurations perform about equal. The result is shown in figure 3.13 'symmetrical'. From these measurements it follows that the geometry of the sensor wires has little or no influence on the performance of the sensor. Furthermore it is observed that an object in the vicinity of the sensor has a large influence on the sensitivity and directivity of the sensor.

Polar diagram of the symmetrical sensor

When sensor wires 1 and 4 or 2 and 3 (see Figure 3.12b) are used a sensor with an expected sensitivity direction 45 degrees out-of-plane is made.

The sensor was rotated in a standing wave tube and for 96 different angles the sensitivity measured. Results are plotted in a polar plot diagram. In Figure 3.16a the line 'standard design' shows the results obtained with the sensor shown in Figure 3.12a. The direction of sensitivity is here around 30 degrees, so a deviation of 15 degrees is present.

The sensor shown in Figure 3.14 is fully rotational symmetric and therefore no deviation is expected. This sensor should have a maximum sensitivity directed to 45 degrees. A polar pattern measurement is performed on this device, for the result of this see figure 3.16a, 'symmetrical design'. The angle of maximum sensitivity is at 51 degrees. Still an error of 6 degrees is found but this is much smaller than with the original sensor shown in

Figure 3.12a (the polar pattern is shown in Figure 3.16a 'standard design'). Additionally the symmetrical sensor has a 1.15 times higher sensitivity than the original sensor.

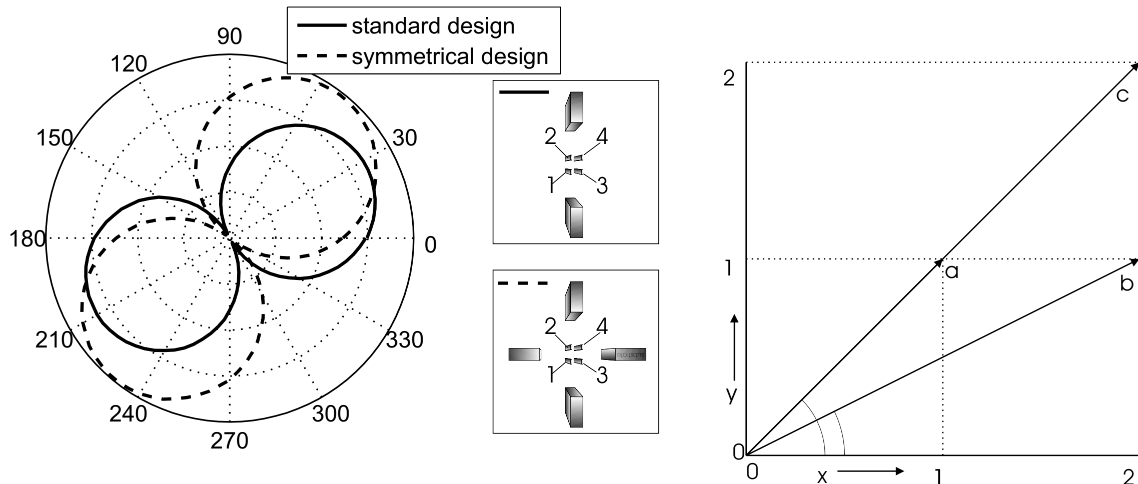

(a) Measured difference in sensitivity and direction between a flat sensor as in Figure 3.12b and a rotational symmetrical version as in Figure 3.14. The scaling of the polar plot is linear.

(b) sensitivity vectors schematically represented. The angle α is 30 degrees and β is 45 degrees.

Figure 3.16: *Effect of the package on the polar pattern.*

An intuitive explanation by linearly combining the (directional) amplification of the package gain is given below. A more detailed theoretical discussion is given in [39]. From Figure 3.13 the difference between the in-plane and out-of-plane sensitivity is a factor two. The package gain in the direction perpendicular to the surface of the chip is therefore assumed a factor two and in the direction of the plane equal to one (or 'no gain'). Using the sensor wires 1 and 4 and measuring the polar diagram of the sensor results in a factor two increased sensitivity in the horizontal direction in Figure 3.16a, 'standard design'. This corresponds to the found deviation of about 15 degrees. In Figure 3.16b this sensitivity is depicted by a vector 'b'. When adding another silicon frame as in Figure 3.15 the sensitivity for particle velocity in the vertical direction is also increased by a factor two, bringing the direction of sensitivity back to 45 degrees (arrow 'c' in the figure). Vectors 'b' and 'c' differ in length with a factor 1.17, which is again in accordance with the measurement results.

Thermal or flow effect

There are two global explanations for the directional deviation. First the effect can be due to a locally disturbed flow profile and secondly a temperature effect due to the local cooling of the surrounding silicon substrate can be of influence. When the heated sensor wires are in the vicinity of a heat source or heat sink the temperature profile around the wires differs from when they are surrounded by air only. Since silicon is a very good heat conductor (thermal conductivity of 157 W/m K), implying that the temperature at the

surface of the silicon is constant over the silicon chip. The temperature of the chip is measured and at most 15 degrees warmer than the surrounding air. This depends on the used mounting, the power supplied to the sensor wires and the size of the silicon chip. Because the sensor wires are operating at a temperature between 200 and 300 ^{o}C the silicon acts as a heat sink.

The flow profile is changed when objects are in the vicinity of the sensor. When a massive object is located in an air-flow, this has to find another path. For acoustic particle velocity this also seems to be valid. Whether the deviation is due to a flow change or a thermal effect has to be investigated.

The surrounding objects can have an effect on the flow but also on the thermal profile around the sensor wires. To investigate which effect has the largest influence the effects must preferably be separated. For the isolation of the thermal effect this is quite difficult; a thermal sink without any influence on the flow profile is hard to fabricate. A thermal source can be added in the form of a nearby heater wire, assumed that the wire has negligible effect on the local flow profile.

The flow effect can be separated from the thermal effect by using an obstacle with the same thermal resistance as air, and the same specific heat, but with a rigid shape. Such a material however is hard to find. A so called 'aero-gel' is suitable, but this material is very hard to pattern in the preferred shape. Therefore balsa wood has been used, which has also a very low thermal conductivity of 0.048 W/m K, which is almost twice that of air (thermal conductivity of 0.024 W/m K). When the experiment with balsa wood as object versus the experiment with silicon as object is compared there would at least be a distinct difference when the effect is largely of thermal origin.

The same symmetrical sensor as shown in Figure 3.14 is made, but now the ridges that are mounted on the sides are made of balsa wood. So the sensor with the 4 wires does now consist of a silicon substrate with sensor wires and an out of plane construction of balsa wood.

Measurements results show that the deviation is about equal to the experiment with silicon as construction material for the ridges. Since the sensor is assembled by hand with an estimated precision of tenths of millimeters, while the total sensor size is in the order of millimeters, the mounting is not very precise. Therefore quantitative results on how much effect the change of material has is hard to give. Nevertheless the precision is good enough in order to conclude that the deviation effect is mainly due to flow disturbance around the sensor wires.

3.5.4 The shape of the polar pattern

From the polar pattern it can hardly be seen whether the directional sensitivity is a vector sensitivity or an added effect. If the sensitivity is indeed a pure vector the sensitivity pattern must have a strong resemblance with a sine function. In the figure 3.17 below

the measurement result is fitted with a sine function. The residual error in terms of angle mismatch is depicted in the figure below that. Clearly a sine is a very good matching function for the polar plot, with a very small residual error. At the maximum sensitivity point the residual error seems to be large (-5 degrees).

Essentially the *arcsine* of an amplitude value results in a certain angle (and then there are multiple solutions). The difference between the *arcsine* of both the measurement point and the fitted data point is equal to the difference found in terms of an angle between the fitted data and the measurement data. Since this error angle is calculated through $arcsine(measurement_data) - arcsine(fitted_data)$, a very small amplitude variation results in a large error-signal [1], especially at places where the sinusoidal shape is at its maximum. From the graph it can be concluded that the error displayed is more due to a small amplitude variation than a directivity error and that the directivity is a pure vector.

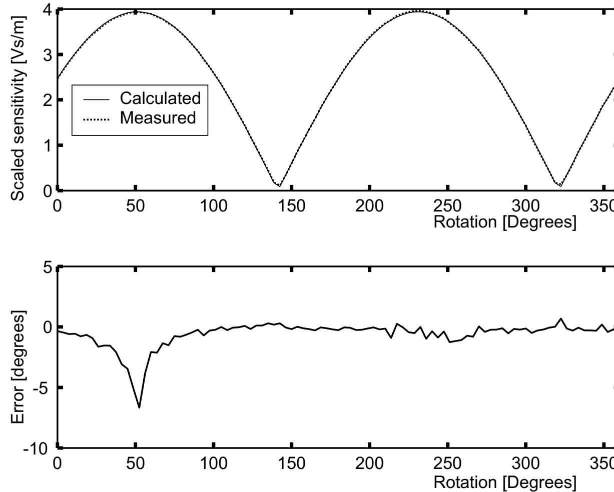

Figure 3.17: *Resemblance of the measurement results with a sinusoidal function. Only a small residual error exists.*

3.5.5 Influence of the element housing temperature

The sensor is modified again. In this experiment a small platinum temperature sensor (Pt 100 type) is placed on the silicon substrate. First the sensor is rotated and the sensitivity pattern is recorded, thereafter the sensor substrate is heated by means of heating the temperature sensor with an electrical current. After some time the temperature stabilized at approx 130 degrees Centigrade. Following the measurement is repeated. From this measurement the directivity does not noticeably change. Thus the substrate temperature does influence the direction of sensitivity, but the sensitivity is decreased a slightly.

[1] Or, the derivative of $arcsine(x)$ around $x = 1$ is large, so for small Δ the solution of $arcsine(x - \Delta) - arcsine(x + \Delta)$ is large. A small errors represented by Δ has therefore a large effect.

3.5.6 Measurement on loose wires

When the sensor wires are heated more the wire tension becomes less. When this happens the wires start 'dangling'. In final designs this effect can be avoided by placing wire end-points with a spring constant, as discussed in part 2.3.3. Still when the wires are heated too much the springs are not able to compensate and eventually the wires move with the particle velocity.

To investigate if this is the reason for the deviation of the polar pattern the sensor is subjected to power levels at which this dangling occurs. Even then the sensor continues working; there is a small deviation on the shape of the polar pattern in the form of a oddly shaped cosine function. However the overall direction of sensitivity remains the same. So the dangling wires have indeed an effect on the polar sensitivity pattern, but they do not explain the global change of the direction directivity and this effect does only occur when power in excess of the recommended values are used.

3.6 A second 3D integrated particle velocity sensor design

From measurement results on the first prototype it seemed that surrounding objects such as the silicon chip had a large influence on the directivity of the sensor. An attempt is made to improve the directivity by making the design acoustically more transparent. This is accomplished by keeping the amount of silicon to a minimum.

While the first design simply had a cross shaped window in the silicon chip the second design has silicon only at places were conductive traces to the sensor wires are, and for structural reasons. It is assumed that the particle velocity flow is much less disturbed by this design. In Figure 3.18b both designs are shown.

Furthermore in the design an opening with two sensor wires for a sound pressure sensitive element is placed. When equipped with a pressure-back chamber this type of sensor is a fully integrated three dimensional particle velocity sensor on one chip. The sound pressure sensor is discussed more in depth in chapter 4.

3.6.1 Measurement results

Sensor performance in terms of self noise is comparable with the first type of sensor, measurement results of the self noise are shown in Figure 3.19. These results differ mainly from the previous results in terms of the visual graph. In this graph the transfer function of the standing wave tube is canceled out, while in the previous graph the self noise results are interpolated from the uncorrected measurement data. A similar self noise compared with the previous sensor is measured.

The polar pattern unfortunately seemed to show no improvement over the previously fabricated sensor. While the acoustically transparent sensor has smaller supporting

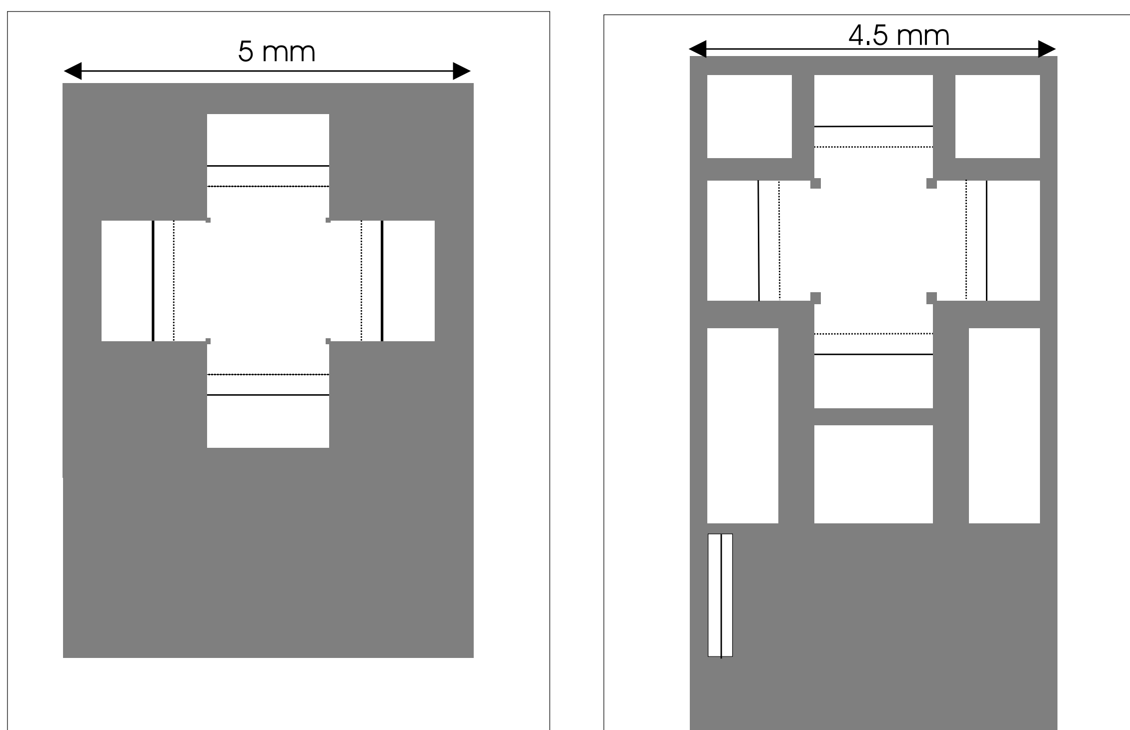

(a) The first type 3D- particle velocity sensor (b) An acoustically more transparent design

Figure 3.18: Integrated three dimensional particle velocity sensors, the first and acoustically transparent version.

beams, is smaller in total width and has additional holes this has barely effect on the directivity compared with the first type of chip.

From this point on a standing wave tube is used for directivity measurements, since the standing waves for frequencies under the cut off frequency of the tube are well defined and directed in the length axis of the tube. A small stepper motor is used to rotate the element inside the tube, thereby keeping the position of the element at the same place. At the same time the signal of the element is recorded, for 96 angles, delivering a polar pattern with a 3.75 degree step size.

In Figure 3.20 the measurement results with the sensor using the rotation in a standing wave tube is shown. The shape of the polar pattern is smoother than when measuring in the box described in section 3.4, and a cosine function can be fitted through the results with a small residual error. The angle of directivity is hard to determine precisely from the polar plot, however when fitting the cosine function the direction of sensitivity becomes very clear and is plotted with an arrow in the graphs. For the newly made element there was no difference in directivity was seen compared to the first type of element, except for the fact that the element nearest the carrier board had no more deviation than other elements.

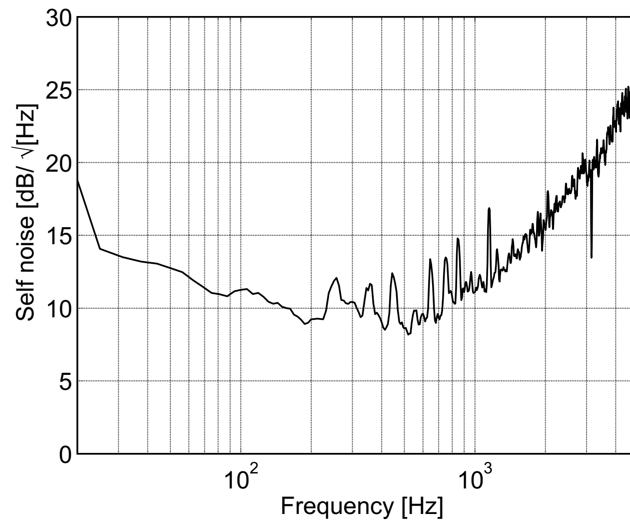

Figure 3.19: *Self noise result of the sensor.*

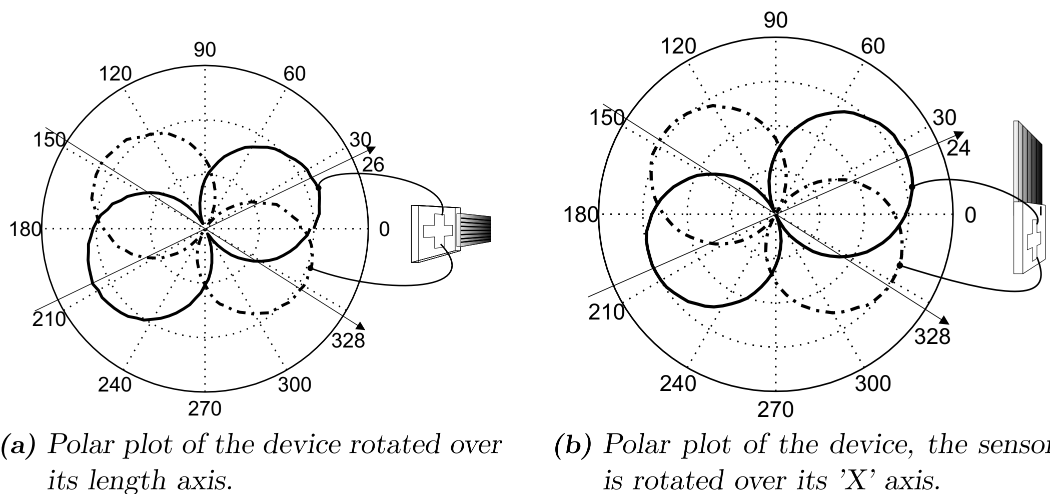

(a) *Polar plot of the device rotated over its length axis.*

(b) *Polar plot of the device, the sensor is rotated over its 'X' axis.*

Figure 3.20: *Polar plot measurement results with the acoustically transparent design.*

3.7 A particle velocity sensor with four wires

The research design as used before to investigate the deviation effects can be connected in another way. Because the sensor has four wires they can all be connected simultaneously. Every pair of two opposite sensors can be used as a particle velocity sensor. The other pair of sensor wires (pair 1 and 4 respectively pair 2 and 3 in figure 3.12b) provide an added temperature effect that enhances the first sensor. Together the sensor principally consists of two separate sensors, so providing two directions of sensitivity. Two of these types of sensors or one additional other 1-D type particle velocity sensor can make a three dimensional particle velocity sensor.

Fabrication is done in a 250 μm thick wafer, with wire width of 3 μm. The design is shown in Figure 3.12a.

3.7.1 Polar pattern and sensitivity

Sensitivity is measured in a short standing wave tube. Two opposite wires are connected as a sensor pair and the signal is connected to an analyzer. Following one extra neighboring wire is heated by electrical current, and finally the other remaining wire is powered also. For each situation the sensor is rotated, and the sensitivity is recorded (see figure 3.21b). When applying power to one or more wires the sensitivity is increased. When one wire was powered the sensitivity increased approx. 2.5dB (1.8 times). With both wires powered the sensitivity increased 3.8dB (2.4 times). When the 4-wire sensor is connected with only two opposite wires powered the expected sensitivity of a figure of eight exists. When measuring the same pair of wires and supplying power to one other wire, the direction of sensitivity does not change. From measurements shown in Figure 3.21b the direction of maximum sensitivity for only the pair of wires connected is 28 degrees, with one extra wire powered it is 26 degrees and with two wires on it is 27 degrees. The mutual deviation of one and two degrees is so small that it is within the measurement error. Also there is the large error discussed earlier of the sensitivity direction which is here 17 degrees.

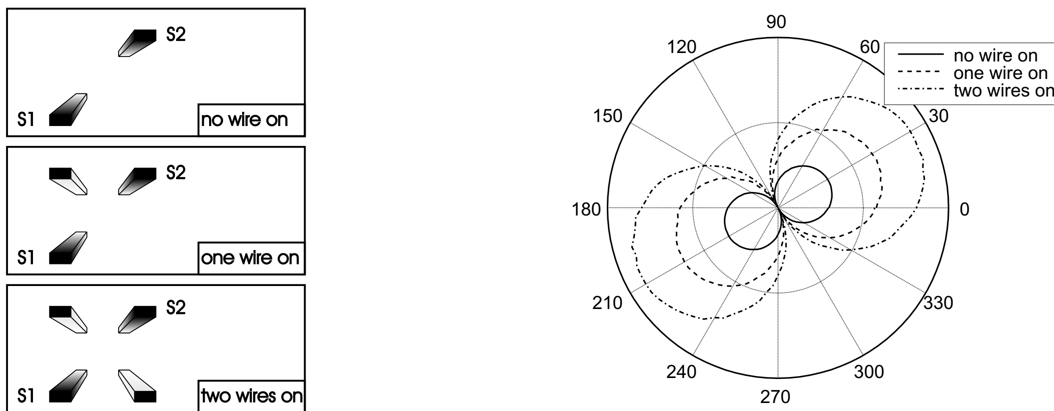

(a) Schematic view of the activated sensor wires.

(b) Two, three and four wires powered, scaling is linear.

Figure 3.21: *Evolution from two wire sensor to four wire sensor.*

3.7.2 Self noise difference between two and four wires

Powering only two or more wires does barely increase the noise of the sensor, however the sensitivity does increase when extra wires are powered. Because of this the self noise decreases. The extra wires form again a sensor pair, with sensitivity in another direction and again with a lower self noise compared with a two-wire sensor. In Figure 3.22b below the difference between a configuration with one pair powered and two pair of wires powered is shown with respect to sensitivity and self noise.

Clearly the sensor performs much better, and has additionally a second sensor with its own directivity integrated at virtually the same place. So a two dimensional particle

velocity sensor is made taking not more space than a regular one dimensional particle velocity sensor.

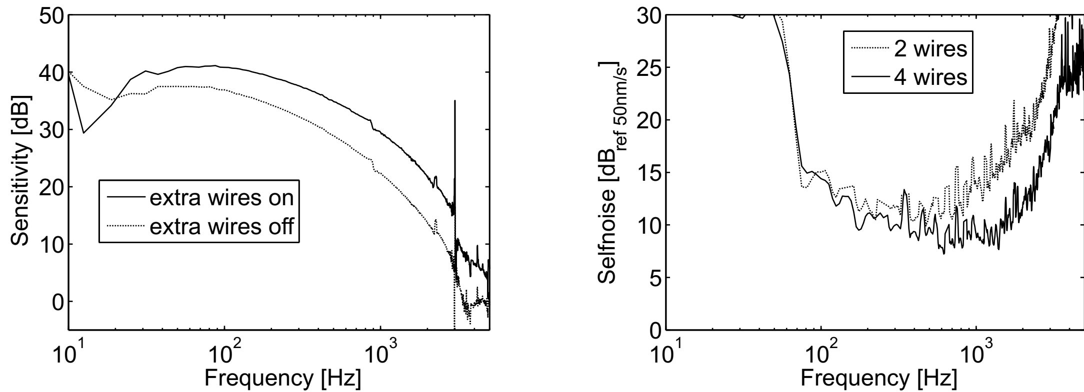

(a) *Sensitivity with two and four wires.*

(b) *Self noise of the sensor, with two and four wires powered.*

Figure 3.22: *The performance increases when more wires are heated.*

3.8 An integrated four-wire 3D design

With the four wire principle a three dimensional sensor can be made. Use is made of a pair of four wire sensors placed close to each other. If the sensor plane is in the (x,y) plane then sensitivity directions of (1 0 1),(-1 0 1),(0 1 1) and (0 -1 1) are obtained by doing this. For two pairs of sensor wires these directions are shown in Figure 3.23. Together with this sensor a sound pressure design is integrated, see chapter 4, enabling the sensor for use as a three dimensional sound intensity probe.

Two diagonally placed wires are used as one sensor with wire distance of 350 μm, so each four-wire configuration results in two sensor output signals corresponding to perpendicular particle velocity directions. For each sensor, there is now an additional heat source in the form of the other pair of sensor wires, and this result in a higher sensitivity. Therefore, both a smaller size and better performing sensor is realized. To make a three dimensional type two of these sensors are places in a silicon chip as shown in the schematic Figure 3.24.

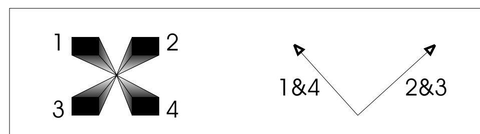

Figure 3.23: *Schematic view of directions of sensitivity of the sensor wire pairs, the arrows indicate the directions of sensitivity for the sensor pairs 1&4 and 2&3.*

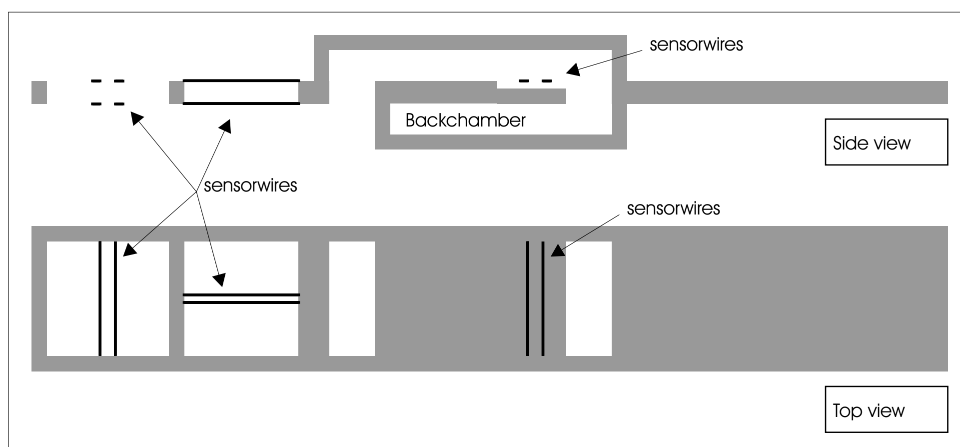

Figure 3.24: *Schematic view of the design.*

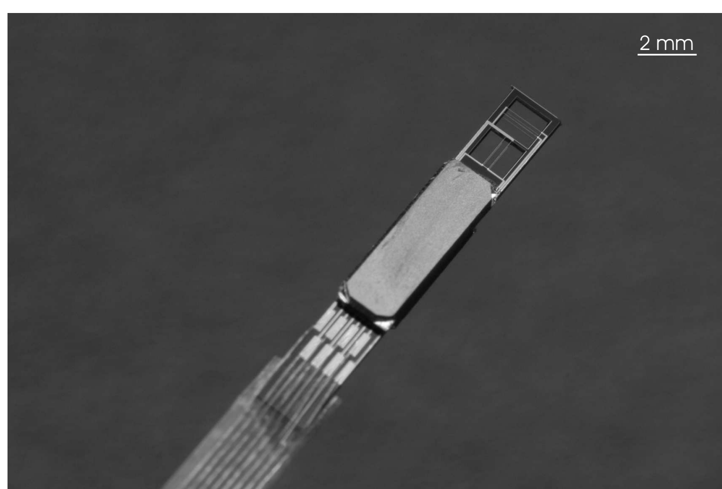

Figure 3.25: *Photograph of the 3D four wire particle velocity sensor, equipped with a pressure back chamber, as described further in chapter 4.*

3.8.1 Fabrication

Fabrication is done on both sides of a 250 μm thick silicon wafer. Figure 3.25 shows a complete mounted 3D sensor with integrated sound pressure sensor. Fabrication of the device is done similarly to the previous designs, only wire width is taken 3 μm (instead of the previously used 2 μm) to gain a higher sensor yield.

3.8.2 Measurement results

Directionality experiments show that this sensor has a better agreement between measured sensitivity direction and the 45 degrees out-of-plane sensitivity as designed. The deviation is around 10 degrees instead of the 15 degrees found in earlier versions. A plot of the measurement is shown in Figure 3.26. Together with this plot, another plot with the name 'corrected' is shown in the figure. This is the directional corrected signal, and is aimed exactly at 45 degrees.

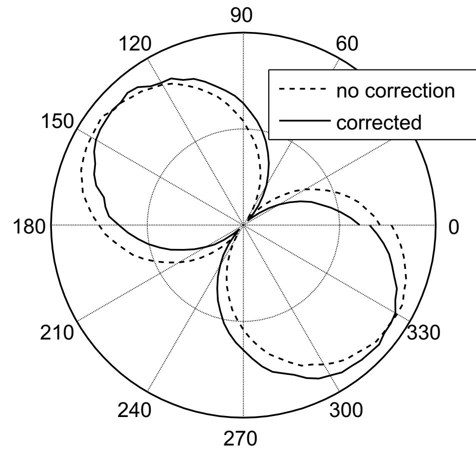

Figure 3.26: *Polar pattern measurement results of the sensor. The scaling is linear.*

This correction method is carried out by subtracting or adding a part of the signal from the other sensor, so that this the polar pattern is changed. Only when the sensors are very close compared with the acoustic wavelength this is possible and since the sensor wires are virtually at the same place (only 250 and maximally 350 μm apart) this is the case. The signal of both elements is amplified, and electronically a part of the signal is subtracted from the other signal, the amount is experimentally found by applying an acoustic wave in the direction where the minimum sensitivity (perpendicular to its maximum sensitivity direction) must be. Here signal variations are large and precision is therefore higher than in the direction of maximum sensitivity. Varying the amount of the signal added or subtracted from the other sensor until the total signal is a minimum results in the proper setting. At this point, the sensor is calibrated in the right direction.

3.9 Conclusions

An investigation to the best possibility configuration of a three dimensional particle velocity sensor is done. A type with four particle velocity sensors placed symmetrically is found to be a good choice. Next a three dimensional particle velocity sensor element with four sensor elements in one chip has been fabricated. Although measurements were satisfactory and proved that the sensor was directional, a better result can be obtained by re-designing the sensor. A smaller outline, providing a more 'acoustically transparent' design is expected to decrease deviations from the expected sensitivity directions, however no improvement is seen.

After exclusion of several trivial possible causes for the deviation in directivity, the 'package gain' effect is found responsible for the deviation. Research leads to the conclusion that obstacles in the vicinity of the sensor wires have a large influence on the

response of the sensor, both on directionality and sensitivity. Experiments further show that this is mainly due to a flow effect.

The newly developed four-wire sensor is a good alternative for three-wire sensor, since the sensor performance is better than a comparable two-wire design. Additionally the sensor is already a two-dimensional sensor. Two of these sensors combine to a very small three dimensional particle velocity sensor. Together with this sensor, a directivity correction method using signal processing is applied. The directivity deviation is smaller than that of earlier designs.

Chapter 4

A silicon pressure sensor based on particle velocity sensing

4.1 Summary

Measurement of the three dimensional sound intensity vector requires besides a three dimensional particle velocity sensor also a sound pressure sensor. Integration of a three dimensional particle velocity sensor has been discussed in the previous chapter. This chapter will focus on integration of a sound pressure sensor on the same chip.

A commercially available sound pressure microphone can be placed close to a three dimensional particle velocity sensor, resulting in a small sound intensity probe. Commercially available sound pressure sensors are of size 2.5 mm diameter and 2.5 mm length [59] and 2.3 * 1.6 * 0.8 mm [60], but for some applications a small integrated design can be advantageous.

The basic particle velocity sensor as discussed in the previous chapter is able to operate over a wide temperature range and in chemically reactive environments, generally known as a 'harsh environment'. There are several cases, e.g. close to or inside an engine exhaust, where a sound field reconstruction or prediction is required. In such situations, a regular sound pressure microphone cannot be used. Standard electret based sound pressure microphones stop functioning above approximately 70 ^oC due to the failure of the electret layer which looses its built in charge at high temperatures. Other types of sound pressure microphones often operate with a built in amplifier that generally stops functioning well above 120 ^oC, since most active elements (semiconductor devices) loose their function at these temperatures.

In this chapter, a sound pressure microphone that uses a particle velocity sensor as a sensing element is presented. This is made possible by using a sound pressure to particle velocity converter, so that sound pressure is converted into particle velocity. The particle velocity signal in the converter due to the pressure fluctuations is measured, thereby indirectly measuring sound pressure. Because the used sensor element and the converter is mechanically stable enough to withstand high temperatures the device can be used up

to temperatures of 300 ^oC.

The total size of the sound intensity probe can be smaller than a separate assembly of particle velocity sensors and a sound pressure microphone. Additionally, the sound pressure sensitive opening is located very close to the particle velocity measuring point. This is crucial for 'single point' measurements. Because of the similar fabrication process of both types of sensors, they can be integrated on the same chip. A fully integrated 3D sound intensity probe is made possible.

4.2 Introduction

A sound pressure microphone measures sound pressure that is a scalar, a perfect sound pressure microphone has therefore an omni-directional response. The use of both particle velocity and sound pressure sensors provides information on the sound field at the measurement spot, such as sound intensity and acoustic impedance. Especially sound intensity is an important value for sound engineers [61].

Sound pressure sensor designs based on the membrane deflection principle are relatively hard to integrate with existing particle velocity sensor designs in terms of clean room fabrication. There are major compatibility problems with the fabrication process, especially in the etching steps of the process. Furthermore, silicon sound pressure sensors based on membrane deflection are commercially available and optimized. Because of this, the road to the integration of membrane based silicon pressure sensors is not taken and a different approach is considered.

A conversion method from sound pressure to particle velocity is described and fabricated. Using this converter allows the use of a particle velocity sensor as transducer for indirectly measuring sound pressure. This sound pressure sensor together with particle velocity sensor(s) creates a sound intensity probe that is solely based on the principle of particle velocity sensors. Using particle velocity sensors for (indirect) measurement of sound pressure has the advantage that there is a good match with the regular particle velocity sensors in terms of stability and temperature dependence, humidity etc. Additionally in both cases the same type of amplifier and signal conditioning can be used. Eventually it is well possible to integrate the two types of sensors in a single silicon chip. Except for the possibility to measure sound intensity another use of such a transducer is measuring sound pressure in a high temperature environment, since the particle velocity sensor can withstand and work at high temperatures.

With the design based on particle velocity sensors the fabrication process is relatively straightforward, since the processes used is very much alike the original process for fabricating particle velocity sensors.

Basically the sound pressure to particle velocity transformer consists of an enclosed cavity with one open end, an increasing pressure will result in an inwards particle velocity and vice versa. A small tube is used as a cavity here. Placing the particle velocity sensor

at the open end seems to be the most obvious, nevertheless the particle velocity sensor can be placed at various locations inside this tube. Placement elsewhere than the open end can have some advantages regarding frequency response. It is furthermore possible to create a damped tube or a tube with different shapes to suppress standing waves in the tube. By doing this a different transfer function is obtained. A well defined transfer function is crucial if the sensor is used for measurement purposes, so special attention is paid to design a response characteristic that is as flat as possible, thereby keeping the sensitivity as high as possible.

Below the results of different designs, prototypes and measurements are discussed.

4.3 The Helmholtz realization

When pressure at the entrance of a cavity increases, air is forced into the cavity and the pressure inside increases. Once the external pressure that forces the air into the cavity lowers, the now higher-pressured air inside will flow out through the channel again. By measurement of the particle velocity at the entrance of the tube the variations in pressure are indirectly measured. For the small structures that we will be dealing with, the wavelength of sound is typically much longer than the dimensions of the structure, so that we can safely assume that the pressure will be equal everywhere inside the volume of air.

A tube that is terminated by a volume of air creates a so-called Helmholtz resonator. When due to a sudden pressure increase outside the cavity air is forced in to the cavity is attains a certain speed, depending on the area of the opening and the volume of the cavity. Due to inertia of the air in the entrance of the cavity the pressure reaches a slightly higher pressure. Due to this pressure difference the air flows out again resulting in a slightly lower pressure. This process repeats itself at the resonance frequency of the device but with a diminishing amplitude due to damping effects. When measuring particle velocity in the entrance there is a higher sensitivity to pressure fluctuations at this resonance frequency.

4.3.1 Theory

In order to calculate the resonant frequency of a tube of length l terminated with a volume V, we first calculate the mass of the air inside the tube with cross-sectional area A:

$$m = \rho l A \tag{4.1}$$

with ρ the density of air. The value of Δp is the variation in pressure due to the sound waves. A movement of the volume V of air by a distance x inside the tube results in a variation in density (and so a variation in pressure) inside the volume:

$$\frac{\Delta p}{p_0} = \kappa \frac{\Delta v}{v_0} = \kappa \frac{Ax}{V} \tag{4.2}$$

with p_0 the initial (atmospheric) pressure, v the speed of the air in the tube, and κ the bulk modulus, which can be described as $\kappa = \gamma p_0$ with the ratio of specific heats $\gamma = C_p/C_v$ of air. The change in sound pressure results in a net restoring force given by:

$$F = -A\Delta p = \kappa \frac{A^2 x p_0}{V} \tag{4.3}$$

We can now easily derive the resonance frequency by applying Newton's second axiom:

$$m\frac{d^2x}{dt^2} = F \tag{4.4}$$

and inserting (4.1) and (4.3) for the mass and restoring force:

$$\frac{d^2x}{dt^2} = -\frac{\kappa}{\rho} p_0 \frac{A}{Vl} x \tag{4.5}$$

It follows that the resonance frequency is given by:

$$f_0 = \frac{\omega_0}{2\pi} = \frac{1}{2\pi}\sqrt{\frac{\kappa}{\rho} p_0 \frac{A}{Vl}} = \frac{c}{2\pi}\sqrt{\frac{A}{Vl}} \tag{4.6}$$

with c the speed of sound.

$$c = \sqrt{\frac{\kappa}{\rho} p_0} \tag{4.7}$$

To get an impression of dimensions: a tube with a diameter of 5 mm and a length of 7 mm ends in an enclosed volume of one cubic centimeter of air has a resonance frequency in the order of 2.9 kHz.

4.3.2 Measurements

A test setup was realized in which a particle velocity sensor is placed inside the entrance tube of the Helmholtz resonator [62]. The enclosed volume was made variable by means of a piston. Figure 4.1 shows a photograph of the setup. The frequency response of the particle velocity sensor inside the tube was compared with the response of an unpackaged sensor (in the free field). Figure 4.2 shows the result. The influence of the resonator is clearly visible through the peak observed at 3 kHz. Note that the absolute value of the sensitivity of the two devices cannot really be compared since the unpackaged sensor is sensitive to particle velocity whereas the Helmholtz resonator is sensitive to pressure variations.

The difference between a device being sensitive to particle velocity and a device that is sensitive to sound pressure becomes clear in a standing wave tube. Inside a standing wave tube and at a certain frequency, there are certain positions with a maximum sound pressure. At these places there is a minimum value of particle velocity and vice versa. Figure 4.3 shows a measurement again comparing the Helmholtz resonator with an unpackaged particle velocity sensor. The device is clearly sensitive to sound pressure and less to particle velocity, although the minimum (pressure) and maximum (particle velocity) values in the two curves do not perfectly coincide. An explanation besides a not perfectly functioning transducer is a slight misalignment of the sensors in the standing

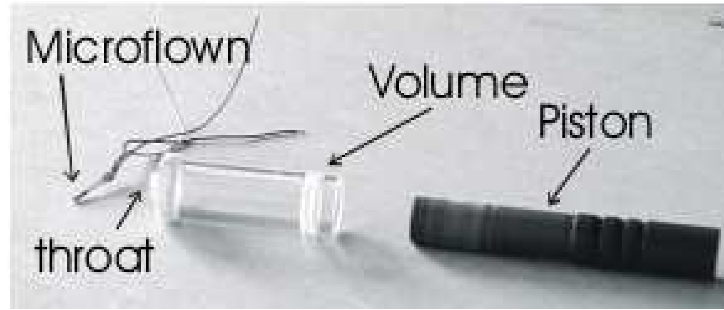

Figure 4.1: *A photograph of a Helmholtz resonator with a particle velocity sensor mounted in the entrance tube. The volume enclosed is 1 cm^2.*

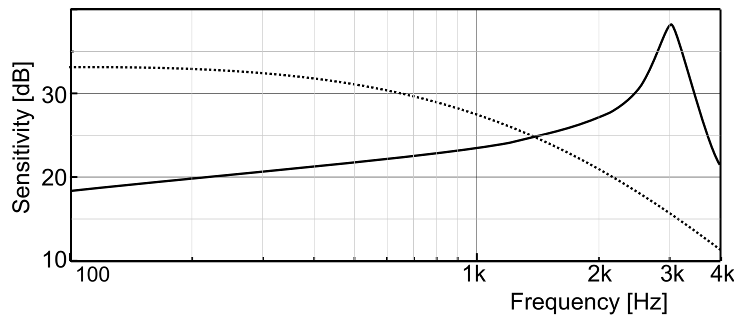

Figure 4.2: *Frequency response of an unpackaged particle velocity sensor (dotted line) and a similar sensor placed in the entrance tube of a Helmholtz resonator. Both devices are placed in the standing wave tube where a clear distinction between pressure and particle velocity exists. This measurement proves that the device is sound pressure sensitive.*

wave tube. Additionally, a disturbance in the standing wave pattern due to the presence of the bulky Helmholtz resonator can have influence. A particle velocity signal travels just past the opening of the entry tube of the device, and can still influence the particle velocity sensor so that the sensor is somehow a little sensitive for particle velocity.

4.4 A standing wave tube

4.4.1 Response of an undamped standing wave tube

A standing wave tube can be used for calibration of both sound pressure sensitive devices as well as particle velocity devices, see for a detailed explanation [12] or [45]. Figure 4.4 shows a schematic drawing of a standing wave tube setup. It consists of a tube that is rigidly terminated at $x = l$, and driven by a vibrating piston at x=0. For frequencies lower than the so-called cut off frequency, the vibrating piston generates a sound wave inside the tube that can be approximated by a plain wave. Above the cut off frequency, standing waves can occur perpendicular to the propagation direction. The cut off frequency for a cylindrical tube is given by [63]:

$$f_c = \frac{c}{1.71 \cdot d} \tag{4.8}$$

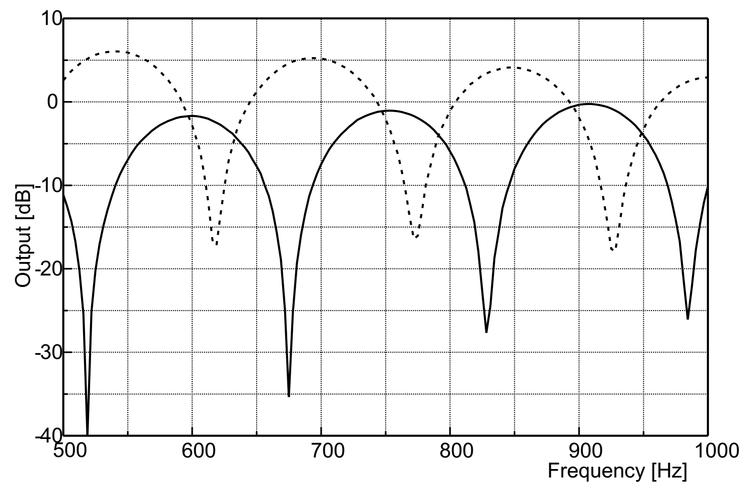

Figure 4.3: *Frequency response of an unpackaged particle velocity sensor (dotted line) and a similar sensor placed in the entrance tube of a Helmholtz resonator, both measured inside a standing wave tube.*

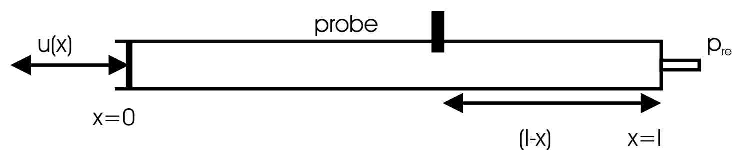

Figure 4.4: *A standing wave tube that is rigidly terminated at $x = l$ and in which air is driven at $x = 0$.*

with d the diameter of the tube. For tubes with a square cross section this is a little different:$f_c = \frac{c}{2 \cdot d}$ with d the length of a side. The graph in Figure 4.5) illustrates this.

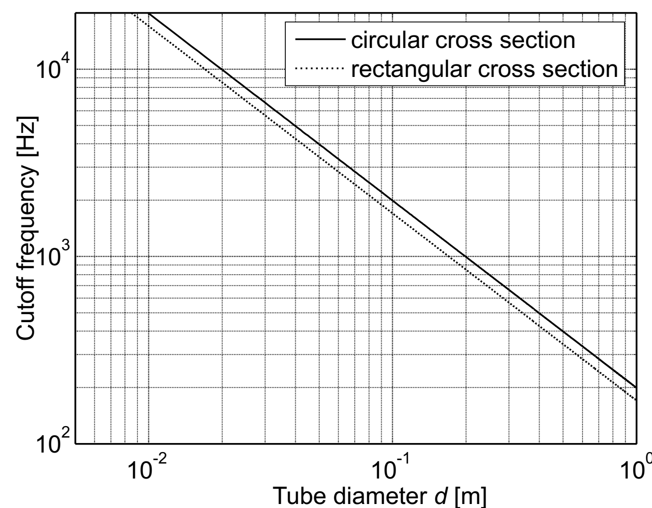

Figure 4.5: *Illustration to equation* (4.8).

Below the cut off frequency, the solution to the wave equation can be represented as a superposition of the complex sound pressure associated with plane waves traveling in the positive and negative direction. This can be written as follows:

$$p(x,t) = p_0(Ae^{-ikx} + Be^{ikx})e^{i\omega t} \tag{4.9}$$

With A and B arbitrary complex numbers representing the amplitude and relative phase of the traveling waves. Using the conservation of momentum,

$$\rho\frac{\partial u}{\partial t} = -\frac{\partial p}{\partial x} \tag{4.10}$$

and given that $c = \omega/k$, the associated particle velocity (in the x-direction) can be obtained:

$$u(x,t) = \frac{1}{\rho c}p_0(Ae^{-ikx} - Be^{ikx}) \cdot e^{iwt} \tag{4.11}$$

At the rigidly terminated end of the tube ($x = l$) the particle velocity must be zero. At the open end (at $x = 0$) the particle velocity is u_0. From this the constants A and B can be found. Since $u(l) = 0$,

$$Ae^{-ikl} = Be^{ikl} \tag{4.12}$$

And $u(0) = u_0$

$$A - B = u_0 \cdot i\rho c \tag{4.13}$$

Combining eq.(4.12) and eq.(4.13) results in a solution for A and B :

$$A = -iu_0\rho c\frac{e^{ikl}}{2sin(kl)} \quad B = -iu_0\rho c\frac{e^{-ikl}}{2sin(kl)} \tag{4.14}$$

Combining this with (4.11) and omitting the time dependent results in a solution for amplitude of the the particle velocity:

$$u(x) = u_0\frac{sin(k(l-x))}{sin(kl)} \tag{4.15}$$

From the conservation of momentum (4.10) the sound pressure can again be calculated:

$$p(x) = -i.\rho c u_0\frac{cos(k(l-x))}{sin(kl)} \tag{4.16}$$

If the particle velocity sensor is positioned at a place x in the tube, the ratio of sound pressure and particle velocity, which is the acoustic impedance Z_a, is given by:

$$Z_a = \frac{p(x)}{u(x)} = -i\rho c.\frac{cos(k(l-x))}{sin(k(l-x))} = -i\rho c \cdot cot(k(l-x)) \tag{4.17}$$

A sound pressure fluctuation at position $x = 0$ at the entrance of the tube results in a particle velocity signal in the tube. The particle velocity signal at $x = 0$ is related to the sound pressure at $x = 0$ by the inverse acoustic impedance of the tube Z_a^{-1}:

$$Z_a^{-1} = \frac{u(0)}{p(0)} = \frac{i}{\rho c} \cdot \frac{sin(kl)}{cos(kl)} = \frac{i}{\rho c} \cdot tan(kl) \tag{4.18}$$

This inverse impedance varies from zero to infinity as function of k and so does the frequency response of the system. If the particle velocity sensor is positioned half way the tube, the ratio between the sound pressure (at the open end of the tube) and the particle velocity is given by:

$$\frac{u(\frac{1}{2}l)}{p(0)} = \frac{i}{\rho c} \frac{sin(\frac{1}{2}kl)}{cos(kl)} \tag{4.19}$$

This transfer function does not have the zero sensitivity point at 4.5 kHz, see figure 4.6. A disadvantage of this arrangement is that the transfer function, and thus the sensitivity, is about 10 dB lower at lower frequencies for tubes of the same length.

For tubes with a proposed length of 38 mm the configuration with the particle velocity sensor at the entrance of the tube is preferable for low frequency applications and the configuration with the particle velocity sensor half way the tube is more suited for higher frequencies. For shorter tubes the frequency response is shifted to a higher frequency.

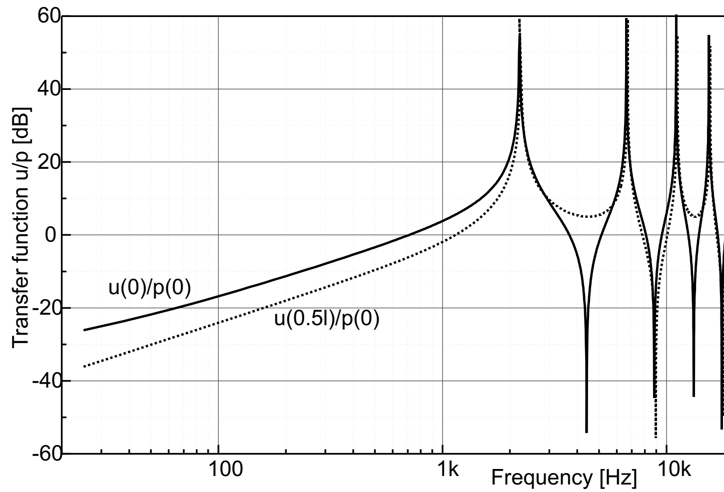

Figure 4.6: *Transfer function u(x)/p(0) for a tube with length L=38mm with at sensor at the open end of the tube (u_0/P_0) and halfway ($u_{0.5l}/P_0$) the tube.*

Temperature sensitivity

The sensitivity of the particle velocity sensor element is barely temperature dependent (less than 0.02 dB/K, see [64], the particle velocity sensor) and the temperature sensitivity of the sound pressure microphone mainly depends on the temperature sensitivity of the acoustic impedance. Initial measurements show that the working temperature of a particle velocity sensor element can be up to 300 degrees centigrade. The temperature dependence of the several constants in the equation of the acoustic impedance is given by:

$$c = \sqrt{\kappa RT} \qquad \rho = \frac{P_0}{RT} \qquad k = \frac{2\pi f}{c} \tag{4.20}$$

With c the speed of sound, κ is the adiabatic index (1.402 for air), R is the universal gas constant (287 J/(kgK) for air), T is the absolute temperature in Kelvin and P_0 the ambient pressure (100 kPa).

Open end correction

A tube of a certain physical length behaves acoustically as if it were longer than this length. This phenomenon is due to mass loading of the tube in the form of an air column protruding out of the tube at the open end. From [65] this correction between the physical length and the acoustical length is exactly equal to 0.41 times the diameter of the tube. Due to the effect of objects in the open end of the tube (e.g. a sensor device) the acoustical length may differ a little from what is stated above.

Maximum attainable sensitivity

The maximum sensitivity of such a sound pressure to particle velocity converter would theoretically be two times the sound pressure divided by ρc. This can be attained by placing a particle velocity sensor inside a small opening in a rigid wall. The value ρc is simply the acoustic impedance of the air, the factor two is due to the pressure doubling against a rigid wall, for this the size of the wall must be much larger than the acoustic wavelength. Both sides of the wall are assumed isolated from each other except for the hole where the sensor is in.

4.4.2 Damping effects

Sound is damped by the air itself but also due to interaction with other materials. Damping inside a tube is due to viscous friction and thermal effects. Effects due to friction of (moving) air against the (stationary) walls of the tube are generally called viscous friction. In a small region near the wall there is a transition area between the non-moving particles at the wall and the moving particles at a larger distance from the wall. Between these points the viscosity of air accounts for damping inside the tube. The distance over which the particle velocity speed gradually increases from zero to the applied particle velocity speed is in the range of hundreds of microns to millimeters, depending on the frequency of the movement [66].

Sound in the free field is assumed to be an adiabatic process, or a process without heat transfer. Between two points of a different pressure there is a thermal difference as well. For acoustic propagation in air the heat transport between a high and low pressure point is negligible, and therefore the process is called adiabatic. Near surfaces of a material with a relatively large heat capacity compared with the heat capacity of the air or large heat conductivity, the walls can be assumed to be at a constant temperature. At the walls the process is therefore not adiabatic, but isothermal. The region over which this is the case is generally small compared to the total volume of moving air and in the case of

large tubes there is no noticeable influence of damping. [44].

When narrowing the tube the effect of the isothermal layer at the walls is becoming large compared with the total volume of air. So when using small tubes the acoustic process is not adiabatic anymore. For the 3mm wide tubes as used in the prototypes of the pressure to particle velocity transformers, and for audible frequencies, the damping effect does not play a significant role, but when using smaller tubes it will. To find an expression for the damping inside the tube a propagation coefficient is included in the propagation of sound in the standing wave tube.

From the solution of the one dimensional Helmholtz equation [48] one can write for the pressure inside the tube:

$$p(x,t) = p_0(Ae^{-\Gamma kx} + Be^{\Gamma kx})e^{i\omega t} \tag{4.21}$$

with again x the distance to the open end of the tube. The propagation coefficient Γ can be described as follows; when it is the purely imaginary unit i there is no damping inside the tube. This approximates measurement results roughly when using tubes with large diameters. For κ with a real part $\neq 0$ the real part gives the amount of damping.

Using the one dimensional equation of conservation of momentum (4.10) one can find the particle velocity u.

$$u(x,t) = \frac{-i\Gamma}{\rho c} p_0(Ae^{-\Gamma kx} - Be^{\Gamma kx})e^{i\omega t} \tag{4.22}$$

With $c = \omega/k$. Note that for $\Gamma = i$ the equation reduces to (4.11).

Similar to the case with the tube without damping the constants A and B are solved.

$$Ae^{-\Gamma kl} = Be^{\Gamma kl} \tag{4.23}$$

And $u(0) = u_0$

$$(A - B) = u_0 . \frac{i\rho c}{\Gamma} \tag{4.24}$$

Combining eq.(4.23) and eq.(4.24) results in :

$$B(e^{2\Gamma kl} - 1) = u_0 \frac{i\rho c}{\Gamma} \tag{4.25}$$

And A and B are solved.

$$A = u_0 \frac{i\rho c}{\Gamma} \frac{e^{\Gamma kl}}{2sinh(\Gamma kl)} \qquad B = U_0 \frac{i\rho c}{\Gamma} \frac{e^{-\Gamma kl}}{2.sinh(\Gamma kl)}; \tag{4.26}$$

Which gives with (4.22) for the particle velocity amplitude at position x:

$$u(x) = u_0 . \frac{-i\Gamma}{\rho c} . \frac{i\rho c}{\Gamma} \left(\frac{e^{\Gamma k(l-x)} - e^{-\Gamma k(l-x)}}{sinh(\Gamma kl)} \right) = u_0 \cdot \frac{sinh(\Gamma k(l-x))}{sinh(\Gamma kl)} \tag{4.27}$$

For the sound pressure signal a similar approach can be followed, or alternatively a solution can be found from (4.27) with the equation for the conservation of momentum:

$$p(x) = u_0 \frac{i\rho c}{\Gamma} \left(\frac{cosh(\Gamma k(l-x))}{sinh(\Gamma kl)} \right) \tag{4.28}$$

When $\Gamma = i$ the solution for the sound pressure in a tube without damping (as in equation (4.16)) is obtained.

For the acoustic impedance at x in the tube the solution is then:

$$Z(x) = \frac{p(x)}{u(x)} = \frac{i\rho c}{\Gamma} . \frac{cosh(\Gamma k(l-x))}{sinh(\Gamma k(l-x))} = \frac{i\rho c}{\Gamma} . \frac{1}{tanh(\Gamma k(l-x))} \tag{4.29}$$

The sound pressure to particle velocity converter works by transforming the pressure at position $x = 0$ to particle velocity. A particle velocity sensor at location x therefore has an output signal due to the sound pressure at $x = 0$ and the effect of the transformer. The relation between the sound pressure at point $x = 0$ and the particle velocity at some point x is described by a transfer function S.

$$S(x) = \frac{u(x)}{p(0)} = \frac{\Gamma}{i\rho c} \frac{sinh(\Gamma k(l-x)}{cosh(\Gamma kl)} \tag{4.30}$$

The relation between particle velocity and sound pressure for a freely propagating wave is described by the specific acoustic impedance ρc. For the propagation inside a tube the acoustic impedance is altered. The acoustic impedance for the tube is evaluated by the Kirchhoff approximation or the LRF-approximation [48]. In equation 4.30 the acoustic impedance is the part $\frac{\Gamma}{i\rho c}$ which is replaced by $\frac{G}{\rho c}$ for use with the models.

The Kirchhoff approximation for damping inside circular tubes

The Kirchhoff approximation for damping in circular tubes is a helpful design tool for estimating damping inside circular tubes. The approximation is valid for shear wave numbers much larger than one. The Kirchhoff approximation for damping in small circular tubes uses for the damping coefficient:

$$\Gamma = i + \frac{i+1}{\sqrt{2}} (\frac{\gamma - 1 + \sigma}{s\sigma}) \tag{4.31}$$

with s the shear wave number and γ the ratio of specific heats C_p/C_v of air. The following equation shows that the shear wave number is based on the characteristic length of the cross section l, in the case of a tube with a circular cross section this is equal to the radius r, and μ is the dynamic viscosity of air.

$$s = l\sqrt{\frac{\rho_0 \omega}{\mu}} \tag{4.32}$$

Sigma (σ) is here the square root of the Prandtl number, which in its turn is a function of the specific heat at constant pressure C_p, the dynamic viscosity μ and the thermal conductivity λ.

$$\sigma = \sqrt{\frac{\mu C_p}{\lambda}} \tag{4.33}$$

This model is only appropriate for circular tubes. However, for tubes with other cross sectional shapes it can still approximate the damping well enough to be useful as a design rule. Other cross sectional shapes are for example square shapes with sides r, a tube with this cross section can be approximated by the Kirchhoff approximation model taking the diameter d equal to the length of a side r.

A coefficient depending on the cross section is introduced in the impedance equation, which brings the particle velocity signal due to a pressure fluctuation at $x = 0$ to [48]: note[0]

$$S(x) = \frac{u(x)}{p(0)} = \frac{G}{\rho c} \cdot \frac{sinh(\Gamma k(l-x)}{cosh(\Gamma kl)} \tag{4.34}$$

With for the coefficient $G = \frac{i}{\Gamma}$ for the Kirchhoff approximation.

For a number of different cross sections the damping effect on the response of the tube is shown in the Figure 4.7. For high damping values the response of the tube is more smooth, the less damping the more the resonance peaks are present. The length of the tube was set to 14 mm.

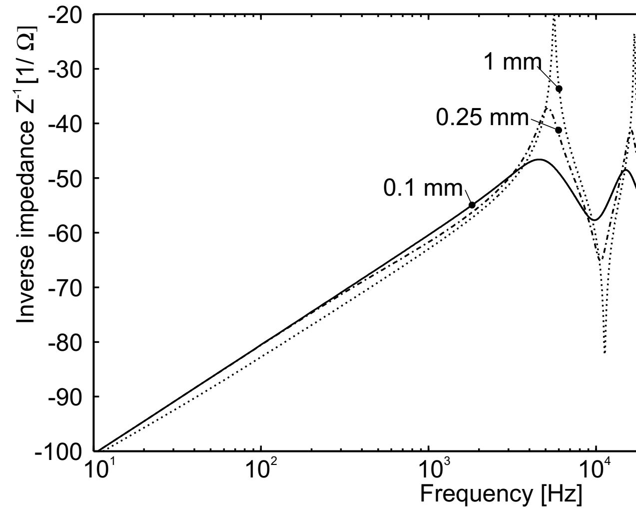

Figure 4.7: *Comparison of different tube diameters for the Kirchhoff solution.*

[0]the sign differs from the solution presented in [48], due to the definition of $p(x) = Ae^{-\Gamma kx} + Be^{\Gamma kx}$ instead of $p(x) = Ae^{\Gamma kx} + Be^{-\Gamma kx}$

The Low Reduced Frequency model for damping inside tubes with a rectangular cross section

For the LRF-model the values of the propagation coefficient Γ are obtained by a numerical method described in appendix B.

For the cross-section dependent coefficient is $G = -i\Gamma F(\frac{\mu}{\rho_0})$. From equation (4.34) the response can be evaluated. In the appendix the function $F(\frac{\mu}{\rho_0})$ is described. Only the solutions for rectangular cross sections are described, since the MEMS devices presented here below are have a rectangular cross section. For circular cross sections and shear wave numbers well below 1, the Kirchhoff model gives a good approximation.

Practical use of the models

When designing the sensor it is useful to have a model for the acoustic impedance of the tube, since the response of the system is largely dependent on it. Take the case that the particle velocity sensor has typically low pass behavior. With the use of a small tube with resonance frequencies tuned to the response and (tuned) damping inside the tube the response of the particle velocity sensor sensor can be adjusted to a more flat response, therefore the correction of the response can be simpler or even omitted.

For the designs described here and the use of the damping models there are some remarks though. Inside the tube a particle velocity sensor is placed, which disturbs the sound field inside, and the designs can have a cross section that is not fully constant over their length. Theory does not account for this for the following reason: firstly modeling is becoming increasingly complex, and secondly the model is used to predict roughly the damping inside a tube.

After fabrication the sensor is to be calibrated, and the response can still be corrected afterward by signal processing.

4.5 Prototype construction

A prototype is constructed to verify the theoretical results. For the construction of the converter two tubes of steel with lengths of 38 mm and 58 mm and an inner diameter of 3 mm are used. One end is closed with a steel rod and at the other (open) end of the tube a particle velocity sensor is placed. The particle velocity sensor is mounted on a carrier board to make the connections to the measurement amplifier and the carrier board is placed in the tube. in figure 4.8 the prototype is shown.

4.5.1 Measurement results

To test if the device works as expected several experiments have been carried out. The sensitivity of a sound pressure sensitive device should not be dependent on the orientation of the probe. In an anechoic chamber the probe was rotated with a stationary sound source to check the directivity. For the sound pressure transducer the most important property is that it is indeed sound pressure sensitive. In a standing wave tube the difference between sound pressure and particle velocity is distinct; this can be used to check the sound

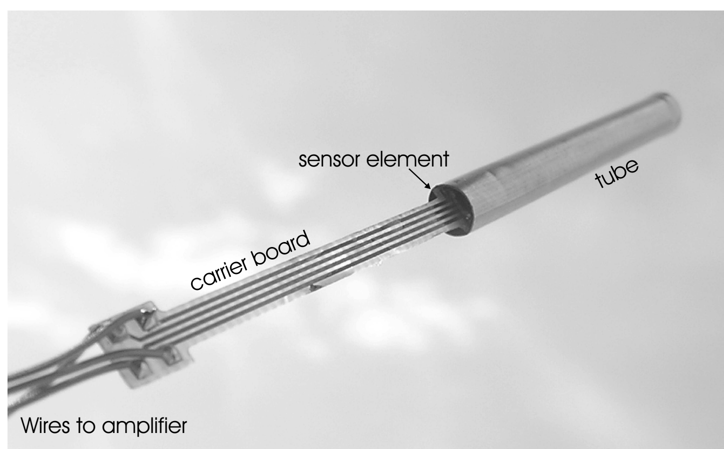

Figure 4.8: *First prototype of the SWT sound pressure to particle velocity converter.*

pressure sensitivity of the device. Finally the Frequency response has been obtained and compared with theory.

Polar pattern measurement

Sound pressure is a scalar value, in theory this sound pressure microphone must have an omni directional sensitivity. Inside an anechoic room with one sound source the sound must be purely directional, so when the device is rotated in such environment the response must stay constant. The measurement is performed by rotating over two axes in 96 steps (rotation over a and b as depicted in figure 4.9).

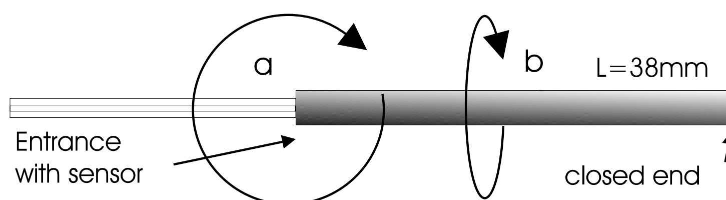

Figure 4.9: *The two axes of the directivity measurement.*

The measurements show that sensitivity is nearly independent on the orientation of the tube; the sound probe under test shows to be omnidirectional, see Figure 4.10. Mostly due to imperfections in the anechoic room the polar pattern is a little 'wobbly', this is so random that this can not be caused by directionality effects of the sensor at the measured frequencies, but is due to an imperfect anechoic room and acoustic disturbances.

Frequency response

Measurements of the frequency response are performed with the sensor placed close to a reference microphone. The calculated distance between the terminated end and the particle velocity sensor is 38.0 mm while the distance from acoustical measurement is 38.5 mm; the small deviation may partly be explained due to the mass loading of the

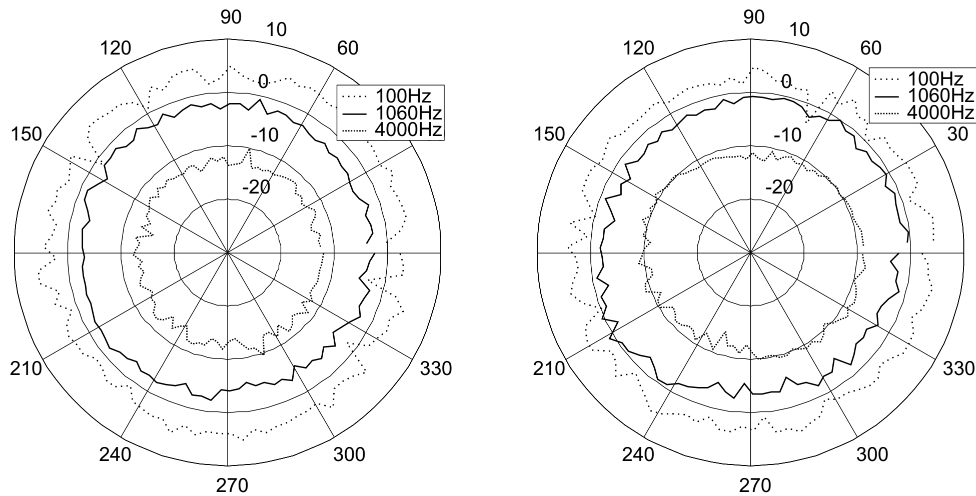

Figure 4.10: *Polar plots of the device (logarithmic scale).*

open end, which should theoretically be responsible for an acoustically 0.41 * 3 mm longer tube. The limited precision in mounting gives additional errors, still the result is as expected. Another tube was mounted and measured. With this tube the actual and calculated length was 58 mm. The theoretical (without damping) inverse acoustic impedance of the tube is shown in Figures 4.11 and 4.12, the dotted lines. It is observed that the measurement results are quite similar, with a small frequency shift between the location of the peaks.

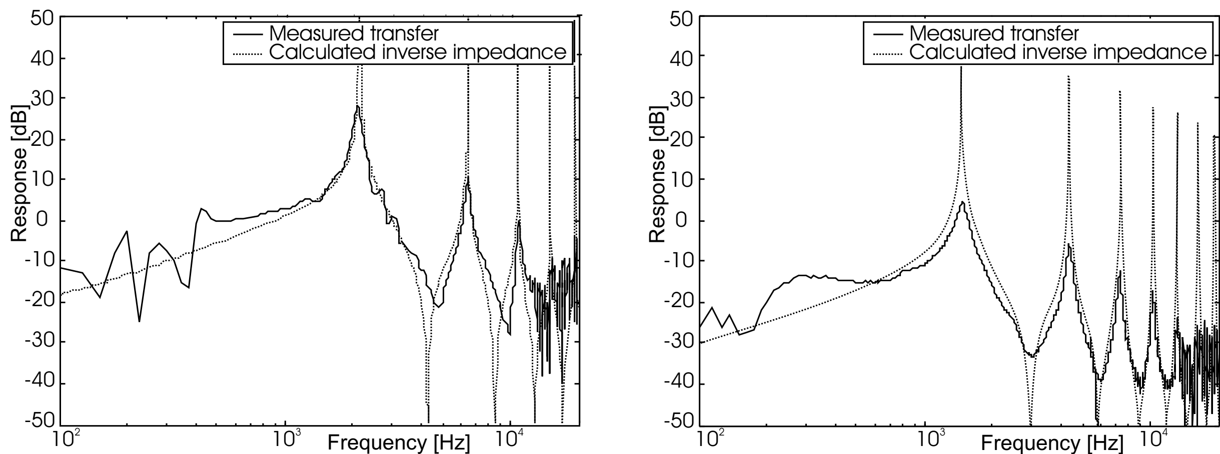

Figure 4.11: *The frequency response of a particle velocity sensor mounted at the open end of a 38 mm (left) and a 58 mm tube (right).*

Signal to noise ratio

Apart from the frequency response, the equivalent acoustical noise of the sensor is measured to be able to compare the sensor to regular sound pressure microphones. In a silent environment the electrical output signal is measured. This is the noise level and is measured in 1 Hz bandwidth. Compared with a frequency response (the sensitivity of the

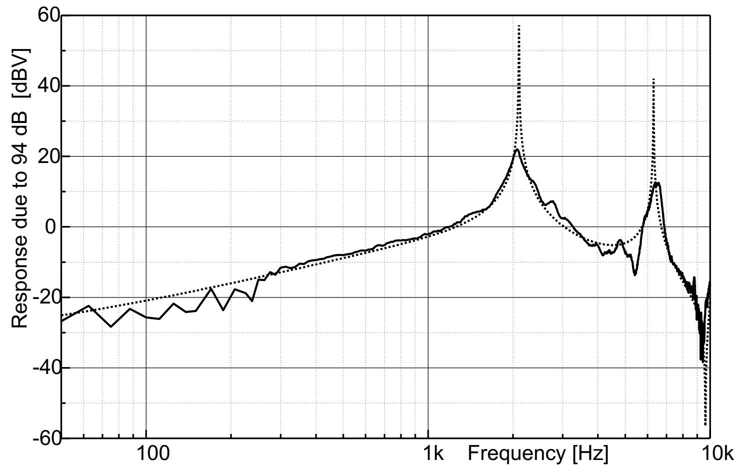

Figure 4.12: *The frequency response of a particle velocity sensor mounted at the middle of the 38 mm tube (dotted line model, black line measurement result).*

microphone as function of the frequency) the equivalent self noise level can be determined. The self noise of a sensor is given by the 94dB reference level minus SNR, where SNR represents the signal(in dB) due to 94 dB minus the noise level (in dB). In Figure 4.13 the signal, noise and signal-to-noise levels are shown.

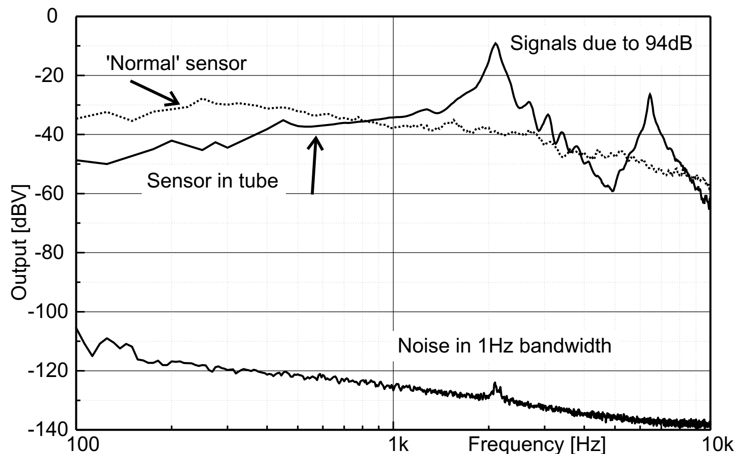

Figure 4.13: *Signal of regular particle velocity sensor, the 38mm device (particle velocity sensor at the open end of the tube) and the noise of both.*

A regular sound pressure microphone has a SNR larger than 100 dB at 1 kHz and excitation at 94 dB and the device has an SNR between 60 and 90 dB (120 dB at resonance frequency). Regarding noise level and frequency characteristic the sensor might not be useful for audio recording of music or speech. For measurement purposes the noise level is of less importance because averaging and cross spectral measurements can be done, for example for intensity measurements the cross spectrum of the sound pressure and the velocity signal is determined. Taking the cross spectrum of two sensor signals reduces the effect of uncorrelated noise significantly [11].

Additionally this type of probe is quite resistant to elevated temperatures, and can be used nearby hot (and noisy) objects like engines and exhausts. At these places the sound level is generally high, so the high selfnoise is not problematic here.

4.5.2 Sound pressure sensitivity measurement

Up to a certain frequency (for the used tube: f_{max}=4.2 kHz) in a standing wave tube the difference between sound pressure and particle velocity is distinct. At a point and frequency where the sound pressure is maximum, the particle velocity is minimum and vice versa. So from the frequencies where the maximum and the minimum in response occur it can be derived if the sensor is sound pressure sensitive or particle velocity sensitive. A steel tube of 70 centimeters is used with a reference microphone at one end, the 38 mm sound probe under test together with a particle velocity sensor and a reference particle velocity sensor at one third of the tube and a loudspeaker is used as sound source. Transfer functions of both reference sensors and the sound probe under test clearly show that the device is not sensitive to particle velocity but only to sound pressure variations.

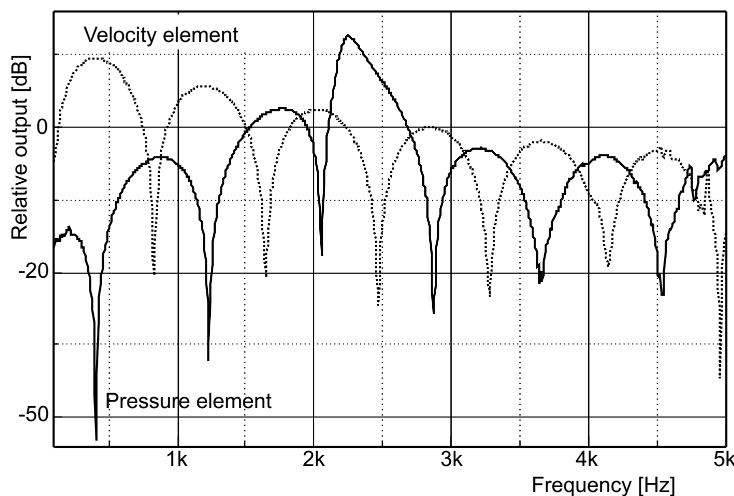

Figure 4.14: *The transfer function between a reference sound pressure sensor and a reference particle velocity probe and the sound pressure sensor under test clearly shows that the device is only sensitive to pressure variations.*

4.5.3 Temperature measurements

The velocity sensor was tested up to 300 ^{o}C (573 K) and functioned properly. The self noise did not increase significantly (less than 3 dB). This is because the noise of the particle velocity sensor is caused by thermal noise. The change in sensitivity of the velocity sensor element was measured to be 5 dB over a 300 K (0.017 dB/K) temperature range.

4.6 Integration into a MEMS sensor

A three dimensional sound intensity probe (i.e. the particle velocity sensor in three dimensions and a sound pressure microphone) has been made in silicon: see Figure 4.19 Simulation of the design has been used to optimize the design.

4.6.1 Design

As described before in section 4.4.2 the package may be used to tune the response of the system such that a more flat response is obtained. An attempt to do this is depicted in Figure 4.15. Theory of modeling of the response of the sound pressure to particle velocity converter is studied. With this model the converter can be simulated first and so an optimum converter can be designed. First of all there are a number of design rules, such as that the size of the converter must be as small as possible, or must extend into the carrier board. In this design it is chosen to keep the converter on the chip only. Next it is desirable to have a frequency response that has a small frequency dependency, or has at least a well defined response. The dimensions of the tube are chosen such that it can be integrated in the final design. A width of 1.5 mm is determined by the length of the sensor wires, short sensor wires have a negative effect on the performance of the sensor in terms of noise level. Inner height from almost zero up to 0.4 mm would be a feasible choice here. Higher tubes would require multiple wafer stacking.

The particle velocity element has a low pass filter characteristic, which can be successfully approximated by a second order low pass filter. Since this element is inside the converter the responses of both the converter and the element have an effect on the response of the device. Fortunately the converter has a transfer function that increases with frequency for frequencies below resonance. Combining these effects leads to a more flat frequency characteristic. In Figure 4.15 the effect of combining the transfer function of the particle velocity sensor with the response of the sound pressure to particle velocity transformer is shown. For a frequency range between 400 Hz and 3 kHz the response can be tuned to an almost frequency independent characteristic (less than 3 dB). With damping included, the response becomes even smoother, especially the large resonance peak vanishes.

When the frequency response of the particle velocity sensor element is estimated and superposed on the acoustic impedance of the tube this gives a fair estimate of the expected response of the complete sensor. This is used to design the final sensor. In Figure 4.16a the effect of the tube length with the estimated response of the particle velocity sensor is observed. Damping is here left out. Clearly there is a consideration between sensitivity and 'flatness' of the response. Here the importance of the sensitivity is chosen over the flatness, because the sensitivity of the element is already low compared with regular sound pressure sensors. Due to this tubes shorter than 10 mm are discarded.

One could choose a tube with length of 10 mm, because of the good flatness and relatively good sensitivity. However, the tube with length of 15 mm has 4 dB extra sensitivity at low frequencies and the frequency response does not decrease before the resonance peak,

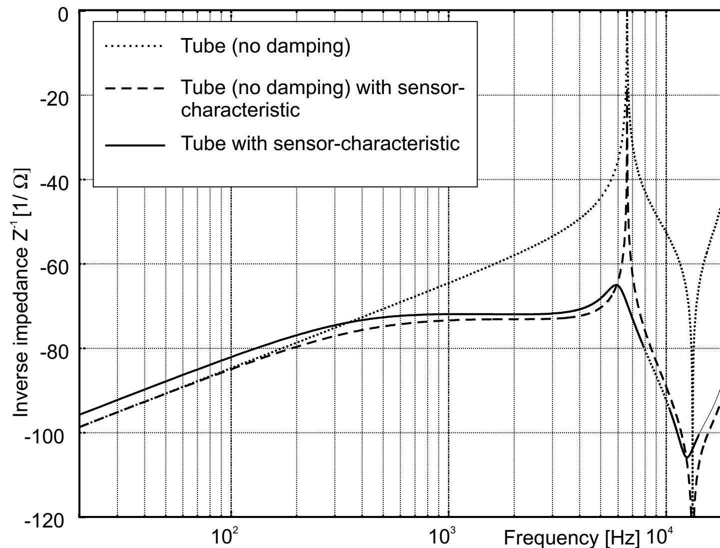

Figure 4.15: *The inverse acoustic impedance with and without damping and the particle velocity sensor response of the proposed tube.*

in contrast to the tube of 10 mm length. For low frequency applications a longer tube can be chosen, this results in higher sensitivity. Operation at frequencies higher than the resonance frequency is not considered here, since the frequency characteristic is varying sharply here. Next the influence of damping is investigated. The width of the entrance opening is fixed at 1.5 mm, which is equal to the length of the particle velocity sensor wires. Sensor wire length can be adjusted but is kept at this length because of the predictive behavior of this configuration. Looking at the result '1 mm', which represents thus a rectangular cross section of 1.5 mm width and 1 mm height, the amount of damping is still not too high and therefore the resonance peak of the sensor is pronounced. With decreasing height of the tube the damping becomes higher and at 0.1 mm height the frequency range is even limited. A slightly higher value of 0.15 mm seems to be a perfect value.

Translated to fabrication possibilities, the precision must be quite high, since the back chamber is to be mounted manually on top of the sensor with epoxy glue, which in its turn lifts the cap a little and increasing the height. For this the error range is high compared with the height of 0.15 mm, to be able to compare the theory more successfully with experiments the height is chosen as 0.25 mm, with a deviation of 0.05 mm. The damping associated with this height still is fairly good so resonance is fairly well suppressed. Another reason to choose a little higher tube is that the particle velocity sensor sensitivity is much less predictable when the wires are very close to an other object; normally the sensor wires are located at least 0.25 mm from the nearest object.

4.6.2 Final discussion of the design

The sound pressure part of this probe is made with the approximate dimensions derived from the simulations above, with an approximate length of 14 mm in a small meandering

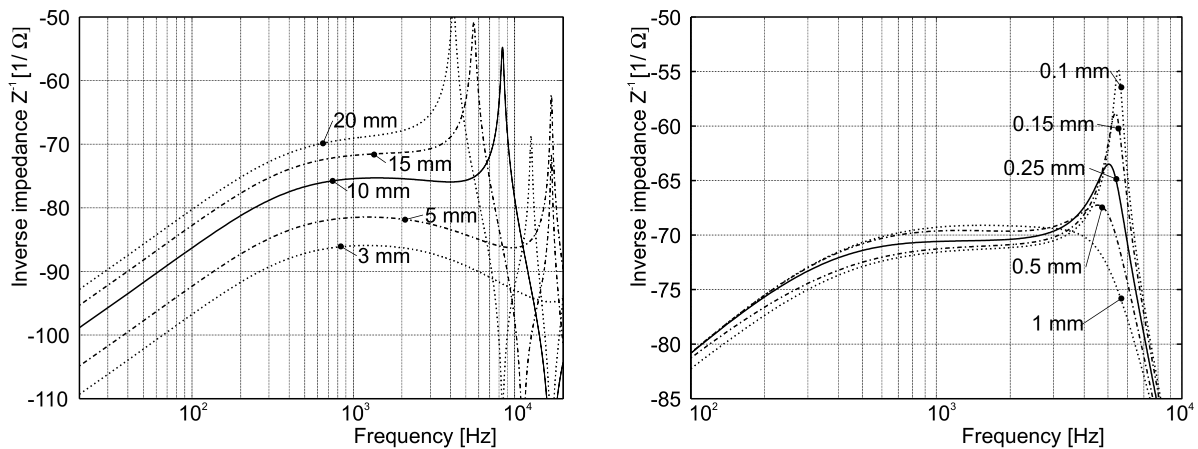

(a) *The effect of tube length on the frequency response.*

(b) *The effect of damping on the frequency response.*

Figure 4.16: *Design choices regarding the length of the tube and damping inside the tube.*

tube and a cross sectional area of 0.25 height *1.5mm width. Schematically this looks as shown in Figure 4.17

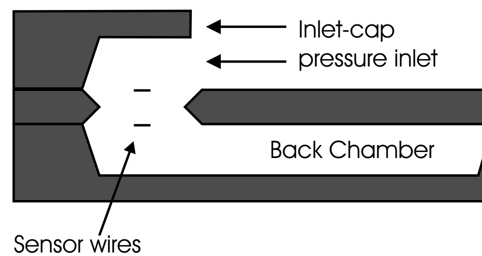

Figure 4.17: *A schematic representation of the tube.*

The sound pressure inlet is a small rectangular hole at the upper part of the device, see Figure 4.18a. A hollow cap with a meandering tube is glued at the back side. This cap forms the standing wave tube, see Figure 4.17. The sensor wires of this sound pressure probe are found at the top and bottom of the sound pressure inlet.

4.6.3 Fabrication and assembly of the sensor

The sound pressure sensor is made in the standard process described in chapter 5, and the back chambers are processed by patterning a silicon wafer with photo resist foil and powder blasting of a cavity in silicon, see chapter 5, following which the chambers are diced so that one cavity remains, see Figure 4.18b.

Both a back chamber and a sound pressure inlet are made using this method. The back chambers are glued manually to the chip. Figure 4.19a shows the sensor chip with back chamber and 4.19b shows the other side with the sound pressure inlet which is inside the inlet cap.

After mounting the caps the whole element is mounted on a carrier printed circuit board to provide a usable sensor element. The pair of sensor wires for the sound pressure element is just as with the particle velocity elements connected in series and powered with a low noise voltage supply; the series signal is amplified with a low noise transistor amplifier to obtain a reasonable signal level suitable for further processing.

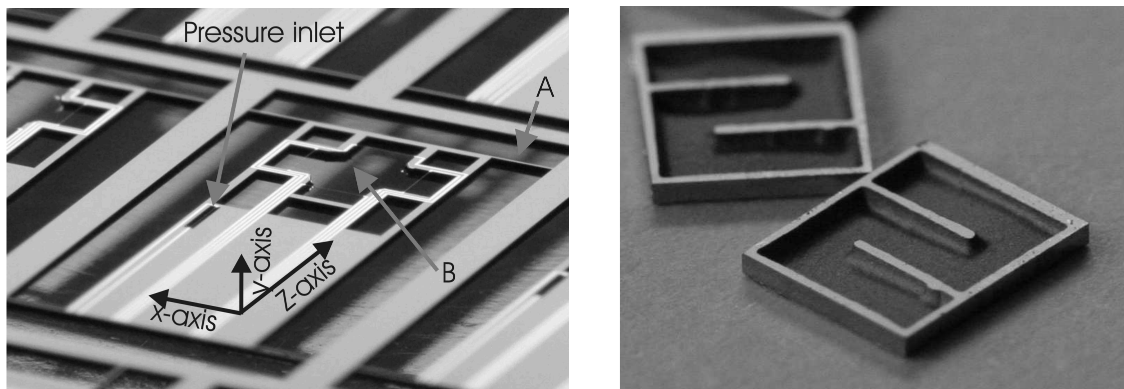

(a) Photograph of the sensor still in its wafer. *(b) The pressure chamber after processing*

Figure 4.18: *Components of a three dimensional intensity probes based on only particle velocity sensors, the sound pressure sensitive sensor is made with the standing wave tube technique.*

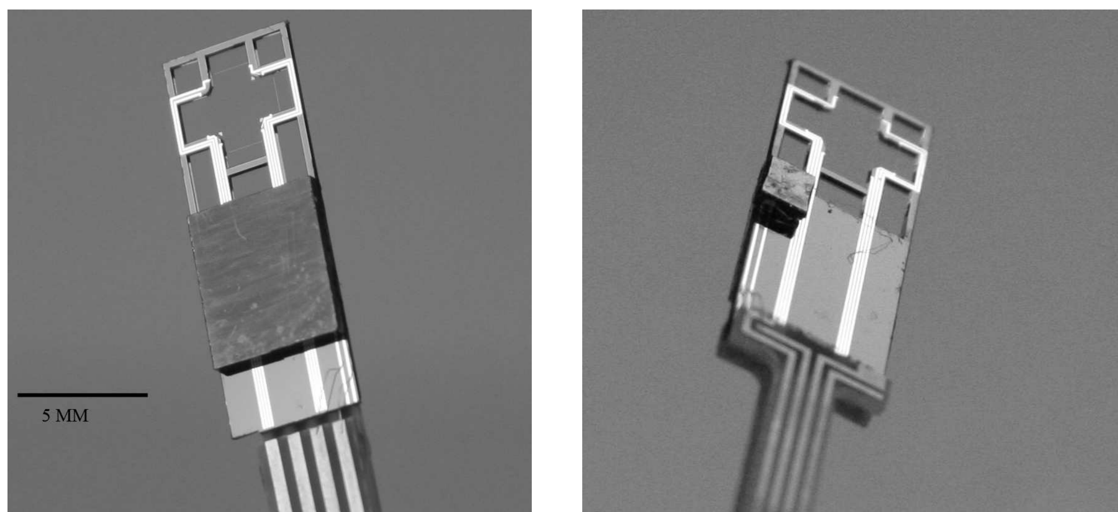

(a) Photograph of the sensor, seen from the side with the back chamber. *(b) Photograph of the sensor, seen from the side with the pressure opening.*

Figure 4.19: *A three dimensional intensity probe based on only particle velocity sensors.*

4.6.4 Measurement results

The measurement results are divided into: 1.) frequency response, 2.) polar pattern measurement and 3.) sound pressure sensitivity. The frequency response is of interest

for the calibration of the sensor and actual measurement results, while directionality and sound pressure sensitivity measurement are mainly to verify that the sensor is working as expected.

Frequency response

For measurement of the (frequency) response, the device was compared with a calibrated sound pressure microphone in a sound field. When looking at Figure 4.15 (the undamped tube without the sensor), the inverse acoustic impedance of the back chamber has a high pass behavior for frequencies below resonance. In contrast the particle velocity element response has a low pass behavior. These effects combine to a more flat response. When the inverse acoustic impedance of the tube is divided through the known low pass frequency response of a standard particle velocity sensor thereby compensating for the frequency response of the particle velocity element inside the tube, the theoretical response of the device shown in Figure 4.20a (the Kirchhoff and Low Reduced Frequency solution), emerges.

The measurements can be compared with theory and are also shown in Figure 4.20a. The overall sensitivity of the device is roughly 5 dB lower than expected and at low frequencies the response is much lower than expected.

The self noise of the sensor is not low as shown in Figure 4.21, but still good enough to perform measurements in many situations. In combination with sound intensity measurement the cross correlation between the particle velocity signal and the sound pressure signal is taken, thereby improving the signal to noise ratio [11].

Polar pattern measurement

A polar pattern has been measured to show that the sound pressure sensor is omnidirectional. For this the sensor is subjected to a known sound field inside a standing wave tube. For frequencies below the cut off frequency of this tube the sound field is defined to be in the length axis of the tube. A sound source is at the open end of the tube, at the closed end a reference sound pressure microphone is placed. Rotating the sensor and thereby measuring the transfer function between the sensor and the reference pressure sensor at one end of the tube the directivity of the sensor can be determined. Measurement results are plotted in Figure 4.22. Clearly the sensor is fully omni directional. The first results of the sensor without the small inlet-cap were not satisfactory, at angles of the device in the standing wave tube where the sound waves travel parallel to the sensor surface there was an increased and oddly shaped signal, and the polar plot was not omni directional. The reason for this odd result was that one sensor wire is placed on the sensor plane and therefore directly in the particle velocity flow. Due to this the single sensor wire cooled with every particle velocity flow in the direction with the plane. Intuitively thinking a solution would be to place a small shielding cap on top of the element, which should keep the sensor wire from undesired disturbances. After placing such a cap the measurements were satisfactory.

Sound pressure sensitivity

Testing the sensor for sound pressure sensitivity in a standing wave tube reveals that the sensor is sound pressure sensitive indeed. Inside the standing wave tube again the transfer function between a probe and a reference sensor at the closed end is recorded. From this it is clear that the device performs as a normal sound pressure sensor and that the particle velocity sensor responds exactly complementary. At peaks in the response of the sound pressure sensors the particle velocity is zero and vice versa. In Figure 4.20b a sound pressure sensitive device, a particle velocity sensor and the device are compared.

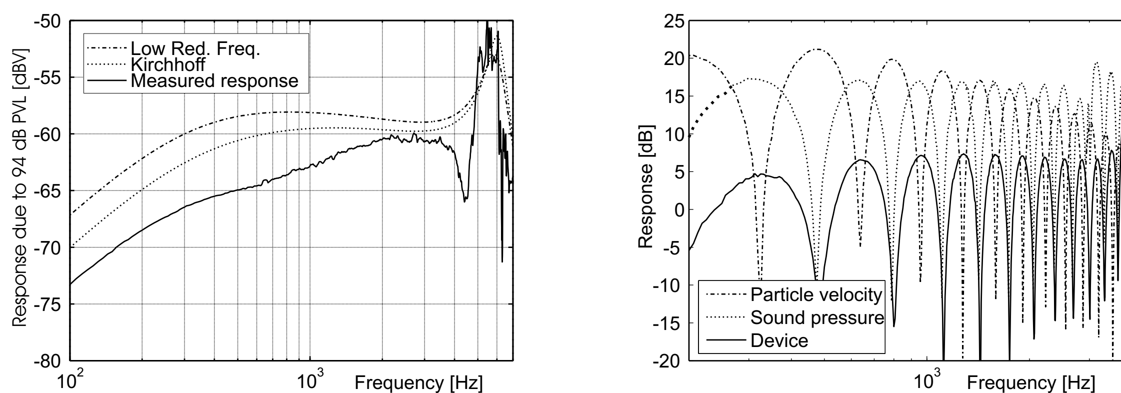

(a) *Response of the sound pressure device.* ***(b)*** *Pressure sensitivity verification.*

Figure 4.20: *Frequency response and proof of sound pressure sensitivity in the standing wave tube.*

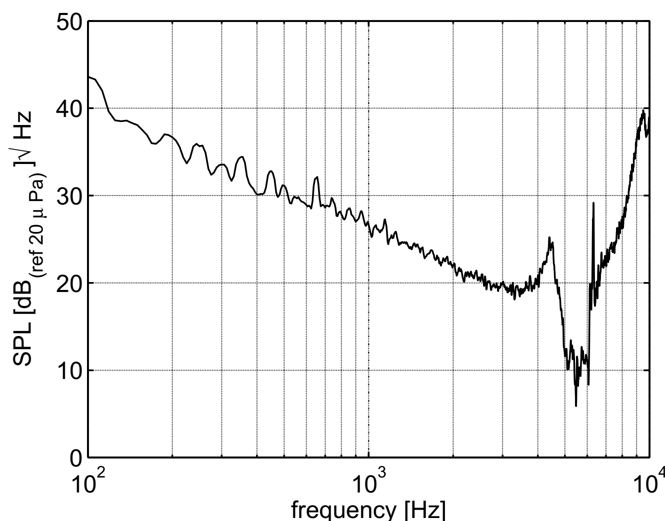

Figure 4.21: *Self noise of the device.*

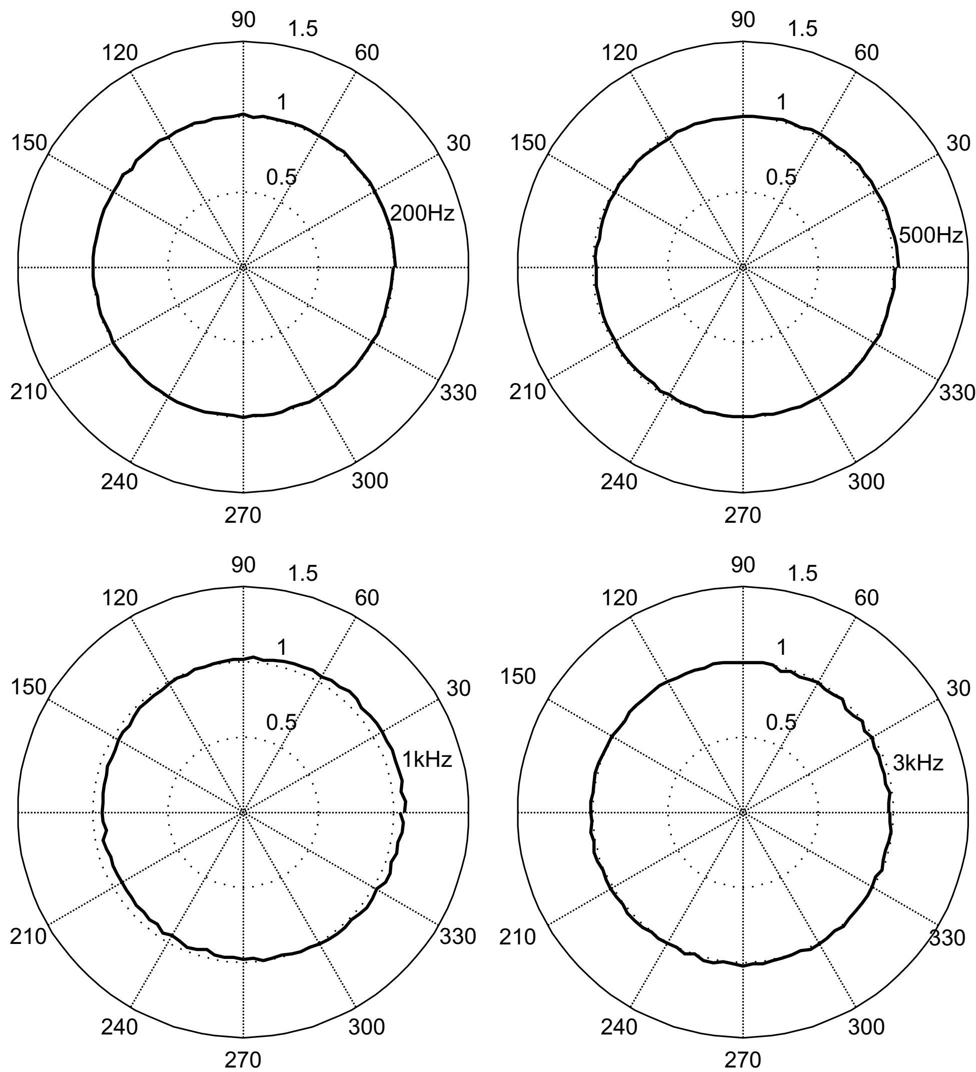

Figure 4.22: *The directionality of the sensor plotted in a polar plot.*

4.7 A second implementation of a MEMS sound pressure device

As shown before the particle velocity element can be placed halfway the sound pressure to particle velocity converter. In a micromechanical design this can be implemented as shown in the Figure 4.23. For the frequency response the sizes are chosen such that the response is as flat as possible over the whole frequency range. For the sake of this and the small size of the chip a little of the low frequency response is sacrificed. For environments where the signal level is high this is not a problem, but for measurements where low levels have to be detected the sensor is not a good choice. With temperature resistent glue this sensor is able to withstand temperatures up to 300 ^{o}C.

Another major difference between this sensor and the previous realization is that this is even smaller. The sound pressure converter is here folded on two sides of the sensor

chip. This is done manually, but with the help of a self-assembling design mounting is relatively straightforward. When applying a small amount of epoxy glue on the edges of the sensor chip and then placing the caps on the chip, the caps float on the glue to their designated positions. Then the whole device is baked until the glue has hardened.

In Figure 4.24a the upper cap is placed next to the sensor chip, epoxy glue is applied on the edges of the cap and the cap is placed over the sensor chip. Sideways this looks as shown in Figure 4.24b. The mounting with the epoxy glue is straightforward due to the self alignment of the caps and the epoxy glue gives a good air tight seal between chip and cap, which is necessary to prevent undesired particle velocity sensitivity (due to leakage of air) instead of pure sound pressure sensitivity.

In a mass-production scenario whole wafers with caps can be sprayed or dipped with glue and placed on top of a whole wafer with sensors. Even bonding of a whole wafer could be an option.

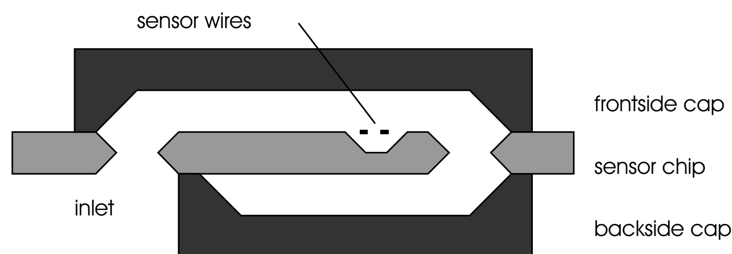

Figure 4.23: *The schematic design of the sensor.*

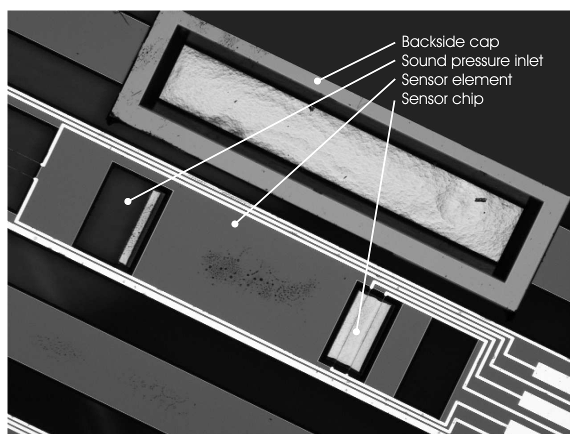

(a) *The sensor chip and back chamber element.*

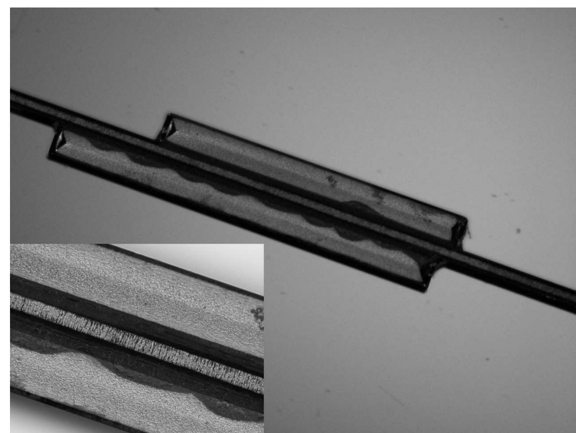

(b) *View from the side. Both caps glued on the sensor chip, due to the glue the distance between cap and sensor chip is increased somewhat.*

Figure 4.24: *Mounting of the sensor.*

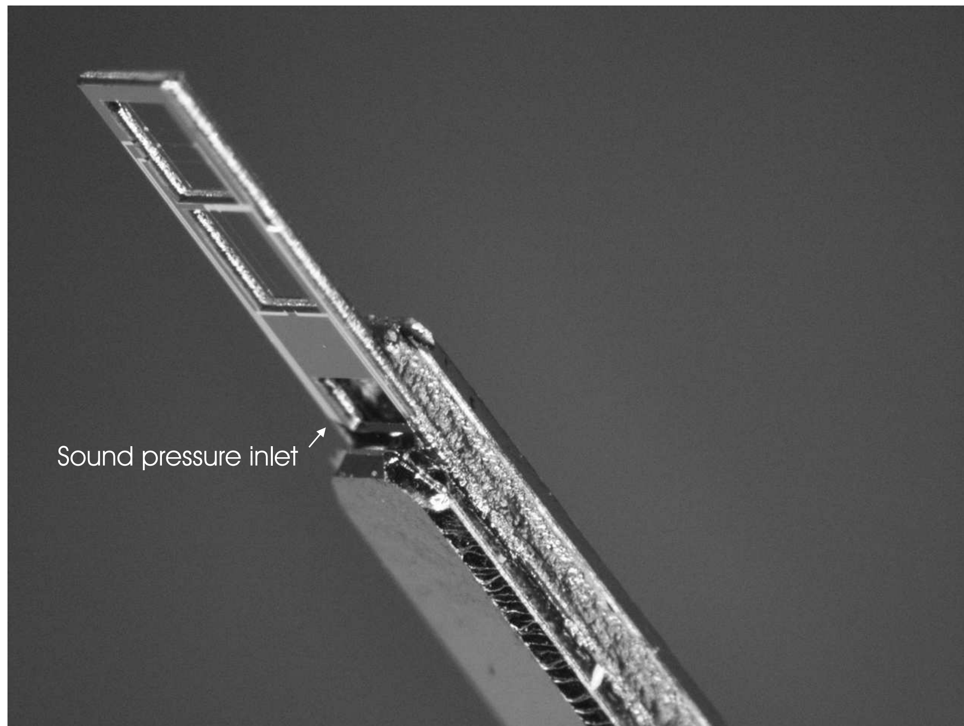

Figure 4.25: *Photograph of the final sensor. The pressure inlet can be seen just as a small hole.*

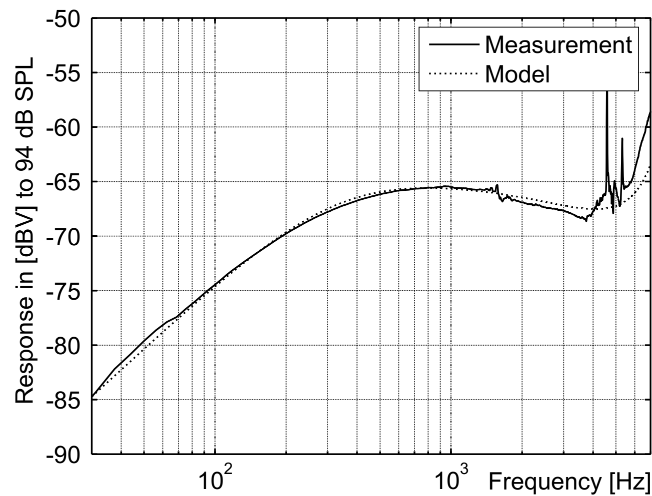

Figure 4.26: *Frequency response of the sound pressure device compared with theory.*

4.7.1 Measurement results

Measurement of the frequency response reveals that the sensor operates as expected. There is a remarkable similarity between theory and measurement. Further measurement of sound pressure sensitivity and omni-directionality is conducted with expected results; the sensor is omni directional and purely sound pressure sensitive.

4.7.2 Effect of ridges inside the sound pressure to particle velocity converter

In the surface of one type of sensor chip small ridges have been etched with a periodicity of 50 micrometers over a distance of 3 mm. Acoustically this could have influence on the damping inside the tube, since the total surface is enlarged and the surface roughness is much higher. Whether this has effect on the response is of influence on future designs. The ridges are shown in the Figure 4.27.

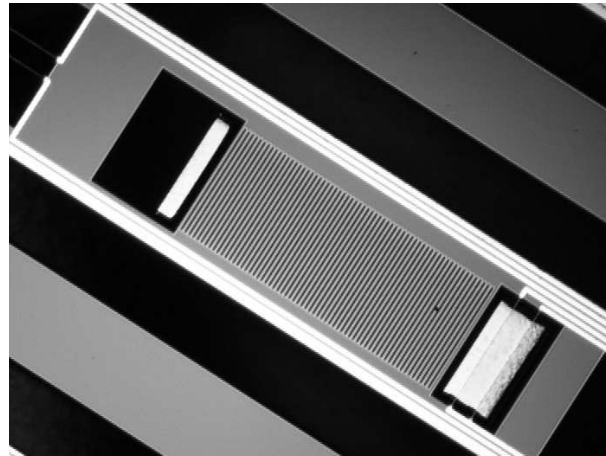

Figure 4.27: *The ridges inside the tube.*

Two sensors from the same area of the sensor chip wafer are mounted with their caps. Sensitivity measurement does reveal that the response of the sensors is identical within 0.5 dB. This is remarkably, and proves that the ridges do not have a noticeable effect on the acoustic performance of this type of design. Furthermore the result shows that two sensors can be practically identical and the (manual) mounting does not have an influence here on the reproducibility in making the sensors. Noise level is also found to be identical. The sensors are embedded in the plane of the silicon sensor chip as shown in the figure.

4.8 Other designs

The design is working properly but a number of design choices can be adjusted so that the sensor may perform better. Whether to place the sensor at the entrance of the tube or at another place is a point of discussion, the placement halfway the tube has a positive effect on the frequency response of the sensor, but a lower sensitivity level and hence higher self noise level is a trade off here. Using shorter tubes has a similar effect, choosing between these two options depends mainly of the shape of the frequency response.

Space is the limiting factor in the design in terms of sensor noise. In choosing larger tubes the overall size increases further and enables further improvements in signal to noise and frequency characteristics. For example the tube can be made longer, which has a direct effect on the frequency response, the resonance peaks shift to a lower frequency, but the sensitivity for lower frequencies increases. Shorter tubes show the opposite effect.

More sensors can be placed in parallel thereby improving the signal to noise ratio.

Figure 4.28 shows possible designs. Picture a) is the design discussed before, compared with b) which has the sensor placed differently, thereby increasing sensor wire to substrate distance and enabling a little higher sensitivity. In figure c) the sound pressure entrance opening is not 'through the wafer' but at the endpoint of the cap. This can be geometrically beneficial and space can be used more efficiently, here the lower cap is extended to just below the sound pressure opening. Figure d) finally shows the placement of the sensor near the entrance. Care must be taken that the sensor is far enough inside the tube so that no particle velocity sensitivity or disturbances can occur. In practice one or two mm from the entrance is sufficient to avoid this.

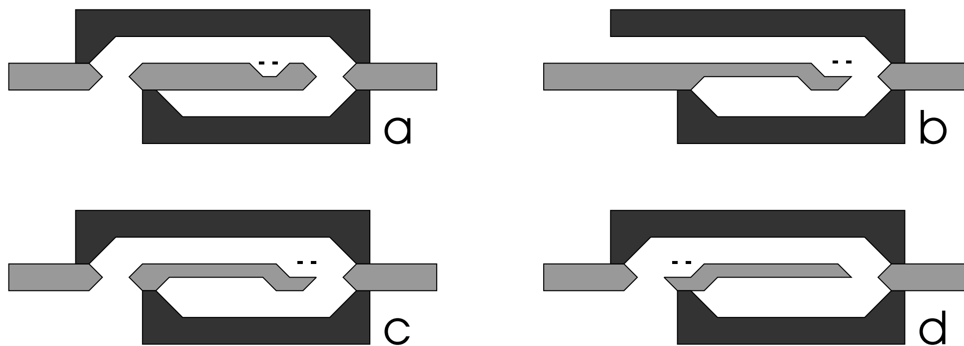

Figure 4.28: *Other designs.*

Resonance in this tube design can also be exploited to gain extra sensitivity in a certain frequency range. Assume that signals with a frequency around 1 kHz are of interest for a specific application. The length of the tube is then set to 8 cm, the resonance frequency is then tuned to 1 kHz. In Figure 4.29 a theoretical sensitivity curve is shown. To increase the effect of the resonance the damping inside the tube must be small, for this a tube with diameter of 1 cm is sufficiently large, the damping is estimated to be 1 dB lower than the when the tube diameter is taken as large as 1 meter. Signals with this frequency are filtered and other frequencies are suppressed successfully.

A realistic design of such a sensor consists of a tube with a particle velocity sensor at the open end and the other end terminated similar to the configuration discussed before in 4.5, but preferably wider. When the termination point is made variable by replacing it by a piston the resonance frequency can easily be tuned to other frequencies.

4.9 Fields of application

With its small size and integrate ability on a particle velocity chip the proposed sensor can be used as a very small sound intensity sensor. For example the acoustic intensity or acoustic impedance inside a cavity can be measured, this cavity can be down to three millimeters diameter. An example involving small cavities is the human ear; the acoustic

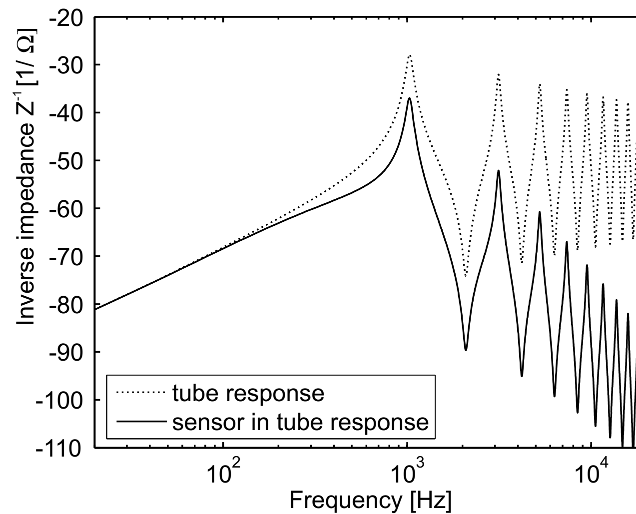

Figure 4.29: *Selective frequency design, the frequency of interest is 1 kHz.*

impedance of this cavity extended with the eardrum gives information on the operation of the hearing system.

Sound source localization of small sound sources is possible with particle velocity sensors, however with the sound pressure signal actual direction information and acoustic impedance can be measured. This combination gives a complete sound field description at the measurement point. When measuring sound intensity (which is the real part of the cross-spectrum between sound pressure and particle velocity) the uncorrelated sensor noise is diminished [11], therefore the relatively high noise level of the sound pressure sensor is of less concern here.

Particle velocity sensors are able to operate within a wide temperature range, and since the sound pressure sensor is mainly a particle velocity sensor with a rigid back chamber the sound pressure sensor is also able to operate in this temperature range. Within the range of -50 ^oC to 300 ^oC the combination of particle velocity sensors and the pressure sensor is expected to operate without problems, extended temperature ranges can be made possible with adapted materials. A recalibration of the sound pressure sensor is necessary since the response is temperature dependent.

The sound pressure sensor is not particularly sensitive over a large frequency range compared with existing pressure microphones. For high levels the sensor is suited well, and cross-correlating signals can partly compensate the high self noise. Furthermore the sensor is nicely embedded into a back chamber and consists of materials that are very stable, measurement of sound pressure in chemical aggressive, high temperature and high sound pressure levels such as in exhaust systems is therefore possible.

4.10 Conclusions

In this chapter a sound pressure sensor is presented with a particle velocity sensor as sensor element. Sound pressure is converted to a particle velocity signal by means of a sound pressure-to-particle velocity converter. The converter is in principle a cavity connected to the outside. Pressure fluctuations outside the cavity result in particle velocity in the entrance of the opening. Placing a particle velocity sensor in the opening results therefore in a sound pressure sensitive device.

A device with an enclosed cavity and an entrance tube (a Helmholtz resonator) is discussed, the device proved to be a sound pressure sensitive device. A following sound pressure sensitive design is based on a small tube with a particle velocity sensor inside. Measurements prove that the device is indeed sensitive to sound pressure and that the device has an omnidirectional characteristic.

Such a microphone has a frequency response that is not flat; however a model of the response is presented and verified. Both standing waves in the converter and damping inside the tube influence the response of the device. Both effects are discussed and a model for the response of the device as a function of the tube size is presented.

The sound pressure device is integrated successfully with an existing design of a three dimensional particle velocity transducer. The total device can be made very flat (1.3 mm is feasible), which is an advantage when measuring in small confined spaces or when non-intrusiveness of measurement devices is of importance. Another advantage of this new sound pressure microphone is that it can be used in harsh measurement environments such as high temperature or chemical reactive environments.

Chapter 5

Fabrication and assembly

5.1 Introduction

In this chapter the fabrication of the sensor elements and additional structures is discussed. The sensor chips are fabricated in a clean room environment. Process steps include deposition of sensor wires, wet- and dry- etching and finally dicing or separating chips. Furthermore the chips are assembled and packaged into a sensor element that is handled easier for further characterization. The chapter starts with a discussion of the clean room fabrication process. Next, in section 5.3, the assembly into complete functional sensors is discussed.

5.2 Clean room fabrication

A clean room is necessary for the process of making particle velocity sensors with small dimensions. Even a small dust particle can destroy the pattern of the photo resist layer defining the metal sensing layer. Since sizes of the sensing wires are in the order of micrometers, a dust particle is relatively large and influences the process. A number of process steps are less susceptible to dust particles, such as the etching of silicon in potassium hydroxide (KOH).

Although not every process step is necessarily done in a clean room, for convenience, safety and to avoid cross pollution between processes and machines the whole process is done inside. A class 10000 clean room environment, with class 100 process benches is used.

First, in section 5.2.1, the fabrication of a traditional particle velocity sensor is discussed. Next, in 5.2.2, the modifications needed for fabrication of the three-dimensional particle velocity sensors are described. Finally, in section 5.3, the fabrication of the back chamber structures for the pressure sensitive device is discussed.

5.2.1 Fabrication of a single-sided particle velocity sensor

Basic fabrication sequence

The fabrication of a standard particle velocity sensor is described along the steps indicated in Figure 5.1. A single side polished silicon wafer of 0.5 mm thickness and with a diameter of 10 cm is used. The silicon is in fact purely for the mechanical structure of the sensor and not very critical in terms of conduction or roughness. Wafers with crystal orientation of <100> are used, which defines the etching profile after etching in KOH. On top of the silicon wafer a thin layer (200nm) of silicon nitride is deposited by Low Pressure Chemical Vapor Deposition (LPCVD) at 850 ^oC. Next the wafer is covered with a photo resist layer, which is then exposed to UV with the pattern of the conducting platinum layer. This platinum layer forms the conducting part of the sensor wires and the electrical connection to the bond pads. After development of the photo resist layer the silicon nitride underneath the illuminated areas becomes exposed. Subsequently, a thin layer of chromium is sputtered on the wafer, which acts as a primer for the platinum sensing layer, and the actual sensing layer of 150 nm thick platinum is deposited. Deposition of the layers is done in a low pressure (0.0066 mBar) sputtering system, with chromium and platinum targets. To remove the metal at other areas than the sensor wires and contact pads the wafer is placed in an ultrasonic agitated bath with acetone. Acetone dissolves the remaining photo resist layer which is still covered with chromium and platinum, resulting in lift off of the metal pattern. What remains is a silicon wafer covered with silicon nitride and patterned sensor wires in chromium/platinum.

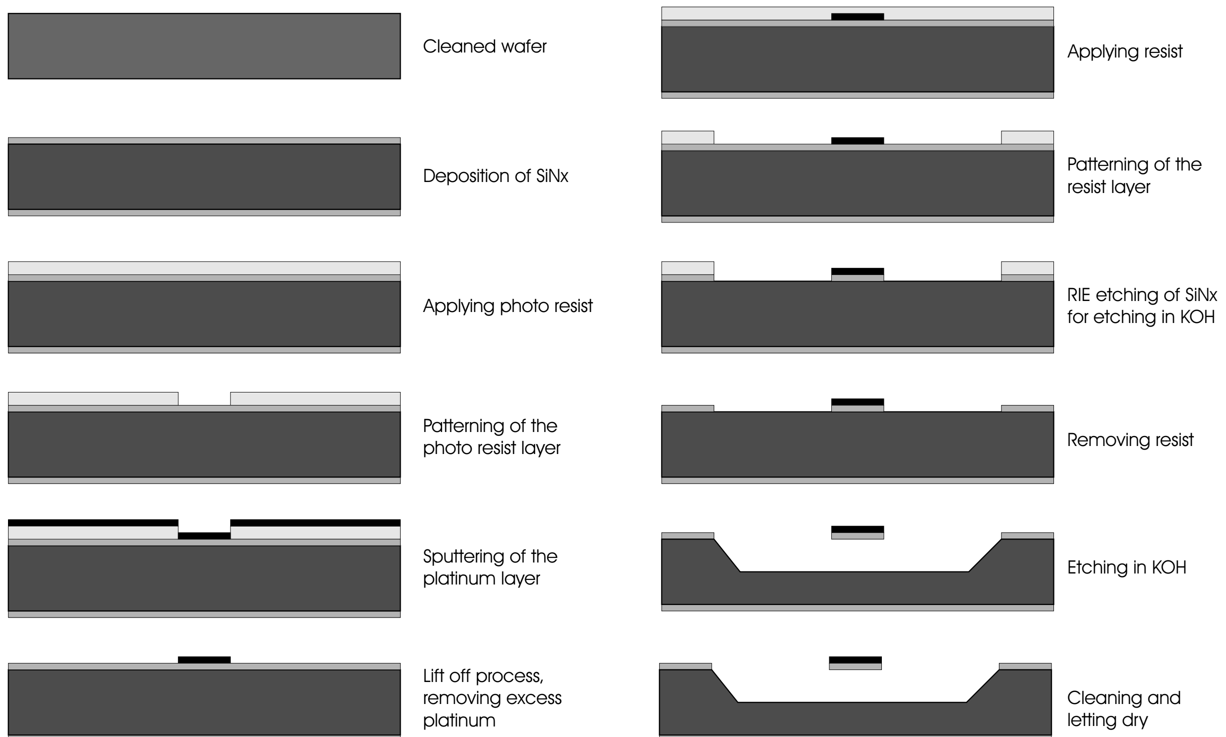

Figure 5.1: *Survey of the fabrication process.*

Another layer of photo resist is patterned, now defining the etching mask for the KOH etching step and thus determining which part is etched away in KOH and which not. After development of this photo resist layer the wafer is etched using Reactive Ion Etching (RIE). This etch process attacks the silicon nitride layer until it is etched completely through until the silicon substrate. The photo resist layer is attacked to a certain extent, but does remain in place.

After removal of the remaining photo resist in an oxygen plasma the wafer is etched in KOH. This etchant leaves the silicon nitride and metals intact, but at places where the silicon is not protected by the silicon nitride the silicon is etched in a specific shape, see Figure 5.2b. Just before this step there is an optional etching step with $HF : HNO_3 : H_2O$ described in the following section. Rinsing the KOH from the wafer and drying in isopropanol leaves a processed wafer patterned with the sensors. A detailed description of the process can be found in appendix C. After dicing the wafer into individual chips the sensors are ready to be mounted and connected.

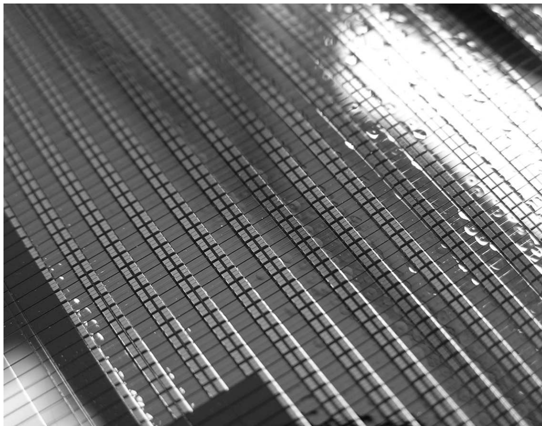

(a) *Fully processed wafer.*

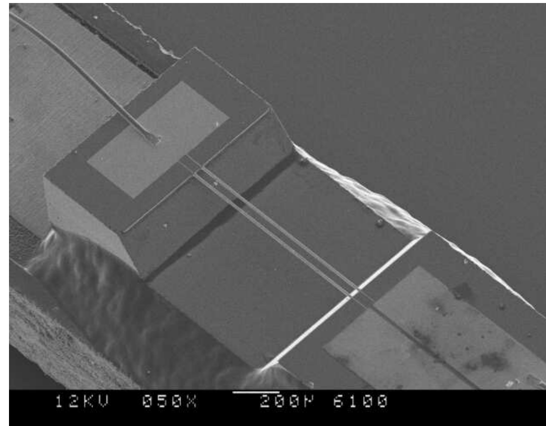

(b) *Bridge type two wire sensor mounted on carrier board.*

Figure 5.2: *Fabricated sensors using a single sided process.*

Under etch step with $HF : HNO_3 : H_2O$

A slight misalignment between the wafer crystal orientation and the lithography process is generally sufficient to ensure that the wires are released. However this works for sensor wires with widths below 3 μm. For wires with larger widths the misalignment must be larger, and still there is a chance that material is not completely etched away. When the silicon underneath the sensor wires in not etched completely away or even not at all this results in non uniform sensors or non functional sensors.

The selectivity of etching of <100> silicon planes compared with <111> planes in 25% KOH of 75 ^{o}C is approximately 80 times [67], so for an etch depth of 125 μm in the <100> plane the etch depth of the <111> plane is 1.5 μm. Since the <111> planes are at an angle of 54.7 degrees with respect to the wafer surface, this results in 2.3 μm

undercut at each side of a wire (when no misalignment is present between the crystal orientation and the wire length axis). This value corresponds to the experimental result shown in Figure 5.3. In this experiment a number of slits are made in a silicon nitride mask on a silicon wafer with orientation <100>. The slits are 25 μm wide and a couple of millimeters long. After etching for two and a half hour in 25% KOH of 75°C the depth at other parts of the wafer was 130 μm. The amount of undercut at the edges of the slits is found to be within 1.5 and 3.5 μm, at the upper edges of the slits in the figure the amount of undercut is on the smaller side. Possibly due to a small misalignment there is a deviation in width. Still the undercut is found to be at least 1.5 μm.

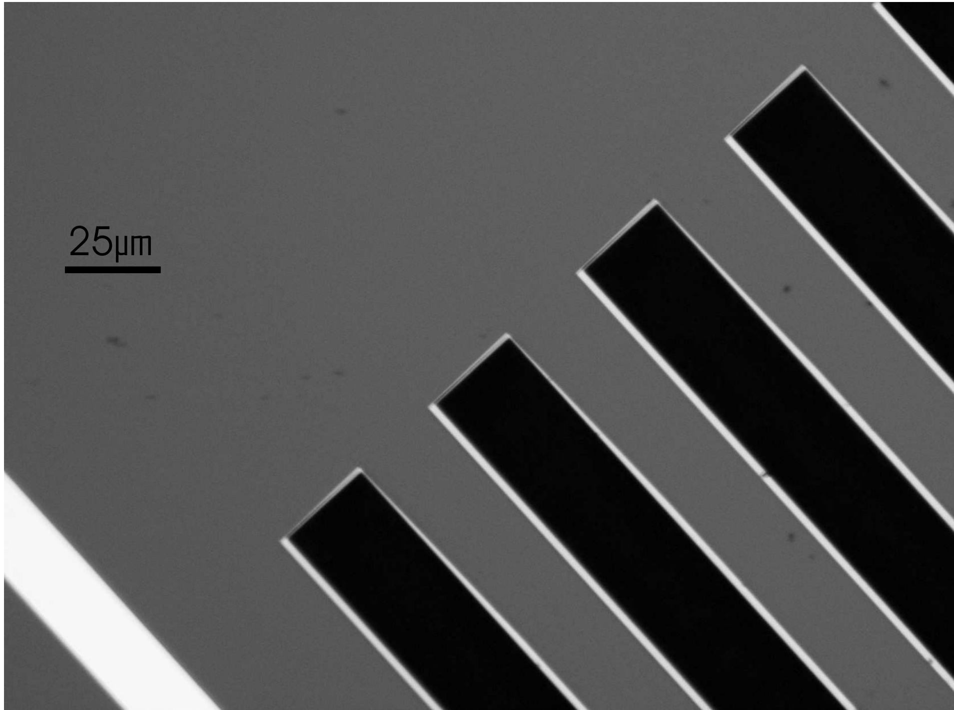

Figure 5.3: *Undercut after etching in KOH, the ridges are shown as black holes, the white lines surrounding it are the under cut areas.*

This means that when etching 125 μm in the depth direction, wires with a width of 3 μm are etched free and a pyramidal shape remains underneath the wire. This pyramid is attacked fast, however this still takes time. When etching up to 250 μm depth this pyramid has vanished almost completely.

An etching solution of HF(50%) : HNO_3(69%) : H_2O (1:2:6) is used to etch the silicon isotropically underneath the wires [68] to avoid the problem. Etching time is between 30 seconds to one minute and is empirically adjusted. The etch rate of the solution is expected to be 3 μm per minute. For wires up to ten micrometers in width this means that after one minute the silicon underneath the wire is attacked to a width of 4 μm instead of ten, assuming that the etch rate is maintained at 3 μm per second. The remaining 4 μm is etched by KOH and assisted by possible misalignment between the crystal orientation and the wire.

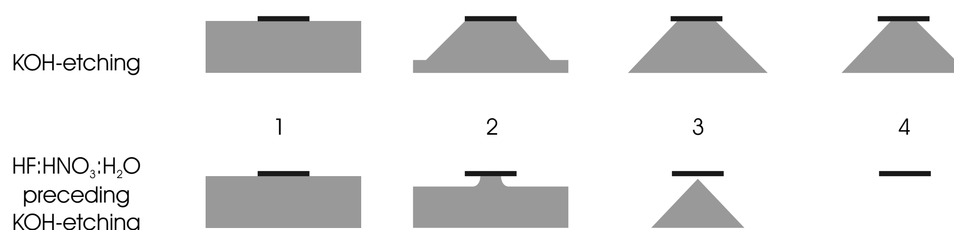

Figure 5.4: *Etching in of silicon in $HF : HNO_3 : H_2O$ preceding the etching in KOH.*

Separating devices from the wafer

Chips can basically be separated from the wafer by two means: dicing using a saw or using a break out structure. Sawing has the advantage that the edges are perpendicular to the surface and the diced sensors can therefore easily be handled with tweezers. On the other hand dicing is not feasible without protecting the fragile sensor wires, and alignment of the dicing saw and dicing itself is time consuming.

The other method is to design a break out sensor. The main advantage is that there is no extra time involved by dicing and the problem as described in 2.3.2 where conduction between the metal and bulk silicon can occur by sawing does not occur. On the other hand due to the normally slanted edges of a chip due to the KOH etching it is more difficult to handle the chip with tweezers and the amount of sensors on one wafer drops due to the extra space needed for the break out design. Straight edges are possible however; over etching with KOH will remove the slanted edges, but also the design is etched more.

Dicing of sensors

Sensors can be diced with a 50 micrometer wide saw rotating at 25000 RPM, at a surface speed of 130 m/s, avoiding to saw through the electrically conducting connection pads, see also 2.3.2. The name 'dice' means small cube, and is in chip fabrication a synonym for a chip which is separated from a wafer. One method to dice the particle velocity chips with a saw is to use an extra plate, covering it with wax and placing the wafer to be diced on top.

The wax fixes the wafer on the plate and can be melted later to remove the elements easily. Inside the sawing machine the sensor wires do not survive, since the dicing saw moves just next to it at high speed, and is cooled with a water jet. The high speed water jet and the dicing debris easily destroys the sensor wires. Applying a very thick layer of photo resist can protect the wires. A wafer with sensor elements is covered completely with the photo resist layer, such that the sensor wires are just covered in the photo resist. Next the stack is placed on a hot plate allowing the photo resist to dry faster. Together with this the viscosity of the hot dried photo resist is much higher than the cold photo resist allowing the sensor wires to move (very slowly) through the hot photo resist. Because when the photo resist dries it shrinks: causing the wires to be torn apart by the drying resist if the resist was not viscous. After approximately 15 minutes the resist layer has dried, and the stack must be cooled slowly, to prevent the photo resist layer from

cracking and destroying the sensor wires.

Next the plate is mounted in the dicing machine and, after meticulously adjusting the height such that the silicon wafer is just sawn through, the chips are diced apart from the wafer. The layer of photo resist is removed with acetone and the sensors can be taken from the plate when it is heated to 70°C so that the wax melts.

The total yield of good sensors is drastically reduced by this method, since the process of photo resist drying is very difficult to control. With a slightly to fast or too slow cooling or heating combined with a non uniform thickness of the photo resist layer the layer cracks easily, taking the sensor wires along.

Another method has become available with the use of a strongly adhesive foil. This foil sticks to the silicon substrate and is strong enough to withstand the dicing of the wafer, thereby preventing that diced elements come off the foil. Therefore the original method of using a plate with a wafer mounted with wax is not necessary anymore. Protection of the elements when dicing is still a problem, but the use of wax instead of photo resist is now also possible; earlier when the wax was used to fix the wafer on the plate a removal of the wax from the sensor elements would also result in the removal of the sensors from the plate, resulting in a mess. Placing the wafer on the foil and covering it with hot and clean wax protects the sensor wires successfully, after dicing the majority of the wax can be removed easily when heat is applied and the rest can be removed with a chloroform bath. The dicing foil remains stable in chloroform. The foil is removed with ultra violet light exposure; the foil simply loses its adhesive power and the sensors can be picked up.

Break out sensor designs

When etching a narrow slit around the sensor element and supporting the element with small beams this element can be broken out of the wafer. This must be done with care, but a good design facilitates easy use. Figure 5.5 shows a break out design with the elements still in the wafer. Etching is done in KOH, the characteristic slanted sidewalls inside the elements show this. Etching is done from both sides, and is continued long enough to etch completely through the wafer. When etching even longer the slanted sidewalls etch away to the straight beams shown in the figure.

General guidelines for making a break out structure are to make the structures as small as possible, thereby avoiding that the elements come out before finishing the fabrication process. The thicker the beams the more force is necessary to separate the chips and risk of damaging elements increases. Here the width of the beams is chosen 50 μm and the length 1.5 mm. This length can be chosen shorter but must be long enough to etch through the wafer completely, in the case of KOH and <100> wafers this distance is directly dependent on wafer thickness.

Using a break out design results in less sensor elements per chip due to the extra needed space for the break out structures. On the other hand the yield of working elements is

normally very high. For double side processed wafers with sensor wires on both sides dicing is not straightforward and a break out design is a good option.

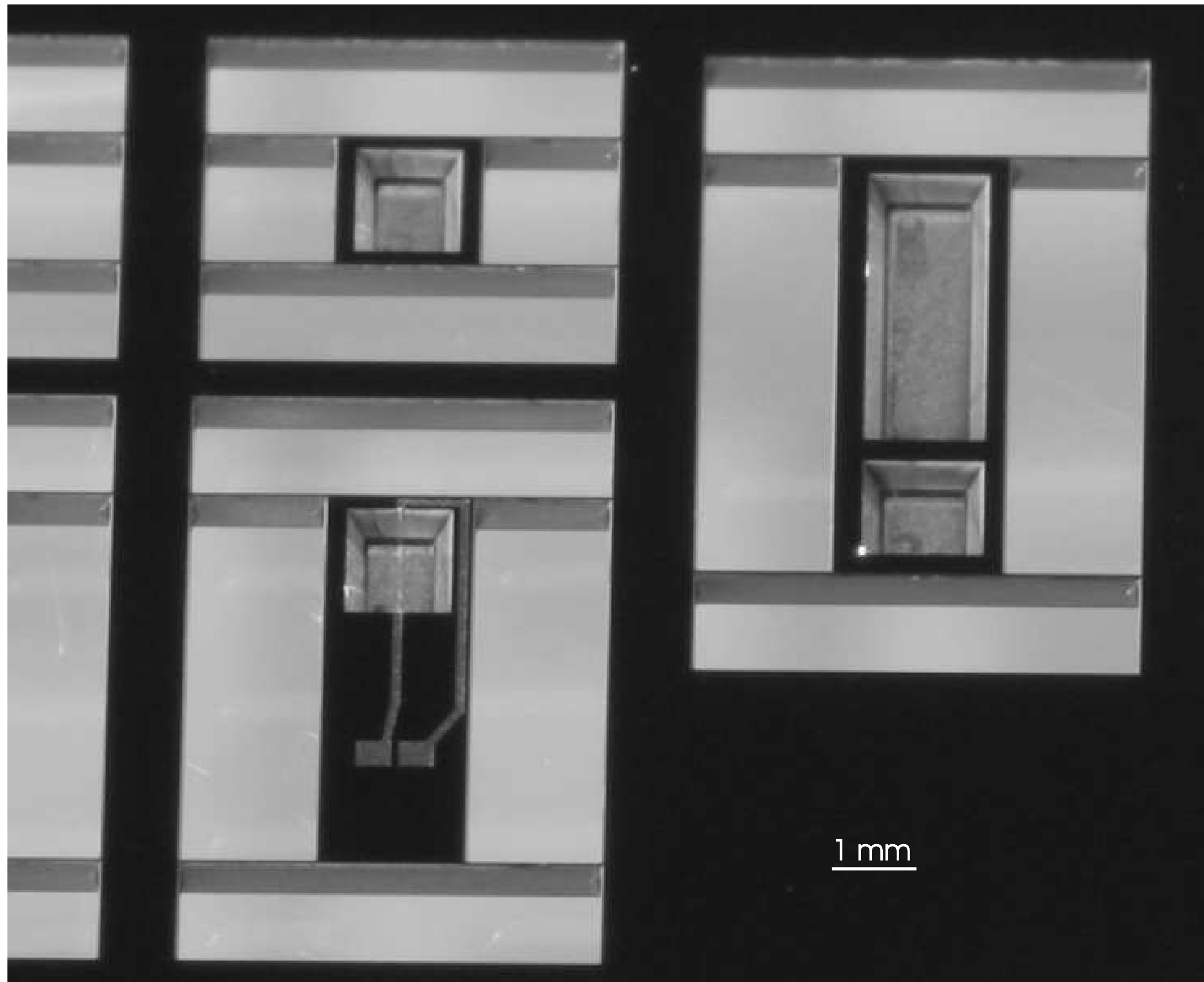

Figure 5.5: *Photograph of a a break out design, the elements are still in the wafer, but suspended by small beams.*

5.2.2 Fabrication of three-dimensional particle velocity sensors

As mentioned in chapter 3, double side polished 250 μm thick wafers are used for the three-dimensional sensor. Figure 5.6 shows a summary of the fabrication process. First, an insulating and construction layer of 200 nm low stress silicon nitride is deposited by LPCVD. After patterning photo resist, a 150 nm thick platinum layer is deposited. Only the platinum which is directly on the silicon nitride remains, the platinum on the photo resist is removed by lift off in acetone. It is essential that both sides of the wafer are processed in exactly the same way to prevent mismatch between the sensor wires. Next, a new layer of photo resist on the silicon nitride is patterned and the exposed silicon nitride is etched away by reactive ion etching (RIE). Both the photo resist and the platinum of the sensor wires act as an etch mask here. Finally, the silicon substrate is etched in KOH,

releasing the sensor wires. The resulting sensor wires consist of 200 nm silicon nitride covered by 150 nm platinum.

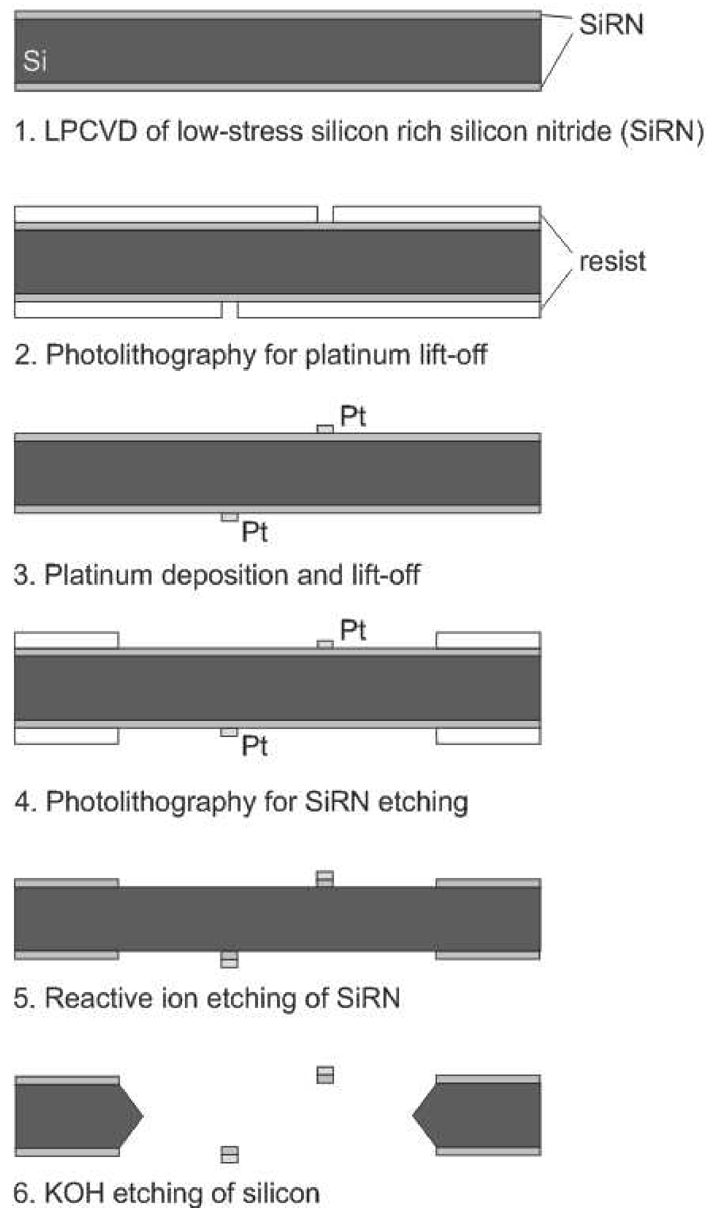

Figure 5.6: *Double sided processing schematic.*

The complete sensor chip is etched free from the wafer except for four small silicon beams holding the sensor in place, as shown in Figure 5.7. The small support beams are indicated by the arrow 'A'. In this way the chips can be broken out of the wafer, which is necessary because standard dicing would destroy the fragile sensor wires, which are just visible in Figure 5.8.

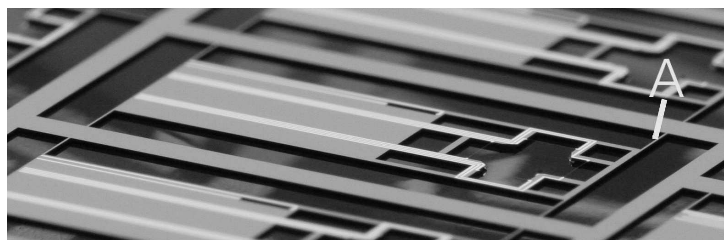

Figure 5.7: *Photograph of the double sided processed sensor, a break out beam is visible at 'A'.*

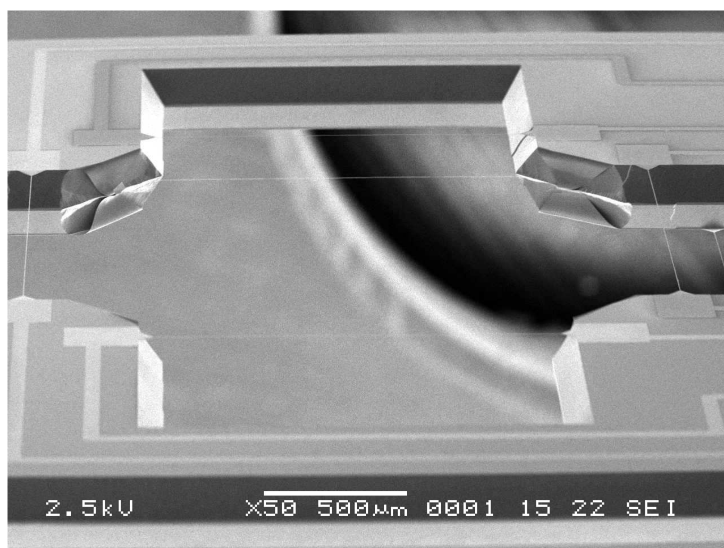

Figure 5.8: *SEM photo of the device. The sensor wires on both sides can be seen clearly.*

5.2.3 Fabrication of pressure cavities

The cavities as described in the making of a pressure sensitive device in chapter 4 are small rigid caps with an etched or micro machined cavity to provide an enclosed volume. These caps can be made by powder blasting a cavity in a silicon substrate [69].

As mask material a foil resist is used, this consist of BF405 photosensitive resist foil which is applied on a silicon or glass wafer. After exposure to UV-light and development the parts that must be etched are exposed. Powder blasting is done by a high pressure air jet with small abrasive aluminum oxide particles that collide with the exposed substrate at high speed. Each collision removes a piece of the substrate until the desired cavity size is attained. At places where the mask material is still present the particles collide with this elastic material so that no damage is done to the substrate. Due to the energy absorbing properties of the mask material the particles have only effect on hard surfaces, so the mask material does not easily degrade. It is possible to etch through a 550 μm silicon wafer with one single mask layer of about 50 μm thickness. Although the powder blasting can be controlled very precisely this is not especially necessary for the fabrication of the caps. A resolution of 100 μm lateral and 50 μm in depth is generally sufficient for the fabrication of the caps. After powder blasting the cavities the substrate is sawed into

separate caps for mounting on the sensor chip. Powder blasting is especially suited since it enables fast fabrication of complex (meandering) shapes in silicon.

Another possibility of making the cavities is etching silicon by KOH, this is a good choice for straight cavities without protruding inner corners so that the etching in KOH does not require compensation structures, see for example Figure 5.5. Both a break out structure and dicing can be used to separate the caps from the wafer.

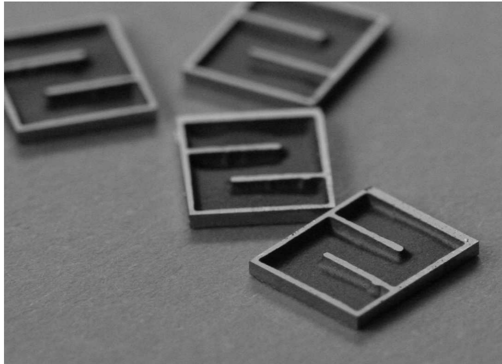

(a) Processed cap with meandering structures etched with powderblasting and sawed apart.

(b) Processed cap, etched with KOH and sawn.

Figure 5.9: *Processed pressure cavities.*

5.3 Assembly of sensors

A diced sensor of the 'standard' design is of size 1 mm * 2.5 mm * 0.5 mm (l*w*h). Further the electrical connection pads are typical of size 0.3* 0.3 mm squared. Transforming this into a more workable element the sensor chip is mounted on a carrier board which acts as a carrier. On top of the carrier board copper traces are used for the electrical contact. With cyano-acrylate glue the sensor chip is mounted on the carrier board. The electrical connections between the chip and the copper traces on the carrier board are made by wire bonding.

Wire bonding is the process of 'welding' a small wire between the contact pads and the copper trace [70]. This can be done with different techniques such as elevated temperature, high pressure electrical current and so on. In our case we used the ultrasonic energy type of wire bonding with a wedge and an aluminum wire of 25 micrometers in diameter. With the help of ultrasonic energy the wire is welded onto the contact pads. In Figure 5.10 the wire bonds are the tiny threads between the chip and the carrier. These formed wire bonds are very vulnerable, and are therefore protected by epoxy glue with a low expansion / shrinking coefficient. Expansion or shrinking could tear off the welded metals, leaving a disconnection. The sensor is now ready for use, however the sensor wires are still exposed and can be destroyed easily. A protective cap can be glued on this element, leaving only a small hole perpendicular to the wires, in practice this is a very robust sensor which can

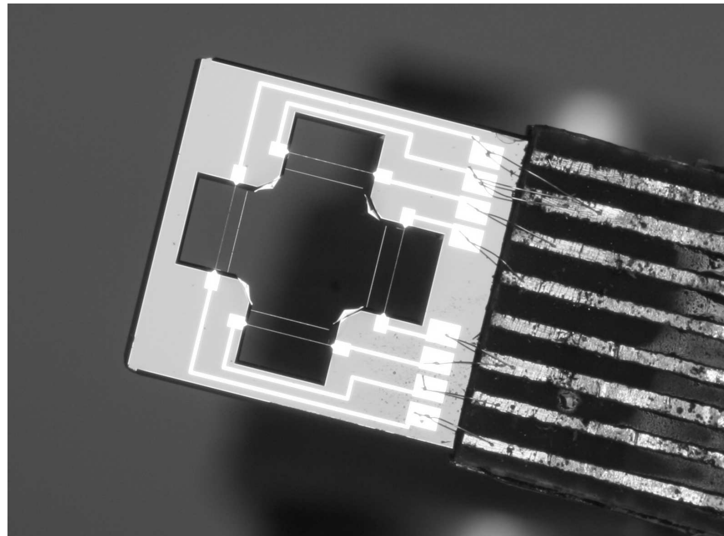

Figure 5.10: *Processed sensor mounted on a carrier board and wirebonded.*

hardly be destroyed. Connecting the now acquired element to external circuits can easily be done by soldering wires to the printed circuit board.

5.3.1 Mounting in a Zero-Insertion-Force connector

Mounting and wire bonding of the sensor chips is a tedious and very meticulous process. Especially when mounting sensors with multiple electrical connections on both sides of the chip this is a difficult and time consuming process.

For chips with multiple connections on both sides of the chip an alternative is available; a zero insertion force socket. Commercially available connectors especially designed for connecting small flat cables between electronic printed circuit boards are used. These sockets have a small lever which closes the contacts tightly after the cable is loosely inserted. Regular sockets would require the cables pressed inwards with force, when applying this handling to a fragile sensor chip the chip is easily destroyed.

In the figure below (Figure 5.11) a photo with an element inserted and an exploded view of the connector is given. Contact points of the used connector are on both sides of the chip and are interconnected, so by using this type of connector connections on both sides of the chip can be made. For 250 μm thick wafers standard available connectors can be utilized. A sensor chip with pre-aligned contact pads is placed into the connector and the clamp is closed. Experiments have shown that the chip is tightly connected in the connector and that electrical contact is good. The pressure on the contact points is not too high to destroy a connection pad and even removing the chip forcefully from its socket while the clamp is closed did not damage the chip. When necessary the clamp can be opened again, thereby loosening the contacts and the chip can be taken out of the connector, again without mechanical resistance.

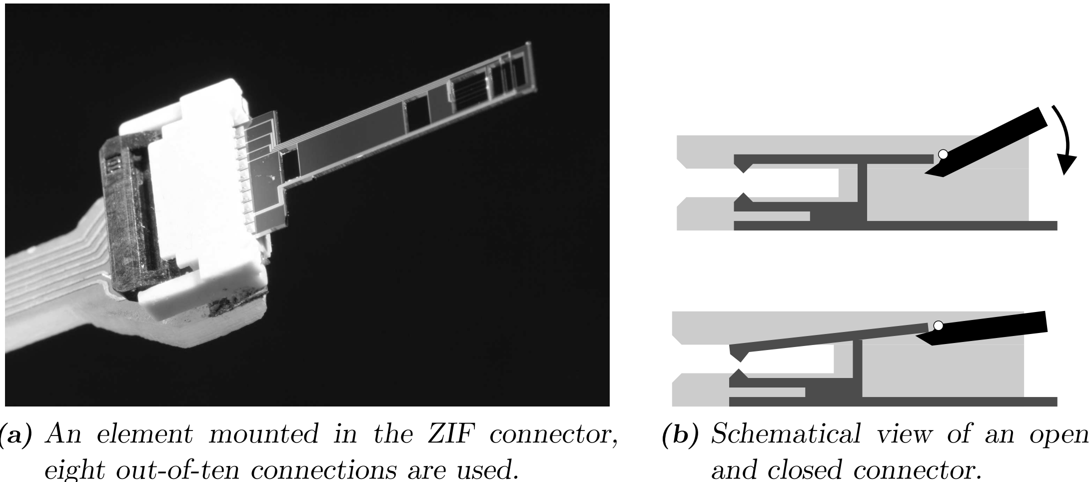

(a) An element mounted in the ZIF connector, eight out-of-ten connections are used.

(b) Schematical view of an open and closed connector.

Figure 5.11: The Zero Insertion Force connector explained.

Assembling the connector onto a carrier board results in a good way of connecting sensor chips with thickness between 150 μm and 300 μm. These types of connectors are available in many sizes and probably a model for thicker sensor chips can be found. A disadvantage is that the minimum separation of the connecting pads is 0.5 mm pitch. This can make a sensor chip larger than strictly necessary when multiple conections must be used.

Application to sensors

For the three dimensional particle velocity sensor types with pressure microphones an interconnection can be designed such that all sensors are connected properly with only ten connection pads. In the Figure 5.12 this is shown for the most complex sensor designs, dotted lines are connections on the back side, solid lines on the front side.

5.3.2 Interfacing to MEMS devices by a soldered connection

Care must be taken when applying high temperatures combined with physical force and/ or chemicals to the sensor elements, since the silicon nitride electrical insulation properties must be maintained. Experiments involving the soldering of wires to the platinum contact points resulted in sensors exhibiting excessive noise. When soldering at lower temperatures than 300 ^{o}C this problem is avoided.

Standard 40 % Pb/ 60% Sn solder material melts at around 220 ^{o}C. Applying solder paste, which is a paste with the solder metal and flux (an oxide removal agent), on a printed circuit board, placing the element with the conductive pads to the copper plane and heating the stack results in a strong electrical and mechanical connection and no damage to the elements.

Heating temperature is held at 230 ^{o}C and the element is subjected to this temperature until after the solder material starts to flow. An element with size 3 mm * 5 mm

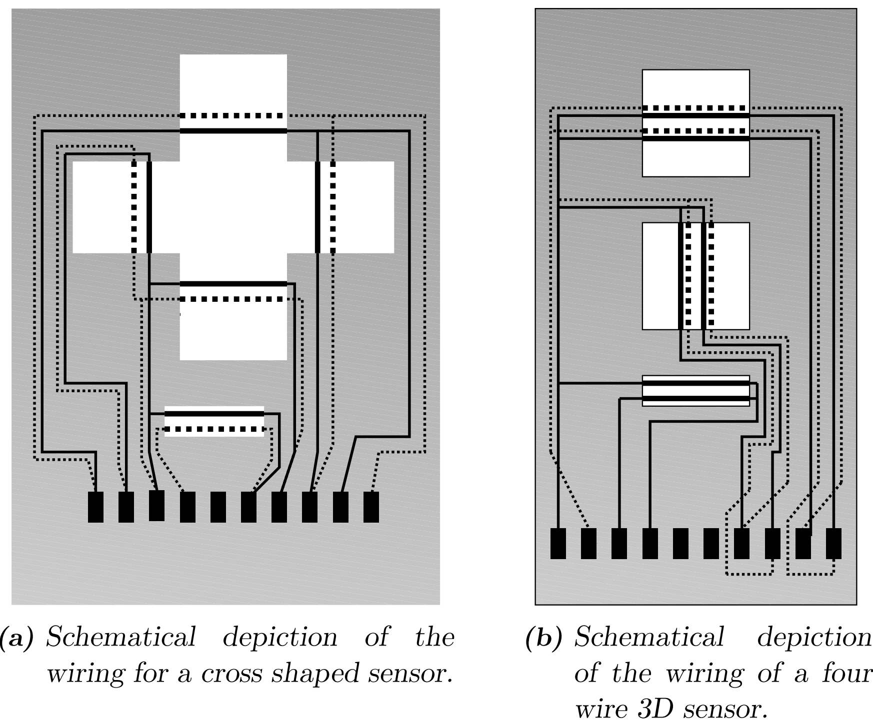

(a) Schematical depiction of the wiring for a cross shaped sensor.

(b) Schematical depiction of the wiring of a four wire 3D sensor.

Figure 5.12: *Electrical connections for the 3D chips suited for use with a connector.*

and 0.25 mm thick is used. Alignment of the contact pads to the printed circuit traces does not have to be very precise since the element moves to the place with minimum total contact area of the solder material by capillary force. This is the place where the contact pads of the element and the printed circuit board are just above each other. This technique is used commonly in the industry for the assembly of electronic components on printed circuit boards, however this is in general done only with already fully packaged chips. In Figure 5.13 a successful mounting of an element using only solder metal is shown.

In practice this method seems to be very suitable as a low cost and fast assembly method of the fabricated devices on a carrier board. Additionally the place where the element is connected to the carrier board is not larger in contrast to wire bonding or the use of a connector, enabling a smaller total size.

Soldering at high temperatures

Measurement results on a large particle velocity element which was soldered with regular solder material at 350 ^{o}C showed disappointing results; the noise level was extremely high. The insulating properties of the 200 nm silicon nitride layer were suspected to be insufficient and this was tested. A double side polished wafer with platinum on both sides and silicon nitride in between was subjected to increasing voltages and the current through the wafer was measured. The results shown in Figure 5.14 show an exponential behavior, which is characteristic for a semiconductor.

Similar elements which were not soldered did barely conduct current. Assuming that

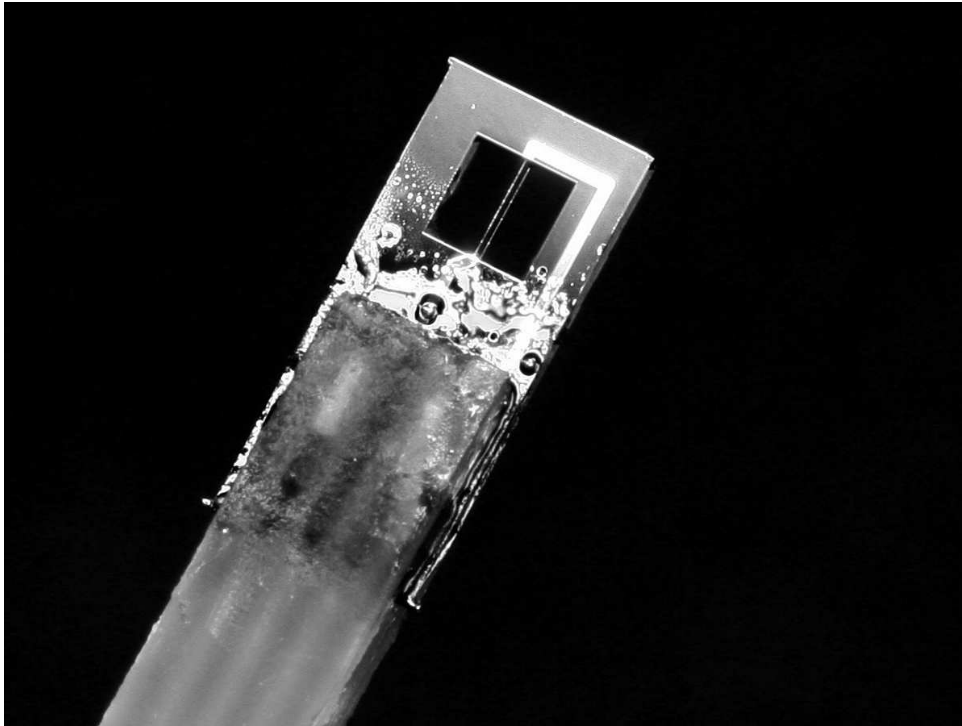

Figure 5.13: *Soldered element between two carrier boards. The fluid-like substance is the remains of the used solder flux, this has no influence on the working of the sensor but can be removed for aesthetic reasons in isopropanol.*

the metal layer and silicon bulk layer conduct perfectly compared with the silicon nitride layer there must be around 20 volts over each nitride layer. With a thickness of 200 nm the field strength is 1.0 MV/cm, which is still much lower than regular nitride break-through voltages reported to be above 10 MV/m [71]. Concluding the soldering at high temperatures (350 degrees Centigrade or higher) can destroy the insulating properties of silicon nitride.

5.3.3 Alignment by capillary force

The pressure caps are to be mounted on the sensor element. For single element assembly this is done manually. With the use of glob-top epoxy glue this can be simplified. The glue has a certain wetting action so is sticks to the substrate. When the upper part, as depicted in Figure 5.15, is placed with epoxy glue on the lower part, the glue wets both surfaces. With a slight misalignment of the caps there is an enlarged exposed glue-surface, as is shown in the figure to the left. Due to this enlarged surface and the contact angles between the glue and the substrate a force exists on the upper cap to the right. Since the glue is also a good lubricant (when not cured) the upper cap moves to the right until a minimum in exposed surface and an optimum contact angle is obtained. The cap aligns itself on the right place. This alignment is observed to be better than 0.1 mm in the case of the back chamber mounting process.

For a successful assembly the amount of glue has to be controlled precisely. When

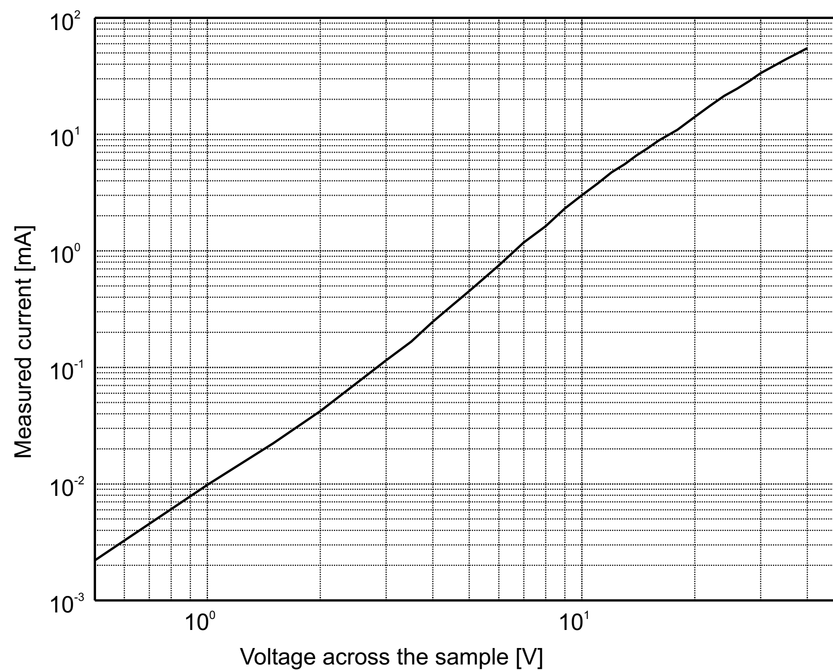

Figure 5.14: *The current through the sensor versus applied voltage. A logarithmic behavior is observed, indicating a semiconductor behavior.*

there is too little glue there will be friction and the alignment will be incomplete. On the other hand when too much glue is applied the capillary forces are lower and the precision is also less. A good practice is to apply the glue with a metal wire to cover all interfacing areas with a layer of 0.05- 0.1 mm. The obtained thickness depends on the viscosity and curing-speed of the glue. The cap must be of the same shape as the sensor to maximize capillary force. In Figure 4.24a the end result of the process is illustrated.

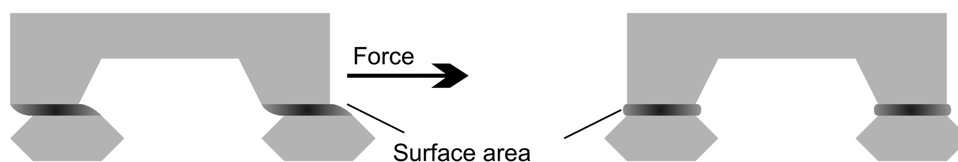

Figure 5.15: *Alignment by capillary force.*

5.4 Conclusions

The fabrication of platinum wires with a width of 2 μm is discussed. Underneath the sensor wires the silicon substrate is etched away, leaving these wires only supported by their endpoints. For single sided and double sided designs almost the same process is used. Separating the fragile devices from the wafer by sawing and using break out structures are discussed. When protecting the fragile parts with a removable protecting material dicing

is successful. Sensors on double side processed wafers are separated through a break-out design. Design rules for a practical break out design are discussed.

A multiple layer design is discussed involving the mounting of chip with a small cavity on top of a sensor chip. A successful fabrication of the cavity chip with both etching silicon in KOH and powder blasting is possible. The cavity chips are finally separated from the wafer by sawing. The cavity chip is manually put on the sensor chip and assisted by capillary forces towards the designated place. Resolution of alignment is high enough for the purpose of developing a sound pressure device.

The assembly of sensors to a sensor element is normally done by bonding an element to a substrate and wire bonding of the electrical connections. This is a complex and time consuming method for chips with multiple and double sided electrical contacts. The mounting of a device in a connector is a fast and simple way to mount sensors but the size of the assembly is increased by the size of the connector. Soldering elements to a carrier board provides both a mechanical and electrical connection with a minimum increase in size.

Chapter 6

Applications

6.1 Introduction

Applications of a device are situations where the device can be of use to solve a problem. To find an application for a device is a process that is exactly the opposite of what is resourcefulness in general. Normally when a situation requires a solution, the particular needs to find a solution are derived, and from this a specific tool can be found or made that can fulfill those needs.

The other way around, when designing a certain tool, a basic application is generally known. In the case of a three dimensional sound intensity probe this is indeed true, one can measure the three dimensional sound intensity vector, but there are many more possible applications for such a sensor.

Some applications are:

- Sound intensity: by measuring this quantity a measure of the radiated sound energy is obtained, giving information on the sound. Using a three dimensional sound probe enables the user to measure the 3D sound Intensity flow profile, which is useful especially for complex sound fields [72]. The direction of the sound intensity (flow profile) can be used to find the origin of a noise source, while the magnitude is useful to compare sound sources or to derive the sound pressure or particle velocity field at other places.

- Acoustic impedance: this value can give valuable information on e.g. a structure, material or sound source. With the use of a sound pressure sensor and a particle velocity sensor the measurement can be done in-situ [25] [26] [27] [28] [29].

- Particle velocity measurement is a valuable quantity in several cases; in some situations the particle velocity signal has a better signal to noise ratio than with the sound pressure sensor. Also the particle velocity signal can be used to measure structural velocity, implying a small and contact-less measurement of vibration [73].

- Multiple sound pressure and Particle velocity sensors can be formed to an array. Visualization of these signals can be very useful in sound source finding [74].

- High temperature measurement: the integrated 3D sound intensity probe is able to work at elevated temperatures and chemically reactive environments [75], this can open up application fields where regular sensors cease working, for example for acoustic measurement in a combustion engine.

Only some of the many possible applications are discussed in this chapter, mainly focusing on the goal to detect sound sources. Sensor configuration, methods and accompanying instrumentation are discussed. Instrumentation is in some cases of large importance; when e.g. speaking of 'a hand held noise source finder' the size and weight of the apparatus must not inhibit the user from carrying the apparatus. Or in applications involving the use of a large number of sensors the amount of cabling can be a problem.

6.2 Acoustic Noise Source Finder application

The following is based on the paper presented at the automotive congress FISITAS 2007 [76].

6.2.1 Introduction

An apparatus has been developed to find acoustic sound sources in the near field of a radiating object operating in a noisy environment. It is based on two orthogonally placed particle velocity probes. The complete signal processing is done in real time with battery powered analogue circuitry, resulting in a very small and hand held measurement device. One particle velocity sensor is used to display the sound level and to provide the possibility to listen to the source whilst rejecting the background noise and another particle velocity sensor is used to indicate in which direction the device must be moved to pinpoint the noise source.

6.2.2 Description

In complex sound fields, e.g. diffuse sound fields, with reflections or many simultaneous radiating sound sources, it is often difficult to find specific sound sources with only sound pressure microphones. However, in the near field of sound sources the use of a particle velocity sensor is advantageous over a sound pressure microphone [77]:

1. The sound pressure level and particle velocity are related by ρc in the free field. When approaching an acoustic hard surface that does not vibrate, sound pressure due to other (background noise) sources doubles against this surface and particle velocity in the normal direction of the plane reduces to zero. Therefore a particle velocity sensor with sensitivity in the normal direction to the plate surface picks up only a small percentage of the background noise. The sound pressure microphone picks up this (doubled) noise.

2. Vice versa, close to a point sound source the acoustic impedance is determined by the near field effect $Z_a = \rho c \frac{ikr}{1+ikr}$, implying that for small distance r the particle velocity is much higher compared with sound pressure than in situations further away.

3. A sound pressure microphone is omnidirectional and thus measures the sound field in all directions. A particle velocity sensor measures the particle velocity in one direction only (assuming here a measurement in the direction toward the source). Therefore when measuring in a diffuse sound field a (directional) particle velocity sensor measures less of the total diffuse background sound field whereas a sound pressure microphone (omnidirectional) measures the total sound pressure field. This on its turn results in a lower signal to background-noise level. As described in [77] when measuring with a directional sensor in a complete diffuse sound field only one third of the total field squared is detected compared with measuring with an omnidirectional sensor.

The hand held Acoustic Noise Source Finder (ANSF) consists of two particle velocity sensors placed orthogonally to each other. Particle velocity sensor A with sensitivity vector $S1$ aims in the forward direction and particle velocity sensor B is placed perpendicular so that the sensitivity is zero in the forward direction. See the photograph in Figure 6.1 for a graphical representation. On top of a printed circuit board a black piece of silicon is shown, wires are placed in a small gap, and for this element the sensitivity direction is in line with the printed circuit board (S1). The other element is placed on the other side and has sensitivity direction $S2$.

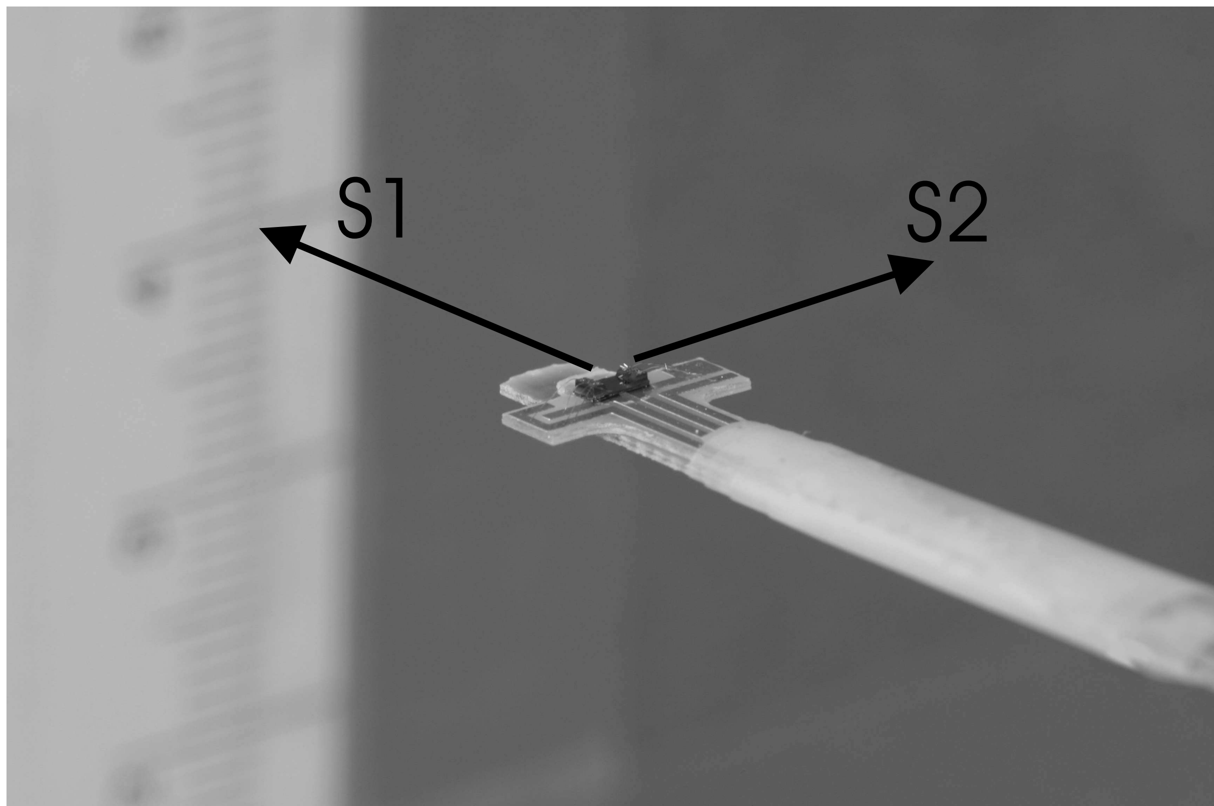

Figure 6.1: *Photo of the particle velocity sensors*

The signal of sensor A ($S1$) is amplified and fed to a pair of headphones. Because of the three effects mentioned before, this sensor has the benefit of a rejected background noise

level and a relatively high signal from the source. So with this particle velocity sensor A is already able to find sound sources in a better way than a single sound pressure microphone.

The source is found at the position where the sound is at its loudest. Although it is possible to find sound sources with only one particle velocity sensor, a second, perpendicularly placed particle velocity sensor is added. With the use of the second sensor it is possible to obtain a signal that indicates the direction of the particle velocity signal, enabling both indication of direction and an enhanced precision in noise source finding.

With some additional electronics there is now a possibility to send directivity information to the ears of the user. Once the two particle velocity sensors are moved over the sound source, the source signal distributed between the headphones left and right channel so that the source can be located easier.

6.2.3 Sound source localization

When a particle velocity signal is present with a component in the plane of sensitivity of the two sensors the signals can be used to determine the direction and magnitude of that particle velocity signal. Assume that the particle velocity signal is a pure sine signal. When multiplying the signals there is a resulting signal given by:

$$U_s = \frac{1}{2}A.B \cdot sin(2\alpha) \cdot sin^2(\omega t) \tag{6.1}$$

With A the amplitude of the signal from sensor A and B the amplitude of the signal from sensor B, ω the angular frequency and α the angle of incidence. Depending on the value of α the sign of U_s changes. The time average of this signal divided by the amplitude A of the particle velocity signal (extractable from sensor A and B) gives a direct measure of the angle of incidence of the particle velocity direction and level. The signal U_s can be used together with the signal obtained from particle velocity sensor A to locate the source of an acoustic noise source when connected to an indicator displaying the average voltage.

Measurements procedure

The apparatus is hand held and turned on. The frequency filters are adjusted in such a way that the sound to be located is heard clearly through the headphone in an as small as possible bandwidth. When the source of the noise is on the left side of the sensors the voltmeter, showing the averaged multiplied signal, shows a negative voltage (meter is turned to the left), and vice versa when the noise source is on the right side. When the source is exactly in front of the sensor the meter shows "zero", or "straight ahead". Together with this voltmeter two variable gain amplifiers are steered in such a way that the user experiences the noise going from left to right when moving the noise source finder from right to left. This assists the finding of the noise source.

6.2.4 Implementation

Since the processing is relatively simple an analog processing circuit has been used for this prototype. Schematically the electronics fulfilling the desired functions can be summarized as shown in Figure 6.2. The signal of sensor A is amplified, band pass filtered and then supplied to a headphone section with AC voltmeter. Band pass filters are needed for two reasons: First they enable the user to focus on a specific noise source, and secondly to get a useful output from multiplying the signals in the time domain. When for example, multiplying 1/f (pink) noise signals with a specific bandwidth the lower frequencies in that bandwidth has a large influence on the output level. If the bandwidth is not too large this effect is less.

In principle it is now already possible to find an acoustic hot spot in a certain frequency band. The use of headphones facilitates finding of specific noises. When the audio signal is at its loudest, the acoustic hot spot has been found. Advantage of filtering is that one can localize a specific (band pass filtered) sound among other sounds.

The signal of sensor B is also band pass filtered and then multiplied with the band pass filtered signal of sensor A. The resulting signal is averaged in time. This results in a signal that is zero if the sensors are located exactly in front of the hot spot, a negative DC signal when the sensor is on the right of the hot spot and a positive DC signal when the sensor is on the left of the hot spot. This signal is fed into a voltmeter which can be used for indicating where to move the ANSF in order to locate the hot spot. The multiplied and integrated signal is also used to operate two voltage controlled amplifiers feeding the audio signal to the headphones. Panning of the audio signal between the left and right channel is controlled by the DC signal. When the hot spot is on the left side of the ANSF the left headphone signal is louder and vice versa. Only when the hot spot is in front of the ANSF the signal is equal on both headphone channels.

Amplifiers $A1$ and $A2$ can be replaced by voltage controlled amplifiers as well, improving the working of the system in terms of a larger dynamic range. Optionally there is a frequency correction circuit; this is implemented to correct the frequency response of the particle velocity sensors in terms of a high frequency amplification to improve audio fidelity.

6.2.5 Measurement results

Next a series of measurements is performed, starting with the intuitive Acoustic Noise Source Finder or ANSF. Use is made of an automated robot to ensure exact positioning of the device and reproducibility of the measurements. Firstly the ANSF is tested in a quiet environment with only one source near the sensor. Then the usefulness of sound pressure sensors and particle velocity sensors when measuring near a sound source are compared. Dependent on the outcome of these measurements the measurements with the ANSF are continued, but now with background noise present.

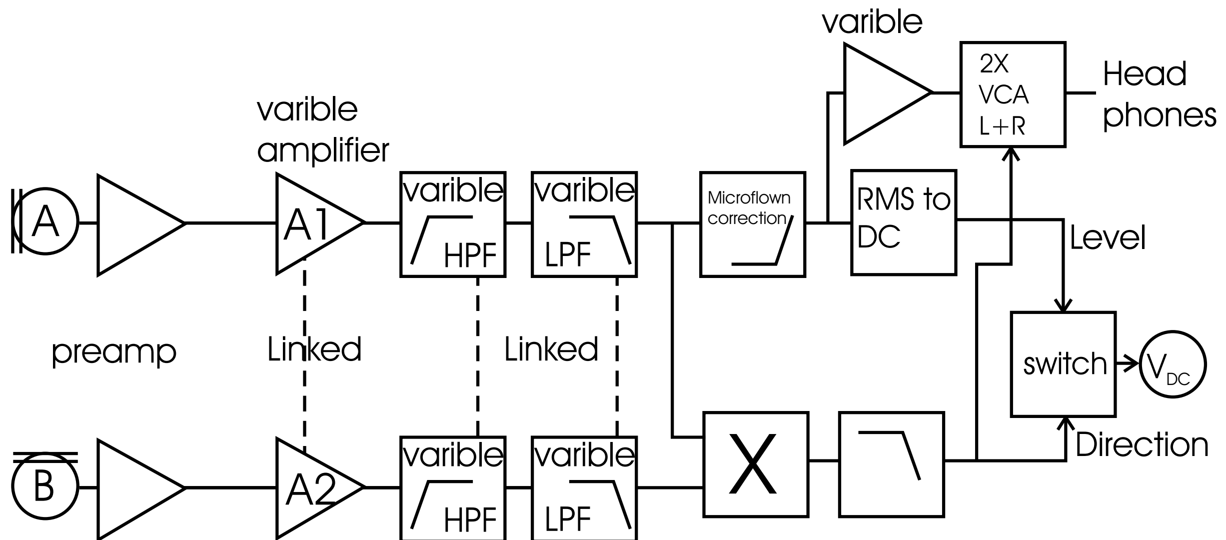

Figure 6.2: *Schematic representation of electronics*

Measurements with the ANSF

Measurements are performed using the direction signal and the band pass filtered signal from sensor S1. The two particle velocity sensors were placed at a distance of 2.5 cm from a plate with a sound source in it. Next a scan was made in a plane parallel to the plane with the source, see Figure 6.1, the plate can be seen fuzzy in the background, and was placed vertically. The source consisted of a loudspeaker behind a hole with diameter of 2 cm and was excited with white noise. For these measurements a band pass filter was chosen with a pass band from 100 Hz to 1 kHz, which is very wide and a more difficult test for the system when using a narrow band. A scan with 15 points in the horizontal direction and 9 points in the vertical direction was made, the distance between neighboring points was one centimeter. First a scan is made with the sensitivity axis of sensor two (S2 in Figure 6.1) in the horizontal direction and next in the vertical-direction. The resulting output signals of the scan with sensitivity in the horizontal direction are plotted in Figure 6.3a. As can be observed the amplitude of the signal is maximum when approaching the source, and changes sign when crossing the source. Using sound pressure sensors instead of particle velocity sensors would not result in a change of sign. The same measurement has been performed with sensor two's sensitivity axis parallel with the vertical axis. Results of these measurements are shown in Figure 6.3b, which are clearly similar to results shown in Figure 6.3a, except that the figure is rotated 90 degrees when seen from above. Since measurements were done in the whole plane at a fixed distance both in the horizontal and vertical direction, this creates the possibility to display a vector plot of the measurements which is shown in Figure 6.4a. Clearly the arrows point toward the point source; however at larger distances the arrows are too small to recognize a direction. Therefore the same graph is printed in Figure 6.4b, but with a logarithmic scale of the values. At the edges the values do not point toward the source anymore, there the system is not sufficiently sensitive since the sensor pointing to the plane with the source has barely signal strength because the component in this direction is very small. At 6 cm distance the vector plot

is much smoother and values all over the whole grid point toward the source, the signal is now much more constant over the scanning surface. See Figure 6.5 for the 2-D vector plot of this data.

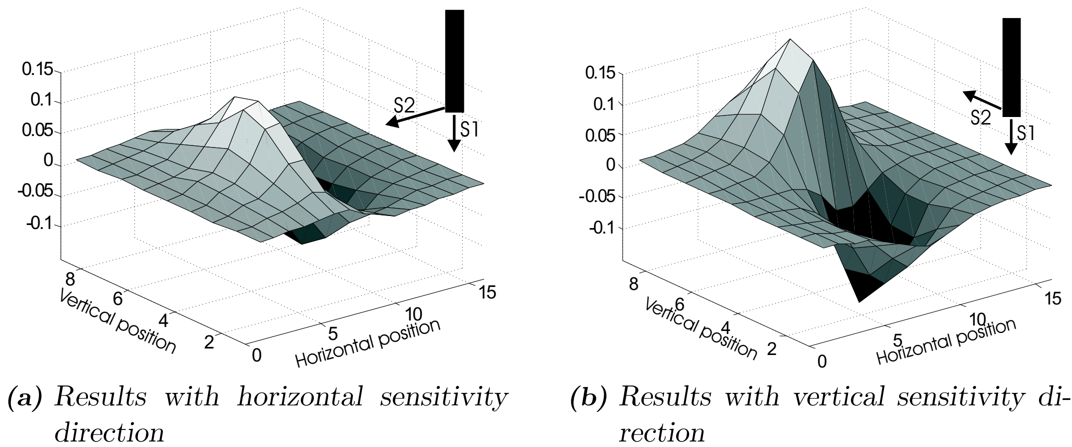

(a) *Results with horizontal sensitivity direction* ***(b)*** *Results with vertical sensitivity direction*

Figure 6.3: *Measurement results of scanning a point source and plotting the averaged multiplied signal source.*

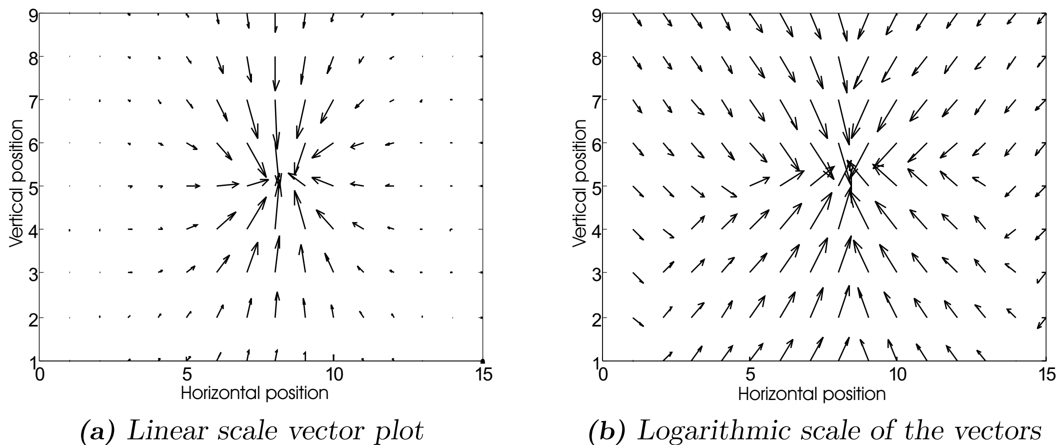

(a) *Linear scale vector plot* ***(b)*** *Logarithmic scale of the vectors*

Figure 6.4: *Vector plot of measurements at 2.5 cm distance.*

6.2.6 Comparison between the sound pressure and particle velocity signal

To illustrate the difference between using a sound pressure microphone or a particle velocity sensor when scanning near a sound source a comparing test has been made. A measurement scan over the source with one particle velocity sensor pointing in the direction normal to the plane with the source and with a sound pressure sensor was performed. The measured auto spectrum in the frequency range of 100 Hz to 200 Hz of both sensors is taken for each place in the scan. The results of the measurements are shown in Figure 6.6a. It is seen that the sound pressure sensor signal shows a clear peak in the

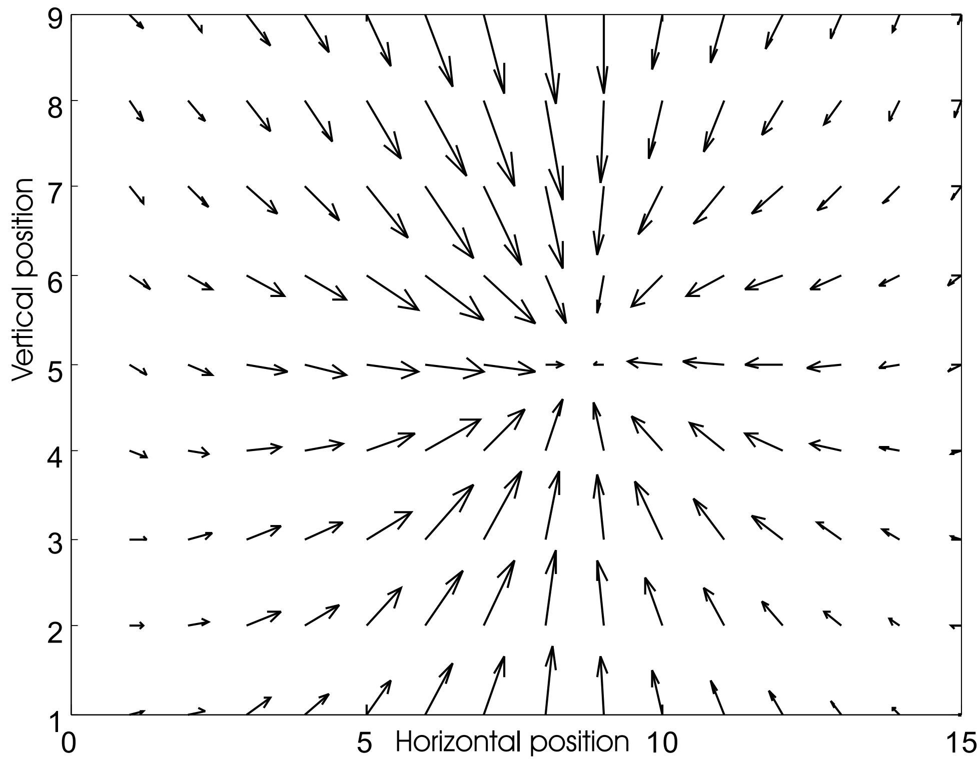

Figure 6.5: *Measurement results at 6 cm distance, linear scale*

response when near to the source. The particle velocity sensor has a sharper peak, which originates from the directive nature of the particle velocity sensor. Both methods can be of use. However, in much cases background noise is present. So the scanning test was repeated, but now with an external sound source generating background noise. The background noise level is set so that when a sound pressure microphone is positioned 5 cm away from the sound source in the plate the background noise level results in a higher sound pressure signal than the source in the plate produces. Clearly the sound pressure signal now gives at best a very rough indication about the location of the sound source, whereas the particle velocity sensor signal gives a similar result as in the situation without background noise as shown in Figure 6.6b.

6.2.7 Measurements with the ANSF and background noise

Another scan with the two sensor system was performed with 5 cm distance from the plane with the source and with background noise. The background noise level was the same as in the test described above. Together with the direction signal (the averaged multiplied signal) the amplitude of the signal from sensor A, pointing toward the plane, is monitored. This time the filters are adjusted to a smaller bandwidth. To evaluate the frequency response of the filters a frequency response of one channel of the system is shown in Figure 6.7a, showing that the filter is set to a relatively narrow pass band of 150 Hz to 225 Hz. In Figure 6.7b both signals are plotted versus the horizontal distance. The values are scaled, since absolute values are not of importance here. The source can be

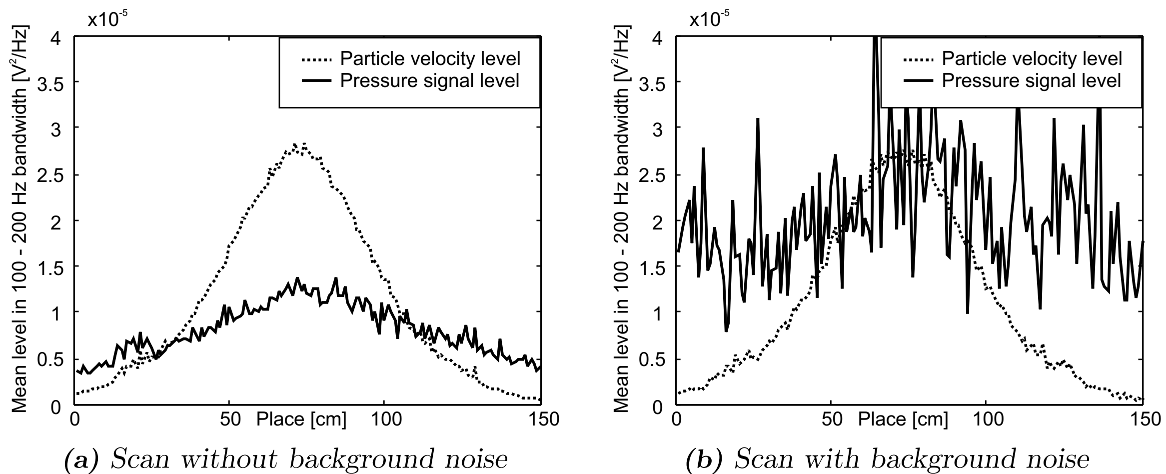

(a) Scan without background noise *(b) Scan with background noise*

Figure 6.6: *The response of the sound pressure sensor and the particle velocity sensor with and without background noise are compared.*

found at the maximum of the amplitude of the signal from sensor one and the changing of the sign of the direction signal. Here the use of the direction signal comes to its right; with help of the output signal of sensor A the source can be found globally, but the direction signal gives the exact point.

The results that are depicted in Figure 6.7b are measured in the presence of background noise level equal to the level used in the experiment before. From the previous results it was shown (see Figure 6.6a and Figure 6.6b) that the particle velocity sensor aimed in the direction normal to the plane with sensitivity direction $S1$ is not or barely affected by background noise. A particle velocity sensor pointed in the lateral direction ($S2$) however is affected more by background noise because the lateral component of the background noise does not reflect on the surface. However because the lateral velocity is multiplied with the normal velocity and averaged, the effect of the background noise is theoretically averaged to zero and has therefore low effect.

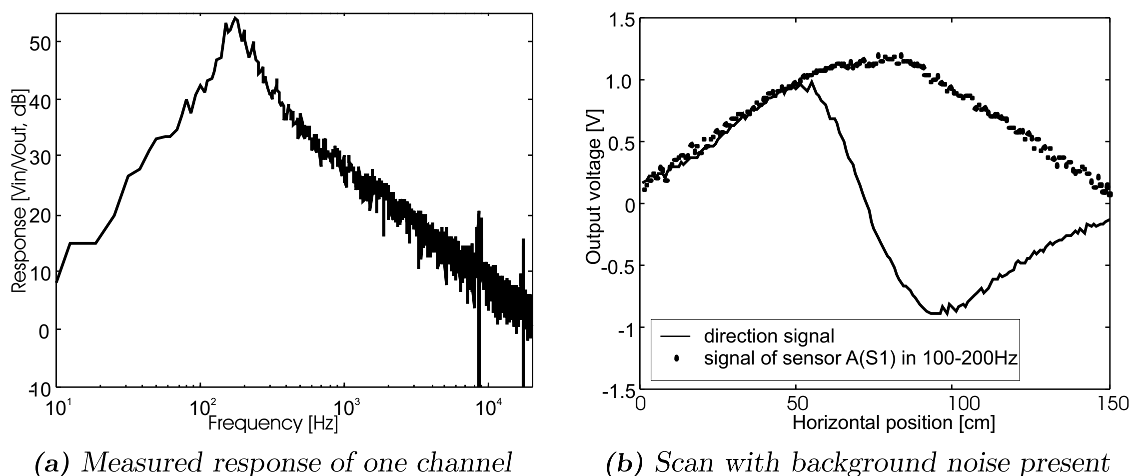

(a) Measured response of one channel *(b) Scan with background noise present*

Figure 6.7: *Measurement at 5 cm distance and background noise present.*

6.2.8 Conclusions

An intuitive acoustic noise source finder for use in an environment with background noise has been presented. A direction indicator pointing toward the source enables the user to find a noise source quickly and intuitively. It has been shown that background noise has less influence on the measurements near a sound source when measuring particle velocity than when measuring with sound pressure microphones.

6.3 Very small sound source localization

As shown in the previous part sound sources are more difficult to identify with single sound pressure microphones than with particle velocity sensors when close to a sound source. Good results are possible with a multi-microphone setup, but this normally requires a measurement setup with low background noise and complicated signal processing.

When using the particle velocity signal for locating small sound sources both the direction can be determined and the effect of background noise is diminished, see the previous section or [76], [78] and [79]. Here measurements on a very small sound source are presented, showing the possibility to measure the sound field generated by small (electronic) components together with background noise immunity. This enables for example automated end of line control in a factory even in a noisy environment. End of line control is testing whether the end product is working well or not. Acoustic end of line testing is done for electrical toothbrushes, small pumps , loudspeakers, car mirror adjustment units and numerous other products.

6.3.1 Measurement setup

A three dimensional particle velocity sensor together with a commercially available sound pressure microphone (a Knowles FG type) was used to determine the sound field around a known sound source emitting sound at a frequency of 2 kHz. At a distance of 7 mm above this sound source the sound field was scanned with a step size of 1 mm. In Figure 6.8 the three dimensional particle velocity sensor is shown, together with the sound pressure sensor mounted just above the element. The sensor element was positioned by a pen-plotter.

A small point source was used. When applying an AC voltage across another particle velocity element, heating the wires periodically, a sound is emitted at twice the excitation frequency. Since the actual size of the particle velocity element is 1.5 mm long and 300 μm width it can be treated as a nearly perfect point source.

6.3.2 Measurement results

For all measurement results the sensor is calibrated for both directionality and signal strength.

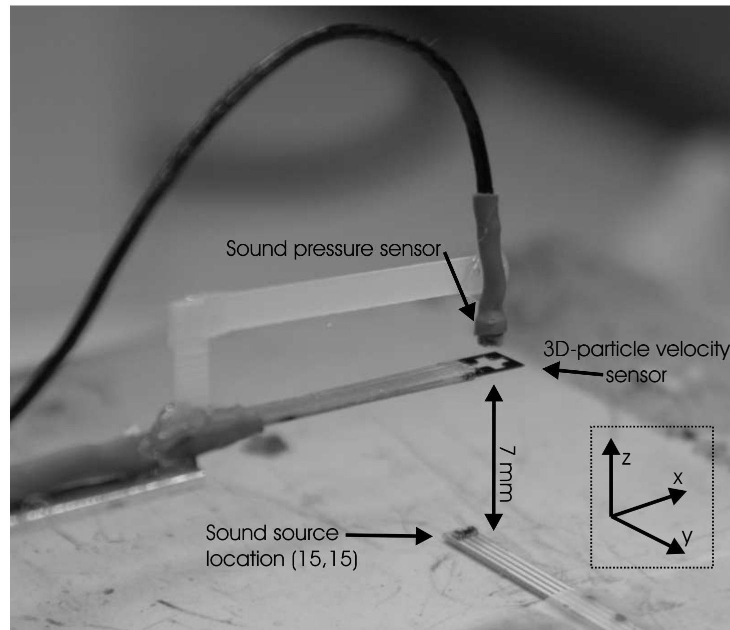

Figure 6.8: *Measurement setup*

Results of a 27 times 27 points scan over a small sound source

Measurement results of the auto spectrum are plotted in Figure 6.9. In the center of the figure the auto spectrum contour plot from the sound pressure sensor is shown. From the contour it is observed that the signal is point symmetric around the sound source which is found in the middle, near location (15,15). The dynamic range between maximum and minimum level in this graph is 14 dB, and is only dependent on the distance of the source and the near field effect. A distance increase from 7 mm just above the source to the outer measurement corner of 22 mm in total, gives a decrease of ten times (10 dB) regarding sound intensity as expected. From the near field effect the sound pressure at 7 mm compared with the sound pressure at 22 mm drops another 4 dB, adding up to 14 dB.

For a directional sensor the dynamic range is much larger, since for particle velocity directions perpendicular to the sensitivity direction the sensitivity is theoretically zero. In this experiment this angle of incidence is reached, so in principle without accounting for reflections the dynamic range must be equal to the maximum recorded signal minus the self noise of the sensor. Together with this the earlier mentioned dynamic range loss of 4 dB due to the near field effect for the sound pressure microphone is added to the dynamic range of the particle velocity sensor. However due to reflections at the surface and sensor imperfections the dynamic range is here limited to 40 dB.

Because a three dimensional particle velocity sensor has been used it cannot be determined whether the direction of the particle velocity signal points to or from the sound source. From particle velocity signal measurement results at different places it is possible to derive the direction of the sound source at every measurement point, or when using the pressure signal (which is non directional) the direction can be found.

Combining the signals of the auto spectra from the particle velocity sensors the directions were obtained and a vector plot was constructed, here the direction of the particle velocity signals is set to be in the direction of the sound source. In Figure 6.10 this vector plot is shown, with only a limited number of the available 27*27 arrows. Of course, not all measurements have to be made to identify a single sound source, the sound source can also be identified with one or two measurements, when no errors are made. In the measurement results no measurement errors are found in the made scan.

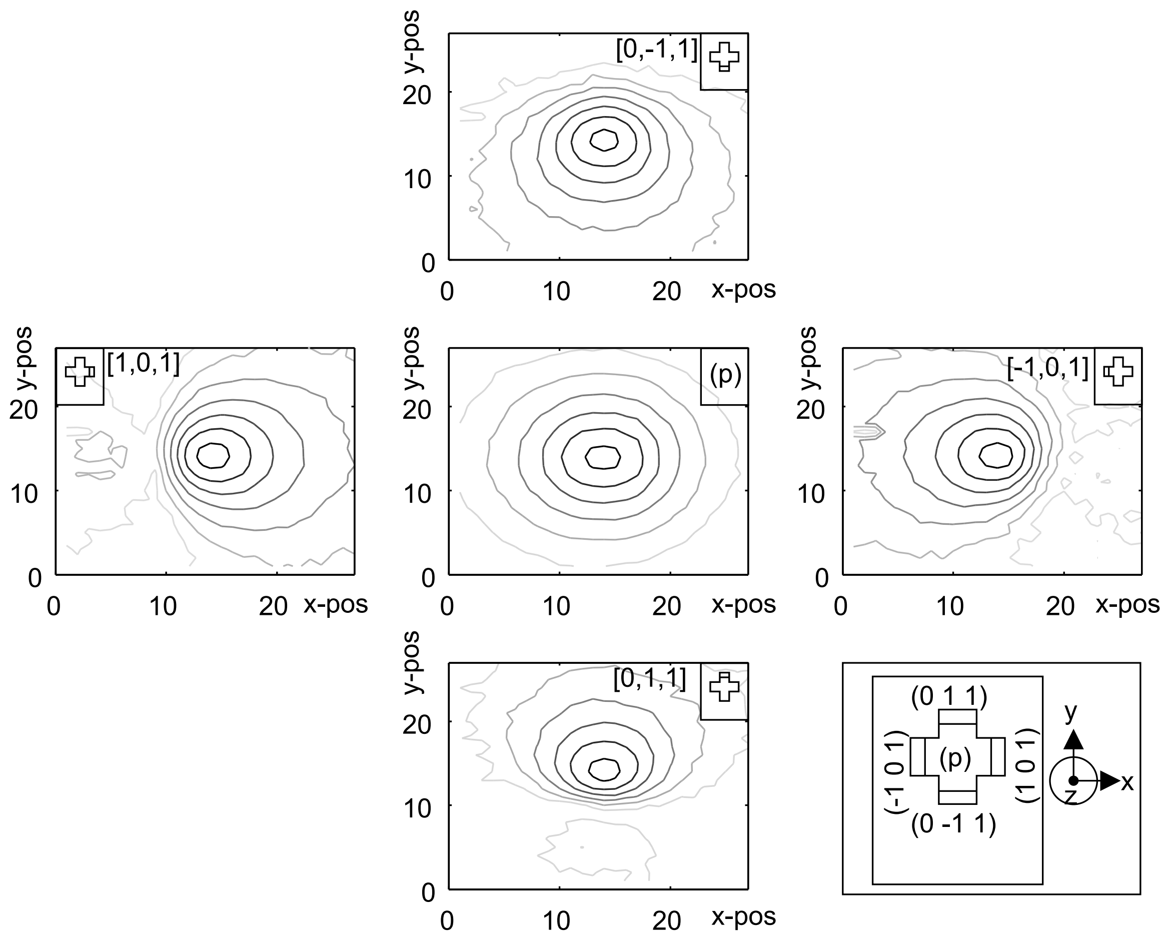

Figure 6.9: *Contour plots of the signals acquired by scanning the surface above a sound source. The middle plot shows the contour of the sound pressure signal, Between the lowest contour and the highest contour is 14 dB, for the particle velocity signals this is 40 dB. Horizontal axes correspond to the x-axis, vertical axes to the y-axis.*

Results in the presence of background noise

Measuring near a sound source better results can be obtained using particle velocity sensors. Following the results of a measurement scan with background noise are presented. The particle velocity sensor shown in the most right plot in Figure 6.9 is used, with

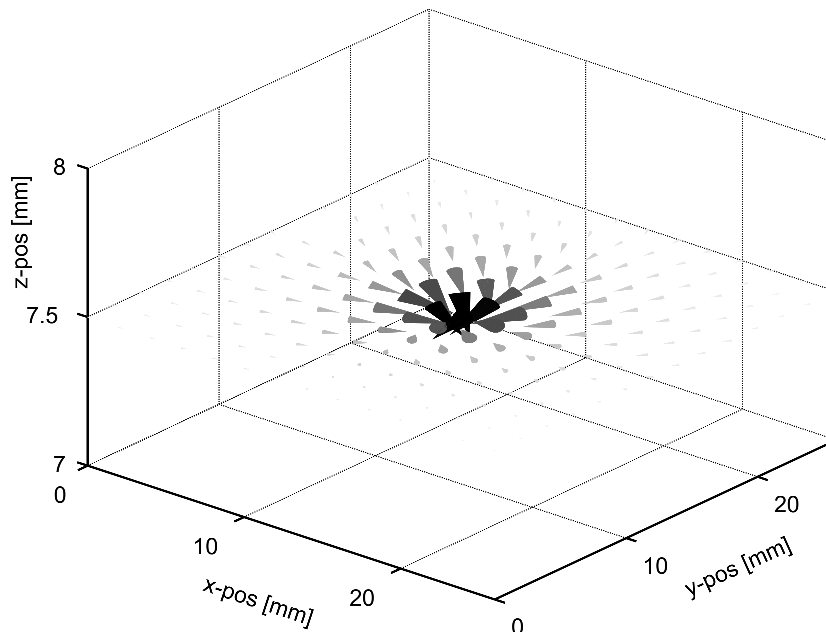

Figure 6.10: *Cone plot of the particle velocity vector field, strength is related to color (black is largest signal level) and the arrows are pointing toward the sound source*

further the same measurement setup as described in the previous experiment. Both for the background noise and for the signal from the sound source a tone with frequency 2 kHz was used. The background noise increased from a low level of some dB's below the signal strength to an intermediate level where the background noise detected by the pressure sensor is just somewhat smaller (1 dB) than the signal from the source (at position (15,15)) and finally a louder background noise level was used.

Due to the increasing background noise the pressure signal is increasingly disturbed, from Figure 6.11a to Figure 6.11c to 6.11e the shape of the contour plot is disturbed and the dynamic range lowers significantly. At the right side of Figure 6.11b to Figure 6.11f, where the contour plots of the particle velocity signal are plotted, no remarkable influence of the background level is seen, apart from a higher noise level on the left side of the center position (at (7,7)). Also the dynamic range is lower, but it is still much larger than the pressure signal.

From the auto spectra of the particle velocity signals for every case a plot similar to that in Figure 6.10 plot can be made, resulting in similar pictures, even with background noise present.

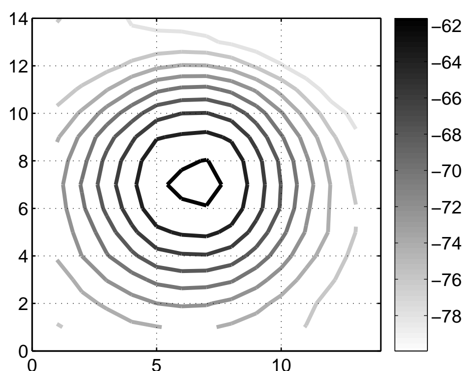

(a) Measurement with no background noise present, pressure signal.

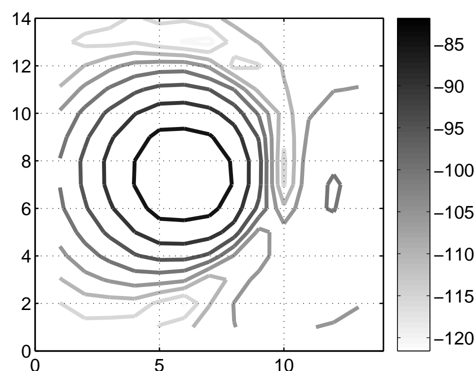

(b) Measurement with no background noise present, particle velocity signal.

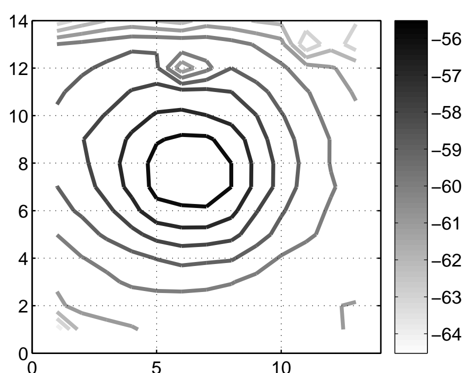

(c) Measurement with some background noise present, pressure signal.

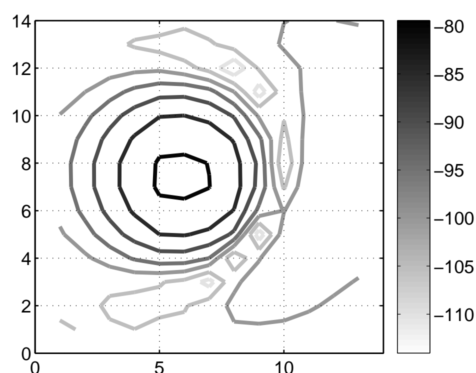

(d) Measurement with some background noise present, particle velocity signal.

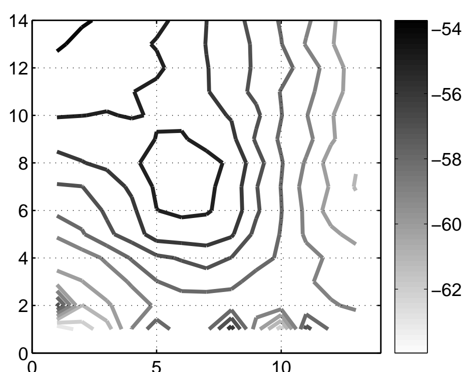

(e) Measurement with loud background noise present, pressure signal.

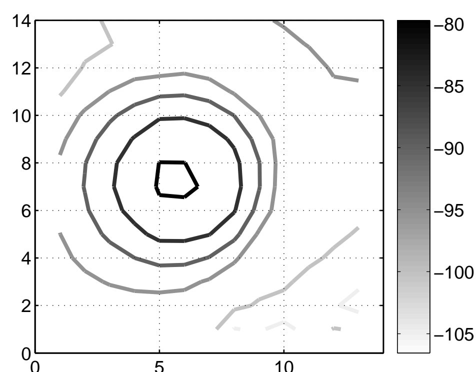

(f) Measurement with loud background noise present, particle velocity signal.

Figure 6.11: *Measurement at 5 cm distance from a piezo loudspeaker and various levels of background noise. Figure (a) and (b) show results without background noise, (c) and (d) are measured with background noise level just below the signal level detected by the pressure microphone exactly above the source. Figures (e) and (f) are the results of a measurement with a high level of background noise.*

6.4 A portable sound intensity array system

In an array setup the sound intensity from a number of spatially distributed sensors is measured, and visualized by colors in two dimensions as shown in Figure 6.12b. This principle is commercialized as an 'acoustic camera' [22]. Only one specific bandwidth is used at a time and the sound intensity in that bandwidth is displayed as a color in a two dimensional plane. The setup enables the user to investigate the sound intensity measured by the array in real time, and observe effects on the sound field immediately.

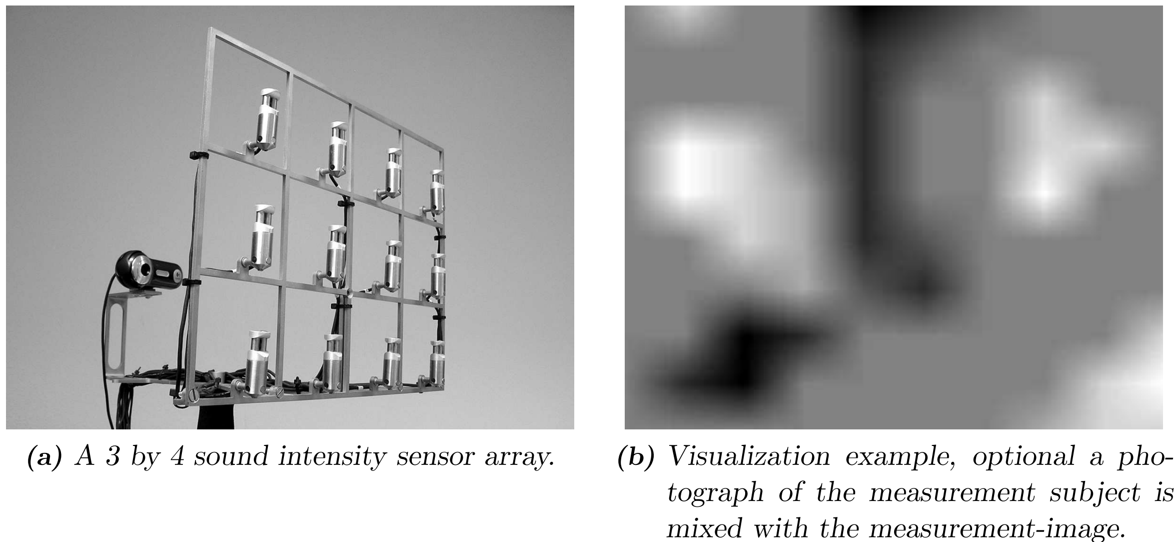

(a) *A 3 by 4 sound intensity sensor array.*

(b) *Visualization example, optional a photograph of the measurement subject is mixed with the measurement-image.*

Figure 6.12: *An array of sensors and application example.*

6.4.1 The regular approach of an array system

The existing solution works as schematically shown in Figure 6.13. The signals from the sensor array to the visualization unit are analog and require one wire per sensor. Sound intensity is the product of particle velocity and pressure, so in a (one-dimensional) sound intensity probe two sensors are present. The analog signals from the sensors enter a processing unit. After processing the averaged sound intensity signal in a certain bandwidth is displayed on a screen.

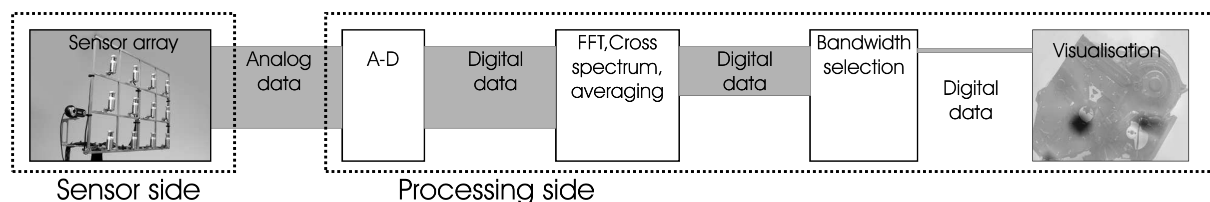

Figure 6.13: *An array approach depicted, on the right side the post processing unit is shown, on the left side the sensor array is shown and the blocks are electrically connected.*

For such a system, a sensor array, amplifiers, an analyzer or analog-to-digital converter and a visualization unit are needed. Using this approach requires much cabling and processing power both increasing with the number of sensors in an array. In case an object is measured only once and the obtained data is post-processed or when the sound is not stationary this approach is appropriate. The amount of data from the sensors at full bandwidth is for an array with 12 sound intensity probes 18 Mega bytes per second (48 kHz (the sample rate) times 16 bits (sampling resolution) times the amount of channels, which is here 12 'p' and 12 'u' channels).

Assuming that it is desirable to display the sound intensity (which is the product of the 'p' and 'u' signal) as colors in a plane as depicted in Figure 6.12b. With a graphical update speed of ten times per second and a resolution of 16 bits (two bytes) per sound intensity probe this requires the signal of 12 P-U sensors, times 10, times 2 bytes = 240 bytes per second. Clearly the amount of data that remains for this is very small (≈ 0.01 $^{o}/_{oo}$ of the original data rate).

6.4.2 A realization with a low data transfer rate

Figure 6.14 shows a different approach, leading to a much lower data transfer between the array and visualization unit. In the block named 'FFT' in Figure 6.13 the digital time-data signals are transformed to the frequency domain and averaged over a certain time. Next a frequency band is selected and the sound intensity values are displayed on screen as a color. The colored image obtained is refreshed several times per second to provide a 'camera' view. From the original data stream effectively only one data point per sound intensity probe per update remains.

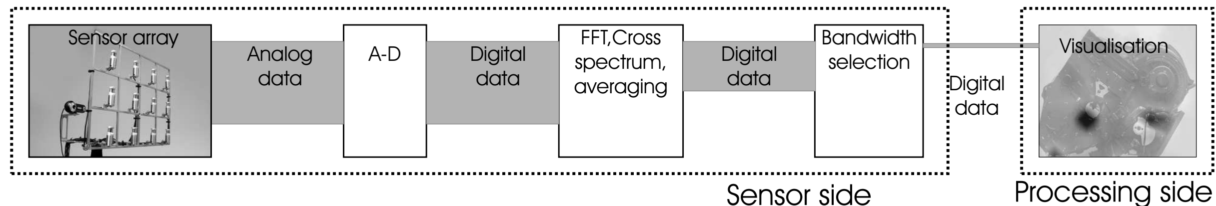

Figure 6.14: *The reduced data approach depicted schematically.*

The data reduction takes place in the processing unit. When the processing unit is moved to the sensor location and only the data which is really needed for visualization has to be transmitted between the array and the visualization unit. Each sound intensity probe can have its own processing unit but it can be profitable to combine several units in one (larger) box. The probes are then connected by analog wiring to this box, but wire length between the probes and the box can be kept short. One cable connects the processing units to an external visualization unit. On a single cable multiple processing units can be connected, sharing wires.

Figure 6.15 shows a possible realization of such a system, which will be called Sound Intensity Measurement Device or SIMD. In the figure two amplifiers are shown, which

adjust the 'p' and 'u' signals to match the D-A converters in the DSP chip. Processing is done a little different as in the 'full bandwidth' approach, the signals are filtered by the DSP to the desired bandwidth, so avoiding the FFT transform. The output (a digital signal) is fed to a micro-controller which multiplies and averages the filtered 'p' and 'u' signals. A power supply and a single clock source are used to operate the digital circuitry.

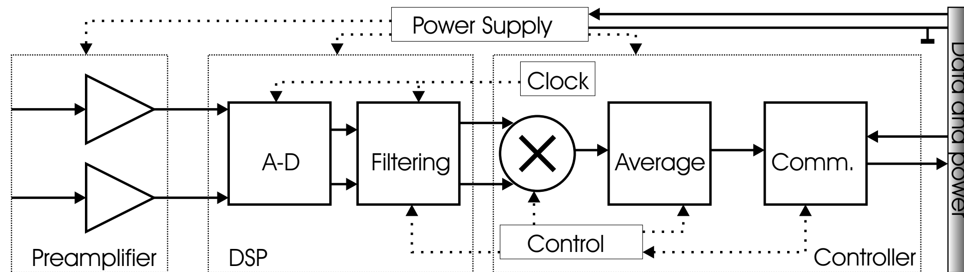

Figure 6.15: *Block diagram of the device.*

When the SIMD is not measuring, the controller takes care of the communication over a low voltage serial port running at 56 kbps, although higher speeds can be achieved. The visualization unit communicates with a simple serial data protocol requiring two wires. Power has to be fed to the sensor and processing device which requires another conductor. With the necessary ground lead the total number of conductors is four. This is not less than needed for a single analog sound-intensity probe, but multiple probes can be connected on the same cable, all sharing the same power supply connections and data bus. To complete the system a small computer to initiate and display the measurements and a power supply is needed. Figure 6.16 shows a photograph of a realized prototype.

Figure 6.16: *Photo of the prototype, the size of the printed circuit board is 7 * 5 cm.*

6.4.3 Measurements with the prototype

To measure with the SIMD first the measurement bandwidth is defined, which takes around 100 Bytes. Including other delays, such as updating the configuration of the devices, this takes only several milliseconds. All devices on a bus can be configured simultaneous or one device at a time, enabling different configurations for each sensor. A start measuring command is issued. When the measurement is finished one node at the time is requested for its measurement data. At the used connection speed of 56 kbps the filter configurations, start of measurement and data readout takes 1 to 2 seconds, excluding the measurement time.

With the prototype a measurement scan was made to test the possibility of sound source localization with this device. A sound source emitting white noise was connected to a short square tube of 4 x 4 cm cross section. The filters in the device were set to a frequency of 200 Hz and the sound intensity was measured at 5 x 5 positions along the x, y and z axis, see the Figure 6.17. The measurements shown in the figure are composed from the x,y and z results.

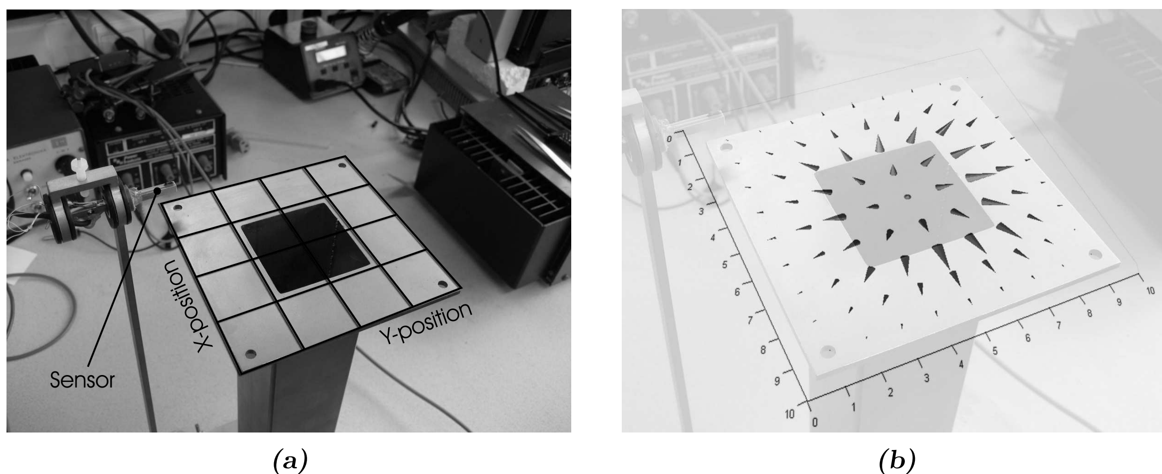

Figure 6.17: *Figure a) shows a photo of the measurement setup and Figure b) shows the measurement results superimposed on the photograph.*

6.4.4 Design improvements

After successful operation of the prototype, an improved version is designed. Although the prototype is operational, it has a large size, is mechanically instable, has no signal conditioning for the sensors and lacks a proper power supply. The newly developed SIMD has a smaller size, is capable of correcting the amplitude and phase response. The size is decreased from 5 cm * 7 cm * 1 cm (l*w*h) to 7 cm * 1.8 cm * 0.5 cm, including power supply and signal conditioning. In Figure 6.18 a box with three of these SIMDs (one is located just behind the black front side) with a wireless transmitter is shown. This configuration is able to measure the three dimensional sound intensity vector, together with receiving and wireless transmitting its data to the receiver. A battery pack is necessary to operate the system. The nodes can be addressed individually (request for

measurement data) or simultaneously (setting the filters and starting the measurement). A short summary of the properties of the new SIMD is given in Table 6.1.

Table 6.1: *Device properties (single unit).*

Property	Value	Units	Remarks
Power supply	12 to 15	V	Extension possible
Current consumption	< 0.1	A	Can be reduced
Size	7*2*0.5	cm (l*w*h)	
Inputs	2	channels	
Sampling rate	48	kHz	32 kHz possible
Sampling depth	16	bits	24 bits possible
Filter type	bi-quad		
Filter order	max. 14		
DSP type	TAS 3002		
Controller type	ATMEGA 88		
Interface type	RS232 and wireless		
Interface speed	300 - 115200	bps	

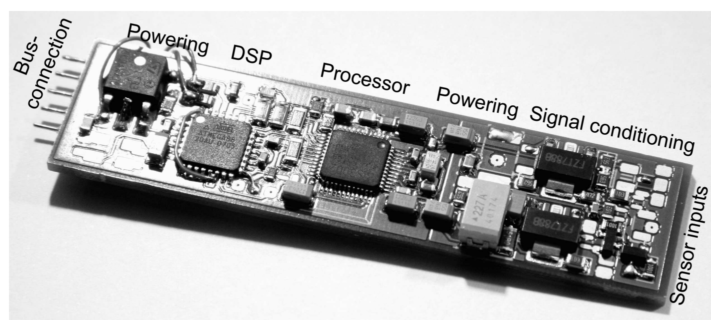

(a)

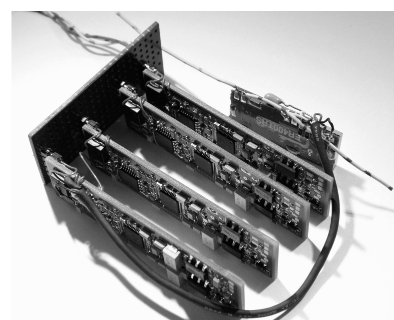

(b)

Figure 6.18: *Figure a, photograph of the improved design, a device is 1.8 x 7 cm large. Figure b, four devices are combined together with a wireless transceiver module.*

6.4.5 Applications with the SIMD

The SIMD is in fact an analyzer, suited for measuring sound intensity. Compared with regular approaches to measure sound intensity, the advantage is that this device is smaller compared with a normally used analyzer, the output data-rate is very low and the device is able to operate in a bus-structured connection. Altogether this leads to a very compact multichannel sound intensity analyzer.

Since the SIMDs are small, they can be located near the sensors in an array, and a lightweight and small sound intensity array can be made. Visualization requires a PC or laptop.

For a three dimensional sound intensity probe as described in this thesis, four particle velocity signals and one sound pressure signal must be processed. Each particle velocity signal is multiplied with the same sound pressure signal. For such a probe a block of four SIMDs makes up for a complete 3D-sound-intensity analyzer, but of course without the visualization unit. Figure 6.19 shows the setup schematically.

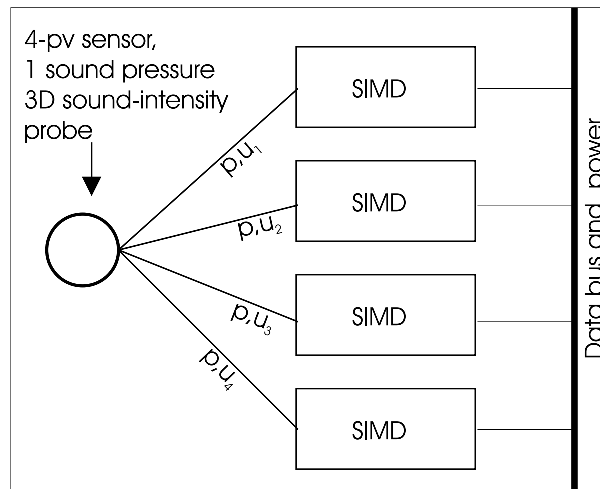

Figure 6.19: *Four individual SIMD devices are combined to one 3D Sound-intensity analyzer.*

An application with finding a sound source using two 3D- sound intensity probes is presented in [80]. In the article a sound card is used and the results are calculated afterward. Instead of the large analyzer a similar system can be made with the presented device, only smaller.

Sound source localization with the sound-intensity measurement device

In [80] and [81] use is made of the possibility to locate sound sources with three dimensional sound intensity probes. In [80] a 3D sound intensity probe (see also Figure 1.6) is used together with a data acquisition device and a computer to calculate the 3D sound-intensity vector. The direction is calculated by multiplying the particle velocity signals with the sound pressure signal and combining this to a three dimensional vector pointing to the sound source. An acoustic pulse is used for the experiment, generated with a starting gun.

With the device presented in the previous section these experiments can be performed similarly, but with the difference that the 3D probes including processing can be small and even wireless connected to the visualization unit. Experiments are performed to investigate whether there is agreement between the results in the article [80] and results obtained when using the device. To investigate this the measurement signals used in both experiments were identical in order to compare both methods in an objective way.

Measurement procedure and results

The 3D sound-intensity probe was connected to a personal computer with a sound card. Time domain measurements presented in [80] were re-used for this project. Five gunshot sounds were used for intensity based estimation of fire direction with respect to the sensor location.

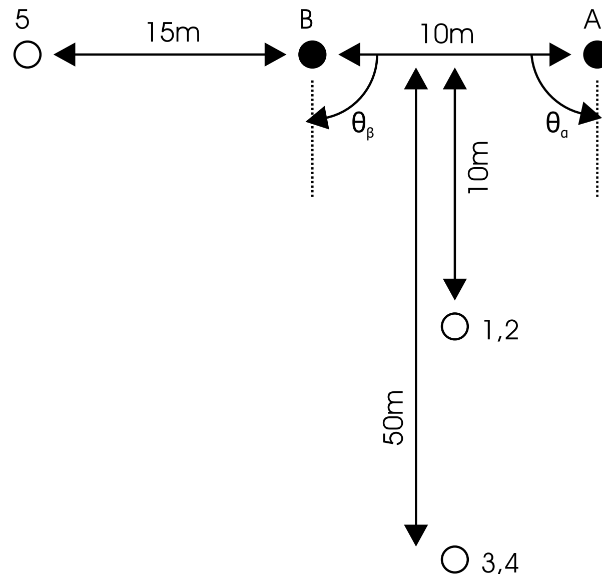

Figure 6.20: *The locations of the starting gun for the respective measurements in the original measurement setup.*

The measurement was initiated by the personal computer, which at the same time plays the time domain measurements used before through a sound card. These time domain signals were input to the SIMD and the results were further converted to the incoming-sound angles and compared with the results given in the paper.

The calculations were performed by direct multiplication of the particle velocity and the sound pressure input signal and averaging the result in the time domain. Results are given in Table 6.2, where the measured m and real angles between source and the two probes are given with the method presented in the paper. In the column m_{SIMD} the results when calculating intensity with the SIMD are shown. Results found through calculating the vector directly from the measured time data and using the SIMD connected to a sound card playing the same measurement data are similar. Altering the signal strength of the output signal of sound card (and therefore the direct input signal of the device) did not influence the measured angles, but of course a difference in the magnitude is observed.

Small differences occur however, and are presumably due to differences in input data. For the measurement results presented in the paper the processed time data is tailored

to the actual gunshot event, with the sound intensity device this is not done. To be sure that the actual impulse is recorded the measurement is started half a second before the impulse and stopped after the impulse is finished, thus calculating the result over a longer time period. This is an explanation for the differences in outcome.

Table 6.2: *Measured and real source directions. The values of θ correspond to the angles in Figure 6.20.*

Measurement	θ_A **m**	θ_A $\mathbf{m}_{SIMD}$	θ_A **real**	θ_B **m**	θ_B $\mathbf{m}_{SIMD}$	θ_B **real**
1	67	62	63	60	67	63
2	55	48	63	81	72	63
3	87	87	84	86	87	84
4	86	85	84	89	89	84
5	-16	-16	0	20	21	180

6.4.6 Conclusions

An approach to reduce the data rate of a multichannel sound intensity system was considered. A prototype was developed and tested. With the system an array can be made capable of measuring sound intensity in a predefined bandwidth. Only one single cable is needed for the whole array, avoiding the problem of large cabling. Additionally a completely wireless approach can be used enabling measurement on moving objects or at large distances. With the SIMD similar results are obtained as with the approach presented in [80] but without the need of the sound cards and large cabling, which enables a far more convenient use.

Chapter 7

Conclusions and recommendations

7.1 Summary of conclusions

In this thesis the successful integration of particle velocity sensors with a sound pressure sensor is discussed in detail.

To facilitate the development of such a sensor an investigation of particle velocity sensors has been performed. This serves two purposes. Firstly better understanding of the sensor and its characteristic behavior enables a good starting point for a new design. Secondly the results are useful for the improvement of sensor quality. In chapter two it is shown that self noise is an important parameter in judging the quality of a sensor. The power consumption of the particle velocity sensor is not considered of main importance for use in measurement systems, lowering the demands on the design of an integrated sensor. A solution is presented to keep the mechanical wire tension of the sensors more constant thereby avoiding problems with the operation of the sensor. The maximum admissible operating temperature of a standard element is found to be 300 degrees centigrade.

For sensors with two sensor wires and sensors with an heater between the sensor wires (the three wire design) an optimum operating power and optimum sensor wire separation distance is found. This makes it possible to compare sensor types and results in insight in optimization of the designs. Three wire sensors are found to exhibit a lower self noise for frequencies above 1 kHz at their optimum operating power, whereas the two wire sensors require a lower power consumption for their optimum operating power. For frequencies below 1 kHz the self noise of two wire sensors and three wire sensors is roughly comparable and wire separation does not have a large influence on the self noise.

In chapter three the design of an integrated three dimensional particle velocity sensor is discussed. Starting with a manually assembled version of a 'four particle velocity sensor' design, it evolves into an integrated version. Measurement results were satisfactory and proved that the sensor was directional in the expected directions but improvements are possible.

Small obstacles in the vicinity of the particle velocity element were shown to have a

large influence on the particle velocity direction and magnitude near the sensor, leading to deviations in directivity of the sensor. An investigation to this effect was performed leading to the conclusion that the main reason for the deviation is found to be due to flow disturbance. A minor part can be due to a thermal effect of neighboring heat sinks. Since the particle velocity sensor element needs a substrate to be mounted on, an obstacle is unavoidable and deviation is hardly avoidable. However the effect can be minimized by minimizing the size of surrounding objects. Another way is to correct for the deviation by adjusting the orientation of the sensor wires, or by signal processing either with the help of a computer or with an analog circuit.

A particle velocity sensor with four separate wires has been developed, in the length of the wires axis seen as four wires running through the corners of a square. Connecting opposite sensor wires as one sensor results in two sensors with their sensitivity directed differently. This way a two dimensional sensor is created with lower self noise than designs with two wires. The four wire sensor is a good alternative for using a three wire sensor, since it offers an improved self noise and ease of fabrication. Placing two of these sensors close to each other and rotated in one chip results in an integrated three dimensional particle velocity sensor with increased performance compared with earlier designs in terms of self noise.

For a three dimensional sound intensity probe both particle velocity and sound pressure must be measured in one probe. Often, sound pressure devices make use of a deflecting membrane but this principle is hard to combine with the fabrication process of particle velocity sensors, together with the fact that silicon sound pressure sensors based on membrane deflection are commonly available. A sound pressure sensor suitable for integration in a chip together with particle velocity sensors has been developed and tested. The operating principle is based on indirect sound pressure measurement by means of a sound pressure to particle velocity transformer and measuring the particle velocity signal. Measurements with the device show that it is sound pressure sensitive and omni-directional. The response of the device is successfully modeled by theory. This enables the design of a device with a predefined response.

The self noise is not very low compared with existing sound pressure sensors, but the sensor can be designed having a very small size and it offers the possibility to use it in a harsh environment (high temperature or chemical aggressive environments). With increasing size the self noise can be decreased. A successful integration with particle velocity sensors on one chip has been achieved.

Fabrication of the devices presented in the chapters three and four is discussed in chapter five. In the first part of the chapter the fabrication process is discussed, explaining the various process steps. The fabrication of the sensor is done with a reliable process with high a yield. For the double sided processes dicing of the chips is impossible and a break out design is required. The fabrication of a back chamber for the sound pressure device by both etching and powder blasting in silicon is discussed and both methods give satisfactory results. This back chamber is fixed on the sensor chip with glue and alignment by capillary forces, enabling a relatively simple manual assembly of the sensor.

In the fabrication chapter also the assembly of sensor elements on a carrier board is discussed, with various connection methods. Mounting of the MEMS devices in a standard available connector enables an easy assembly of probes and fast replacement of defect sensors. Soldering MEMS devices directly on a carrier board results in both a good electrical and mechanical connection. This process seems promising for mass assembly of elements on carrier boards.

The final chapter focuses on applications involving the use of the particle velocity signal and the use of the integrated elements. A signal processing device is presented which works with a two dimensional particle velocity setup. The device helps the user to find a noise source by acoustic feedback of the measurement signals on a pair of headphones and a visual indication. Sound source localization in the presence of background noise is made possible with the system in an intuitive way.

An integrated three dimensional particle velocity device is used to successfully determine the location of a very small sound source. The device is able to measure the three dimensional particle velocity vector, from which the direction to the sound source can be obtained. Two measurements are in principle sufficient for a three dimensional localization of a sound source. Even in the presence of background noise at a level where sound pressure measurement is useless the system is able to perform well. The system does not rely on correlating signals but only on particle velocity measurement.

The main disadvantage of using multiple (three dimensional) sound intensity probes is the large amount of post processing required to generate a useful result. A device that is capable of measuring the sound intensity vector in a certain predefined frequency band is presented, thereby minimizing cabling and total size. Where normal data acquisition of sound intensity probes measuring particle velocity requires a large data stream, the presented device is able to tailor the amount of data to what is needed for the display of sound intensity in this bandwidth only. The device is suited for application in an array, where the small size and low data rate are especially beneficial. Where needed the possibility to compensate the response of particle velocity sensors and sound pressure sensors can be used. Furthermore the device can operate as a stand alone sound source detection unit transmitting the detection results (wireless) to a receiving station. With such a setup the acoustic detection and localization of airplanes, animals, thunder or gunshots can be automated.

7.1.1 Recommendations and future research

A particle velocity sensor with four wires has been developed, with a lower self noise level than a configuration with only two wires. The mutual wire separation distance is fixed at 250 μm but a different distance may result in a lower self noise level. Future research of the sensor can reveal this.

Some testing has been performed to operate a particle velocity device in a high temperature environment. From [10] it follows that a three dimensional sound intensity probe capable of operating at high temperatures is a very useful tool for application in the automotive industry, measurements near exhaust systems or close to running engines are made possible by this. Further research to the capabilities of high temperature operation and further extension of the allowable operation temperature is needed. Calibration of the sensors at these high temperatures is still problematic and needs to be improved.

Appendix A

Appendix to section 3.3

Section A

In this appendix the equation A.1 is written out.

$$C_{12} = \int_0^{\pi} sin(\alpha)d\alpha \int_0^{2\pi} d\beta.(\boldsymbol{\mu_1} \cdot \boldsymbol{v_m})(\boldsymbol{\mu_2} \cdot \boldsymbol{v_m}) = \frac{v_{rev.}^2}{3}(\mu_1 \cdot \mu_2) \tag{A.1}$$

Multiplication of the vector quantities results in:
$(\boldsymbol{\mu_1} \cdot \boldsymbol{v}_m) \cdot (\boldsymbol{\mu}_2 \cdot \boldsymbol{v}_m) =$

$v_m^2\{\mu_{1x}.\mu_{1x}.sin^2(\alpha).cos^2(\beta) + \mu_{1y}.\mu_{2y}.sin^2(\alpha).sin^2(\beta) + \mu_{1z}.\mu_{2z}.cos^2(\alpha)\}+$

$v_m^2.[\mu_{1x}.\mu_{2y}.sin^2(\alpha).cos(\beta).sin(\beta)+ \mu_{1x}.\mu_{2z}.sin(\alpha).cos(\alpha).cos(\beta)+$

$\mu_{1y}.\mu_{2x}.sin^2(\alpha).cos(\beta).sin(\beta) + \mu_{1y}.\mu_{2z}.sin(\alpha).cos(\alpha).sin(\beta)+$

$\mu_{1z}.\mu_{2x}.sin(\alpha).cos(\alpha)cos(\beta) + \mu_{1z}.\mu_{2y}.sin(\alpha).cos(\alpha).sin(\beta)].$

The integration $\int_0^{\pi} sin(\alpha)d\alpha \int_0^{2\pi} d\beta$ of the terms between [] brackets results in a zero value (e.g. $\int_0^{2\pi} cos(\beta).sin(\beta)d\beta$=0 etc.). The integration $\int_0^{\pi} sin(\alpha)d\alpha \int_0^{2\pi} d\beta$ of the terms between {} results in:

$\frac{4\pi}{3}.v_m^2. \{\mu_{1x}.\mu_{2x} + \mu_{1y}.\mu_{2y} + \mu_{1z}.\mu_{2z}\} = v_{rev.}^2(\boldsymbol{\mu_1} \cdot \boldsymbol{\mu_2})/3$

(e.g. $v_m^2 \int_0^{\pi} sin(\alpha)d\alpha \int_0^{2\pi} sin^2(\alpha).cos^2(\beta)d(\beta) = v_m^2 \int_0^{\pi} sin^3(\alpha)d\alpha = 4\pi v_m^2/3$

or: $v_m^2 \int_0^{\pi} sin(\alpha)d\alpha \int_0^{2\pi} cos^2(\alpha)d(\beta) = -v_m^2 2\pi \int_0^{\pi} cos^2(\alpha)dcos(\alpha) = 4\pi v_m^2/3$

Instead of writing out all the components of the arbitrary vectors $\boldsymbol{\mu_1}$ and $\boldsymbol{\mu_2}$ a faster derivation of equation (3.3) is possible. Since the integration should be performed over all mirror sources equally distributed over the sphere the result of the integration is independent of any rotation of the Cartesian coordinate system. Rotate then the coordinate system such that $\boldsymbol{\mu_1} = [0, 0, 1]$ and $\boldsymbol{\mu_2} = [0, sin(\alpha_\mu), cos(\alpha_\mu)]$. The angle between $\boldsymbol{\mu_1}$ and

$\boldsymbol{\mu_2}$ is α_μ and the inner product $\boldsymbol{\mu_1} \cdot \boldsymbol{\mu_2}$ is equal to $cos(\alpha_\mu)$. The integral equation for the contribution of the reverberant field to the cross-spectrum becomes:

$$v_m^2. \int_0^\pi sin(\alpha).d\alpha. \int_0^{2\pi} d(\beta) \{cos(\alpha).sin(\alpha_\mu).sin(\alpha).sin(\beta) + cos(\alpha_\mu).cos(\alpha)\} =$$
$$2\pi v_m^2. \int_0^\pi sin(\alpha).cos^2(\alpha)cos(\alpha_\mu).d\alpha = \frac{v_{rev.}^2}{3}.(\boldsymbol{\mu}_1 \cdot \boldsymbol{\mu}_2)$$

Section B

When the free field is known, the reverberant field can be solved from the measurement of auto spectra (or cross spectra).

For the case of $A_i.A_j - (C_{ij})^2$ with i=1 and j=2:

$$A_1.A_2 - (C_{12})^2 = \{\tfrac{1}{2}v_x^2 + \tfrac{1}{2}v_z^2 + v_x.v_z + \tfrac{1}{3}v_{rev}^2\}.\{\tfrac{1}{2}v_y^2 + \tfrac{1}{2}v_z^2 + v_y.v_z + \tfrac{1}{3}v_{rev}^2\} -$$

$$\{\tfrac{1}{2}v_z^2 + \tfrac{1}{2}v_x.v_y + \tfrac{1}{2}v_x.v_z + \tfrac{1}{2}v_y.v_z + \tfrac{1}{6}v_{rev}^2\}^2 =$$

$$\tfrac{1}{4}v_x^2.v_y^2 + \tfrac{1}{4}v_x^2.v_z^2 + \tfrac{1}{2}v_x^2.v_y.v_z + \tfrac{1}{3}(v_{rev}^2).(\tfrac{1}{2}v_x^2 + \tfrac{1}{2}v_z^2 + v_x.v_z + A_2) + \tfrac{1}{4}v_y^2.v_z^2 + \tfrac{1}{4}v_z^4 +$$

$$\tfrac{1}{2}v_y.v_z^3 + \tfrac{1}{2}v_x.v_y^2.v_z + \tfrac{1}{2}v_x.v_z^3 + v_x.v_y.v_z^2 - \{\tfrac{1}{4}v_z^4 + \tfrac{1}{4}v_x^2.v_y^2 + \tfrac{1}{4}v_x^2.v_z^2 + \tfrac{1}{4}v_y^2.v_z^2 +$$

$$(\tfrac{1}{6}v_{rev.}^2)^2 + \tfrac{1}{2}v_x.v_y.v_z^2 + \tfrac{1}{2}v_x.v_z^3 + \tfrac{1}{2}v_y.v_z^3 + (\tfrac{1}{3}v_{rev.}^2).(\tfrac{1}{2}v_z^2 + \tfrac{1}{2}v_x.v_y + \tfrac{1}{2}v_x.v_z + \tfrac{1}{2}v_y.v_z) +$$

$$\tfrac{1}{2}v_x^2.v_y.v_z + \tfrac{1}{2}v_x.v_y^2.v_z + \tfrac{1}{2}v_x.v_y.v_z^2\} =$$

$$(\tfrac{1}{3}v_{rev.}^2).(A_1 + A_2 - \tfrac{1}{3}v_{rev.}^2) - \{(\tfrac{1}{6}v_{rev.}^2)^2 + (\tfrac{1}{3}v_{rev.}^2).(C_{12} - \tfrac{1}{6}v_{rev.}^2)\}$$

or:

$$3.(\tfrac{1}{6}v_{rev.}^2)^2 - 2.(\tfrac{1}{6}v_{rev.}^2).(A_1 + A_2 - C_{12}) + (A_1.A_2 - C_{12}^2) = 0,$$

from which $v_{rev.}^2$ can be solved.

For the case of $A_i.A_j - (C_{ij})^2$ with i=1 and j=2:

$$A_1.A_3 - (C_{13})^2 = \{\tfrac{1}{2}v_x^2 + \tfrac{1}{2}v_z^2 + v_x.v_z + \tfrac{1}{3}v_{rev.}^2\}.\{\tfrac{1}{2}v_x^2 + \tfrac{1}{2}v_z^2 - v_x.v_z + \tfrac{1}{3}v_{rev.}^2\} - \{-\tfrac{1}{2}v_x^2 + \tfrac{1}{2}v_z^2\} =$$

$$\tfrac{1}{4}v_x^4 + \tfrac{1}{4}v_x^2.v_z^2 - \tfrac{1}{2}v_x^3.v_z + (\tfrac{1}{3}v_{rev.}^2).(\tfrac{1}{2}v_x^2 + \tfrac{1}{2}v_z^2 + v_x.v_z + \tfrac{1}{2}v_x^2 + \tfrac{1}{2}v_z^2 - v_x.v_z + \tfrac{1}{3}v_{rev.}^2) +$$

$$\tfrac{1}{4}v_x^2.v_z^2 + \tfrac{1}{4}v_z^4 - \tfrac{1}{2}v_x.v_z^3 + \tfrac{1}{2}v_x^3.v_z + \tfrac{1}{2}v_x.v_z^3 - v_x^2.v_z^2 - \tfrac{1}{4}v_x^4 - \tfrac{1}{4}v_z^4 + \tfrac{1}{2}v_x^2.v_z^2 =$$

$$(\tfrac{1}{3}v_{rev.}^2).(A_1 + A_3 - \tfrac{1}{3}v_{rev.}^2)$$

or:

$4.(\frac{1}{6}v_{rev}^2)^2 - 2.(\frac{1}{6}vrev^2).(A_1 + A_3) + (A_1.A_3 - C_{13}^2) = 0,$

from which $v_{rev.}^2$ can be solved.

An alternative way is as follows: Write $A_1 = A_1 + 2R$, where $R = \frac{1}{6}v_{rev}^2$; $A_2 = A_2 + 2R$, $A_3 = A_3 + 2R$, $C_{12} = \sqrt{A_1.A_2} + R$ and $C_{13} = \sqrt{(A_1.A_3)}A_1.A_2 - C_{12}^2 = (A_1 + 2R).(A_2 + 2R) - (\sqrt{A_1.A_2} + R)^2 = 2R.\{A_1 + A_2 - \sqrt{A_1.A_2}\} + 3R^2$.

$A_1 + A_2 = A_1 + A_2 - 4R$ and $\sqrt{A_1.A_2} = C_{12} - R$, thus $A_1.A_2 - C_{12}^2 = 2R\{A_1 + A_2 - 4R - C_{12} + R\} + 3R^2$ or $-3R^2 + 2R.(A_1 + A_2 - C_{12}) = A_1.A_2 - C_{12}^2 A_1.A_3 - C_{13}^2 =$

$A_1.A_3 + 2R.(A_1 + A_3) + 4R^2 - A_1.A_3 = 2R.(A_1 + A_3 - 4R) + 4R^2 = -4R^2 + 2R.(A_1 + A_3),$

which are the same equations as above.

Appendix B

Propagation coefficient for a damped tube

Propagation coefficient for a tube with rectangular cross section

For a one-dimensional viscothermal wave propagation the pressure and particle velocity due to an acoustic disturbance are given by:

$$p(x) = Ae^{-\Gamma kx} + Be^{\Gamma kx} \qquad u(x) = \frac{G}{\rho c}\left(Ae^{-\Gamma kx} - Be^{\Gamma kx}\right) \tag{B.1}$$

where Γ is a coefficient describing the damping.

The solution for damping in small tubes is derived in [66]. Here the propagation coefficient Γ is calculated:

$$\Gamma = i \cdot \sqrt{\frac{\gamma - (\gamma - 1)F(\frac{\gamma}{\rho_0 C_p})}{F(\frac{\mu}{\rho_0})}} \tag{B.2}$$

The coefficient G is dependent on the cross section of the tube and is given by:

$$G = i\Gamma F(\frac{\mu}{\rho_0}) \tag{B.3}$$

Both equations involve the function $F(\eta)$. For a rectangular cross section with sides 2a and 2b the function $F(\eta)$ is evaluated as follows:

$$F(\eta) = i \cdot \frac{4\omega}{\eta a^2 b^2} \sum_{n=0}^{\inf} \sum_{m=0}^{\inf} \left(\alpha_n^2 \beta_m^2 (\alpha_n^2 + \beta_m^2 + \frac{i\omega}{\beta})\right)^{-1} \tag{B.4}$$

$$\alpha_n = (n + \frac{1}{2})\frac{\pi}{a} \qquad \beta_m = (m + \frac{1}{2})\frac{\pi}{b} \qquad n, m = 0, 1, 2 \ldots \tag{B.5}$$

At least 25 iterations of i and j were used for evaluation of the function.

Appendix C

Fabrication process sheet

Process sheets

Table C.1: *Process sheet single sided process*

Step	Process	Process parameters	design remarks
1	select wafers	-orientation <100> -Dia. 4" -Thickness 500μm -Curvature <10μm -Single Side Polished	
2	Preparation LPCVD cleaning	-Fuming nitric acid, 5 min -Quick dump rinse DI <5μS -Boiling Nitric acid 95 ^{o}C, 15 min. -Quick dump rinse DI <5μS -Spin dry	
3	Preparation LPCVD, native oxide strip	-HF 1%, 60 s -Quick dump rinse DI <5μS -Spin dry	
4	LPCVD SiRN	**-Tempress LPCVD furnace** -SiH_2Cl_2 flow: 70 sccm -NH_3 flow: 18 sccm -Temperature: 850 ^{0}C -deposition rate: 7 nm/min -Nf: 2.14 -stress: 10.6 E-10 dyne/cm^2 -pressure: 200 mTorr	Cleaning required

Step	Process	Process parameters	design remarks
5	Lithography	**-EVG 602-mask aligner** -Dehydration bake/priming: 120 ^oC /15 min. -Gas/liquid priming with HDMS -Resist: Olin 907-17 4000 rpm, 20 s -Prebake 95^oC, 90 s -Hard contact exposure: 60 mJ -After exposure bake 120 ^oC, 90 s -Development OPD 4262, 45-60 s -Quick dump rinse, DI, <0.1 μS -Spin dry -Microscopic inspection	No postbake, (lift off process)
6	Sputtering Cr/Pt	**-Sputterke (custom design)** -Base pressure: 10 E-6 mBar -Water cooled electrode -Gas flow: 45 sccm Ar -Sputter pressure: 6.0 E-3 mBar -Power: 200 W -Deposition rate Cr: 10 nm/min -Deposition rate Pt: 20 nm/min	 Cr: 10 nm Pt: 200nm
7	Lift off resist	**-Wet bench** -Acetone technical grade -Acetone VLSI-grade -Isopropanol VLSI-grade -Spin dry -Microscopic inspection	User made solutions Ultrasonic excitation for better lift off

Step	Process	Process parameters	design remarks
8	Lithography	**-EVG 602-mask aligner** -Dehydration bake/priming: 120 ^oC /15 min. -Resist: Olin 907-17 4000 rpm, 20 s -Prebake 95^oC, 90 s -Hard contact exposure: 60 mJ -After exposure bake 120 ^oC, 90 s -Development OPD 4262, 45-60 s -Quick dump rinse, DI, <0.1 μS -Spin dry -Microscopic inspection -Post bake 120 ^oC, 20 min.	No postbake, (lift off process)
9	RIE etching SiRNx	**-Electrotech PF 310/340** -dirty chamber -Styros electrode -Electrode temp: 10 ^oC -CHF_3 flow: 25 sccm -O_2 flow: 5 sccm -Pressure 10 mTorr -Power 75 W -etchrate SiRNx: 60-90 nm/min. -etchrate resist: 95 nm/min. -Directional profile	Etching time 4 min.
10	Oxygen plasma stripping	**-Nanotech Plasmaprep 100** -O_2 flow 55 sccm -Power: 500 W for 4 wafers -pressure 1 mBar -Time: 30 min -visual inspection	
11	Etching Si HF/HNO_3H_2O	**-Wet bench** -recipe: -HF 50% : 11ml -HNO_3 69%: 67 ml -DI: 22ml -wafer horizontal in etchant -No stirring -Quick dump rinse DI$<0.1\mu S$ -spin dry	See [68] time: $30 \cdots 60$ s

Appendix D

Polar plot measurement

Measuring the polar pattern of a device

Polar pattern measurements give information about the directivity of a sensor. For measuring a polar pattern of an acoustic sensor the direction of sound field relative to the sensor must be varied. Either the location of the sound source or the orientation of the sensor can be varied to accomplish this, see Figure D.1. Although both methods could be used in this thesis the probe is rotated inside a standing wave tube.

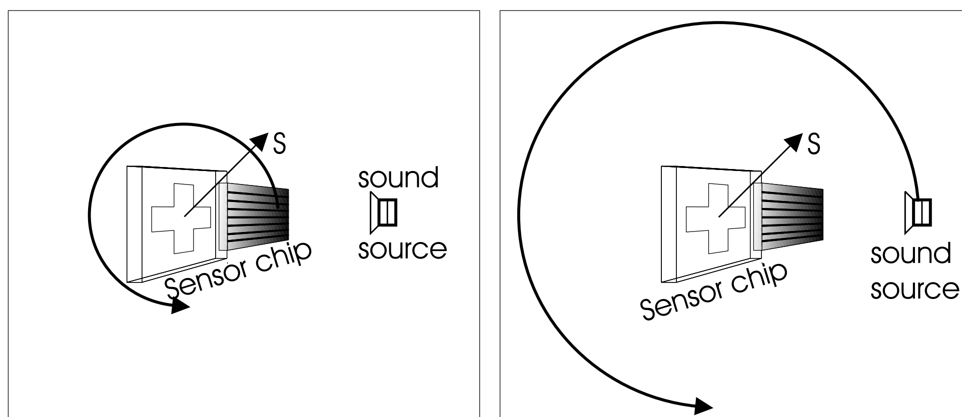

Figure D.1: *On the left the sensor is rotated in a sound field, on the right side the sound field is rotated around the sensor.*

The sensitivity of the device is measured for a number of rotational positions of the element. In figure D.1 the arrow with designator 's' represents the sensitivity direction of a directional sensor, in the direction of the arrow and in the direction opposite to the arrow the sensor is maximally sensitive.

Starting at an angle of zero degrees and plotting the results in a regular graph would result in a figure similar to Figure D.2. Plotting the same data in a polar plot would look like Figure D.3.

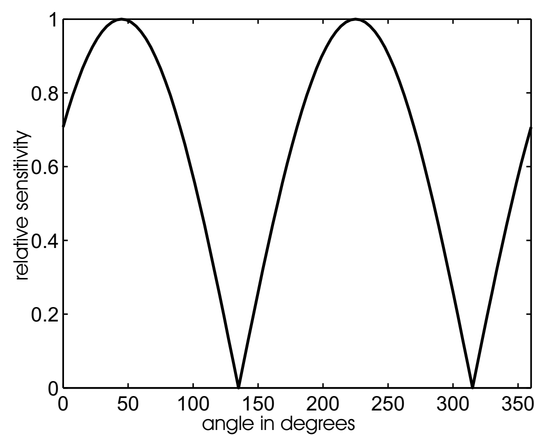

Figure D.2: *Rotational sensitivity in a regular graph.*

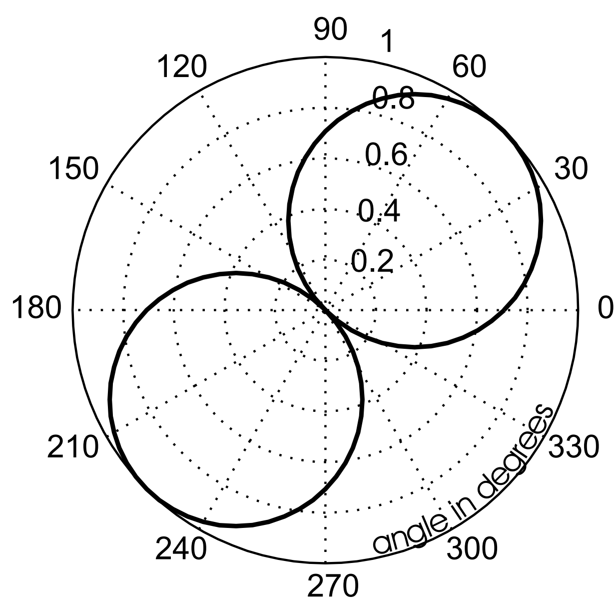

Figure D.3: *The same data plotted in a polar plot.*

References

[1] C.L. Morfey. *Dictionary of acoustics.* academic press, 2001.

[2] A. Nordby and O.-H. Bjor. *Proceedings of Internoise*, pages 1107–1109, 1984.

[3] O.-H. Bjor and H.J. Krystad. *Proc. Of the Autumn Conference*, pages p.B7.1–B7.5, 1982.

[4] H-E. de Bree. The microflown: An acoustic particle velocity sensor. *Acoustics Australia*, 31:91–94, 2003.

[5] H-E. de Bree et al. The microflown: a novel device measuring acoustical flows. *Sensors and Actuators*, 54:552–557, 1996.

[6] H-E. de Bree et al. Use of a fluid flow measuring device as a microphone and system comprising such a microphone, pct/nl95/00220.

[7] H-E. de Bree. An overview of microflown technologies. *Acta Acustica*, 89:163–172, 2003.

[8] V.B. Svetovoy and I.A. Winter. Model of the microflown microphone. *Sensors and Actuators*, 86:171–181, 2000.

[9] J.W. van Honschoten, G.J.M. Krijnen, V.B. Svetovoy, H-E. de Bree, and M.C. Elwenspoek. Analytic model of a two-wire thermal sensor for flow and sound measurements. *J. Micromech. Microeng*, 14:1468–1477, 2004.

[10] H-E. de Bree, A. Koers, E. tijs, R. Platenkamp, et al. Private discussions with members of the microflown company.

[11] J.W. van Honschoten, W.F. Druyvesteyn, H. Kuipers, R. Raangs, and G.J.M. Krijnen. Noise reduction in acoustic measurements with a particle velocity sensor by means of a cross-correlation technique. *Acta acustica united with Acustica*, 90:349–355, 2004.

[12] Ron Raangs. *Exploring the use of the Microflown.* PhD thesis, University of Twente, The Netherlands, 2005.

[13] H-E. de Bree, V.B. Svetovoy, and R. Visser. The very near field II , an introduction to very near field holography. In *SAE International*, 2004.

[14] Wieslaw Woszczyk, Masakazu Iwaki, Takehiro Sugimoto, Kazuho Ono, and Hans-Elias de Bree. Anechoic measurements of particle-velocity probes compared to pressure gradient and pressure microphones. In *Audio Engineering Society*, 2007.

[15] H-E. de Bree. Add-on microflown for a high-end pressure gradient microphone. In *LA-AES*, 2000.

[16] Finn Jacobsen and Hans-Elias de Bree. A comparison between p-p and p-u sound intensity measurement systems. In *International Congress on Sound and Vibration (11th ICSV)*, 2004.

[17] Frank J. Fahy. *Sound intensity*. E & FN Spon, 1989.

[18] Frank Fahy. *Foundations of Engineering Acoustics*. Elsevier Ltd, 2003.

[19] Finn Jacobsen and Hans-Elias de Bree. Intensity-based sound power determinateion under adverse sound field conditions: P-p probes versus p-u probes. In *12th International Congress on Sound and Vibration (ICSV)*, 2005.

[20] Finn Jacobsen and Hans-Elias de Bree. A comparison of two different sound intensity measurement principles. *JASA*, 118:1510–1517, 2005.

[21] S.Weyna. Acoustic flow visualization based on the particle velocity measurements. In *Forum Acousticum*, 2005.

[22] Microflown Technologies B.V. (www.microflown.com).

[23] J.-P. Dalmont. Acoustic impedance measurement, part I: a review. *Journal of Sound and Vibration*, 243(3):427 439, 2001.

[24] Bruel & Kjaer. Two-microphone impedance measurement tube: Type 4206. Product data sheet, 1995.

[25] R. Lanoye, G. Vermeir, W. Lauriks, R. Kruse, and V. Mellert. Measuring the free field acoustic impedance and absorption coefficient of sound absorbing materials with a combined particle velocity-pressure sensor. *JASA,*, May, 2006.

[26] H-E. de Bree, M. Nosko, and E. Tijs. A handheld device to measure the acoustic absorption in situ. In *SNVH, GRAZ*, 2008.

[27] Tijs et al. Non destructive and in situ acoustic testing of inhomogeneous materials. In *ERF33, Kazan, Russia*, 2007.

[28] J.D. Alvarez and F. Jacobsen. In-situ measurements of the complex acoustic impedance of porous materials. In *Internoise*, 2007.

[29] Martin Nosko, Emiel Tijs, and Hans-Elias de Bree. A study of influences of the in situ surface impedance measurement technique. In *DAGA*, 2008.

[30] Earl G. Williams. *Fourier Acoustics*. Academic Press, Harcourt Brace & Company, Publishers, 1999.

[31] Earl G. Williams. Fourier acoustics: Uncovering the origins of sound. In *International Congress on Sound and Vibration (ICSV)*, 2004.

[32] Finn Jacobsen and Yang Liu. Near field acoustic holography with particle velocity transducers. *JASA*, 118(5):3139–3144, 2005.

[33] Finn Jacobsen and Yang Liu. Near field acoustic holography based on an array of particle velocity sensors. In *Internoise 2005*, 2005.

[34] Johan de Vries and Hans-Elias de Bree. Scan & listen: a simple and fast method to find sources. In *Society of Automotive Engineers*, 2008.

[35] T.G.H. Basten, H-E. de Bree, and E.H.G. Tijs. Localization and tracking of aircraft with ground based 3d sound probes. In *ERF33, Kazan, Russia*, 2007.

[36] Kenbu Teramoto and MD Tawhidul Islam Khan. Acoustic blind source separation based on the particle velocity vector measurement. In *International Congress on Sound and Vibration (ICSV) 13 - Vienna*, 2006.

[37] J.W. van Honschoten. *Modeling and optimisation of the Microflown*. PhD thesis, University of Twente, The Netherlands, 2003.

[38] H-E. de Bree. *The Microflown*. www.microflown.com, 2001.

[39] J.W. van Honschoten, D.R. Yntema, R.J. Wiegerink, and M.C. Elwenspoek. Analysis of a three-dimensional particle velocity sensor for design optimization. *Journal of micromechanics and microengineering*, 17:S137–S146, March 2007.

[40] R.Raangs, T. Schlicke, and Richard Barham. Calibration of a micro-machined particle velocity microphone in a standing wave tube using a lda photon correlation technique. *Measurements Science and Technology*, 16:1099–1108, 2005.

[41] H-E. de Bree, W.F. Druyvesteyn, and M. Elwenspoek. Realisation and calibration of a novel half inch p-u sound intensity probe. In *106th AES Munchen*, 1999.

[42] Hans-Elias de Bree and Tom Basten. A full bandwidth calibrator for a sound pressure and particle velocity sensor. In *DAGA proceedings*, 2008.

[43] Finn Jacobsen and Virginie Jaud. A note on the calibration of pressure-velocity sound intensity probes. *JASA*, 2006.

[44] J.W. van Honschoten, H-E. de Bree, F.J.M. van Eerden, and G.J.M. Krijnen. The influence of viscothermal effects on calibration measurements in a tube. In *presented at the LA AES*, 2000.

[45] H-E. de Bree. *The Microflown*. PhD thesis, University of Twente, The Netherlands, 1994.

[46] Samara L. Firebaugh, Klavs F. Jensen, and Martin A. Schmidt. Investigation of high-temperature degradation of platinum thin films with an in situ resistance measurement apparatus. *Journal of microelectromechanical systems*, 7:128–135, March 1998.

[47] R. Tiggelaar. *Silicon-technology based microreactors for high-temperature heterogeneous partial oxidation reactions*. PhD thesis, University of Twente, The Netherlands, 2004.

[48] F.J.M. van der Eerden. *Noise reduction with coupled prismatic tubes*. PhD thesis, University of Twente, The Netherlands, 2000.

[49] W.F. Druyvesteyn, H-E. de Bree, and M. Elwenspoek. A new acoustic measurement probe; the microflown. In *IOA, London, UK*, 1999.

[50] Meyer Sound. 3-DP, three dimensional sound probe. Product folder, 2002. Product folder of impulse response measurement with the USP.

[51] S.Weyna. Application of "microflown probe" to visualization of acoustic power flow. In *proceedings of the Polish-Scandinavian structured conference on acoustic*, 2005.

[52] Davide Bonsi and Domenico Stanzial. Realizzazione di un systemadi acquisizione di risposte all 'impulso intensimetriche mediante sonda microflown per lo stodio delle proprieta spaziali del campo acustico. In *31 Convegno Nazionale AIA (Associazione Italiana di Acustica), Venezia, Italy, 5-7 May*, (2004).

[53] H-E. de Bree, W.F.Druyvesteyn, E.Berenschot, and M.Elwenspoek. Three-dimensional sound intensity measurements using particle velocity sensors. In *Micro Electro Mechanical Systems,Proceedings IEEE The Twentieth Annual International Conference on, Orlando,USA*, pages 1–4, 1999.

[54] D.R. Yntema, W.F. Druyvesteyn, and M.C. Elwenspoek. A four particle velocity sensor device. *Journal of the Acoustical Society of America*, 119:943–951, February 2006.

[55] V.A. Gordienko, B.I. Goncharenko, and Ya.A. Ilyushin. Basic rules of vector-phase structure formulation of the ocean noise field. *Acoustical Physics*, 39:237–242, 1993.

[56] V.A. Shchurov. Modern state and prospects for use of underwater acoustic intensity measurements. *Pacific Oceanological Institute Vladivostok*, 1998.

[57] D.R. Yntema, J.W. van Honschoten, H-E. de Bree, R.J. Wiegerink, and M.C. Elwenspoek. A three dimensional microflown. In *Micro Electro Mechanical Systems, 2006. MEMS 2006 Istanbul. 19th IEEE International Conference on, Instanbul - Turkey*, pages 654–657, Los Alamitos, January 2006. IEEE Computer Society Press.

[58] J.W. van Honschoten, D.R. Yntema, R.J. Wiegerink, and M.C. Elwenspoek. Directional sensitivity of a three dimensional particle velocity sensor. In *Proceedings of the 17th workshop on Micromachining, Micromechanics and Microsystems, Southampton*, pages 201–204, Southampton, September 2006. Southampton University Press.

[59] Knowles FG-series microphones.

[60] Simic^{tm} analog silicon microphone, type TC200A.

[61] W.F. Druyvesteyn and H-E. de Bree. A new sound intensity probe; (comparison to the 'pair of pressure microphone' intensity probe). In *AES 1998 conference, Amsterdam, The Netherlands*, 1998.

[62] H-E. de Bree et al. The sound pressure microflown; a novel way of transducing sound pressure. In *In Proceedings of the MME convention, Sweden*, 2000.

[63] A.P. Dowling and J.E. Williams. *Sound and Sources of Sound*. Ellis Horwood Pub., 1983.

[64] D.R. Yntema and H-E. de Bree. A microflown based sound pressure microphone suitable for harsh environments. *NOISE-CON 2005, Minneapolis, Minnesota,October 17-19*, 118(3):1923–1924, 2005.

[65] J.W.S. Rayleigh. *The theory of sound*. Dover publications, New York, 1877.

[66] Michael R. Stinson. The propagation of plane sound waves in narrow and wide circular ducts, and generalisation to uniform tubes of arbitrary cross section. *Journal of the Acoustical Society of America*, 89:550–558, 1991.

[67] Database transducer science and technology, university of twente.

[68] R.W. Tjerkstra. *Isotropic etching of silicon in fluoride containing solutions as a tool for micromachining*. PhD thesis, University of Twente, The Netherlands, 1999.

[69] H. Wensink, J.W. Berenschot, H.V. Jansen, and M.C. Elwenspoek. High resolution powder blast micromachining. *Micro Electro Mechanical Systems, MEMS 2000*, pages 769–774, 2000.

[70] George Harman. *Wire bonding in microelectronics materials*. McGraw-Hill, 1997.

[71] S. Habermehl and R. T. Apodaca. Dielectric breakdown and poole–frenkel field saturation in silicon oxynitride thin films. *Applied Physics Letters*, 86(7):072103, 2005.

[72] S.Weyna. An experimental study of sound intensity distributions in real acoustic flow field. In *Proceedings of the Institute of Acoustics*, volume 29, 2007.

[73] H-E. de Bree, V.B. Svetovoy, R. Raangs, and R. Visser. The very near field, theory, simulations and measurements of sound pressure and particle velocity in the very near field. In *International Congress on Sound and Vibration (ICSV) 11, St. Petersburg*, 2004.

[74] H-E. de Bree, E.Tijs, and T. Basten. Real time sound field visualization in the near field, far field and at absorbing surfaces. In *Acoustics*, 2008.

[75] H-E. de Bree, T. Basten, and D.R.Yntema. A pu sound intensity probe designed for high temperature use. In *SAE proceedings*, 2007.

[76] D.R. Yntema, H-E. de Bree, and J.G.A.M. van Heck. An intuitive handheld noise source finder. In *proceedings from the FISITA 2006 World Automotive Congress*. FISITAS, 2006.

[77] H-E. de Bree and W.F. Druyvesteyn. A particle velocity sensor to measure the sound from a structure in the presence of background noise. *Forum Acousticum*, 2005.

[78] D.R. Yntema, W.F. Druyvesteyn, and R.J. Wiegerink. Choosing the most appropriate sensor for acoustic measurements. In *International Congress on acoustics, ICA, Madrid*, 2007.

[79] D.R.Yntema, W.F.Druyvesteyn, and R.J.Wiegerink. Choosing the most appropriate sensor for acoustic measurements. In *International Congress on Acoustics (ICA, Madrid)*, 2007.

[80] T.G.H. Basten, H.E. de Bree, and S. Sadasivan. Acoustic eyes, a novel sound source localization and monitoring technique with 3d sound probes. In *ISMA*, 2008.

[81] H-E. de Bree. *The Microflown, E-Book*. www.microflown.com, 2008.

Summary

This thesis deals with the development of an integrated three dimensional sound intensity probe. Although a 3D sound-intensity probe based on an (manual) assembly of multiple particle velocity sensors and a sound pressure microphone exists, by integrating all sensors into one chip the size can be reduced further. A small sensor size is preferable, because it enables the user to do measurements on small objects, very close to objects and with a minimum disturbance of the sound field.

An investigation on various types of particle velocity sensors with respect to sensitivity and self noise is done. The results give insight in the optimum sensor configuration as well as how much a different design affects the signal quality of the sensor. When designing a 3D sensor geometry this is useful. Following the design of a three dimensional particle velocity is discussed. Based on experiments with a manually assembled 3D-particle velocity probe, a chip with four integrated particle velocity sensors is developed. The device is fully functional and used in experiments described in the second to last chapter. Experiments with this sensor show that the expected direction of sensitivity did not match the observed direction very well and that objects in the direct vicinity were responsible for this behavior. It is investigated what the origin of the deviation is. The deviation can be compensated for, either in signal processing or an adapted design.

Furthermore a sound pressure sensitive device is developed for integration with particle velocity sensors on one chip. The sound pressure sensor is not based on a membrane deflection principle. Instead a sound pressure to particle velocity transformer is used, and the particle velocity is measured. Integration of both types of sensors can easily be achieved with this design because the fabrication process is almost the same. Additionally, just as the particle velocity sensors, the sound pressure sensor is capable of operating at temperatures up to 300 ^{o}C. Integrating the 3D particle velocity sensor with this sound pressure sensor results in a fully integrated three dimensional sound intensity sensor. The complete sensor is flatter compared with the existing manually assembled 3D probe (1.3 mm instead of 7 mm). Although the sensor is functional, improvements to the design in terms of self noise and size are possible.

A two-dimensional particle velocity sensor with four sensor wires is invented. Compared with similar two-dimensional two-wire designs the sensor exhibits a better self noise together with a smaller size. Combining two of these 2D sensors with a sound pressure sensor in one chip results in a smaller 3D sound intensity sensor with a better self noise. The size of this sensor is 2 mm wide and 1.3 mm thick. The length of the bare element

is 1.5 centimeters.

Fabrication of the sensor elements is done in a clean room environment. The fabrication process is done on both sides of the wafer, resulting in fragile sensor wires on both sides of the wafer. Instead of dicing the chips from the wafer, a 'break out' design proves to be a good solution to separate the chips from the wafer. Assembly of the fragile sensors to a useful element requires a carrier board. The assembly of the sensor element to the carrier board normally done with glue and wire bonding is a time consuming process. The use of a small connector with a sensor design specially adapted to this connector proves to be of great use. With the connector the sensor elements can easily be mounted and replaced if necessary.

The integrated 3D sensor can be used to measure the sound field near (small) sound sources, as described in the second to last chapter. In an experiment demonstrating this it is also demonstrated that measuring particle velocity near a sound source has advantages compared to measuring the sound pressure.

Measuring sound intensity is normally done by a sound intensity analyzer, where the sound intensity signal is distilled from a large data stream. When this is done nearby the sensor and only the value of the sound intensity is transmitted, the system can be made less complex. A small and modular sound intensity analyzer is made, capable of measuring sound intensity in a predefined bandwidth. The system is easily expandable with a large number of sound intensity channels, requiring only simple cabling and little space.

In conclusion, a very small 3D sound-intensity probe has been developed, tested and proved useful. Application of the sensor in a commercial product has become feasible with a fast and reliable assembly method.

Samenvatting

Dit proefschrift beschrijft de ontwikkeling van een geïntegreerde driedimensionale geluidsintensiteit probe. Hoewel een driedimensionale geluidsintensiteitsprobe gebaseerd op (handmatige) montage van een aantal particle velocity[1] sensoren en een drukmicrofoon bestaat, door de integratie van de sensoren in een enkele chip kan de sensor nog verder verkleind worden. Een kleine sensor maakt het mogelijk om aan kleine objecten en dicht bij objecten te meten met een minimale verstoring van het geluidsveld.

Een onderzoek naar de gevoeligheid en zelfruis van verschillende particle velocity sensorconfiguraties is gedaan. De resultaten hiervan maken inzichtelijk wat de optimale sensorconfiguratie is en in hoeverre een daarvan afwijkend ontwerp van invloed is op de signaalkwaliteit. Dit is nuttig bij het ontwerpen van een driedimensionale sensor. Vervolgens wordt een ontwerp van een driedimensionale sensor besproken. Gebaseerd op experimenten met een handmatig geassembleerde driedimensionale particle velocity sensor is een chip met vier geïntegreerde sensoren ontwikkeld. De sensor is functioneel en wordt gebruikt in experimenten beschreven in het op één na laatste hoofdstuk. In experimenten met deze sensor wijkt de verwachte gevoeligheidsrichting af van de gemeten gevoeligheidsrichting. Objecten in de directe omgeving hebben hier invloed op. Er is onderzocht wat de oorzaak van de afwijking is. Compensatie voor deze deviatie is eenvoudig mogelijk met signaalverwerking of door het ontwerp aan te passen.

Verder is een geluidsdruksensor ontwikkeld die geschikt is voor integratie met particle velocity sensoren op een enkele chip. De geluidsdruksensor werkt niet met een membraan. In plaats daarvan is een geluidsdruk-naar-particle-velocity converter gebruikt, en de particle velocity wordt gemeten. De integratie van beide typen sensoren kan gemakkelijk bereikt worden doordat het fabricage proces van beide typen sensoren vrijwel gelijk is. Net als de particle velocity sensoren is de geluidsdruksensor bruikbaar tot 300 ^{o}C. De integratie van de sensoren resulteert in een volledig geïntegreerde driedimensionale geluidsintensiteitsensor. Deze sensor is platter dan de bestaande handmatig geassembleerde sensor (1.3 mm in plaats van 7 mm). Hoewel de sensor volledig functioneel is, zijn er verbeteringen mogelijk.

Een tweedimensionale particle velocity sensor met vier sensor draden is ontworpen. Vergeleken met andere tweedimensionale tweedraads ontwerpen heeft de sensor een betere zelfruis en is hij kleiner. Twee van deze sensoren gecombineerd met

[1] deeltjessnelheid

een geluidsdruksensor resulteert in een driedimensionale geluidsintensiteitsensor met een betere zelfruis. De sensor is 2 mm breed en 1.3 mm dik en heeft een lengte van 1.5 cm.

Fabricage van de sensoren wordt in een 'clean room' omgeving gedaan. De fabricage is dubbelzijdig uitgevoerd, en resulteert in fragiele daden aan beide kanten van de wafer. In plaats van de sensoren van de wafer te zagen wordt gebruik gemaakt van een 'break out' ontwerp, wat een goede manier blijkt om de sensoren van de wafer te scheiden. Assemblage van de sensor tot een bruikbaar element vereist een drager. De normale assemblage van het sensor element op de drager door lijm en 'wire bonding' is een tijdrovende bezigheid. Het gebruik van een connector met een sensor ontwerp aangepast op die connector blijkt zeer bruikbaar te zijn. Met de connector kunnen de elementen eenvoudig gemonteerd en vervangen worden.

De gëintegreerde driedimensionale sensor kan gebruikt worden om het geluidsveld dicht bij (kleine) geluidsbronnen te meten, zoals beschreven in het één na laatste hoofdstuk. In een experiment dat dit beschrijft is tevens gedemonstreerd dat het meten van particle velocity dicht bij een geluidsbron voordelen heeft ten opzichte van het meten van geluidsdruk.

Geluidsintensiteit wordt normaal gesproken gemeten met behulp van een intensiteitanalysator, waarin de geluidsintensiteit gedestilleerd wordt uit een grote datastroom. Wanneer dit dicht bij de sensoren gedaan wordt en alleen de waarde van de geluidsintensiteit verzonden wordt kan het totale systeem eenvoudiger gemaakt worden. Een kleine en modulaire geluidsintensiteit analysator is ontwikkeld, met de mogelijheid de geluidsintensiteit in een vooraf instelbare bandbreedte te meten. Het systeem kan makkelijk uitgebreid worden, heeft slechts eenvoudige bedrading nodig en is klein.

Een zeer kleine, driedimensionale geluidintensiteitprobe is ontwikkeld, getest en bruikbaar gebleken. De toepassing van de sensor in een commerciëel product is mogelijk geworden met een snelle en betrouwbare assemblagemethode.

Publications

Journal papers

D.R. Yntema, W.F Druyvesteyn and M.C. Elwenspoek. A four particle velocity sensor device. *Journal of the Acoustical Society of America, 119. pp. 943-951.*

D.R. Yntema, J.W. van Honschoten, R.J. Wiegerink and M. Elwenspoek. A complete three-dimensional sound intensity sensor integrated on a single chip. *Accepted for publication in Journal of Micro Mechanics (JMM).*

J.W. van Honschoten, D.R. Yntema, V. Svetovoy, M.A. Dijkstra, R.J. Wiegerink and M.C. Elwenspoek. Analysis of the performance of a particle velocity sensor between two cylindrical obstructions. *Journal of the Acoustical Society of America, 121 (5). pp. 2711-2722, (2007). ISSN 0001-4966*

J.W. van Honschoten, D.R. Yntema, R.J. Wiegerink, and M.C. Elwenspoek. Analysis of a three-dimensional particle velocity sensor for design optimization. *Journal of Micromechanics and Microengineering, 17. S137-S146, (2007).*

D.R. Yntema, J.W. van Honschoten, R.J. Wiegerink and M.C. Elwenspoek. Design and analysis of a four-wire particle velocity sensor (part I). *To be submitted.*

J.W. van Honschoten, D.R. Yntema, R.J. Wiegerink and M.C. Elwenspoek. Design and analysis of a four-wire particle velocity sensor (part II). *To be submitted.*

Conference contributions

D.R. Yntema, H-E. de Bree and J.G.A.M. van Heck. An intuitive handheld acoustic noise source finder. *Proceedings from the FISITA 2006 World Automotive Congress, Yokohama, Japan.*

D.R. Yntema, J.W. van Honschoten, H-E. de Bree, R.J. Wiegerink and M.C. Elwenspoek. A three dimensional microflown. *Micro Electro Mechanical Systems.*
MEMS 2006, Istanbul.

D.R. Yntema, R.J. Wiegerink, J.W. van Honschoten and M.C. Elwenspoek. Fully integrated three dimensional sound intensity sensor. *Micro Electro Mechanical Systems, MEMS 2007.* Kobe, Japan.

D.R. Yntema, W.F. Druyvesteyn and R.J. Wiegerink. Choosing the most appropriate sensor for acoustic measurements. *Proceedings of the 19th International Congress on Acoustics, 2007.* Madrid, Spain

D.R. Yntema, J.W. van Honschoten, R.J. Wiegerink. Integrated 3D sound intensity sensor with four-wire particle velocity sensors. *Proceedings of DTIP of MEMS & MOEMS 2008.*

D. R. Yntema and H-E. de Bree. A Microflown Based Sound Pressure Microphone Suitable For Harsh Environments. *Acoustical Society of America Journal (ASAJ), 118. pp. 1923-1924 .*

J.C. Winkel, D.R. Yntema, W.F. Druyvesteyn and H-E. de Bree. A particle velocity based method for separating all multi incoherent sound sources. *Proceedings of the FISITA 2006 World Automotive Congress.* Yokohama, Japan.

H.E. de Bree, T. Basten, D. Yntema. A single broad banded 3D beamforming sound probe. *Proceedings of DAGA, 2008.*

J.W. van Honschoten, D.R. Yntema, M.A. Dijkstra, V. Svetovoy, R.J. Wiegerink, M.C. Elwenspoek. Analysis of packaging effects on the performance of the microflown. *Proceedings of DTIP of MEMS & MOEMS 2006.*

J.W van Honschoten, D.R. Yntema, R.J. Wiegerink, M.C. Elwenspoek. Directional sensitivity of a three dimensional particle velocity sensor. *Proceedings of the 17 workshop on Micromachining, Micromechanics and Microsystems, pp. 201-204, 2006.* Southampton.

Dankwoord

De afgelopen vier jaar heb ik samengewerkt met diverse mensen, en dat meestal met veel plezier. Een aantal mensen wil ik speciaal bedanken. Allereerst mijn promotor Miko Elwenspoek, bedankt voor de leerzame en leuke tijd die ik heb mogen doorbrengen in de vakgroep TST. Verder bedank ik mijn copromotor Erik Druyvesteyn voor de zeer aangename samenwerking. Uw kritische kijk op problemen, enthousiasme en combinatie van geduld en gedrevenheid heeft mij geïnspireerd. En mijn dagelijkse begeleider Remco, bedankt voor een uiterst prettige begeleiding en ontspannen samenwerking.

Het onderzoeksproject is uitgevoerd in samenwerking met het bedrijf Microflown Technologies dat de Microflown sensoren vermarkt. Hans-Elias, zonder wie ik waarschijnlijk niet in dit vakgebeid terecht gekomen zou zijn, bedankt voor de altijd enthousiaste samenwerking en goede vriendschap. En Alex, ik denk dat je mijn beste voorbeeld bent van een ‘ruwe bolster blanke pit’. Het Microflown team: een groep innovatieve mensen, bedankt voor de fijne samenwerking.

Aan mijn mede- projectgenoten en betrokken mensen zoals Kechun, die altijd iets werkends uit de cleanroom haalt en Meint, die dat proces liever wat meer geoptimaliseerd ziet. Erwin, in de cleanroom is verassend veel mogelijk als het aan jou ligt. Remco, qua opruimen in het lab zie ik wel een overeenkomst tussen ons, gelukkig pak jij het wat groter aan. Joost, bedankt voor de hulp inzake theoretische problemen. In het project zijn ook een aantal afstudeerders, stagiaires en andere studenten betrokken, daarvan vooral Robert en Sjouke bedankt. Verder wil ik Duy nog extra bedanken voor zijn bijdrage aan de omslag van dit proefschrift, en mijn paranimfen Kechun en Tjeerd-Hans.

De vakgroep TST, ook wel bekend als MicMec, heeft een speciale sfeer. De oorzaak van die sfeer ligt in de omgang met collega’s en de grote vrijheid die iedereen krijgt. Dat moet je als persoon wel liggen, maar als dat zo is dan staat het garant voor een zeer fijne, inspiratievolle werkomgeving. Natuurlijk hebben alle collega’s een grote invloed daarop. Daarom ook alle collega’s, ex-collega’s en indirecte collegas bedankt, ik noem een aantal van de vele: Arjan, Arno, Boudewijn, Dannis, Dennis, Dick, Duy, Edin, Erwin, Gijs, Hanh, Hans, Henk, Henry, Imran, Ingrid, Gijs, Jelmer, Jeroen, John, Joost, Judith, Laura, Leon, Marcel & Marcel, Marcus, Meint, Mink, Natalya, Niels, Nima, Rahm, Sandeep, Saravanan, Shahina, Srinivas, Susan, Toon, Theo, Vitaly, Yi Ping.

Verder is er natuurlijk nog een leven naast werken, waar invulling aan gegeven wordt door een biertje te drinken op een terras, lekker te eten, te praten enzovoort. Hoewel er

veel mensen zijn met wie ik dat graag doe zijn er een paar die ik specifiek wil noemen, namelijk Tjeerd Hans, Anne, Duy, Remco Seesink, Rolf, Lissa, Remco, Ilona, Marcus, Dennis, Marjolijn, Jeroen en Maartje.

Aan mijn vader en moeder, die mij opgevoed hebben met het idee dat je moet doen wat je kunt en niet te snel tevreden met jezelf moet zijn: gelukkig vind ik dat nog leuk ook. Marian, je zou vast een beetje trots zijn. Ernst en Maren, die vroeger toch altijd weer de moed hadden mijn uitvindingen te testen. Verder alle familie en schoonfamilie hartelijk bedankt voor de getoonde interesse en een altijd fijn welkom.

Marije Jildou, mijn lieve vrouw, dank je voor het vertrouwen: 'hij maakt zich wel druk maar het komt toch wel goed', ik houd heel veel van je!

September 2008